

## September, 1958

*published monthly by The Institute of Radio Engineers, Inc.*

# Proceedings of the IRE<sup>®</sup>

*contents*

	<b>Poles and Zeros</b> .....	1571
	<b>Donald B. Sinclair, Director, 1958</b> .....	1572
	<b>Scanning the Issue</b> .....	1573
<b>PAPERS</b>	Analysis and Experimental Results of a Diode Configuration of a Novel Thermoelectron Engine, <i>G. N. Hatsopoulos and J. Kaye</i> .....	1574
	Sputnik I's Last Days in Orbit, <i>J. D. Kraus and E. E. Dreese</i> .....	1580
	Correction to "Thermoelectric Effects," <i>Frank E. Jaumot</i> .....	1587
	Noise in Maser Amplifiers—Theory and Experiment, <i>J. P. Gordon and L. D. White</i> .....	1588
	The Spherical Coil as an Inductor, Shield, or Antenna, <i>Harold A. Wheeler</i> .....	1595
	Error Probabilities for Binary Symmetric Ideal Reception through Nonselective Slow Fading and Noise, <i>G. L. Turin</i> .....	1603
	Diffraction by Smooth Cylindrical Mountains, <i>H. E. J. Neugebauer and M. P. Bachynski</i> ....	1619
	Refraction Anomalies in Airborne Propagation, <i>Ming S. Wong</i> .....	1628
	A Cathode Test Utilizing Noise Measurements, <i>W. Dahlke and F. Dlouhy</i> .....	1639
	Correction to "IRE Standards on Radio Aids to Navigation: Definition of Terms, 1954" .....	1645
	IRE Standards on Information Theory: Definitions of Terms, 1958 .....	1646
<b>CORRESPONDENCE</b>	Optimum Finite Code Groups, <i>J. E. Storer and R. Turyn</i> .....	1649
	WWV Standard Frequency Transmissions, <i>W. D. George</i> .....	1649
	Storage Capacity in Meteor-Burst Communication Systems, <i>Walter A. Helbig</i> .....	1649
	Radio Engineering Use of the Cayley-Klein Model of Three-Dimensional Hyperbolic Space, <i>E. F. Bolinder</i> .....	1650
	Properties of Root Loci, <i>C. S. Lorens</i> .....	1651
	A Proposed Technique for the Improvement of Range Determination with Noise Radar, <i>Harry Hochstadt</i> .....	1652
	Estimates of Entropy of a Message Source, <i>Carmen N. Campopiano</i> .....	1652
	Minimum Weight Solenoid Systems, <i>G. M. Clarke</i> .....	1652
	Various Definitions of the Delta Entities, <i>Otomar Pankraz</i> .....	1653
	Some Comments on Minimum Triggering Signals, <i>J. L. Dautremont, Jr.</i> .....	1654
	A Low-Noise Nonlinear Reactance Traveling-Wave Amplifier, <i>R. S. Engelbrecht</i> .....	1655
	The Electron Optical Action of an Annular Aperture Lens, <i>L. A. Harris</i> .....	1655
	Pulse Modulation Transmitted through a Linearly Modulated Transit-Time Device, <i>V. Met</i> ..	1656
	Phase Dependence of a Ferromagnetic Microwave Amplifier, <i>W. L. Whirry and F. B. Wang</i> ..	1657
	Analysis of Traveling-Wave Tubes with Tapered Velocity Parameter, <i>D. V. Geppert</i> .....	1658
<b>REVIEWS</b>	Scanning the TRANSACTIONS .....	1661
	Books:	
	"Mass Spectroscopy," by H. E. Duckworth, <i>Reviewed by Harold C. Mattraw</i> .....	1662
	"Introduction to Electromagnetic Engineering," by R. F. Harrington, <i>Reviewed by L. A. Manning</i> .....	1662

# Proceedings of the IRE®

continued

	"Transients in Electrical Circuits," by G. V. Lago and D. L. Waidelich, <i>Reviewed by G. B. Herzog</i> .....	1663
	"Modern Computing Methods," <i>Reviewed by L. N. Ridenour</i> .....	1663
	"Einführung in die Mikrowellen-Elektronik Teil II: Lauffeldröhren," by Werner Kleen and Klaus Pöschl, <i>Reviewed by W. J. Albersheim</i> .....	1663
	"Principles of Electricity," (3rd ed.) by Leigh Page and N. I. Adams, Jr., <i>Reviewed by E. T. Jaynes</i> .....	1664
<b>ABSTRACTS</b>	Abstracts of IRE TRANSACTIONS .....	1665
	Abstracts and References .....	1668
<b>IRE NEWS AND NOTES</b>	Calendar of Coming Events and Authors' Deadlines .....	14A
	Call for Papers, 1959 IRE National Convention .....	14A
	Obituary .....	20A
	1958 IRE WESCON Convention Record .....	20A
	IRE Canadian Convention .....	22A
	Annual Conference on Industrial Electronics .....	26A
	Annual Broadcast Symposium .....	26A
	National Symposium on Engineering Writing and Speech .....	28A
	National Symposium on Extended Range and Space Communications .....	28A
	Professional Groups .....	30A
	Sections and Subsections .....	30A, 34A
<b>DEPARTMENTS</b>	Contributors .....	1659
	IRE People .....	42A
	Industrial Engineering Notes .....	106A
	Meetings with Exhibits .....	8A
	Membership .....	62A
	News—New Products .....	40A
	Positions Open .....	134A
	Positions Wanted by Armed Forces Veterans .....	138A
	Professional Group Meetings .....	84A
	Section Meetings .....	94A
	Advertising Index .....	186A
<b>COVER</b>	A novel diode-type of thermoelectronic device has been developed at M.I.T. for converting heat directly into electrical energy with an efficiency of better than 10 per cent, as described on page 1574.	

**BOARD OF DIRECTORS, 1958**

\*D. G. Fink, *President*  
 C. E. Granqvist, *Vice-President*  
 \*W. R. G. Baker, *Treasurer*  
 \*Haraden Pratt, *Secretary*  
 \*J. D. Ryder, *Editor*  
 A. V. Loughren,  
*Senior Past-President*  
 \*J. T. Henderson,  
*Junior Past President*

1958  
 A. N. Goldsmith  
 H. R. Hegbar (R4)  
 E. W. Herold  
 K. V. Newton (R6)  
 A. B. Oxley (R8)

F. A. Polkinghorn (R2)

D. B. Sinclair  
 \*Ernst Weber  
 J. R. Whinnery

1958-1959  
 R. I. Cole (R3)  
 G. A. Fowler (R7)  
 \*R. L. McFarlan (R1)  
 D. E. Noble  
 E. H. Schulz (R5)  
 Samuel Seely

1958-1960  
 G. S. Brown  
 W. H. Doherty

\*Members of Executive Committee

**EXECUTIVE SECRETARY**

George W. Bailey

Evelyn Benson, *Assistant to the Executive Secretary*

John B. Buckley, *Chief Accountant*

Laurence G. Cumming, *Technica Secretary*

Emily Sirjane, *Office Manager*

**ADVERTISING DEPARTMENT**

William C. Copp, *Advertising Manager*

Lillian Petranek, *Assistant Advertising Manager*

**EDITORIAL DEPARTMENT**

Alfred N. Goldsmith, *Editor Emeritus*  
 J. D. Ryder, *Editor*  
 E. K. Gannett, *Managing Editor*  
 Helene Frischauer, *Associate Editor*

**EDITORIAL BOARD**

J. D. Ryder, *Chairman*  
 F. Hamburger, Jr., *Vice-Chairman*  
 E. K. Gannett  
 Keith Henney  
 E. W. Herold  
 T. A. Hunter  
 G. K. Teal  
 W. N. Tuttle



PROCEEDINGS OF THE IRE, published monthly by The Institute of Radio Engineers, Inc., at 1 East 79 Street, New York 21, N. Y. Manuscripts should be submitted in triplicate to the Editorial Department. Responsibility for contents of papers published rests upon the authors, and not the IRE or its members. All republication rights, including translations, are reserved by the IRE and granted only on request. Abstracting is permitted with mention of source.

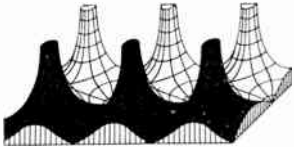
Fifteen days advance notice is required for change of address. Price per copy: members of the Institute of Radio Engineers, one additional copy \$1.25; non-members \$2.25. Yearly subscription price: to members \$9.00, one additional subscription \$13.50; to non-members in United States, Canada, and U. S. Possessions \$18.00; to non-members in foreign countries \$19.00. Entered as second class matter, October 26, 1927, at the post office at Menasha, Wisconsin, under the act of March 3, 1879. Acceptance for mailing at a special rate of postage is provided for in the act of February 28, 1925, embodied in Paragraph 4, Section 412, P. L. and R., authorized October 26, 1927. Printed in U.S.A. Copyright © 1958 by The Institute of Radio Engineers, Inc.

**Airborne Instruments Laboratory Monograph on page 4A.**

# Proceedings of the IRE



## Poles and Zeros



**D-Day in Engineering Education?** This is written under a cloud of discouragement created by attendance at the annual convention of the American Society for Engineering Education at the University of California in Berkeley.

The dejection comes not from attendance at any of the sessions of the Electrical Engineering Division (chaired by former IRE Director Eastman), nor as a result of visits with E. E. Department Head John Whinnery (present Director-at-large) but from conversations with other engineering teachers and administrators and attendance at certain sessions.

In Year I A.S. (After Sputnik) it seems appropriate to be discouraged over the future of engineering and of our world after attending a session of engineering teachers where it was necessary ardently to argue the desirability of graduate work for the engineer, and that a graduate degree should not be based upon the development of specialized technical abilities, but rather as a further deepening and broadening of the scientific base of the student. To listen to other arguments justifying the retention of a freshman course in surveying for all engineers as training in measurement, without introducing error theory or recognition that you may measure things you cannot see, or arguments on the need for a lengthy drawing course by stating that the student will then know the standard symbols for screw threads, or a shop course because he will then learn to design parts that fit, is certainly disheartening. Especially so when we face this great and once-in-many-lifetimes opportunity to uplift the whole profession by making it a study of the science of nature as against training in technique. In the future it is not going to be enough to know how it *was* done—the problems of tomorrow have never been solved before.

While we admit our evolution from the early civil engineers, we wonder how long it will be before some of our educators recognize that we are not ALL civil engineers; that electronics, rockets, and research have introduced a whole new dimension to the spectrum of engineering knowledge, where conception and design of ideas may be of equal value to visualization and design of structures.

The widening of this spectrum of engineering knowledge is going hand in hand with increased utilization of mathematics. The fields which are moving and solving the new problems for tomorrow seem to be the fields in which mathematical proficiency is at its highest level of advance—and we venture a theorem without further proof: A field of engineering can advance only as fast as its members acquire mathematical proficiency. How can members of a field be expected to understand what mathematics can do for them when they have no proficiency in mathematics? How can they realize that the electronic computer can now solve insoluble problems

of an earlier age? Or that a mathematical analysis can often save kilobucks and kilominutes otherwise to be expended in the wrong experiment?

Take mechanical engineering as an example (*note*: always choose a field which is not your own) where in only recent years has the differential equation been studied, and where the partial derivative is still of somewhat questionable ancestry. Theoretical progress is just now really beginning, whereas electronics with its longer history of mathematical study now has graduates who are mathematics majors as well as engineers, and teachers to whom Laplace, Fourier, Bessel, Riemann, Cauchy, are old buddies.

Can the profession of engineering long remain divided, with members in one segment as unable to talk to other segments as if their languages were Aramaic and bebop, with some schools well advanced in the teaching of the science formerly contained in classical physics, and other schools still concerned with the apparatus and hardware of a swiftly passing day?

Are the engineering teachers, the engineering schools, and the engineering profession, at the point of decision—to choose between surveyors of technique or purveyors of science as teachers, hardware or ideas as our course material, drawing or mathematics as our language, and technicians or engineering scientists as our output? Which is it going to be?

**Nothing Really New?** Certain evidence indicates that history may have a repetition rate of about 2.5 per century. Micro-waves returned in 1940 after original investigation before 1900, the crystal diode lived in 1900 and again in 1940, and now we are seeing a return of the battery almost forty years after its heyday in the early 1920's.

Which reminds us that our first battery experience came with the soldering of fifteen flashlight cells into a candy box to beat the price of those 1920 B batteries. We learned that battery life was inversely proportional to length of soldering iron contact, which was inversely proportional to the cleanliness of the iron, which was some never-determined function of the gas burner adjustment on the kitchen stove.

Be that as it may, the review paper on batteries in last month's issue is timely as we move into the transistor and solar-cell era. Besides, you asked for it—more review papers, that is.

**Number Ninety-Nine!** To show that the IRE is aware of progress in all fields from polyethylene to polarization to politics, may we remark that the Executive Committee recognized the importance of Alaska four days *before* it was approved as the forty-ninth state, by recommending the formation of the Anchorage IRE Section as Number 99. Greetings, polar bears!—J.D.R.

## *Donald B. Sinclair*

*Director, 1958*



Donald B. Sinclair (J'30-A'33-M'38-SM'43-F'43) was born in Winnipeg, Manitoba, Canada, on May 23, 1910. He attended the University of Manitoba from 1926 to 1929, and worked part-time as a radio operator for Western Canada Airways. He then transferred to Massachusetts Institute of Technology, where he received the degrees of S.B. in 1931, S.M. in 1932, and Sc.D. in 1935. During this period he was enrolled in a cooperative course in electrical engineering, and worked at the New York Telephone Company, the Western Electric Company at Hawthorn, and the Bell Telephone Laboratories. While studying for his doctorate he was a research assistant in the Department of Electrical Engineering at M.I.T., and spent one year working on his dissertation at the General Radio Company. He remained at M.I.T. for one year after receiving his degree.

He was employed by General Radio Company in 1936, and subsequently became Assistant Chief Engineer, and Chief Engineer. In 1955 he was appointed Vice-President, and in 1956 was elected a Director. He is also a member of General Radio's Management and New Products Committees, chairman of the Patents and Development Committees, and a trustee of the General Radio Profit-Sharing Trust.

During World War II he was in charge of the search-receiver work for radar countermeasures at the Radio Research

Laboratory at Harvard University, and was a member of Division Five of the National Defense Research Committee on guided missiles. In 1943 he went to North Africa with the first *Ferret* plane to be sent to the European theater of operations. For his work on countermeasures and guided missiles he received the President's Certificate of Merit in 1948. From 1954 to 1958 he was a member of the Technical Advisory Panel on Electronics of the Department of Defense.

Dr. Sinclair was President of the IRE in 1952, following a term as Treasurer in 1949-1950. He served on the Executive Committee in 1948-1950 and again in 1952-1953, and was previously on the Board of Directors from 1945 to 1954. He has represented the Institute on the Radio Technical Planning Board, the Joint IRE-AIEE Coordination Committee, and most recently, at the 1958 meeting of the A. S. Popov Society in Moscow.

In the Boston Section he has been a member of the Executive Committee, 1946-1948 and 1952-1958, member and chairman of the Awards Nominating Committee, and chairman of the Program Committee. This latter term of office included the first NEREM meeting in 1947.

He is a Fellow of the American Institute of Electrical Engineers, and a member of Sigma Xi and the American Association for the Advancement of Science.

## Scanning the Issue

**Analysis and Experimental Results of a Diode Configuration of a Novel Thermoelectron Engine** (Hatsopoulos and Kaye, p. 1574)—One of the most interesting developments now being worked on in any field of engineering concerns a device which by means of thermionic emission will convert heat directly into electrical energy without requiring any moving mechanical parts. This paper describes the construction and operating results of one of the few such thermoelectron engines to be built so far. The word "engine" aptly describes this device because it is a true heat engine in the same sense that a steam power plant is. Heat is supplied to a working fluid at high temperature to produce a gas which performs useful work and gives up heat at a lower temperature. The cycle is completed by pumping the fluid back to the high-temperature end of the system. The working fluid in this case is an electron gas which is boiled out of a hot cathode and passed through a vacuum to a cold anode. Useful work is produced by the passage of the electrons through a retarding field between cathode and anode. The experimental results show an efficiency of over 10 per cent is now attainable and that considerably higher efficiency can be expected in future models.

**Sputnik I's Last Days in Orbit** (Kraus and Dreese, p. 1580)—Last March the PROCEEDINGS published three letters to the Editor which 1) suggested that certain variations in the observed signal from the transmitter of Sputnik I were due to a bunching of ionized air molecules in front of the onrushing satellite as they rebounded from its nose, 2) reported that this ionization could be detected by reflections of signals from radio stations located on the ground, and 3) by means of reflections of WWV signals, traced the gradual disintegration of Sputnik into a dozen or more pieces. These reports, especially the latter, attracted world-wide attention in the technical and lay press and among many scientific groups engaged in satellite tracking and ionospheric investigations for the IGY, because they offered the only evidence in existence of when and how Sputnik I met its demise. This paper is a complete description and interpretation of the observations reported in brief earlier. The widespread interest in this work is heightened by the fact that a divergence of opinion exists in scientific circles concerning the suitability of the statistical methods and extrapolations which were needed to explain and interpret the results. This in no way detracts from the value of this paper. On the contrary, this paper will provide an exceedingly valuable reference point for further investigation of the ingenious methods proposed by the authors, as well as results which are of importance to all those concerned with the problem of reentry of orbiting objects and with the physics of the upper atmosphere.

**Noise in Maser Amplifiers—Theory and Experiment** (Gordon and White, p. 1588)—One of the liveliest subjects in radio engineering at this time concerns low-noise microwave amplification. Recent advances in traveling-wave tubes have lowered their noise levels to well below earlier predictions. Meanwhile, parametric-type amplifiers have been developed with even lower noise figures. The lowest of the low, however, is the maser. Its low-noise properties have already been put to important use in the field of radio astronomy to extend substantially the range of radio telescopes. This paper presents an excellent theoretical analysis of noise in maser amplifiers and the results of experimental measurements of the noise of an ammonia beam maser, contributing substantially to our understanding of this important subject.

**The Spherical Coil as an Inductor, Shield, or Antenna** (Wheeler, p. 1595)—This paper considers a unique form of

inductor, a spherical coil, which because of its geometry lends itself to unusually simple and exact mathematical formulations of its magnetic and related characteristics. Since the spherical coil is an idealized rather than a practical form of inductor, these exact results will be of direct interest mainly to teachers and students of field theory, who should find the simplicity of the concepts quite intriguing. However, the results can be useful to the practicing engineer, as well. The principles of coupling, shielding, and the effects of core materials, for example, are reduced to such simple expressions that from them the effects of nonspherical geometries can be readily estimated.

**Error Probabilities for Binary Symmetric Ideal Reception Through Nonselective Slow Fading and Noise** (Turin, p. 1603)—An excellent study has been made of the effects of fading and noise on the accuracy with which a receiver will guess which of the two known wave shapes was transmitted over a binary data transmission system. The paper, while somewhat specialized, will find quite wide application in the fields of communications systems, information theory, and wave propagation. The author shows, as an example, how his results can be used to determine the effects of pulse shape and frequency separation on the performance of a frequency-shift-key teletype system working through a scatter propagation link.

**Diffraction by Smooth Cylindrical Mountains** (Neugebauer and Bachynski, p. 1619)—During the Korean War, soldiers in the field found to their surprise that in some cases the presence of a mountain between transmitter and receiver caused better reception than if there had been no obstacle at all. Studies of propagation over the mountainous terrains of Japan, Hawaii, and Alaska confirmed this unexpected result and the phenomenon, known as obstacle gain, was reported in the PROCEEDINGS five years ago. It was recognized that the effect, which occurs at VHF and above, was caused by diffraction of radio waves as they passed over the sharp edge of a mountain. While the principles have thus been well established, the detailed mathematical descriptions of what occurs are at some variance with experimental evidence, enough so as to make it difficult to design accurately a system to take advantage of obstacle gain. This paper presents an interesting combination of geometric-optical theory with corroborative experimental measurements obtained with models of mountains in the laboratory which make an important contribution to the solution of practical engineering problems involving obstacle gain.

**Refraction Anomalies in Airborne Propagation** (Wong, p. 1628)—Ray tracing techniques are used to explain the irregularities of radio wave propagation caused by various refractive index patterns of the atmosphere, determined from airborne measurements. This is one of the first correlations of refractive index structure and radio signal strength, and opens up a new field of prediction of communication and radar propagation characteristics that will be of wide interest in those fields.

**A Cathode Test Utilizing Noise Measurements** (Dahlke and Dlouhy, p. 1639)—This paper describes a simple and sensitive method for measuring the quality of oxide cathodes by means of shot-noise measurements. The method proposed is a fundamental contribution to tube testing techniques and will probably be widely adopted by manufacturers.

**IRE Standards on Definitions of Terms on Information Theory** (p. 1646)—This important Standard sets forth the definitions of 34 basic terms relating to measures of information that are central to the field of information theory.

*Scanning the Transactions* appears on page 1661.

# Analysis and Experimental Results of a Diode Configuration of a Novel Thermoelectron Engine\*

G. N. HATSOPOULOS† AND J. KAYE†

**Summary**—The direct conversion of heat into useful electrical work without utilization of moving mechanical parts has been successfully achieved in a novel device called the thermoelectron engine. This device is a heat engine in the thermodynamic sense because the working fluid, an electron gas, receives heat at a high temperature, rejects heat at a lower temperature, and delivers useful electrical work to an external load. This heat engine is also a thermionic device in that the electron gas is produced by emission from a hot cathode in a vacuum and by absorption or condensation of the electrons on a colder anode at a higher negative potential.

The basic principle underlying this heat engine is that a calculable fraction of electrons emitted from a hot cathode possess sufficiently high values of emission velocity to overcome a retarding electrostatic potential barrier between cathode and anode in a vacuum. Thus these electrons can transform their high initial value of kinetic energy into useful potential energy at the colder anode; this potential energy can then be utilized by connecting cathode and anode externally through a matched impedance in the form of a load. Hence, this engine utilizes a selection process which results in a large value of output voltage per unit cell compared with the output of a thermoelectric generator per unit thermocouple.

The important engineering aspects of this successful heat engine comprise, first, the use of emissive surfaces which can be machined carefully to high tolerances and thus permit very small spacing between cathode and anode, of the order of 0.001 inch or less, and secondly, the heat transfer designs which can greatly reduce unnecessary heat losses at the required high temperatures.

A brief analysis of the diode configuration of a thermoelectron engine is given to predict the performance of several models. Out of a total of ten successful models of the diode configuration, the experimental results for one model have been selected for presentation here. A thermal efficiency of between 12 to 13 per cent has been attained based on measured power output and calculated values of heat input. Power outputs of the order of 1 watt/cm<sup>2</sup> of emissive surface have been measured with this small feasibility model.

If the theory and the presently available data are used as a basis of extrapolation it appears that thermal efficiencies greater than 15 per cent may be attained. The power output might reach values of the order of 10 to 30 watts/cm<sup>2</sup> of emissive surface. Multiplate designs also indicate the attainability of fairly large values of power output per total volume or per total weight of equipment.

## NOMENCLATURE

$A$  = constant in Richardson's (1), amp/(°K<sup>2</sup> cm<sup>2</sup>).

$J_0$  = output current density, amp/cm<sup>2</sup> of emissive surface\*.

$J_s$  = saturation current density, amp/cm<sup>2</sup> of emissive surface\*.

$k$  = Boltzmann's constant,  $0.8616 \times 10^{-4}$  ev/°K.

$P_1$  = ohmic power loss in external leads, watts/cm<sup>2</sup>\*.

$P_0$  = power output, watts/cm<sup>2</sup>\*.

$q$  = heat flux, watts/cm<sup>2</sup>\*.

$q_c$  = heat flux by conduction, watts/cm<sup>2</sup>\*.

$q_r$  = heat flux by radiation, watts/cm<sup>2</sup>\*.

$T$  = temperature.

$V_0$  = output voltage, volt.

$\epsilon$  = thermal emissivity of electron emissive surface.

$\phi$  = work function, volt.

$\eta$  = thermal efficiency.

$\sigma$  = Stefan's radiation constant, watts/(°K<sup>4</sup> cm<sup>2</sup>)\*.

## Subscripts

<sub>0</sub> refers to output of engine.

<sub>1</sub> refers to hot cathode.

<sub>2</sub> refers to cold anode.

## Superscript

\* refers to unit area of emissive surface.

## INTRODUCTION

A METHOD for the efficient conversion of heat directly into useful electrical work without the utilization of moving mechanical parts, which shows promise of becoming a practical engineering device, has been successfully tested. The conversion device to be described is the result of a basic research program started about four years ago at M.I.T. in the Research Laboratory of Heat Transfer in Electronics. Several different types of conversion devices have been analyzed and feasibility models have been constructed and tested. All are, in reality, heat engines which employ electrons or an "electron gas" as a working fluid undergoing a cyclic process. These conversion devices, which are based on thermionic emission, are labelled herein "thermoelectron engines" to distinguish them from conversion devices utilizing thermocouples in the form of well-known thermoelectric generators. Although several diverse forms of thermoelectron engines have been analyzed, designed, constructed, and tested, only one particular form, namely the diode configuration, will be described herein.

Briefly, the thermoelectron engine is a true heat engine in the customary thermodynamic sense, and is comparable with the steam power plant as a heat engine. In both heat engines, heat is supplied to a working fluid at high temperature, producing a vapor or gas capable of delivering useful work to the surroundings. Heat is rejected from this working fluid at a lower temperature, and then the fluid completes the cyclic process, being finally pumped to the part of the device supplying heat at the high temperature. In the case of the thermoelectron engine, the working fluid is the electron gas. Initially, this electron gas is in the metallic cathode which is heated to maintain it at a high temperature,

\* Original manuscript received by the IRE, May 1, 1958; revised manuscript received, May 29, 1958.

† Dept. of Mech. Eng., Mass. Inst. Tech., Cambridge, Mass.

$T_1$ . The electron gas is then evaporated or boiled out of the cathode and passed through a vacuum to the colder anode. It is then condensed on the anode which is cooled to maintain it at a lower temperature,  $T_2$ . The electron gas delivers useful work to the surroundings as a result of its passage through a retarding electrostatic field in the vacuum between cathode and anode. This useful work is, in fact, the electrical work delivered to the external load.

The use of the Edison effect for the conversion of heat into electric power has often been mentioned in the literature on thermionic devices. Champeix<sup>1</sup> in 1951 gave a qualitative discussion of one such method and concluded that this method was impractical. The first detailed electronic and thermodynamic study on the subject was given by one of the authors in 1956,<sup>2</sup> who analyzed the use of close spacings and of a crossed electric and magnetic field for offsetting the effects of space charge. His diode analysis was based on the approximate Childs-Langmuir equation. Subsequently Moss<sup>3</sup> in 1957 analyzed the diode by means of the exact solution of the Poisson's equation.

#### OBJECTIVES

The objectives of this report are mainly twofold:

- 1) An analysis of the diode configuration of a novel thermoelectron engine is given in detail.
- 2) The experimental results obtained with a feasibility model of the diode configuration are given and discussed briefly.

#### ANALYSIS OF THE DIODE CONFIGURATION

The analysis of this thermionic device operating as a heat engine is based on the laws of thermodynamics, statistical mechanics, and electrical phenomena, including the results available from quantum mechanics. A brief description of this analysis will be given first to acquaint the reader with the basic assumptions used.

Consider a hot plane cathode opposite to a cold plane anode, each being made from the same emissive material. The distribution of electron velocities and energies inside each metal is assumed given by Fermi-Dirac statistics. As the electrons are evaporated from the hot cathode, at say 2500°F, it is assumed that they have a Maxwellian distribution of velocity and energy in the vacuum just beyond the cathode surface. If a negative retarding potential is supplied to the anode, then a calculable fraction of the emitted electrons possess sufficient kinetic energy to overcome this retarding potential barrier in the vacuum between cathode and anode, including the space-charge barrier formed by

the electron cloud just beyond the cathode surface. It is evident that a selection process will then occur, in that not all the emitted electrons will pass through this retarding potential but only those which possess a sufficiently high value of emission velocity normal to the cathode. All those electrons which overcome this retarding potential barrier condense on the colder anode surface, if it is assumed that the reflection coefficient for electrons arriving at the anode is zero; this assumption is not quite true if the quantum-mechanical model of electrons is used.

In addition to the emission of electrons from the hot cathode directed towards the anode, there is also an emission of electrons from the colder anode directed towards the cathode. As in the case of the electrons emitted from the cathode, only a calculable fraction of electrons emitted from the anode will possess a sufficiently high value of emission velocity to overcome the retarding potential barrier from anode to cathode; this barrier is, in general, smaller than that from cathode to anode. Again, it is assumed that the reflection coefficient of electrons reaching the cathode is zero. Hence the net electron flow between cathode and anode is the difference of the two streams described above.

When the cathode and anode are connected by an external circuit through a load, useful electrical work is delivered to this load. In effect, those high-energy electrons which overcome the retarding potential barrier between cathode and anode transform their kinetic energy into useful potential energy at the anode. The output current through the load depends on the temperatures of the cathode and anode, the properties of the emissive materials used, and the spacing between cathode and anode. The thermal efficiency is dependent on these same quantities and also on the heat losses due to radiation and conduction processes.

The analysis of the operation of the diode configuration of the thermoelectron engine is presented briefly.

#### OUTPUT CURRENT

Consider two parallel plates of emissive material, placed in a vacuum and separated by a distance  $y$ , as shown in Fig. 1. For steady-state operation, the cathode is maintained at a temperature,  $T_1$ , by a steady input of heat flux,  $q_1$ , and the anode is maintained at a lower temperature,  $T_2$ , by a steady removal of heat flux,  $q_2$ . The potential distribution from cathode to anode is illustrated in Fig. 2, wherein  $\phi_1$  is the potential barrier for electrons within the cathode relative to its surface, or its work function,  $\delta$  is the space-charge barrier,  $\phi_2$  is the work function of the anode, and  $V_0$  is the output voltage obtained when the cathode and anode are connected externally through a load.

The saturation current density of electrons emitted from either cathode or anode in a vacuum is given by the well-known Richardson equation,

$$J_s = AT^2 \exp(-\phi/kT), \quad (1)$$

<sup>1</sup> M. R. Champeix, "Transformation of heat into electrical energy in thermionic phenomena," *Le Vide*, vol. 6, pp. 936-940; January, 1951.

<sup>2</sup> G. N. Hatsopoulos, "The thermoelectric engine," Sc.D. dissertation, M.I.T., Cambridge, Mass.; May, 1956.

<sup>3</sup> H. Moss, "Thermionic diodes as energy converters," *J. Electronics*, vol. 2, pp. 305-322; January, 1957.

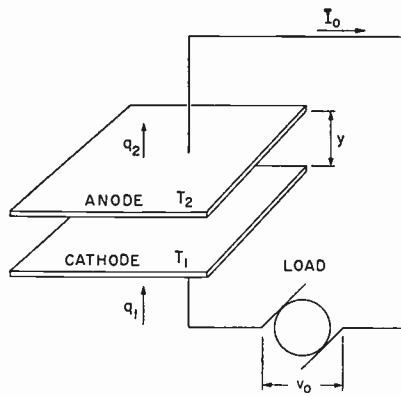


Fig. 1—Thermoelectron engine diode configuration.

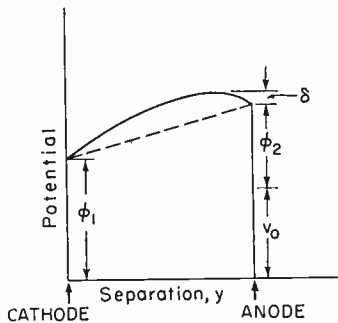


Fig. 2—Schematic representation of potential barrier including space charge.

wherein it is assumed that the surfaces emit electrons uniformly so that nonuniformities based on patch effects are momentarily ignored.

The fraction of the cathode saturation current which reaches the anode is equal to the product of the saturation current and that fraction of emitted electrons which have sufficient initial velocities to overcome the retarding potential barrier of  $(\delta + \phi_2 + V_0 - \phi_1)$ ; *i.e.*,

$$\begin{aligned}
 J_{1-2} &= A_1 T_1^2 \exp(-\phi_1/kT_1) \\
 &\cdot \exp[-(\delta + \phi_2 + V_0 - \phi_1)/kT_1] \\
 &= A_1 T_1^2 \exp(-\phi_2/kT_1) \exp(-\delta/kT_1) \\
 &\cdot \exp(-V_0/kT_1). \tag{2}
 \end{aligned}$$

Likewise, the fraction of the anode saturation current which reaches the cathode is equal to the product of the saturation current and that fraction of emitted electrons which have sufficient initial velocities to overcome the retarding potential barrier equal to  $\delta$ ; *i.e.*,

$$J_{2-1} = A_2 T_2^2 \exp(-\phi_2/kT_2) \exp(-\delta/kT_2). \tag{3}$$

Hence the net current density from cathode to anode is given by

$$\begin{aligned}
 J_0 &\equiv J_{1-2} - J_{2-1} \\
 &= A_1 T_1^2 \exp(-\phi_2/kT_1) \exp(-\delta/kT_1) \exp(-V_0/kT_1) \\
 &\quad - A_2 T_2^2 \exp(-\phi_2/kT_2) \exp(-\delta/kT_2). \tag{4}
 \end{aligned}$$

The physical significance of (4) is that the net flux of

electrons from cathode to anode, or the net current per unit area of emissive surface, depends on the temperatures of cathode and anode, on the space-charge barrier  $\delta$ , and on the work function of only the cold anode  $\phi_2$ , provided that

$$\delta + \phi_2 + V_0 > \phi_1.$$

The net current density is independent of the work function of the hot cathode; this rather surprising result has been known for a long time for the case of the anode current collected from a hot cathode in a retarding field, when the retarding field is sufficiently great (see Becker<sup>4</sup>). This result has also been verified experimentally by Davisson in 1924.<sup>5</sup>

Analysis of the space-charge barrier shows that its effects could be completely eliminated for practical purposes, for a given value of the net current, and for the case of plane cathode and anode, as in Fig. 1, if the plate separation,  $y$ , is made very small, of the order of 0.001 inch. However, the many difficulties of obtaining smooth and uniform emissive surfaces with oxide coatings precluded any practical solution to obtaining such small plate separations. In the last few years, a new engineering emissive material has been developed by the Philips concern in Holland, namely the *L* cathode. This material can be machined to very close tolerances, handled in a rough fashion compared with the delicate and meticulous handling required for oxide coated cathodes, and activated after machining, cleaning, etc., in a fairly straightforward fashion. With this new emissive material, we have been successful, after many arduous efforts, in producing engineering models corresponding to Fig. 1, in which plate separations of less than 0.001 inch have been achieved.

If the space-charge barrier,  $\delta$ , is eliminated from (4), as a result of the use of very small plate separation, and if, as a further approximation, the back current from anode to cathode is made negligibly small by proper selection of  $T_1$  and  $T_2$ , then (4) is reduced to

$$J_0 = A_1 T_1^2 \exp(-\phi_2/kT_1) \exp(-V_0/kT_1). \tag{5}$$

The power output per unit area of emissive surface is then given by

$$P_0 = J_0 V_0 - P_1, \tag{6}$$

where  $P_1$  is the ohmic loss in the external electrical leads per unit area of emissive surface.

#### THERMAL EFFICIENCY OF DIODE

The thermal efficiency of a true heat engine is defined by the ratio of net power output to total heat supplied and, for this case of a diode configuration, by

$$\eta \equiv (J_0 V_0 - P_1) / \sum q_i, \tag{7}$$

<sup>4</sup> J. A. Becker, "Thermionic electron emission and absorption, part I, thermionic emission," *Rev. Mod. Phys.*, vol. 7, pp. 95-128; April, 1935.

<sup>5</sup> C. J. Davisson, "The relation between thermionic emission and contact difference of potential," *Phys. Rev.*, vol. 23, p. 299; 1924.

where  $\sum q_i$  represents the sum of all heat inputs to the cathode per unit area of emissive surface required to maintain it at temperature,  $T_1$ . For the small feasibility model of the diode configuration, which was used to obtain the measured output voltage and current, an accurate measurement of this heat input was most difficult. Hence, the thermal efficiencies given herein are based on measured output voltage and output current and on a calculated value of the heat input to the cathode using the following analysis.

Consider a well-designed engineering model of a multiplate diode configuration of the thermoelectron engine, illustrated schematically in Fig. 3. Such a design can be used as a basis for accurate estimation of the total heat inputs to the hot cathodes. Furthermore, it is evident that such a multiplate design, operating in a vacuum, reduces all unnecessary heat losses to a minimum, since each hot cathode is opposed by two cold anodes. An additional advantage of such a design is that almost any combination of voltages and currents becomes possible by using different ways of electrically connecting cathodes and anodes.

For the engineering model represented by the multiplate design of Fig. 3, the total heat inputs to the cathodes can be given by

$$\sum q_i = J_0\phi_1 + J_0(\phi_2 + V_0 + \delta - \phi_1 + 2kT_1) + q_r + q_c \quad (8)$$

where  $J_0\phi_1$  stands for the heat flux corresponding to the latent heat of evaporation of the electrons from the cathodes;

$$J_0(\phi_2 + V_0 + \delta - \phi_1 + 2kT_1)$$

represents the heat flux corresponding to the kinetic energy of that selected fraction of electrons which can overcome the retarding potential between cathode and anode;  $q_r$  represents the thermal radiation flux between each cathode and the pair of adjacent anodes;  $q_c$  represents the thermal conduction flux between each cathode and pair of corresponding anodes due to heat conduction along the necessary electrical leads. It should be remembered that the average kinetic energy of all electrons emitted from the cathode surface is  $2kT_1$ , but only a selected fraction have a kinetic energy sufficient to overcome the retarding potential equal to  $(\phi_2 + V_0 + \delta - \phi_1)$ .

The thermal radiation flux can be shown, for the geometry of two parallel metallic plates, to be given by

$$q_r = \sigma(T_1^4 - T_2^4)(1/\epsilon_1 + 1/\epsilon_2 - 1)^{-1}, \quad (9)$$

where the emissivities of the cathode,  $\epsilon_1$ , and of the anode,  $\epsilon_2$ , are to be evaluated at temperatures,  $T_1$  and  $\sqrt{T_1 T_2}$ , respectively. The geometric mean temperature is used for calculations of  $\epsilon_2$  rather than the anode temperature because the metallic surfaces of the cathode and anode are not grey bodies.

The conduction flux can be calculated with the aid of Fourier rule and the geometry of the electrical leads between cathodes and anodes, and the resistivity of

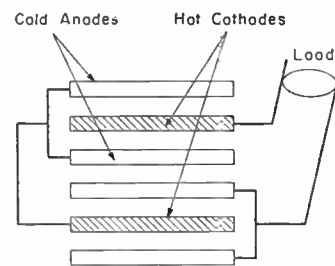


Fig. 3—Multiplate diode configuration of thermoelectron engine.

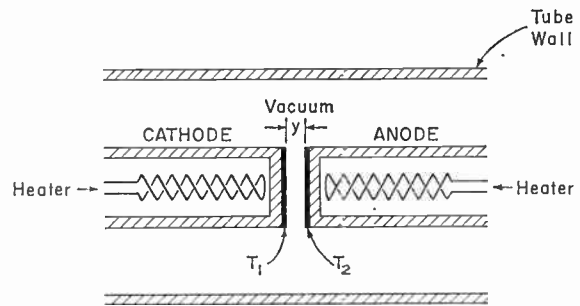


Fig. 4—Details of feasibility model of diode configuration of thermoelectron engine.

these leads. It was found analytically that for maximum efficiency, the cross section of the electrical leads should be selected so that the ohmic loss in these leads equals approximately one-tenth of the thermal conduction losses in the internal electrical leads.

## EXPERIMENTAL RESULTS

### General Description of the Diode

The experimental results presented here are based on the diode configuration described schematically in Fig. 4. Although ten successful models of this configuration have been constructed and tested in this research program, the preliminary data from only one of them will be given here. In this feasibility model, the cathode and anode were hollow molybdenum cylinders about  $\frac{1}{8}$  inch in diameter.

The base of each cylinder was impregnated tungsten, and only these bases of the cylinders, facing each other, were used for electron emission and absorption. Each cylinder was fitted carefully with a separate indirect electric heater, wound to eliminate any magnetic fields. The use of indirect electric heaters permitted us to obtain true equipotential cathodes and anodes. Each cylinder could be used interchangeably with the other as cathode or anode, and each could be heated separately to a given steady temperature. Hence the reproducibility of the test results could be examined by simply interchanging the roles of the two cylinders. The cylinders were mounted on supports, which are not indicated in Fig. 4, so that the separation between the emissive surfaces could be varied carefully and accurately during operation of the diode and without breaking the vacuum.

The results given here are based on use of the same

emissive material for cathode and anode. This material is made from tungsten which has been impregnated with various combinations of oxides of barium, aluminum, and calcium. The activation process to get this material to emit at high temperatures is fairly straightforward and requires only that it be heated to temperatures higher than those used in the final tests.

The output voltage and current were measured separately. The output voltage was also examined for ac components or ripples with the aid of an oscilloscope, but ac components were not present during the measurements reported here.

The temperature of the surface of the hot cathode was measured with an optical pyrometer which was calibrated against a standard source and which was carefully corrected experimentally for the deviations for nonblack body emission of the molybdenum cylinder by actually bringing both cathode and anode up to the source temperature in a series of auxiliary experiments. The temperature of the surface of the colder anode was usually too low to use this optical pyrometer for an accurate measurement; hence, its surface temperature was estimated in this feasibility model from known values of the thermal emissivities of the cathode and anode and the view factor for radiative transfer between them, including the conduction along the leads. Since the temperature of the colder anode is of secondary importance here, this estimation method sufficed for this model.

The distance of separation of the two plates was measured with the aid of an optical comparator in some of the tests.

The work function of the hot cathode was measured from auxiliary tests on saturation currents; its value was about 1.7 v.

#### Output Current Density vs Voltage

Fig. 5 shows the experimental results obtained in Run 17B from the feasibility model of the diode configuration. The data indicate that the output current density increases as the potential difference between cathode and anode decreases. Note that this particular model produced a maximum value of current density of about 3 amp/cm<sup>2</sup>.

Fig. 5 also shows two theoretical values of current density. The dashed curve was computed for the measured temperature of the cathode of 2308°F, the estimated value of the anode temperature of 1000°F, for equal values of work function of cathode and anode, and for a value of separation of the two plates,  $y$ , which was obtained from the tabular values of the solution of the space-charge problem. This solution is found in Kleynen's article.<sup>6</sup> The theoretical dashed curve falls considerably below the experimental points. During

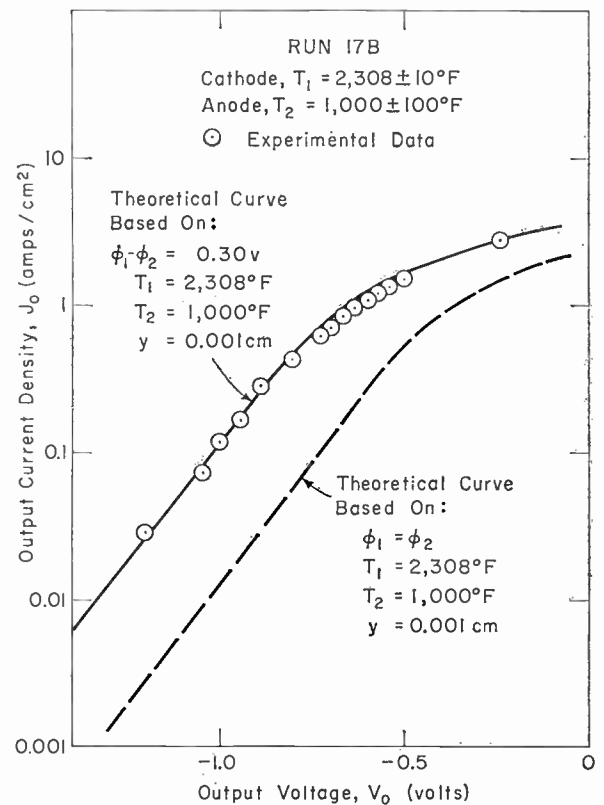


Fig. 5—Comparison of experimental current density with theoretical values for diode configuration.

the course of testing this model, it was found that the change of work function with temperature of this emissive material could be estimated fairly easily and the results agreed roughly with variations of work function in the literature; see review by Herring and Nichols<sup>7</sup> and Nottingham.<sup>8</sup> Hence these variations were included in the computation of a second theoretical curve, presented by the solid line in Fig. 5.

In this second theoretical prediction of current density, the same values of temperature and of plate separation were used, but the work function of the cold anode was assumed to be less by 0.30 volt. This reduction agreed with both our own estimates and with estimates of change of work function with temperature found in the literature.<sup>7,8</sup> The solid line in Fig. 5 shows excellent agreement with experimental data. Furthermore, the slope of the asymptote of both the solid and dashed curves, *i.e.*, that linear portion extending to high voltages, can be shown to be equal to  $(1/kT_1)$ . The value of the cathode temperature deduced from this asymptotic slope for the experimental data points agreed with the measured value of  $T_1$  within  $\pm 30^\circ\text{F}$ .

#### Output Power vs Voltage

Fig. 6 shows the experimental results for Run 17B for

<sup>6</sup> P. H. J. A. Kleynen, "Extension of Langmuir's ( $\xi$ ,  $\eta$ ) tables for a plane diode with a Maxwellian distribution of the electrons," *Philips Res. Repts.*, vol. 1, pp. 79-96; October, 1945.

<sup>7</sup> C. Herring and M. H. Nichols, "Thermionic emission," *Rev. Mod. Phys.*, vol. 21, pp. 185-270; April, 1949.

<sup>8</sup> W. B. Nottingham, "Thermionic Emission," Res. Lab. of Electronics, M.I.T., Cambridge, Mass., Tech. Rep. No. 321; 1956.

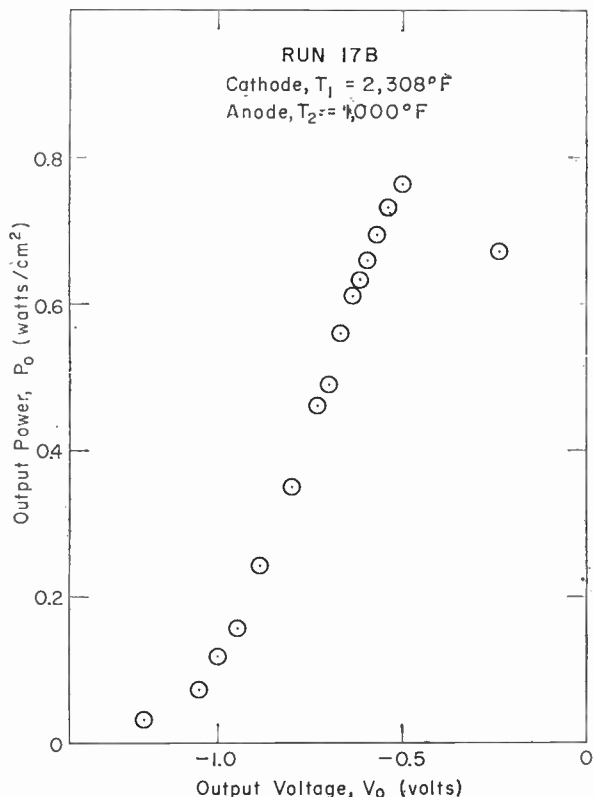


Fig. 6—Experimental power output vs output voltage for diode configuration.

power output vs voltage for the same temperatures as in Fig. 5. The data indicate a maximum exists for a voltage of about 0.5 volt. The optimum impedance matching of internal and external load characteristics will be discussed later in a separate publication. Likewise the theoretical predictions for comparison with the experimental data are omitted.

#### Thermal Efficiency vs Voltage

For simplicity of construction of the experimental models tested, there were no provisions made, such as radiation shields and proper geometric design, to reduce the heat input to a minimum. Hence the thermal efficiencies given here were based on the measured voltage and current and on a calculated heat input as explained previously. Fig. 7 shows a typical set of data for thermal efficiency vs output voltage. For this diode configuration a maximum value of thermal efficiency of about 13 per cent was attained for the cathode temperature of  $2308^\circ\text{F}$ . Comparison of Figs. 6 and 7 illustrates that the maximum values of thermal efficiency and power output do not occur at the same value of output voltage. Analysis has also shown that the optimum voltage for thermal efficiency does not coincide with the optimum voltage for power output.

#### CONCLUSIONS

The analyses presented herein demonstrate that the behavior of the diode configuration of a thermoelectron

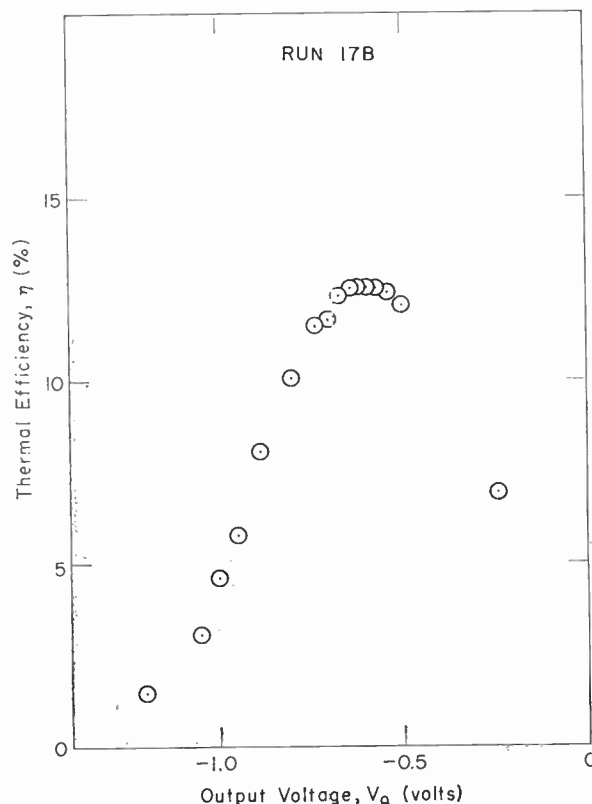


Fig. 7—Experimental results for sample diode configuration of thermoelectron engine.

engine can be predicted accurately. The experimental results show that an engineering model of such a diode configuration is feasible and that values of the thermal efficiency greater than 10 per cent are now attainable and considerably larger values are predicted for future models.

It is also evident that this diode configuration of the thermoelectron engine can be combined with other presently available power plants to yield a value of thermal efficiency of the combined heat engine which will be considerably greater than 10 per cent.

#### ACKNOWLEDGMENT

It is indeed a pleasure to acknowledge the helpful discussions with our many colleagues at M.I.T., especially Profs. William P. Allis, Samuel J. Mason, and Stylianos D. Pezaris, and with our colleagues at Thermo Electron Engineering Corporation. We are also grateful for the spirit of the cooperation given us in the past few months by the staff of Thermo Electron Engineering Corporation, especially by John A. Welsh and Gabor Miskolczy.

Furthermore, we are very happy to thank Pres. J. A. Stratton and Dean C. R. Soderberg of M.I.T. for their approval of the initial financial support of this basic research program and for their continuous help thereafter, and to Peter Nomikos for the generous and understanding financial assistance given us via the Thermo Electron Engineering Corporation.

# Sputnik I's Last Days in Orbit\*

J. D. KRAUS†, FELLOW, IRE AND E. E. DREESE‡

**Summary**—Observations during the last days of Sputnik I's orbiting are presented. These observations were made at The Ohio State University Radio Observatory using a simple CW reflection technique. The data suggest that the breakup of an artificial satellite upon its reentry into the denser atmosphere is a complex phenomenon in which a sequential series of events may occur over a period of days. Graphs of the average height of the satellite and its associated fragments as a function of time are presented, and some conclusions are drawn as to the details of the actual breakup phenomenon.

## I. INTRODUCTION

ARTIFICIAL satellite observations at The Ohio State University Radio Observatory were described which suggested that significant changes in the ionospheric electron density were produced by an artificial satellite<sup>1</sup> and indicated that such changes could be detected by means of a simple CW reflection technique.<sup>2,3</sup> Such a technique is valuable because it makes possible detection of satellites or other objects traversing the ionosphere, without requiring them to have radio transmitters.

It is the purpose of this article to present observational data which appear to be related to passages of Sputnik I and its associated fragments during their last days in orbit. The systematic nature and internal consistency of the data are considered justifications for further analysis involving the drag characteristics of the objects and their rate of fall. Although the results are provisional, they have value as an attempt to reconstruct the events related to the breakup of the first artificial satellite of the earth.

## II. THE SATELLITE IONIZATION PHENOMENON

During observations of radio transmissions from Sputnik I early in October, 1957 it was noted that during the satellite's approach the 20-mc signal was very rough and unsteady. However, some time before the satellite reached its closest point of approach, the signal suddenly became very smooth and steady and remained so during the rest of the pass. Oscillographs of the signal before and after the transition and related data have already been presented.<sup>1</sup>

This effect was observed on a number of passes with the transition from rough to smooth signal occurring when the angle between the satellite path and a line

from the satellite to Columbus, Ohio was about 60°. The effect was observed only on 20 mc and never on 40 mc. The fact that the phenomenon repeated itself from day to day indicated that it could not be due to the satellite transmitter or antenna. Although ionospheric reflections were considered as a cause, this mechanism seemed unlikely since the effect was observed only while the satellite was approaching and not at all while it was receding. The most plausible explanation was that the phenomenon was caused by an anomalous condition of the medium moving just *ahead* of the satellite.

At an altitude of 100 miles the mean free path of air molecules is of the order of 50 meters, and this path lengthens rapidly with further increase in height.<sup>4</sup> For example, at a height of 200 miles the mean free path is estimated to be as large as 100 kilometers. Under such conditions, when a fast moving object (such as an artificial satellite) encounters a gas particle, it may bounce the particle far ahead in the same manner that a golf ball is driven far ahead by a golf club. If the satellite is travelling with a velocity  $v$  and the particle is at rest, the impact can, for a perfectly elastic collision, impart a velocity of  $2v$  to the particle directly ahead of the satellite. If the satellite bounces all the particles it encounters directly ahead in this manner, a column of the same cross section as the satellite will be produced ahead of the satellite having twice the ambient density. If the average velocity after impact is less than  $2v$ , the increase in density would be more than doubled. In the  $F_2$  region, the residual nighttime ionization density may be sufficient (of the order of  $3 \times 10^6$  electrons per cc) so that a two-fold increase would be significant. However, this is an oversimplified picture. Actually, the particles may be scattered into a cone, instead of bunched in a column, and the particles, if not already ionized, may become so by impact. The satellite's velocity (5 miles per second) is sufficient to ionize air molecules (oxygen and nitrogen in either atomic or molecular form) by impact, although the probability of this mechanism producing ionization appears to be low.

The above discussion is intended to be merely suggestive of a possible ionization mechanism. What constitutes the actual ionization mechanism and whether the ionization is actually ahead of or behind the satellite, or both, are not clear. However, as indicated in Section VIII, some form of ionization phenomenon must be involved.

\* Original manuscript received by the IRE, April 24, 1958.

† Dept. of Elec. Eng., The Ohio State University, Columbus, Ohio.

<sup>1</sup> J. D. Kraus and J. S. Albus, "A note on some signal characteristics of Sputnik I," *Proc. IRE*, vol. 46, pp. 610-611; March, 1958.

<sup>2</sup> J. D. Kraus, "Detection of Sputnik I and II by CW reflection," *Proc. IRE*, vol. 46, pp. 611-612; March, 1958.

<sup>3</sup> J. D. Kraus, "The last days of Sputnik I," *Proc. IRE*, vol. 46, pp. 612-614; March, 1958.

<sup>4</sup> R. J. Havens, R. T. Koll, and H. E. LaGow, "The pressure, density and temperature of the earth's atmosphere to 160 km," *J. Geophys. Res.*, vol. 57, pp. 59-72; March, 1952.

### III. CW REFLECTION METHOD

To determine if this ionization could be detected by reflection, the method of Wylie and Castillo<sup>5</sup> was tried. In accordance with this method, the receiver was tuned to the 20-mc transmission of the National Bureau of Standards time service station WWV near Washington, D. C., a distance of about 330 miles from Columbus, Ohio. During the day ionospheric ionization is sufficient to reflect a strong signal from Washington to Columbus on this frequency, but during the winter night, in particular between local midnight and 7 A.M., the ionization decreases to the point where the signal is either undetectable or extremely weak. Under these conditions, any temporary localized increase in ionospheric ionization may result in a detectable burst in signal. Meteors produce brief signal bursts, the signal being reflected by the temporary ion trails. A meteor-induced signal burst is usually only a few seconds long and only rarely (once or twice per night) more than 10 or 15 seconds in duration. In our experiment at The Ohio State University Radio Observatory, more sustained signal bursts were also detected at times corresponding closely with the latitude crossing times for Sputniks I and II. These signal bursts often lasted for one or more minutes. Sample records of such signal bursts have already been presented in the illustrations of Kraus.<sup>2,3</sup>

The receiving antenna has a maximum response in a vertical east and west plane through Columbus along the 40th parallel of latitude, and the signal bursts produced by a satellite or orbiting object appear to occur, in general, within about two minutes of a latitude crossing of the object. This is convenient, since successive latitude passes of a satellite differ in time by its average period or an integral multiple thereof. Because of the broad east-west response of the antenna, a signal burst from a particular satellite object was obtained nearly every day and on some days two successive passes of the same object were recorded. The antenna consists of two horizontal half-wave dipoles separated on an east-west base line by 350 feet, as already described.<sup>1</sup> Each dipole is oriented north-south.

The basic observational data are presented in Fig. 1. Date is plotted as ordinate and time of day as abscissa. The small circles indicate the time of occurrence of large sustained signal bursts of WWV 20-mc signal on a given date. The area of the circle is approximately proportional to the area under the burst deflection, this area being a convenient criterion for the burst intensity. Only bursts of about 15 seconds duration or longer are shown on the chart. The circles indicate *every* large sustained signal burst satisfying this requirement which was observed during the time covered by the graph, that is, between 0220 and 0620 from December 30 to January

<sup>5</sup>L. R. Wylie and R. T. Castillo, "Clustering of meteors as detected by the use of radio technique," *Ohio J. Science*, vol. 56, pp. 339-347; November, 1956.

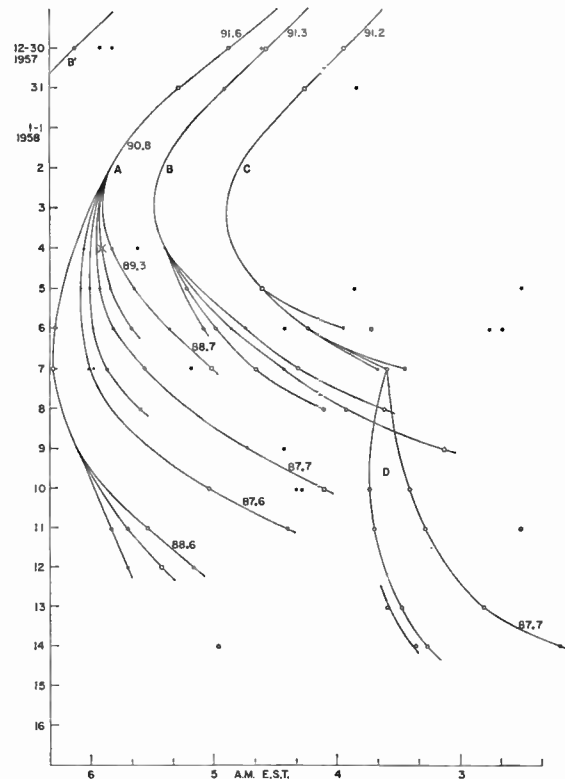


Fig. 1—Observed bursts of WWV signal as a function of date (vertical axis) and time of day (horizontal axis).

16, inclusive. Examples of actual records covering portions of the chart have already been presented.<sup>2</sup>

If all the circles in Fig. 1 were produced by a random phenomenon, such as natural meteors, there would be little tendency toward systematic trends in their positions. However, if the signal bursts were due to orbiting objects, the circles should show a systematic trend. It is significant that most of the bursts in Fig. 1 show a definite systematic trend.

Referring to December 30 on curve A in Fig. 1, there was a large signal burst at 0452. On December 31 a large signal burst occurred 24 minutes later, or at 0516. The total elapsed time between the two signal bursts was 1464 minutes, or the number of minutes in one solar day (1440) plus 24 minutes. If both bursts were made by the same orbiting object, it must have made an integral number of revolutions (in this case 16) during the 1464-minute interval. Hence, its average period, or time for one revolution, was 91.5 minutes (1464/16). Extending the curve to circles corresponding to passages on following days, it is possible to keep track of the progress of an orbiting object in the absence of any other information.

Of course, to identify the curve with any particular earth satellite, such as Sputnik I, it is necessary at some point of the study to know the approximate period and orbital position of the satellite. On dates in December, earlier than those shown in Fig. 1, curve A was tentatively identified with the spherical part of

Sputnik I with whip antennas (designated 1957 $\alpha$ 2 by the Smithsonian Astrophysical Observatory).

As a satellite falls closer to the earth, its period decreases. This decrease in period appears on the chart of Fig. 1 as a change in the slope of the curve. For example, a positive slope corresponds to a period of more than 90 minutes, a negative slope to a period of less than 90 minutes, and a vertical slope to a period of exactly 90 minutes. (Note that  $16 \times 90 = 1440$  minutes.) The 3-digit figures adjacent to the curves in Fig. 1 indicate the period in minutes at that point of the curve. The absence of data for the first three days of January resulted from an interruption in the observations.<sup>3</sup>

By extending curve A from day to day the progress of the satellite was followed in this manner. Connecting the other signal burst circles on the chart yields two other curves, B and C, which follow a trend very similar to that of curve A, suggesting that they also correspond to parts of Sputnik I. For example, object B may have been the nose cone or part of it.

Although only one signal burst had been anticipated for curve A on January 4, three large bursts were noted. (Actually, more were noted but to simplify the following discussion attention will be confined to the three largest ones. In Fig. 1, the three signal bursts correspond to the circles joined by the three earliest or right-hand curves of the A group.) On January 5 and 6 the three signal bursts again appeared, but showed a significant tendency to spread out in time. The early burst moved farther ahead while the late burst dropped farther behind. This is precisely what would be expected to happen to three satellite bodies of slightly different density and drag, the one with most drag getting farther ahead each day and the one with least drag lagging farther behind. Thus, on January 6, the first and third objects were 27 minutes apart, or separated by about 8000 miles along the satellite's orbit. On January 7 the middle (second) object disappeared, and on January 8 the first object was gone. Although the third object was not noted on January 8, it was observed on January 9 and 10.

It would appear that the A object broke into no less than six distinct pieces, each of which could be detected as an orbiting object for several days. The progress of the slowest moving object of the entire A group is shown by the curve farthest to the left in Fig. 1. Since it was in the highest orbit (longest period), it should have stayed up longest, and this is what was observed to happen. On January 9 or 10 it broke into three smaller fragments which were last observed orbiting on January 12, one day after the next slowest object of the entire A group was last observed. Extrapolating the six group A curves back to dates prior to January 4, it appears that the original A object began to break into pieces between January 1 and 3.

Curves B and C follow a similar trend in slope, but show a generally more rapid decrease in period as would be expected for objects running farther ahead (and

lower) in their orbits. Between January 3 and 5 curve B branches into four curves, suggesting a breaking up of the B object between those dates into at least four distinct fragments. The fact that the B fragments show less spread in period than the A fragments would indicate that the B object fragments formed a more homogeneous group.

Referring to curve C, this object appears to have divided on about January 6 into three parts which were last observed on January 7. For a number of days thereafter it was thought that these objects had disappeared entirely, since no bursts were noted which would form a continuation of curve C. However, from January 10–14, at least eight bursts were observed, including one at 0213 (a few minutes ahead of the chart limit) which can be connected in a systematic manner by the curves D. If these curves are significant, they are evidence of an explosion of the C object on or about January 7 into a number of fragments, two of which were raised into a higher orbit where they continued to orbit around the earth until about January 14. The fact that the bursts for the D objects were not observed every day suggests that they were small in size and were observed only on passes with the most favorable signal path geometry. It is also significant that if either object was observed on a given date both were observed. The only other explanation of the D curves is that they are distinctly different objects, not related to the C group, which were noted for the first time on January 10. However, if this were the case, it is difficult to explain why the objects were not observed on earlier dates, the area on the chart where they should have appeared being nearly devoid of signal bursts.

Since all the objects in Fig. 1 had periods between about 87.3 and 91.6 minutes, the question may arise as to why only a single pass of these objects was observed on dates following January 4, whereas two successive passes of the A and B objects had been noted in December (curve B' in Fig. 1). One explanation is that in December the average height of the objects was sufficient to enable their latitude crossings to be observed farther to the east and west of Columbus than was the case later in January, when the heights were appreciably less and decreasing rapidly. The objects were presumably near their average height when passing near Ohio during this period (travelling NNW to SSE) rather than near the perigee or apogee values. That single passes were observed in January is evident from the observations which show that on any given date no burst pairs, with only one or two exceptions, were separated by the proper period. In addition, since signal bursts from the curve C object were not confused with those from the A object, the 40th parallel crossing of the C object orbit must have been some distance west of that for the A object orbit.

#### IV. STATISTICAL CONSIDERATIONS

Referring to the hypothetical date-time diagram shown in Fig. 2, there are four dates with the time scale

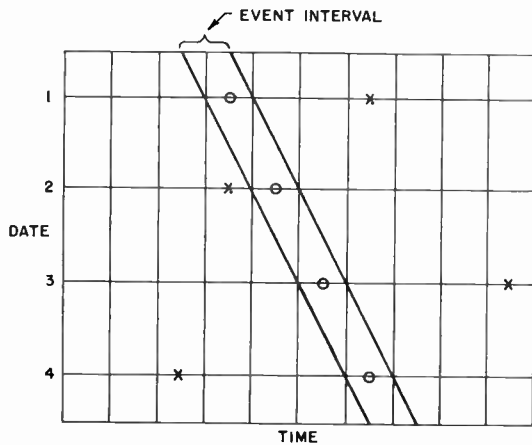


Fig. 2—Date-time diagram for discussion of probability of occurrence of systematically related events.

divided into ten equal intervals. The probability that a single random event will occur in any particular time interval is one in ten. The probability of two events, one on each date, occurring in specified time intervals is one in one hundred. Hence, the probability that the events indicated by the four circles would appear in the designated event interval on four days is only one in ten thousand. Stated in another way, a typical random distribution of four events (one per day) might be as suggested by the crosses in Fig. 2, while the distribution given by the circles would occur on a purely chance or random basis only once in ten thousand four-day intervals. An orbiting object, whose period is decreasing a certain fraction of a minute per day, must follow a definite trend like the event interval in Fig. 2, and any deviations of the observed times of passage amounting to more than a few minutes will obviously not fit such a systematic trend. Applying this type of analysis to the circles of Fig. 1, it follows that the probability of the observed systematic pattern resulting from a random phenomenon is extremely small.

Another important consideration is the self-consistency of the data. This is even more evident from the discussion in later sections of the heights of the objects as a function of time. All of the objects have a generally downward trend in height, with the only abrupt changes in slope occurring at the time of breakups as would be expected. Furthermore, the height data of December 30 and after are entirely consistent with those obtained from other sources for earlier dates (see Fig. 5). Lastly, the fragments were observed only down to heights at which complete disintegration would be expected to occur and no lower.

Another aspect of the data of Fig. 1 concerns the number of bursts observed per night (four-hour period from 0220 to 0620) as a function of date. These data are presented in Fig. 3. Prior to January 5, the number ranged between four and nine bursts, but on January 6 the number reached a peak of 15 bursts during the four-hour period. January 6 was after the breakup of both

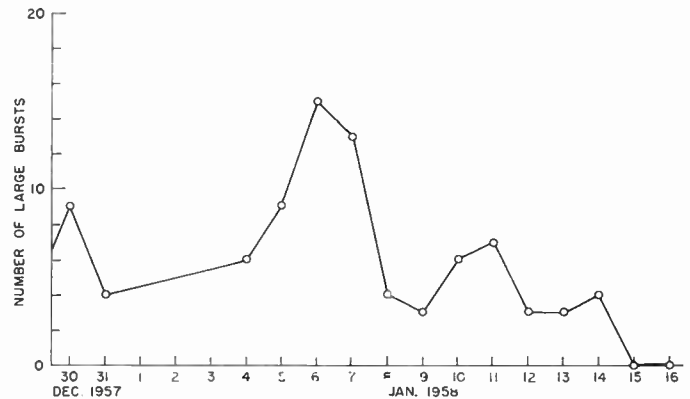


Fig. 3—Graph of number of signal bursts observed as a function of date.

the A and B objects. After January 6 the number decreased as the objects tended to disappear. However, a small secondary peak appeared on January 10 and 11 following the detection of the D objects and the fragmentation of the slowest A object. After this the number again decreased until January 15 and 16, when no signal bursts whatever were detected during the four-hour period. On January 17–19, an average of only one signal burst per night was observed.

Altogether there are 85 signal bursts on Fig. 1, of which at least 66 follow a systematic pattern. The remainder may be meteor-induced signal bursts of unusually long duration. Over the entire period, December 30 to January 16, they averaged only 1.3 per night. During the remainder of January, the number of large sustained bursts was found to average about 1.5 per night (four-hour period from 0220 to 0620). These bursts appeared to have a random time distribution and, hence, probably were of meteoric origin. Accordingly, the background level of large sustained meteor-induced bursts would appear to average about 1.4 per night, thus suggesting that the large increases in bursts observed over many days in late December and early January were not due to meteors, but to artificial satellites as already considered.

Although the general trends in Fig. 1 may be significant, too much importance should not be attached to an individual branch curve with only one or two signal bursts. Actually, several branch curves in addition to those shown could have been added to single bursts which were treated as random in the above discussion.

## V. AVERAGE HEIGHT CALCULATIONS

The data of Fig. 1 become even more significant if converted into a height-time diagram. The slope of any curve in Fig. 1 is a measure of the period of the orbiting object at that time. When the period is known, the height of the object can be calculated from Kepler's third law.<sup>6</sup> Thus, for a circular orbit, the square of the period  $T$  of a small object orbiting around the earth is

<sup>6</sup> C. A. Young, "General Astronomy," Ginn and Co., Boston, Mass., pp. 252–255; 1895.

given by

$$T^2 = \frac{4\pi^2}{g} \frac{5280}{3600} \frac{(r+h)^3}{r^2} \quad (1)$$

where

$T$  = period (min)

$g$  = acceleration of gravity at surface of earth (32.1 ft second<sup>-2</sup>)

$r$  = average earth radius (=3959 statute miles)<sup>7</sup>

$h$  = average height of object (statute miles).

Evaluating (1) for various values of  $T$  (or  $h$ ) a large scale period-height chart was prepared. Then, from the period of a given object as determined from Fig. 1, its average height could be obtained. Actually, the average period for a given object over a one-day interval was used in this conversion, and was found by dividing the total elapsed time between bursts on succeeding days by 16.

The actual orbit of a satellite is elliptical with a point of near approach (perigee) and a most distant point (apogee) which may differ considerably from the average height. However, average height (equal to half the sum of the perigee and apogee heights) is a significant quantity which makes it possible to discuss the trends in height as a function of time in a simple manner. The height values calculated are good approximations of the average height and are sufficient for this discussion of the height vs time behavior of satellites and their associated fragments.

## VI. HEIGHT DATA

The height data, obtained as described above, are presented in Fig. 4. The average height (in miles or kilometers) is given as a function of date for the A, B, and C objects and their fragments. The A group is shown by the solid lines, the B group by the dashed lines, and the C (and also D) group by the dotted lines. Each group exhibits a slightly different behavior which presumably reflects a difference in its drag characteristics. The original object of the A group has the greatest initial height, and after breakup the fragments have the largest dispersion in heights. This group presumably corresponds to the 23-inch diameter, 184-pound spherical antenna-equipped satellite, with the large height dispersion after breakup being due to the wide range of composition of its constituent parts. The original object of the B group has a somewhat lower initial height, and after breakup its fragments show not only less spread in height, but a tendency to fall more rapidly than the A objects. This suggests among other things that the B fragments were of a more homogeneous nature than those of the A group. The original C object had the lowest initial height, and after breakup its fragments

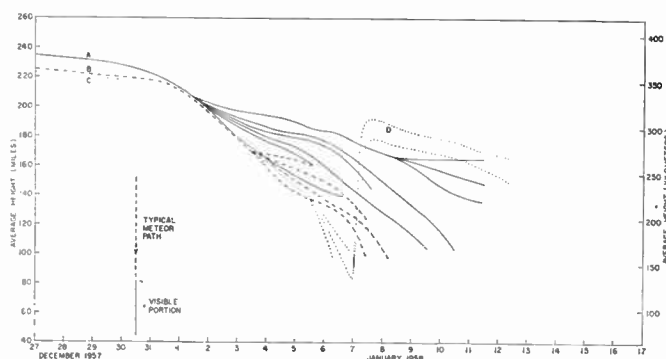


Fig. 4—Average height of Sputnik I objects as function of time as deduced from the signal-burst observations.

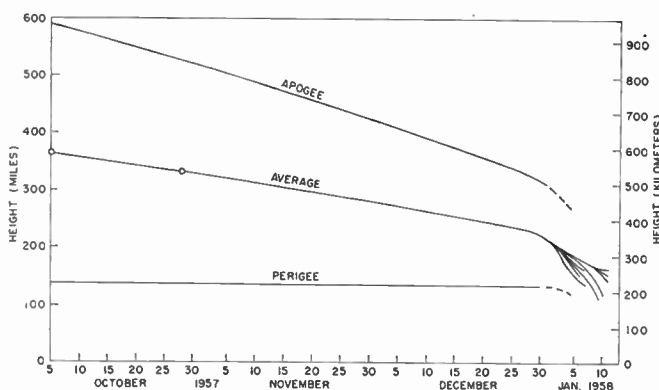


Fig. 5—Average height of Sputnik I during its time in orbit with approximate apogee and perigee heights.

(except for those of the D group) tended to come down much more rapidly. The initial breakup of the A object occurred between January 1 and 3, of the B object between January 3 and 5, and of the C object between January 5 and 6. The D group appears to have consisted of two quite similar objects which were raised into a higher orbit about January 7 by an explosion of one of the C objects. The two D objects are the last orbiting objects observed which appear to have been associated with Sputnik I.

The height variation of object A (presumably the spherical part of Sputnik I) over its entire time in orbit is presented in Fig. 5. The data for A from Fig. 4 appear in Fig. 5 for the dates following December 30 as the average height curve (with branches). The period at the time of launching was 96.2 minutes, giving an initial average height of 365 miles (note circle at left edge of chart). The height circle for October 28 is based on orbital periods given by the Royal Aircraft Establishment, Farnborough.<sup>8</sup> The fact that the height data for December 30 and thereafter, and those for launching and October 28 all join on a smooth curve supports the other evidence that object A corresponds to the spheri-

<sup>7</sup> The statute mile (5280 feet) is meant wherever the unit mile is mentioned in this article.

<sup>8</sup> Staff of the Royal Aircraft Establishment, Farnborough, Eng., "Observations of the orbit of the first Russian earth satellite," *Nature*, vol. 180, pp. 937-941; November 9, 1957.

cal antenna-equipped part of Sputnik I. Curves for apogee and perigee heights are also presented in Fig. 5, but these are intended more to suggest trends than to give precise values. They are based mainly on the values announced soon after the satellite was launched.

### VII. DRAG AND HEATING EFFECTS

One of the most interesting aspects of the data presented concerns its interpretation in terms of the drag of the objects and the mechanism of the actual breakup process. This has great significance in connection with the problem of the reentry of an orbiting object into the denser regions of the earth's atmosphere.<sup>9-13</sup>

An artificial satellite will, in general, have an elliptical orbit. At apogee the satellite may be well outside the denser parts of the earth's atmosphere, but at perigee it may dip close enough to the earth to encounter considerable resistance from the earth's atmosphere. Energy lost by drag at perigee will not affect the perigee height but will result in a decrease in the apogee height. Conversely, drag encountered at apogee will result in a reduced perigee height. Since initially the drag occurs principally at perigee, the effect is to reduce the eccentricity of the orbit by a reduction in the apogee height. This situation is illustrated by the idealized orbits in Fig. 6 with three satellite orbits shown of different apogee but constant perigee height. For convenience, the denser part of the earth's atmosphere is shown with a definite upper edge instead of the actual diffuse limit. The height of the atmosphere and of the orbits is exaggerated for the sake of clarity.

Meteors enter the earth's atmosphere at very high velocities (7 to 45 miles per second) heating up to incandescence by the time they reach heights of 45 to 80 miles above the earth's surface.<sup>14</sup> However, the process is usually of very short duration, lasting only for a few seconds. This is because most meteors enter the atmosphere at angles steeper than tangency. A typical meteor path is shown in Figs. 6 and 4. Because of the long time scale of Fig. 4 a meteor, even of many seconds duration, will appear as a vertical line.

In contrast the satellite objects enter the earth's atmosphere nearly tangent to its surface, but remain in it for relatively long periods (hundreds or thousands of seconds). The resulting heating at each perigee passage

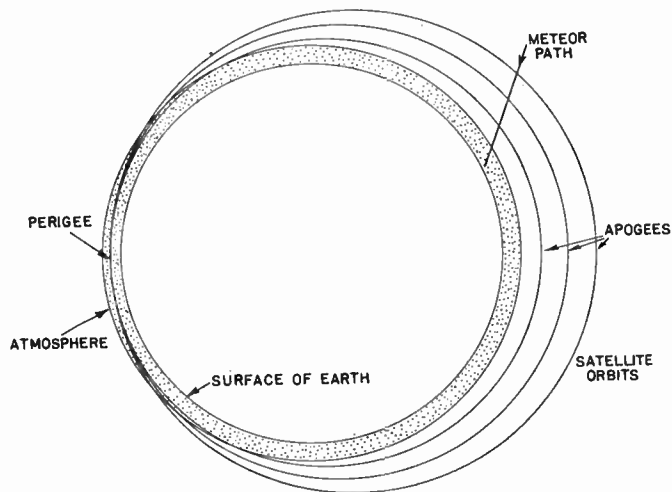


Fig. 6—Diagram illustrating decrease of apogee height of satellite orbit with substantially constant perigee height.

may, accordingly, produce significant effects at perigee heights well above that at which the meteors reach incandescence in their brief flight through the atmosphere. In fact, satellite objects with eccentric orbits are subjected to a cyclical heating process which may cause metal fatigue and cracking long before melting temperatures are reached.

If the satellite were a solid homogeneous metal sphere, the heating might produce little destructive effect until carried to extremes. However, consider for the purpose of discussion two solid homogeneous metal spheres connected by a thin member, as in Fig. 7. As this object moves broadside through the atmosphere, its surface will be heated. Since, however, the thermal capacity of the thin member is less than that of the solid spheres, its temperature will rise faster than the temperature of the spheres. Conversely, in a cooling portion of the temperature cycle (after leaving perigee), the temperature of the thin member will fall faster than the temperature of the spheres. Hence the temperature fluctuations will be greater for the thin member. As the orbit descends, the heating will increase and the thin member will reach destructive temperatures first and the object will separate into two portions. Since the Sputnik I sphere was a complex object fabricated from many parts of different density, it is reasonable to suppose that (with the metal skin removed) the framework holding the heavy and denser components together may have separated at its thinnest and weakest points by a similar process resulting in a breakup into many pieces. The pieces with large drag would fall rapidly, but the more massive objects of lower drag might continue in orbit for somewhat longer.

Specifically, *drag* is a force opposite to the direction of motion of the object.<sup>15</sup> It is proportional to the cross

<sup>9</sup> J. P. Hagen, "The exploration of outer space with an earth satellite," *Proc. IRE*, vol. 44, pp. 744-747; June, 1956.

<sup>10</sup> J. T. Mengel, "Tracking the earth satellite, and data transmission, by radio," *Proc. IRE*, vol. 44, pp. 755-760; June, 1956.

<sup>11</sup> F. L. Whipple and J. A. Hynek, "A research program based on the optical tracking of artificial earth satellites," *Proc. IRE*, vol. 44, pp. 760-764; June, 1956.

<sup>12</sup> J. A. Van Allen, "The scientific value of the earth satellite program," *Proc. IRE*, vol. 44, pp. 764-767; June, 1956.

<sup>13</sup> T. E. Sterne, B. M. Folkart, and G. F. Schilling, "An Interim Model Atmosphere Fitted to Preliminary Densities Inferred from U.S.S.R. Satellites," Smithsonian Institution Astrophysical Observatory, Cambridge, Mass., Special Rep. No. 7; December 31, 1957.

<sup>14</sup> B. Lovell and J. A. Clegg, "Radio Astronomy," John Wiley and Sons, Inc., New York, N. Y., p. 76; 1952.

<sup>15</sup> L. M. Milne-Thomson, "Theoretical Aerodynamics," MacMillan and Co., Ltd., London, Eng., p. 3; 1948.

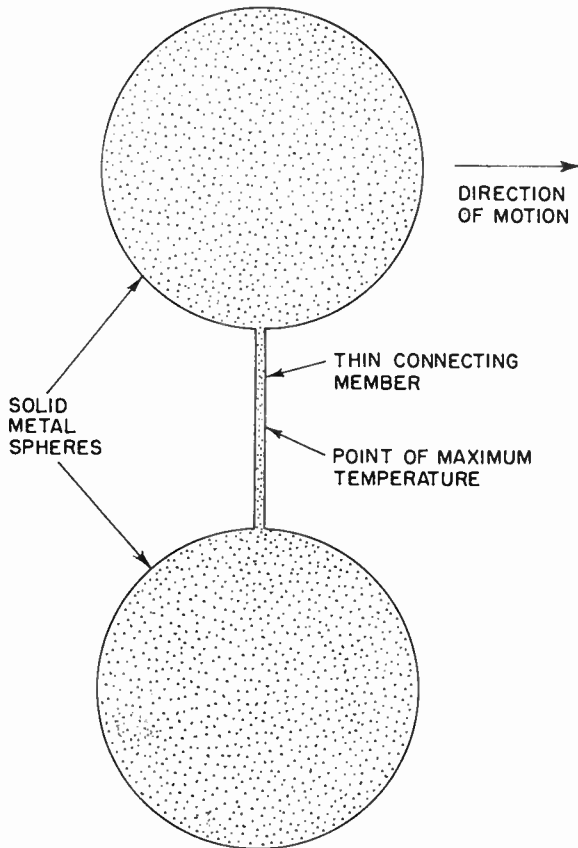


Fig. 7—Thin member connecting two solid spheres will melt first as assembly is heated by motion through the air.

sectional area of the object normal to its direction of motion. It follows that the drag force per unit mass is equal to the negative acceleration or deceleration of the object, and further, that the energy lost by a satellite object due to drag per orbital period is given by

$$W = \oint D dl \quad (2)$$

where

$W$  = energy lost in one period (joules)

$D$  = drag (newtons)

$dl$  = elemental length along orbit ( $m$ ).

The integration is carried out once around the orbit.

Of particular interest in interpreting Fig. 4, it may be shown that at a given average height, the rate of change of average height of an orbiting object is proportional to its average drag per unit mass. Hence, at a given height the objects with steeper slope have higher drag per unit mass than those with smaller (or flatter) slope. Actually, over the range of heights involved, the slope at any height is a good approximation to the drag per unit mass. Several special cases may be considered.

1) A hollow shell containing an assembly of massive or high density parts would, in general, have higher

drag per unit mass than the individual high density components after separation. Since most of the A group fragments had less drag per unit mass than the original A object, it is likely that these fragments were some of the higher density components (such as batteries). It is significant that the object with the least drag per unit mass or its three fragments remained in orbit longest (until January 12). (Although the uppermost curve for the three fragments may appear to have a positive slope, it is actually negative.)

2) The fragments of a homogeneous object will, in general, have higher drag per unit mass than the original object. This would appear to be the case for the C group after breakup about January 6.

3) The fragments of a nonhomogeneous object will, in general, have both higher and lower drag per unit mass than for the original object. Although both the A and B objects were presumably nonhomogeneous, only one fragment of each showed more drag per unit mass than the original object, the remaining fragments having less. This may be explained by the fact that an object with high drag per unit mass falls faster, and unless it remained in orbit for at least one day after the breakup it would not be detectable at all by the method used.

It should be mentioned that although the general trends in Figs. 1 and 4 are significant, too much importance should not be attached to objects for which burst data were observed on only one or two days. To insure a high probability that the bursts corresponded to an orbiting object, it is desirable to have burst data for at least three days.

No direct evidence is available of the ultimate fate of the satellite fragments, but it is likely that as a result of the gradual disintegration process, some very small or dust size particles may have been produced which remained up for some time after all the larger fragments had fallen. It is possible that this residual dust was distributed completely around the orbit in a manner analogous to the distribution of debris in a comet's orbit, forming the material of a meteor stream.

Although no reports were received which gave conclusive evidence of visual sightings of any Sputnik I fragments falling to the ground, a number of observers in the vicinity of Columbus, Ohio did report a bright self-luminous orange-red object moving in horizontal flight from NW to SE across the sky to the NE of Columbus about two hours before sunrise on the morning of January 4. As already reported,<sup>3</sup> this object was on the Sputnik I course and was observed at 0555, or at the same time as the January 4 signal burst marked with an X in Fig. 1. The object was observed for at least 15 seconds and was described by various observers as trailing a thin short streak a few degrees long as though shedding incandescent particles. Its color was described as bright yellow or orange-red when first seen to the north and changing to a dark red as it disappeared to

the east. It is possible that this object was a Sputnik I group A object and, when seen, sharp edges were burning off or connecting members burning apart with visible effect during the object's dip into the lower atmosphere. However, the main body of the object may have continued to orbit for some time longer.

### VIII. ECHO AREA

In connection with the CW reflection method it is of interest to calculate the order of magnitude of extent of the ionospheric reflecting surface required to give the strengths of WVV signal bursts observed at Columbus, Ohio. This may be done by assuming that the path consists of two parts, one from the transmitter near Washington, D. C. to the point of reflection in the ionosphere, and the other from this reflection point to Columbus, Ohio. It will be assumed that at the reflection point the signal from Washington is gathered over an effective aperture  $A_e$  and then retransmitted without loss or gain to Columbus through an aperture of the same effective size. Applying the Friis transmission formula<sup>16</sup> twice to this two-link circuit yields the following value for the square of the effective aperture of the ionospheric reflecting region:

$$A_e^2 = r^4 \lambda^4 \frac{W_r}{W_t A_{et} A_{er}} \quad (3)$$

<sup>16</sup> J. D. Kraus, "Antennas," McGraw-Hill Book Co., Inc., New York, N. Y., p. 54; 1950.

where

- $A_e$  = effective aperture of ionospheric reflection region (m<sup>2</sup>)
- $r$  = distance from point of reflection to Washington or Columbus (m)
- $\lambda$  = wavelength (m)
- $W_t$  = transmitter radiated power (watts)
- $W_r$  = received power (watts)
- $A_{et}$  = effective aperture of transmitting antenna (m<sup>2</sup>)
- $A_{er}$  = effective aperture of receiving antenna (m<sup>2</sup>).

For the case under consideration,  $r = 365$  kilometers,  $\lambda = 15$  meters,  $W_t = 10^3$  watts,  $W_r = 2.5 \times 10^{-15}$  watts (corresponding to 0.1 microvolt per meter at the antenna),  $A_{et} = 0.25\lambda^2$  (m<sup>2</sup>), and  $A_{er} = 0.5\lambda^2$  (m<sup>2</sup>). Introducing these values into (3) gives an effective aperture  $A_e$  of the ionospheric reflecting region of about 600 square meters. This area is nearly a minimum value, and for less favorable path geometry or other factors the aperture would be larger, suggesting that some ionization phenomenon must be involved.

### ACKNOWLEDGMENT

We are indebted to George Veis of the Institute of Geodesy for helpful comments and to James S. Albus of the Department of Electrical Engineering for assistance on some of the observations during the latter part of January.

## CORRECTION

Stig Ekelöf has sent in the following correction to a paper by Frank E. Jaumot, "Thermoelectric Effects," which appeared on pages 538-544 of the March, 1958 issue of PROCEEDINGS. The Ph.D. Dissertation by D. Enskog, referred to in footnote 18, was published at Uppsala University, Sweden, not at Uppsala College, East Orange, N. J.

# Noise in Maser Amplifiers—Theory and Experiment\*

J. P. GORDON† AND L. D. WHITE‡, MEMBER, IRE

**Summary**—This paper contains a theoretical treatment of noise in maser amplifiers and the results of experimental measurements of the noise of an ammonia beam maser. The concept of “effective input noise temperature” is defined and used. The theoretical treatment obtains an equivalent microwave circuit and derives expressions for the gain and effective input noise temperature of both reflection and transmission-type masers. The experimental measurements yielded values of about 80°K for the effective input noise temperature of a reflection-type ammonia beam maser. The experimental values agree with those predicted by theory and the comparison of experiment and theory gives an upper limit of about 20°K for the magnitude of the “beam temperature.”

## INTRODUCTION

IT has been realized for some time that maser amplifiers should be capable of very low noise operation.<sup>1</sup> Recently, several papers have given theoretical calculations<sup>2-6</sup> of the noise generated by “negative temperature” media, and predictions<sup>2-7</sup> of the noise figures of maser amplifiers. Also quite recently, experimental measurements of the noise figures of ammonia maser amplifiers<sup>8-10</sup> and of a solid-state maser amplifier<sup>11</sup> have been made. This paper reviews the theory of maser amplifiers, using an equivalent microwave circuit. This theory applies to two-level masers and also to three-level types in which noise introduced by the pumping source can be ignored. The term “effective input noise temperature”<sup>12</sup> is defined. This term is

quite useful in describing very low noise amplifiers and gives a more immediate idea of the quality of the amplifier than does the usual description in terms of noise figure. Experimental values for the effective input noise temperature of an ammonia maser are given and are compared with those obtained from theory. From this comparison an upper limit for the beam temperature is obtained.

## EFFECTIVE INPUT NOISE TEMPERATURE

The “effective input noise temperature,”<sup>12</sup>  $T_n(f)$ , is defined here as the temperature of the input termination which results at frequency  $f$  in output noise power per unit bandwidth double that which would occur if the same input termination were at absolute zero. The effective noise temperature is related to the noise figure  $F(f)$  of the amplifier with the same input by  $T_n(f) = [F(f) - 1] 290^\circ\text{K}$ . The average effective input noise temperature  $\bar{T}_n$  is defined as the temperature of the input termination which results in a total noise power output double that which would exist if the same input termination were at absolute zero. The average effective input noise temperature is related to the spot effective input noise temperature by

$$\bar{T}_n = \frac{\int T_n(f)G(f)df}{\int G(f)df}$$

where  $G(f)$  is the power gain of the amplifier. Also,  $\bar{T}_n = [\bar{F} - 1] 290^\circ\text{K}$ , where  $\bar{F}$  is the average noise figure. This concept of effective input noise temperature becomes particularly valuable in applications in which both the effective input noise temperature of the amplifier and the noise temperature of the input load (e.g., an antenna looking at the sky) are less than room temperature.

For convenience, it is assumed in the following that the input termination is matched to the input waveguide.

## THEORY OF NOISE IN A CAVITY MASER AMPLIFIER

In this section the noise output of a cavity maser amplifier is considered in detail, using the approach of the microwave circuit. The sources of noise include the

ized previously. In the analysis of noise in conventional amplifiers,  $(F-1)$  has played an important part and has been designated the excess noise figure, and  $(F-1) \cdot 290^\circ\text{K}$  has been termed the excess noise (temperature). (For example, see D. T. McCoy, “Present and future capabilities of microwave crystal receivers,” *Proc. IRE* vol. 46, pp. 61-66; January, 1958.) Also, in dealing with maser noise this concept has been used, being called “noise temperature” by others<sup>2,11</sup> and “effective noise temperature” by the authors.<sup>10</sup>

\* Original manuscript received by the IRE, April 3, 1958; revised manuscript received, May 27, 1958.

† Bell Telephone Labs., Inc., Murray Hill, N. J.

<sup>1</sup> J. P. Gordon, H. J. Zeiger, and C. H. Townes, “Molecular microwave oscillator and new hyperfine structure in the microwave spectrum of  $\text{NH}_3$ ,” *Phys. Rev.* vol. 95, pp. 282-284; July 1, 1954.

—, “The maser—new type of microwave amplifier, frequency standard, and spectrometer,” *Phys. Rev.*, vol. 99, pp. 1264-1274; August 15, 1955.

<sup>2</sup> K. Shimoda, H. Takahasi, and C. H. Townes, “Fluctuations in amplification of quanta with application of maser amplifiers,” *J. Phys. Soc., Japan*, vol. 12, pp. 686-700; June, 1957.

<sup>3</sup> J. P. Wittke, “Molecular amplification and generation of microwaves,” *Proc. IRE*, vol. 45, pp. 291-316; March, 1957.

<sup>4</sup> R. V. Pound, “Spontaneous emission and the noise figure of maser amplifiers,” *Ann. Phys.*, vol. 1, pp. 24-32; April, 1957.

<sup>5</sup> M. W. Muller, “Noise in a molecular amplifier,” *Phys. Rev.*, vol. 106, pp. 8-12; April 1, 1957.

<sup>6</sup> M. W. P. Strandberg, “Inherent noise of quantum-mechanical amplifiers,” *Phys. Rev.*, vol. 106, pp. 617-620; May 15, 1957.

<sup>7</sup> J. C. Helmer and M. W. Muller, to be published.

<sup>8</sup> J. C. Helmer, “Maser noise measurement,” *Phys. Rev.*, vol. 107, p. 902; August 1, 1957.

<sup>9</sup> L. E. Alsop, J. A. Giordmaine, C. H. Townes, and T. C. Wang, “Measurement of noise in a maser amplifier,” *Phys. Rev.*, vol. 107, pp. 1450-1451; September 1, 1957.

<sup>10</sup> J. P. Gordon and L. D. White, “Experimental determination of the noise figure of an ammonia maser,” *Phys. Rev.*, vol. 107, pp. 1728-1729; September 15, 1957.

<sup>11</sup> A. L. McWhorter, J. W. Meyer, and P. D. Strum, “Noise temperature measurement on a solid state maser,” *Phys. Rev.*, vol. 108, pp. 1642-1644; December 15, 1957.

<sup>12</sup> The wording “effective input noise temperature” was chosen after consultation with H. A. Haus. Recently, Subcommittee 7.9 of the IRE approved for the same term a definition similar to that used here. The concept underlying these definitions has been util-

amplifying medium and a number of sources of thermal noise; the cavity walls, the input circuit, the output circuit in the two-port case, and losses in the cavity caused by the presence of the amplifying medium, e.g., dielectric losses in the case of a solid sample or, as was pointed out by Muller and Helmer,<sup>8</sup> absorption due to background ammonia gas in the case of the ammonia beam maser. Noise due to statistical fluctuations in the number of amplifying particles is usually negligible. For example, in the ammonia beam maser, fluctuations amount to about one part in 10<sup>5</sup> (there are about 10<sup>10</sup> molecules in the cavity at any time), and this would be expected to cause gain fluctuations less than 0.1 per cent in a maser amplifier operating at about 20-db gain. Both transmission and reflection-type operation are treated theoretically, although experimental results are given only for the reflection type. It is shown that in most cases the reflection type is better in noise figure as well as in gain-bandwidth product. Finally, the possibility of a traveling-wave maser is mentioned. It is superior to either type of cavity maser if the necessary gain can be obtained.

Consider first the general maser amplifier (Fig. 1) utilizing a resonant cavity. The cavity is coupled by two waveguides, labeled 1 and 2 for input and output respectively, and contains the "negative temperature" amplifying medium. Let there be a circulator on the cavity input so that the power returning from the cavity in waveguide 1 is separated from the input signal power. Furthermore, let there be an isolator in the output waveguide so that a constant matched load is presented to the cavity. Each of the circuit elements has some definite temperature and, if lossy, is a generator of thermal noise. Let  $Q_1$  and  $Q_2$  be equal to the ratio of the energy stored in the cavity to the energy per radian which emerges from the cavity into the input and output waveguides, respectively.

Consider now an equivalent circuit for the maser. At the outset no circuit losses except that of the cavity, represented by  $Q_c$ , and the backward loss of the isolator are included. The losses of the circulator and other input circuitry are taken into account later. First, replace the lossy cavity by a lossless one of the same resonant frequency to which a matched waveguide is appended through a suitable coupling (Fig. 2). The temperature of the load in this waveguide is equal to the temperature of the cavity. As for the amplifying medium, it can be shown directly from Maxwell's equations that the effect of its complex susceptibility,<sup>18</sup>  $\chi = \chi' - i\chi''$ , is to

<sup>18</sup> The electric susceptibility,  $\chi(f)$ , at frequency  $f$  is defined by  $P(f) \cdot \exp i2\pi ft = \chi(f) \cdot \epsilon_0 \cdot E(f) \cdot \exp i2\pi ft$ , where  $P(f)$  is the polarization produced by the electric field  $E(f)$ .  $\chi'$  and  $\chi''$  are related to each other through the Kronig-Kramers relations. See J. H. Van Vleck, "Propagation of Short Radio Waves," M.I.T. Rad. Lab. Ser., McGraw-Hill Book Co., Inc., New York, N. Y., vol. 13, D. E. Kerr, ed., p. 642; 1951.

H. Fröhlich, "Theory of Dielectrics," Clarendon Press, Oxford, Eng.; ch. 1, sec. 2; 1949.

A. M. Portis, "Electronic structure of F centers: saturation of the spin resonance," *Phys. Rev.*, vol. 91, pp. 1071-1078; September 1, 1953.

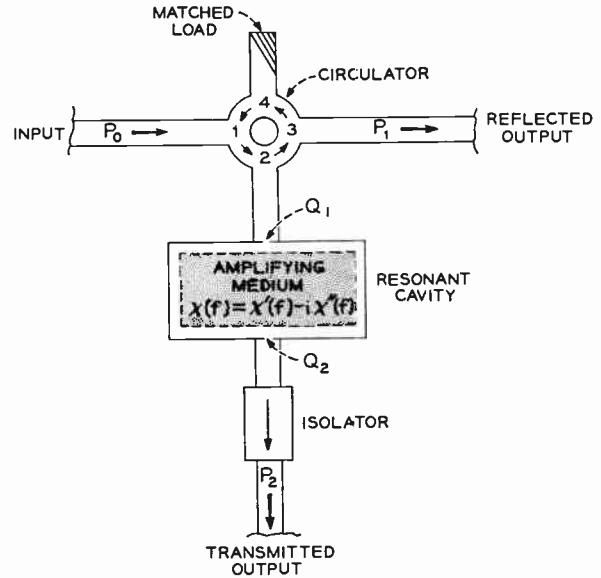


Fig. 1—Schematic diagram of a maser amplifier using a resonant cavity. Both transmitted and reflected power are indicated.

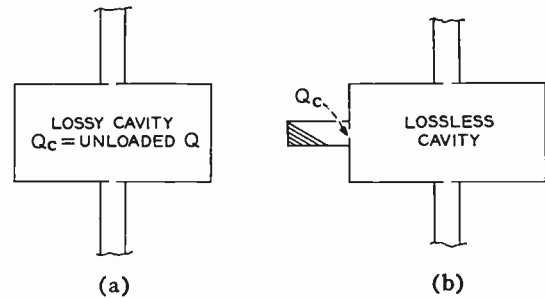


Fig. 2—(a) A lossy cavity. (b) Equivalent circuit for lossy cavity.

change the apparent  $Q$  and resonant frequency of the cavity. The impedance of the cavity plus medium measured at frequency  $f$  is equal to that of a cavity whose resonant frequency differs from that of the actual cavity by the fractional amount  $\Delta f/f_c = \frac{1}{2}\eta \chi'(f)$ , and whose losses differ by an amount  $\Delta(1/Q) = \eta \chi''(f)$ .  $f_c$  is the resonant frequency of the loaded cavity without medium;  $\eta$  is the filling factor<sup>14</sup> and is unity when the medium completely fills the cavity.

According to the results of Slater's<sup>15</sup> analysis, an equivalent microwave circuit may be obtained through replacement of the amplifying medium by another waveguide, whose coupling to the cavity is proportional to the sample susceptibility. This waveguide is terminated at the "plane of the detuned short" by an admittance  $Y$  whose frequency dependence is that of the sample resonance. Let  $\chi_m$  be the maximum absolute value of the imaginary part of the sample susceptibility, and let  $g(f)$  and  $b(f)$  be line shape factors such that  $\chi' = \chi_m b(f)$  and  $\chi'' = \chi_m g(f)$ . The equivalent circuit

$$= \int_{\text{sample}} E^2 d(\text{vol}) / \int_{\text{cavity}} E^2 d(\text{vol})$$

for the case of an electric dipole transition. For the magnetic dipole case  $B$  replaces  $E$ .

<sup>15</sup> J. C. Slater, "Microwave Electronics," D. Van Nostrand Co., Inc., New York, N. Y., ch. 4; 1950.

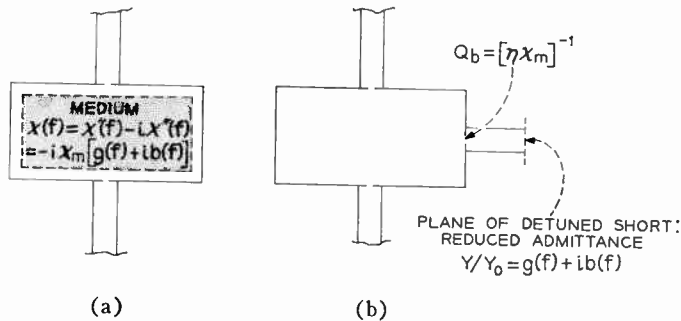


Fig. 3—(a) Resonant cavity with amplifying medium. (b) Equivalent circuit for cavity with amplifying medium.

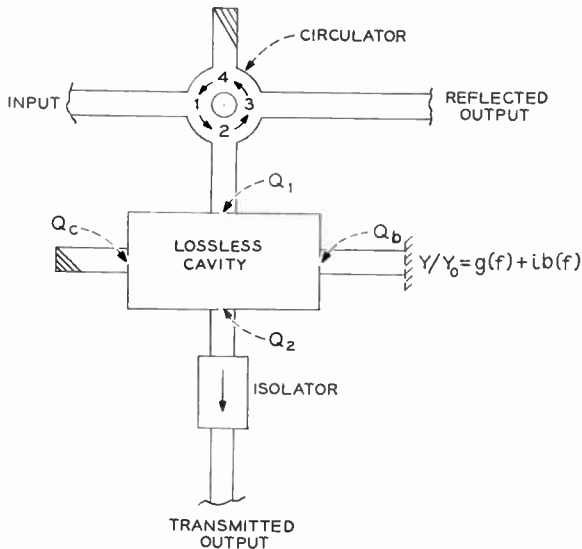


Fig. 4—Complete equivalent circuit for maser amplifier.

(Fig. 3) is then obtained by letting the coupling be  $Q_b = 1/\eta\chi_m$  and the reduced admittance be  $y_b = g(f) + ib(f)$ , where  $y_b = Y/Y_0$ , and  $Y_0$  is the characteristic admittance of the guide. Positive values of  $g$  represent absorption; negative values, emission. From the definition of  $\chi_m$  note that the maximum absolute value of  $g$  is always unity, and that this occurs at the center of the sample resonance. The complete equivalent circuit, then, is as given in Fig. 4.

The sources of noise in the maser amplifier now are easily discernible. Noise power traveling toward the cavity is generated by the load in each waveguide. The output isolator is considered to be an integral part of the amplifier, and therefore the noise it radiates toward the cavity is included in the analysis. This noise power is a full  $kT_i$  per unit bandwidth, corresponding to the infinite attenuation in the backward direction which the isolator is assumed to possess.  $T_i$  is the isolator's temperature. The circulator contributes noise only if it is lossy and/or if it sees a mismatch looking toward the input. Circulator loss is considered later; it is assumed mismatches can be avoided. The amplifying medium also contributes noise. It has been shown by Pound<sup>4</sup> that the noise generator associated with a negative resistance (in this case a negative admittance) follows

the Johnson-Nyquist formulation just as for the positive resistance. Thus, for  $|T_b| \gg hf/k$ , noise power per unit bandwidth of amount  $kT_b g(f)$ <sup>16</sup> is incident on the cavity from this noise source, where  $T_b$  is the "temperature" (negative) of the amplifying medium,<sup>2</sup> defined by  $T_b = -hf/k \ln(n_a/n_b)$ , where  $n_a$  and  $n_b$  are the populations of the upper and lower quantum energy levels responsible for the amplification. This is the same relationship between the level populations and temperature which holds for thermodynamic equilibrium at positive temperature. Dielectric losses in the sample, if any, should be added to the cavity loss in the types of maser in which the sample is permanently affixed to the cavity and takes up the cavity temperature. In the beam-type maser there is no dielectric loss; however, background gas causes some absorption. This absorption should be added similarly to the cavity loss since the molecules responsible for it have bounced, for the most part, at least once off the walls of the cavity, and so have acquired nearly the temperature of the cavity. The relative importance of each noise source is determined by its temperature and the size of the coupling by which it is attached to the cavity.

The calculations necessary to obtain gain and noise figure are quite straightforward from this point. First, however, it is convenient to define some useful symbols:

$$Q_L = \left( \frac{1}{Q_c} + \frac{1}{Q_1} + \frac{1}{Q_2} \right)^{-1}, \text{ loaded cavity } Q,$$

$\beta = Q_L/Q_b$ , beam strength parameter (this factor approaches unity for high gain),

$$D(f) = 4Q_L^2 \left[ \frac{1}{4} \left( \frac{1}{Q_L} + \frac{g(f)}{Q_b} \right)^2 + \left( \frac{f-f_c}{f_c} + \frac{b(f)}{2Q_b} \right) \right],$$

resonant term

$$= (1 + \beta g(f))^2 + \left( \frac{f-f_c}{\Delta f_c} + \beta b(f) \right),$$

where  $\Delta f_c = f_c/2Q_L$  is the half width at half maximum of the cavity resonance. The input power  $P_0$  per unit bandwidth, causes a reflection of amount<sup>17</sup>

$$P_r = P_0 \left[ 1 - \frac{4Q_L^2}{DQ_1} \left( \frac{1}{Q_c} + \frac{1}{Q_2} + \frac{g}{Q_b} \right) \right]$$

and also a transmission into waveguide 2 of magnitude

$$P_t = P_0 4Q_L^2 / Q_1 Q_2 D.$$

Similar equations obtain for the noise power originating from each of the noise sources. Adding up the contributions from all the different independent sources, the power  $P_1$  per unit bandwidth which emerges from the input is

<sup>16</sup> For  $|T_b| \lesssim hf/k$  the exact expression,  $g(f) \cdot hf / [\exp(hf/kT_b) - 1]$ , must be used.

<sup>17</sup> The explicit frequency dependence of  $g(f)$ ,  $b(f)$ , and  $D(f)$  is omitted from here on, and the simple forms  $g$ ,  $b$ , and  $D$  used.

$$P_1 = P_0 \left[ 1 - \frac{4QL^2}{DQ_1} \left( \frac{1}{Q_c} + \frac{1}{Q_2} + \frac{g}{Q_b} \right) \right] + \frac{4QL^2}{DQ_1} \left[ \frac{kT_c}{Q_c} + \frac{kT_i}{Q_2} + \frac{kT_b g}{Q_b} \right]$$

where  $T_c$  is the temperature of the cavity. Similarly, the power  $P_2$  per unit bandwidth emerging into waveguide 2 is

$$P_2 = P_0 4QL^2 / Q_1 Q_2 D + kT_i \left[ 1 - \frac{4QL^2}{DQ_2} \left( \frac{1}{Q_c} + \frac{1}{Q_1} + \frac{g}{Q_b} \right) \right] + \frac{4QL^2}{DQ_2} \left[ \frac{kT_c}{Q_c} + \frac{kT_b g}{Q_b} \right].$$

Now that the basic formulas have been obtained, the gain, bandwidth, noise figure, and relative merit for the transmission and reflection type masers can be evaluated. Also, these results can be compared with the experimental data.

Bandwidth of the amplifier, at high gain, is mainly determined by the resonant term  $D$ . At frequencies near the midband of the maser,  $g$  and  $b$  may be approximated by  $g = -1$  and  $b = (f - f_b) / \Delta f_b$ , where  $f_b$  and  $\Delta f_b$  are, respectively, the center frequency and half width at half maximum of the amplifying resonance. For both reflected power and transmitted power, the difference  $B$  between half-power frequencies is approximately

$$B \approx 2(1 - \beta) \left[ \frac{1}{\Delta f_c} + \frac{\beta}{\Delta f_b} \right]^{-1}.$$

The effective input noise temperature  $T_n(f)$  is obtained by setting  $P_0$  equal to  $kT_n(f)$  and equating the part of  $P_1$  or  $P_2$  originating from this noise source to the combined power per unit bandwidth from the other noise sources. When dealing with the one-port maser,  $Q_2$  is set equal to infinity to eliminate the second waveguide.

The effective input noise temperature for the one-port maser is

$$T_n(f) = \frac{\frac{4QL^2}{Q_1 D} \left[ \frac{T_c}{Q_c} + g \frac{T_b}{Q_b} \right]}{1 - \frac{4QL^2}{Q_1 D} \left[ \frac{1}{Q_c} + g \frac{1}{Q_b} \right]} \quad (1)$$

At resonance ( $f = f_c = f_b$ ) the effective input noise temperature,  $T_{n,0}$ , may be expressed as

$$T_{n,0} = \frac{(\sqrt{G_0} + 1)^2}{G_0} \left[ T_c \frac{Q_1}{Q_c} + |T_b| \frac{Q_1}{Q_b} \right] \quad (2)$$

where  $G_0$  is the power gain at resonance, given by

$$G_0 = \frac{P_r}{P_0} = 1 + \frac{4QL^2}{Q_1(1 - \beta)^2} \left[ \frac{1}{Q_b} - \frac{1}{Q_c} \right]. \quad (3)$$

For the transmission-type maser at resonance

$$T_{n,0} = T_c \frac{Q_1}{Q_c} + |T_b| \frac{Q_1}{Q_b} + T_i \left[ \left( \frac{Q_1}{Q_2} \right)^{1/2} - \frac{1}{\sqrt{G_0}} \right]$$

and

$$G_0 = \frac{4QL^2}{Q_1 Q_2 (1 - \beta)^2}.$$

One further consideration is in order, namely the effect of loss in the input circuit. This loss has two bad effects: it attenuates the signal and at the same time it introduces some noise. The effective input noise temperature  $T_n'$  of the resulting amplifier is increased over that of the maser proper, becoming

$$T_n' = [T_n + T_L(L - 1)/L]L \quad (4)$$

where  $L$  is the loss (reciprocal of the gain) and  $T_L$  is the temperature of the element which introduces the loss. The effect of input loss may be important in maser amplifiers, especially the reflection type where the required circulator may introduce as much as a few tenths of a db of loss.

Contemplation of the above results reveals the following facts, assuming the same sample in both reflection and transmission-type operation.

- 1) For the same value of the loaded cavity  $Q$ , and thus the same bandwidth, the gain of the reflection type is 6 db greater than the maximum gain of the transmission type, which is obtained by setting  $Q_1 = Q_2$ . Also, contributions to the effective input noise temperature from the amplifying material and the cavity walls are higher for the transmission-type maser; they are about twice as large in the case  $Q_1 = Q_2$ .
- 2) For reasonably low noise operation and at the same time high gain, it is essential to cool the isolator of the transmission-type amplifier to a low temperature, whereas the circulator of the reflection type need not be cooled if its loss is kept small.
- 3) For minimum noise operation, it is necessary to cool the input circuit and the resonant cavity for either type of maser.

A word about the possible operation of a traveling-wave maser amplifier is appropriate at this point. The instability and loss in bandwidth, which are common to all types of regenerative amplifiers at high gain, are largely overcome by this method, and its noise properties are similar to those of the cavity maser. However, for some types of amplifying media, e.g., gases, it is very difficult to produce the high concentration of field which is necessary in such a device to obtain useful gain in a reasonable volume.

#### EXPERIMENTAL PROCEDURE

The aim of the experiment was to measure the effective input noise temperature of an ammonia maser and to compare this experimental value with theory.

A block diagram of the apparatus used in making the noise measurements is shown in Fig. 5. With the exception of the liquid nitrogen cooled load, all of the microwave plumbing, including the masers' cavities, was at room temperature. Each maser was similar to that described by Gordon, Zeiger, and Townes<sup>1</sup> and was of the reflection type. The cavities were operated in the  $TM_{010}$  mode. A circulator separated each maser's output from its input. The effective input noise temperature to be measured was that of the first maser. The coupling of its cavity was increased until sufficient gain was achieved with the strongest available beam. A considerable overcoupling, ( $Q_1/Q_c < 1$ ), resulted, giving an expected effective input noise temperature much less than the cavity temperature [see (2)]. The amplification of the first maser was modulated<sup>18</sup> on and off at 35 cps by a square-wave transverse electric field within the cavity. To obtain this field the cavity was split longitudinally and a voltage was applied between the two halves. The resulting inhomogeneous field turned the maser OFF by broadening the ammonia resonance and shifting its peak to the extent that the effects of the beam became negligible. The second maser functioned as a CW low noise RF amplifier. The local oscillator klystron was stabilized with a dc Pound stabilizer circuit.<sup>19</sup> The IF amplifier operated at 70 mc and had a bandwidth of 2.5 mc. The time constant of the dc filter following the lock-in amplifier was about one second.

Measurements were made of the change in RF attenuation  $A$  that followed the second maser required to keep the recorder deflection constant as the temperature of the nonreflecting input termination was changed from one known temperature  $T''$  to another,  $T'$ . This change in termination temperature was accomplished by inserting 20 db of room temperature attenuation between the cold load and the circulator. From these measurements alone an approximate value (within a few per cent) for the effective input noise temperature of the maser plus its input circuitry may be calculated. Measurements also were made of the loss  $L$  and the temperature  $T_L$  of the loss between the input termination and the maser cavity. From the combined measurements, an approximate value  $T_n^*$  may be obtained for the effective input noise temperature of the maser itself. A more exact determination of the effective input noise temperature  $T_n$  requires a knowledge of the relative amount of power leaving the maser when off.

<sup>18</sup> R. H. Dicke, "The measurement of thermal radiation at microwave frequencies," *Rev. Sci. Instr.*, vol. 17, pp. 268-275; July, 1946. This method of modulating the desired signal has a theoretical sensitivity for given IF bandwidth and dc filter time constant comparable to that obtained by making CW measurements. However, in practice, better sensitivity usually is obtained with the modulation technique because it is less sensitive to slow gain fluctuations in the superheterodyne receiver.

<sup>19</sup> R. V. Pound, "Frequency stabilization of microwave oscillators," *Proc. IRE*, vol. 35, pp. 1405-1415; December, 1947.

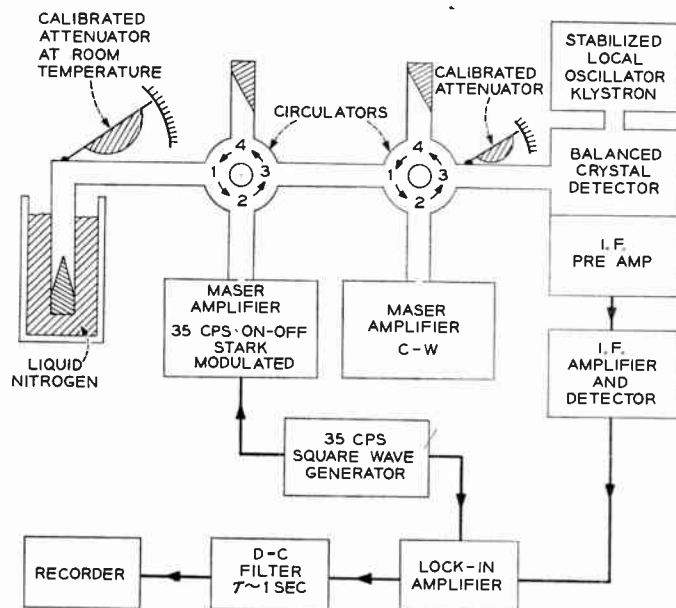


Fig. 5—Block diagram of apparatus.

The difference between  $T_n$  and  $T_n^*$  is of the order of  $T_n/G_0$ , and was obtained from measurements of the maser gain<sup>20</sup> when on  $G_0$ , the maser gain when off  $G'$ , and the temperature of the cavity  $T_c$ .

#### INTERPRETATION OF DATA

Before considering the actual case, consider an ideal case which yields a simpler relationship between the effective input noise temperature and the measured quantities. Assume that there was zero noise power leaving the maser when it was off, that the second maser's gain was high, and that the bandwidth of the second maser was much narrower than that of the first. In this case, the change  $A$  in RF attenuation following the second maser required to keep the recorder deflection constant as the temperature of the first maser's input termination was changed from  $T''$  to  $T'$  is related to the effective input noise temperature  $T_n'(f_2)$  of the combination of the maser and its input circuitry by

$$\frac{T_n'(f_2) + T''}{T_n'(f_2) + T'} = A, \quad (5)$$

where  $f_2$  is the center frequency of the second maser. The effective input noise temperature  $T_n(f_2)$  of the maser itself would be related to the above quantities and to the loss  $L$  and temperature  $T_L$  of the circuitry between the input termination and the maser by (4), or by

$$\frac{T_n(f_2) + T''/L + T_L(L-1)/L}{T_n(f_2) + T'/L + T_L(L-1)/L} = A. \quad (6)$$

<sup>20</sup> The signal used for the gain measurement was derived from that of the local oscillator by a 70 mc modulator and a sideband filter.

Though not stated explicitly, (5) and (6) also assume that both masers were acting as linear amplifiers, which assumption should be valid at the power levels of operation.

The assumptions that the noise leaving the maser when off was zero, and that the second maser's bandwidth was much narrower than that of the first, were only approximately correct. As a result, (5) and (6) are no longer exact. However, for purposes of comparing experiment and theory it is convenient to use a quantity  $T_n^*$  defined by a relation similar to (6):

$$\frac{T_n^* + T''/L + T_L(L - 1)/L}{T_n^* + T'/L + T_L(L - 1)/L} = A. \tag{7}$$

Thus,  $T_n^*$  is a number which may be experimentally determined with no knowledge of the maser's characteristics.

A theoretical value for  $T_n^*$  may be obtained from measurements of the maser's characteristics and the frequency dependence of the amplification between the (first) maser and the IF detector. The recorder deflection was a function of the difference between the power arriving at the detector when the maser was on,  $P$ , and that arriving at the detector when the maser was off,  $P^\circ$ . This difference is

$$P - P^\circ = k \int_0^\infty ([T_n + T/L + T_L(L - 1)/L]G - [T_n^\circ + T/L + T_L(L - 1)/L]G^\circ)G_2' df.$$

$T$  is the temperature of the input termination,  $T_n^\circ$  and  $G^\circ$ , respectively, are the effective input noise temperature and gain of the maser when it is off, and  $G_2'$  is the power gain between the output of the first maser and the IF detector. Equating this power difference for the case of the input termination at the temperature  $T''$  with that for the input termination at  $T'$  and the RF attenuation changed by  $A$ , and arranging the terms into the form of (7), yields for the theoretical value of  $T_n^*$

$$T_n^* = \frac{\int_0^\infty [T_n G - T_c(1 - G^\circ)]G_2 df}{\int_0^\infty (G - G^\circ)G_2 df}, \tag{8}$$

where  $G_2$  has the frequency dependence of the amplification between the first maser and the IF detector.  $A$  is assumed constant over the frequency range of interest. In (8),  $T_c(1 - G^\circ)$  has been substituted for  $T_n^\circ G^\circ$ . This is a valid substitution because the effects of the beam were negligible when the maser was off and thus  $G^\circ$  is the reflection coefficient of the cavity. In our case, a sufficiently accurate evaluation of (8) is possible, even though the exact frequency dependence of  $G$  and  $G_2$  is unknown. In the frequency region where the gain of the first maser is a few db or more, the ratio of

$T_n G - T_c(1 - G^\circ)$  to  $G - G^\circ$  is very nearly independent of frequency. Furthermore, the contribution to (8) from outside this region is negligible (see Appendix I). Thus, (8) reduces to

$$T_n^* = \frac{T_n G - T_c(1 - G^\circ)}{G - G^\circ} = \frac{T_{n,0} G_0 - T_c(1 - G^\circ)}{G_0 - G^\circ} \tag{9}$$

with an estimated uncertainty in  $T_n^*$  of about 1 per cent, arising from lack of exact knowledge of the shape of the ammonia resonance. For these equations to hold, it is required that the resonant frequency of the maser cavity, the resonant frequency of the ammonia beam, and the center frequency of the second maser be identical; it is sufficient if these frequencies are close enough to each other for good operation.

Eq. (9) combined with (2) yields a theoretical value of  $T_n^*$  depending only upon the maser's characteristics. This theoretical value may be compared with the experimental value given by (7). However, since the effective input noise temperature is of more interest than  $T_n^*$ , (7) and (9) were combined to give the following expression for the experimental value of  $T_{n,0}$ :

$$T_{n,0} = \left[ \frac{AT' - T''}{1 - A} \frac{1}{L} - T_L \frac{L - 1}{L} \right] \left( 1 - \frac{G^\circ}{G_0} \right) + T_c \frac{1 - G^\circ}{G_0}; \tag{10}$$

and this experimental value was compared with the theoretical value of  $T_{n,0}$  as given by (2).

RESULTS

Three separate sets of measurements were made. The results are summarized in Table I as follows.

TABLE I  
RESULTS

Date	$T_{room}^\circ K$	$A$	$L$	$G^\circ$	$G_0$	$T_n$ Experimental	$T_n$ Theoretical
June 10, 1957	300	2.00 ±0.05	1.172 ±0.027	0.473 ±0.011	50 ±5	81 ±18	77 ±3
June 25, 1957	307	2.04 ±0.14	1.177 ±0.014	0.505 ±0.030	45 ±7	78 ±30	75 ±7
July 18, 1957	304	1.95 ±0.05	1.232 ±0.020	0.513 ±0.013	71 ±7	74 ±16	68 ±3

$$T'' = (T_{room} - 2)^\circ K$$

$$T' = 77^\circ K$$

$$T_L = T_c = T_{room}$$

The results of June 10, 1957, and July 18, 1957 have been reported previously.<sup>10</sup> In that report, the experimental and theoretical values of the effective input

noise temperature were only approximate; the experimental numbers were the  $T_n^*$  of the present paper, and the theoretical numbers did not include the contribution of the background ammonia.

The experimental values given in Table I for the effective input noise temperature  $T_n$  of the maser, *i.e.*, cavity plus medium, were obtained from (10).

The theoretical values of the effective input noise temperature were calculated from (2) with  $1/Q_c$  representing the losses both in the cavity walls and in the background ammonia. The "temperature" of the beam was negative and probably much smaller in absolute magnitude than  $hf/k$ . As a result, in (2)  $|T_b|$  should be replaced by  $hf/k = 1.1^\circ\text{K}$ . The contribution to the effective input noise temperature by the background ammonia was estimated to be  $3.4^\circ\text{K}$  (see Appendix II). The calculation of the theoretical value was based on measurements of the cavity temperature, the reflection coefficient of the cavity with no beam, the midband maser gain, and the pressure of the background ammonia.

The experimental and theoretical values for the effective input noise temperature of the maser agree well within the experimental error. The contribution of the beam to the maser noise was too small to be measured. However, an upper limit of approximately  $20^\circ\text{K}$  can be placed on the absolute value of the beam temperature.

#### APPENDIX I

The difference in power per unit bandwidth between maser on and maser off is much larger in the frequency region of high gain than in the "tail" of the ammonia resonance. However, the effect of the tail on  $T_n^*$  may be significant, depending upon the frequency dependence of the gain  $G_2$  following the maser. For example, if  $G_2$  is constant over a frequency region which is large compared to the width of the cavity resonance, evaluation of (8) yields

$$T_n^* = T_{n,0} \beta \frac{(Q_c/Q_b) - 1}{(Q_c/Q_b) - \beta}$$

where it is assumed that the ammonia resonance has a Lorentz shape, *i.e.*,  $g = -1/[1 + ((f-f_b)/\Delta f_b)^2]$ . Using values of  $\beta$  ( $\sim 0.8$ ) and  $Q_c/Q_b$  ( $\sim 5$ ) appropriate to the maser as operated gives  $T_n^* \sim (3/4)T_{n,0}$ . The frequency region responsible for most of this difference between  $T_n^*$  and  $T_{n,0}$  is the tail of the ammonia resonance. The exact line shape of the actual resonance is not known.

However, enough is known to be able to state that the relative contribution to  $T_n^*$  from the tail of the resonance is the same order of magnitude as the contribution from the tail of a Lorentz-shaped line. In the actual experiment  $G_2$ , determined by the product of the second maser and the IF amplifier gains, was strongly peaked. In the vicinity of the ammonia resonance  $G_2$  was more than 30 db larger than in the tail. Thus the contribution to  $T_n^*$  from the tail was negligible.

#### APPENDIX II

Eq. (2) can be extended to include the contribution,  $\Delta T_{n,0}$ , to the effective input noise temperature from the background ammonia gas. The loss,  $1/Q_{gas}$ , due to these stray ammonia molecules is simply added to the cavity loss, giving  $\Delta T_{n,0} = [(\sqrt{G_0} + 1)^2/G_0] T_c Q_1/Q_{gas}$ . An estimate of  $1/Q_{gas}$  may be made from the known absorption coefficient of the ammonia 3-3 line,  $\alpha = 7.9 \times 10^{-4} \text{ cm}^{-1}$ ; the background pressure  $p$  of ammonia in the cavity chamber; the gas pressure  $p_0$  at which molecule-molecule collisions and molecule-wall collisions make equal contributions to the line width, and the free space wavelength  $\lambda_0$ . The appropriate relationship for the case  $p \ll p_0$  is

$$\frac{1}{Q_{gas}} \cong \frac{\alpha \lambda_0 p}{2\pi p_0}$$

Taking values approximating the experimental conditions,

$$p_0 = 1 \times 10^{-3} \text{ mm Hg}$$

$$p = 3 \times 10^{-5} \text{ mm Hg}$$

$$\lambda_0 = 1.25 \text{ cm},$$

yields  $1/Q_{gas} \cong 1.8 \times 10^{-6}$ . The resulting contribution to the effective noise temperature is  $\Delta T_{n,0} \cong 3.4^\circ\text{K}$ , where the values  $Q_1 = 1800$ ,  $G_0 = 50$ , and  $T_c = 300^\circ\text{K}$  have been assumed.

#### ACKNOWLEDGMENT

The authors gratefully acknowledge many helpful discussions with Prof. C. H. Townes, Dr. R. Kompfner and Dr. C. F. Quate; circulator components and advice on circulator construction from Dr. E. H. Turner and Dr. E. A. Ohm; considerable experimental assistance from J. M. Dziedzic and J. J. Wiegand; and some valuable comments from the unknown reviewers.



# The Spherical Coil as an Inductor, Shield, or Antenna\*

HAROLD A. WHEELER†, FELLOW, IRE

**Summary**—The spherical coil is an idealized form of inductor having, on a spherical surface, a single-layer winding of constant axial pitch. Its magnetic field inside is uniform and outside is that of a small coil or magnetic dipole. Its properties exemplify exactly some of the rules that are approximately applicable to practical inductors. Simple formulas are given for self-inductance, mutual inductance, coupling coefficient, effect of iron core, and radiation power factor in free space or sea water. This coil is the basis for evaluating the shielding effect of a closed conductive (nonmagnetic) metal shell. A special winding is described which enables simple and exact computation of self-resonance (the length of wire being just  $\frac{1}{2}$  wavelength in some cases).

## I. INTRODUCTION

A SPHERICAL coil is an inductor similar to the solenoid but spherical rather than cylindrical in shape. Its internal magnetic field is constant and its external field is that of a small magnetic dipole.

The spherical coil was described by Maxwell in his monumental treatise [1] but it has been ignored by subsequent workers. It has little practical value in its literal form but its study leads to relationships that have qualitative significance in many practical situations. The present purpose is to present some of these relationships in a form that will suggest their practical implications.

This is an example of one philosophy of approximation, the one that seeks for idealized forms that are susceptible of simple and exact formulation. These forms are then perceived as approximations of practical forms. Being exactly formulated, any relationships are likely to indicate real trends.

The writer first developed some concepts of the spherical coil in 1941 while studying the problems of an electromagnetic detector for buried metal objects [3]. A spherical coil on short-circuit was used to simulate the reaction from an object made of a conducting shell. (The outcome of this work was the SCR-625 mine detector which was the one used by our armed forces in World War II.)

More recently, the writer formulated the ideal properties of a spherical radiator that can be approximated in a loop antenna on a spherical iron core. Also, there will be presented here a set of idealized conditions in which a coil of wire is self-resonant at a frequency such that the length of wire is just  $\frac{1}{2}$  wavelength.

After a preliminary description of spherical coils, there will be formulated their various properties of self and mutual inductance, shielding, radiation and self-

resonance. Attention will be paid to the core space, including a magnetic or antimagnetic sphere partially filling the coil.

## II. SYMBOLS

### MKS Rationalized Units

- $L$  = inductance (henries).
- $C$  = capacitance (farads).
- $R$  = resistance (ohms).
- $\mu_0 = 1.257 \times 10^{-6}$  = magnetivity (permeability) of free space (henries/meter).
- $\epsilon_0 = 8.85 \times 10^{-12}$  = electrivity (permittivity) of free space (farads/meter).
- $R_e = 377$  = wave resistance of free space (ohms).
- $\omega$  = radian frequency (radians/second).
- $\lambda$  = wavelength (meters).
- $\lambda/2\pi$  = radianlength (meters).
- $\sigma$  = conductivity (mhos/meter).
- $\delta$  = skin depth (meters).
- $a$  = radius (meters).
- $c$  = pitch of winding (meters).
- $d$  = thickness of conductor winding or shell (meters).
- $l$  = length of wire on coil (meters).
- $r$  = distance between centers (meters).
- $A$  = total area of turns (meters<sup>2</sup>).
- $V$  = volume of spherical coil (meters<sup>3</sup>).
- $V_r$  = volume of radiansphere (meters<sup>3</sup>).
- $n$  = number of turns.
- $k, k', k_1, k_m$  = magnetic ratio (relative permeability).
- $k_e$  = electric ratio (dielectric constant).
- $k_{12}$  = coefficient of coupling.
- $p = R/L\omega$  = power factor (much less than unity).
- $p_2$  = leakage fraction of spherical shell (free of skin effect).
- $p_s$  = leakage fraction of spherical shell (subject to skin effect).
- $E$  = voltage between ends of coil (volts RMS).
- $I$  = current at middle of coil (amperes RMS).

## III. THE SPHERICAL COIL

Fig. 1 shows some of the properties of the spherical coil. It is to be wound in such a way that the internal magnetic field is uniform, as indicated in Fig. 1(a). This requires a current sheet with the turns pitched uniformly along the axis, as shown in Fig. 1(b). The variation of the length of wire per turn is such that its average is  $\pi/4$  of the middle turn at the equator. The varying area of the turns is graphed in Fig. 1(c). The parabola

\* Original manuscript received by the IRE, February 13, 1958.

† President, Wheeler Labs., Inc., Great Neck, N. Y.

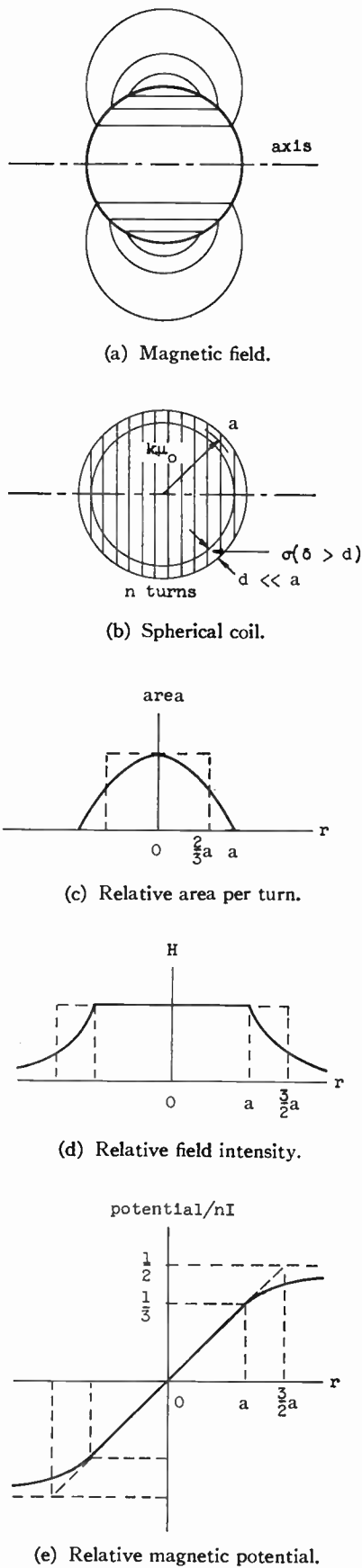


Fig. 1—The spherical coil and its properties.

shows the variation of the area per turn, such that its average is  $\frac{2}{3}$  of the area at the equator. The other curves (d) and (e) will be discussed later.

The concept of the current sheet is familiar in the study of inductance. Ideally it requires many turns of small wire, rather closely spaced but in accordance with the prescribed variation of pitch. As a result, the inductance is mainly obtained by interaction of the turns and is nearly independent of the fine structure of the turns.

Among all forms of inductors, the spherical coil yields the simplest formulation of its properties. The basic reason for this is that its field pattern involves spherical harmonics of orders zero and one, which correspond to a uniform field and to that of a small dipole. Unlike the closed-core or toroidal inductors, the spherical coil has the external field required for radiation or other exterior coupling.

IV. SELF-INDUCTANCE

The inductance formula will be derived in a succession of easy steps relying only on simple rules, referring to Fig. 1.

The starting point is a cylindrical coil of radius  $a$ , length  $2a$ , and  $n$  turns. The cylindrical volume has an air core and is surrounded by a perfect magnetic medium; the respective magnetic ratios are  $k=1$  and  $k'=\infty$ . The interior field is uniform. The inductance is

$$\text{cyl } L(1, \infty) = \mu_0 \frac{\pi a^2 n^2}{2a} = \frac{\pi}{2} \mu_0 a n^2. \tag{1}$$

Taking next the spherical coil with corresponding air core and magnetic surrounding, the volume is  $\frac{2}{3}$  as great so the magnetic energy and the inductance are multiplied by this factor. The inductance of the sphere, with  $k=1$  and  $k'=\infty$ , is

$$L(1, \infty) = \frac{\pi}{3} \mu_0 a n^2. \tag{2}$$

This inductance is limited by the internal reluctance, with no external reluctance.

In order to learn the relative reluctance of internal and external paths for magnetic flux, some computations are made with the spherical coil in air. By integration over the turns of the coil, the magnetic field along the axis is found to follow two laws, graphed in Fig. 1(d). Inside the coil, the magnetic field is uniform. Outside the coil, the field varies inversely with the cube of the distance from the center (as in the case of a small coil or magnetic dipole). Integrating this field along the axis, we obtain the magnetic potential, graphed in Fig. 1(e). The total potential difference along the axis is  $nI$  for  $n$  turns carrying current  $I$ . It is found that  $\frac{2}{3}$  of the potential is inside the coil and  $\frac{1}{3}$  is outside. Therefore the path reluctance outside is  $\frac{1}{2}$  as great as that inside. The in-

ductance of the spherical coil in air is  $\frac{2}{3}$  as great as (2) above:

$$L = \frac{2\pi}{9} \mu_0 a n^2. \tag{3}$$

The general formula, for any magnetic ratios inside and outside, is

$$\begin{aligned} L(k, k') &= \frac{2\pi}{9} \mu_0 a n^2 \frac{1}{2/3k + 1/3k'} \\ &= \frac{2\pi}{9} \mu_0 a n^2 \frac{3}{2/k + 1/k'}. \end{aligned} \tag{4}$$

The resistance of the spherical coil is of interest in some applications. In Fig. 1(b), the conducting shell is indicated as having a thickness  $d$  much less than the radius  $a$ . The conducting cross section of this shell is assumed to determine that of the wires in the current sheet. It is also assumed that this thickness is much less than the "skin depth" in the conducting material at the operating frequency. The resistance per turn is less toward the poles because the turns are shorter and wider; the variation follows the parabola in Fig. 1(c) so the average per turn is  $\frac{2}{3}$  of the resistance of the longest turn at the equator. On this basis, the resistance of the coil is

$$R = \frac{2\pi n^2}{3d\sigma}. \tag{5}$$

The power factor of this inductor (in air) is:

$$p = R/L\omega = \frac{3}{\omega\mu_0\sigma ad} = \frac{3\delta^2}{2ad}. \tag{6}$$

The condition that  $d < \delta$  is still in effect, so this formula is limited to  $p > 3d/2a$ . The last form is simplified to a ratio of length dimensions by introducing the skin depth (though this case is not subject to the skin effect).

If the winding on the spherical coil is subject to the skin effect, no simple evaluation is apparent because the magnetic flux links the winding.

Fig. 2 shows a simple solenoid that has certain properties of the spherical coil exactly, and some other properties approximately. The following properties are the same:

- Radius (at equator)
- Axial pitch of turns
- Total area of turns (and resulting far field)
- Total resistance of turns.

The following properties are different:

- Greater maximum dimension (radius of circumscribed sphere is greater in ratio  $\sqrt{13/9} = 1.20$ )
- Lesser axial length (2/3)
- Lesser number of turns (2/3)
- Lesser field intensity on axis
- Lesser inductance (approximately 0.917 or 11/12).

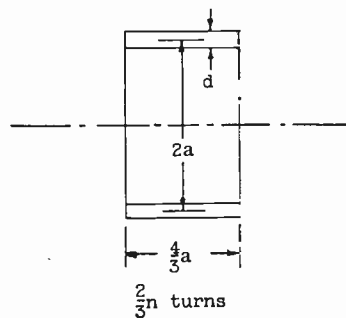


Fig. 2—Solenoidal coil for comparison.

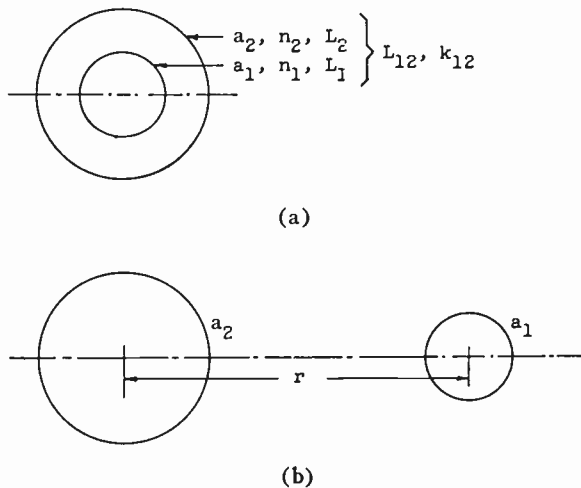


Fig. 3—Two coaxial spherical coils.

The inductance of this solenoid is given by

$$\begin{aligned} \text{sol } L &= \mu_0 \frac{\pi a^2 (\frac{2}{3}n)^2 0.595}{\frac{2}{3}(2a)} = \frac{2\pi}{9} \mu_0 a n^2 \left( \frac{3}{2} 0.595 \right) \\ &= \frac{2\pi}{9} \mu_0 a n^2 (0.893). \end{aligned} \tag{7}$$

The last form shows the ratio by which this inductance is less than that of the spherical coil.

### V. MUTUAL INDUCTANCE

Fig. 3 shows the two cases of mutual inductance between two spherical coils, the smaller coil being inside or outside of the larger coil.

In Fig. 3(a), the smaller of two coils is inside the larger, with parallel axes. They need not be concentric or even coaxial. The mutual inductance is computed easily because of the uniform field inside the larger coil.

$$L_{12} = L_2 \frac{n_1 a_1^2}{n_2 a_2^2} = \frac{2\pi}{9} \frac{\mu_0 a_1^2 n_1 n_2}{a_2}. \tag{8}$$

Their coefficient of coupling is

$$k_{12} = L_{12} / \sqrt{L_1 L_2} = (a_1/a_2)^{3/2} \tag{9}$$

$$k_{12}^2 = (a_1/a_2)^3 = V_1/V_2 \tag{10}$$

in which  $V_1$  and  $V_2$  are the volumes of the spheres.

A practical application of a spherical coil (somewhat different from the ideal) is found in the so-called "variometer." This device is an inductor made of two concentric spherical coils of nearly the same size, the inner one rotating about a transverse axis. The two coils are connected in series (or parallel) to form an inductor that has a wide ratio of variation obtained by changing the mutual inductance from "opposing" to "aiding."

In Fig. 3(b) the two coils are mutually external and coaxial. Since the external field of each coil follows exactly the pattern of a small coil or magnetic dipole, the mutual inductance is expressed by a simple formula (derived from principles given by Harnwell [9]).

$$L_{12} = \frac{2\pi}{9} \frac{\mu_0 a_1^2 a_2^2 n_1 n_2}{r^3} \quad (11)$$

$$k_{12} = (a_1 a_2 / r^2)^{3/2}. \quad (12)$$

The ultimate simplicity of this formula is attributable to the simple properties of the spherical coil.

If instead, the equators of the two coils are coplanar, the values of  $L_{12}$  and  $k_{12}$  are  $\frac{1}{2}$  as great.

The greatest coefficient of coupling between two coils mutually external is obtained with two coaxial coils of the same size in contact:

$$r = 2a_1 = 2a_2 : k_{12} = 1/8. \quad (13)$$

If each of two coaxial coils is filled with a magnetic core ( $k_1$  or  $k_2$ ), their mutual inductance is increased more than their self-inductance, so their coefficient of coupling is increased approximately as follows:

$$k_{12} = \left(\frac{a_1 a_2}{r^2}\right)^{3/2} \left(\frac{3k_1}{2+k_1} \frac{3k_2}{2+k_2}\right)^{1/2} \quad (14)$$

This formula is based on the assumption of a separation far from contact. Perfect magnetic cores increase the coupling by a factor of 3.

Comparing two coaxial coils of the solenoid form (Fig. 2) located far apart, we find that their mutual inductance is the same and their coefficient of coupling is greater approximately in the ratio  $1/0.893 = 1.120$ . This increase is attributed to the larger maximum dimension of each coil.

### VI. SPHERICAL CORE

There has been some mention of a magnetic core completely filling a spherical coil. Fig. 4(a) shows the more general case of a concentric spherical core partially filling the coil. It is regarded as a coaxial smaller coil filled with a core of magnetic ratio  $k_1$ .

Several simple rules enable the computation of the effect of the inside core and coil. First,  $L_1$  and therefore  $L_{12}$  are multiplied by  $3k_1/(2+k_1)$ . Second, the "leakage inductance"  $L_2(1-k_{12}^2)$  is unaffected by the core; it is the inductance of the outer coil with the inner coil on

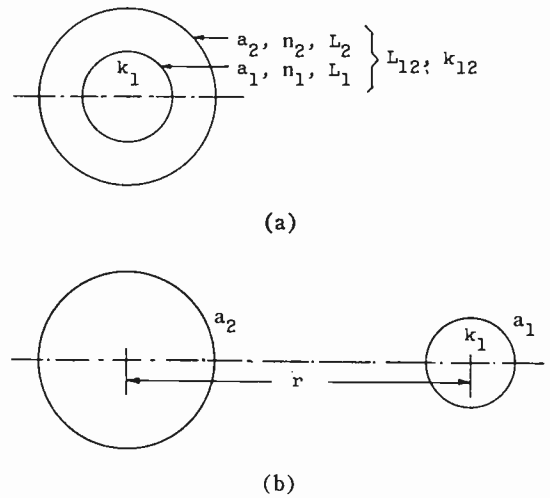


Fig. 4—Spherical core or external object.

short-circuit. With the core, the properties involving the outer coil are changed to the following:

$$k_{12}^2 = \frac{3k_1(a_1/a_2)^3}{2+k_1+2(k_1-1)(a_1/a_2)^3} \quad (15)$$

$$L_2 = \frac{2\pi}{9} \mu_0 a_2 n_2^2 \left[1 + 2 \frac{k_1-1}{k_1+2} (a_1/a_2)^3\right]. \quad (16)$$

The last factor (in brackets) is the ratio in which the inductance of the outer coil is increased by a magnetic core inside, or decreased by an antimagnetic core. The latter might be realized by a conducting core that excludes magnetic flux by virtue of the skin effect, in which case  $k_1 = 0$ :

$$L_2 = \frac{2\pi}{9} \mu_0 a_2 n_2^2 [1 - (a_1/a_2)^3]. \quad (17)$$

This value is reduced in the ratio of the volume outside the antimagnetic core.

As an example, take an iron-dust core of  $k_1 = 4$ , filling  $\frac{1}{2}$  the volume of a spherical coil. The inductance is increased in the ratio  $3/2$ . A solid copper core of the same volume, shielded by the skin effect, would reduce the inductance to  $\frac{1}{2}$ .

Referring again to the solenoid of Fig. 2, and inserting a cylindrical core of the same shape as the solenoid, the change of its inductance would be somewhat less than that computed for the spherical coil.

### VII. EXTERNAL OBJECT

Fig. 4(b) shows a spherical object (of magnetic ratio  $k_1$ ) external to a spherical coil. The reaction of this object on the inductance of the coil forms one basis for the detection of metal bodies, exemplified by the mine detector.

The formulas for this effect are the same as for the internal core, except for the different coefficient of coupling. In (15)–(17) above, we can change:

$$\text{from } (a_1/a_2)^3 \text{ to } (a_1 a_2 / r^2)^3.$$

The inductance of the coil becomes

$$L_2 = \frac{2\pi}{9} \mu_0 a_2 n_2^2 \left[ 1 + 2 \frac{k_1 - 1}{k_1 + 2} (a_1 a_2 / r^2)^3 \right]. \quad (18)$$

The last factor shows the change of inductance caused by the external object; the change is inversely proportional to the sixth power of the distance.

As an example, take the external object to be an antimagnetic (conducting) sphere, and take the dimensions  $a_1 = a_2 = r/10$ . The change of inductance is 1 part in a million.

### VIII. SPHERICAL SHIELD

Fig. 5(a) shows a spherical coil ( $a_1$ ) enclosed by an external spherical shield ( $a_2$ ) that is both coaxial and concentric. The shield is essentially a spherical coil on short-circuit. Its purpose is to confine the magnetic field of the coil inside, that is, to act as a magnetic shield between the inside space and the outside space. The magnetic field that penetrates the shield and reaches the outside space is sampled by the coaxial outside coil ( $a_3$ ).

If the shield has a conductor thickness less than the skin depth ( $d_2 < \delta_2$ ), the shielding action can be represented by the equivalent network shown in Fig. 5(b). (See [2].) In this network, the coupling among three inductors is uniquely reduced to a single transformer with unity coupling, supplemented by a "leakage inductance" in each circuit. The leakage inductance of  $L_2$  becomes zero if  $k_{12}k_{23} = k_{13}$ . This is found to be true for the three spherical coils in Fig. 5(a). Therefore the leakage inductance of  $L_2$  is zero, leaving its resistance  $R_2$  as a direct shunt on the coil  $L_2$  of the coupling transformer. If this resistance were zero, there would be zero coupling between  $L_1$  and  $L_3$ , and hence zero magnetic field outside the spherical shield  $L_2$ .

There is a small amount of leakage through the shield if  $R_2 \ll \omega L_2$ , or  $p_2 \ll 1$ . Assuming that  $L_1$  and  $L_3$  are not too close to the shield  $L_2$ , the short-circuit on  $L_2$  reduces the coupling therebetween by the factor  $p_2$ . Therefore this factor may be denoted the "leakage fraction," and its value is given by (6) applied to  $L_2$ .

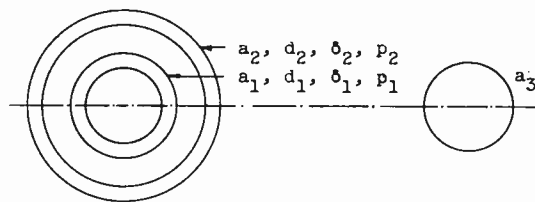
By ordinary circuit theory, it is easy to compute the properties of the inside coil  $L_1$  as modified by the presence of the shield effectively decreasing the inductance and increasing the resistance. The modified properties are:

$$L_1' = L_1(1 - k_{12}^2) \quad (19)$$

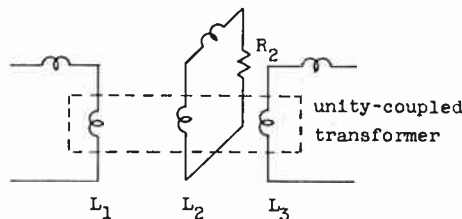
$$R_1' = R_1 \left( 1 + k_{12}^2 \frac{R_2 L_1}{R_1 L_2} \right) = R_1(1 + k_{12}^2 p_2 / p_1) \quad (20)$$

$$p_1' = p_1 \frac{1 + k_{12}^2 p_2 / p_1}{1 - k_{12}^2} \quad (21)$$

$$k_{12}^2 = V_1 / V_2; \quad k_{12}^2 p_2 / p_1 = \frac{a_1^4 d_1 \delta_2^2}{a_2^4 d_2 \delta_1^2}. \quad (22)$$



(a) Geometry.



(b) Equivalent network.

Fig. 5—Spherical shield.

The last expression shows how much the power factor of the shield is coupled into the coil inside.

A spherical shell of conducting material behaves like a spherical coil on short-circuit, so the formulas are valid for this kind of a shield.

If the thickness of the shield is greater than the skin depth ( $d_2 > \delta_2$ ), the leakage is reduced by the skin effect. The modified leakage fraction becomes

$$p_s = p_2(2\sqrt{2}) \frac{d_2}{\delta_2} \exp - \frac{d_2}{\delta_2} = \sqrt{2} \frac{3\delta_2}{a_2} \exp - \frac{d_2}{\delta_2}. \quad (23)$$

It is noted that the formulas give nearly equal values of  $p_2$  and  $p_s$ , as they should, if  $d = \delta$ .

If completely subject to the skin effect, the shield appears to have a higher power factor as follows, substituting  $\delta$  for  $d$  in (6):

$$p_2 = \frac{3\delta_2}{2a_2}. \quad (24)$$

Substituting this for  $p_2$  in (21) and (22), but leaving  $p_1$  the same (no skin effect in  $L_1$ ):

$$k_{12}^2 p_2 / p_1 = \frac{a_1^4 d_1 \delta_2}{a_2^4 \delta_1^2}. \quad (25)$$

As an example, take a spherical shell of copper, operating at 15 kc.

$$a_2 = 25 \text{ mm}; \quad d_2 = \delta_2 = 0.5 \text{ mm}.$$

This is a case of marginal skin effect. The leakage fraction is:

$$p_2 = 0.03 \text{ [see (6)]}$$

$$p_s = 0.03(1.04) = 0.0312 \text{ [see (23)].}$$

The shielding by a closed metal shell is noncritical to the shape, whereas the shielding by a coil on short-circuit is critical to both shape and orientation.

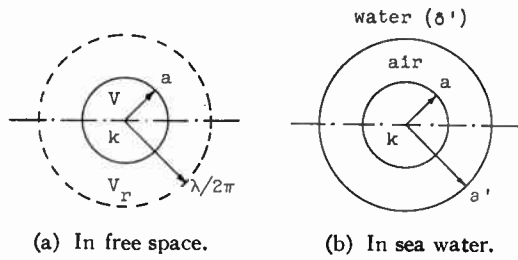


Fig. 6—Spherical coil as small antenna.

IX. SPHERICAL ANTENNA

A spherical coil that is much smaller than the radian-sphere in space has radiation properties that are easily computed. Fig. 6(a) shows such a coil in relation to the radian-sphere. (See [14].)

The reactance may be expressed in terms of the wavelength:

$$\omega L = \frac{4\pi^2}{9} R_c \frac{an^2}{\lambda} \frac{3}{1 + 2/k} \quad (26)$$

The radiation resistance is computed from the basic formula for a small coil:

$$R = \frac{2}{3} \frac{R_c}{4\pi} \left( \frac{2\pi\sqrt{A}}{\lambda} \right)^4 = 20 \left( \frac{2\pi\sqrt{A}}{\lambda} \right)^4 \quad (27)$$

This is in terms of the total effective area of turns, which is, in the spherical coil,

$$A = \frac{2}{3} \pi a^2 n \frac{3}{1 + 2/k} \quad (28)$$

One property of a small antenna is the radiation power factor, which depends primarily on the size and is independent of the number of turns [6]. For the spherical coil, the radiation power factor is:

$$p = \frac{R}{\omega L} = \left( \frac{2\pi a}{\lambda} \right)^3 \frac{3}{1 + 2/k} = \frac{V}{V_r} \frac{1}{1 + 2/k} \quad (29)$$

The greatest value would be obtained with a perfect magnetic core ( $k = \infty$ ), in which case the radiation power factor would equal the volume ratio of the two spheres. This is an upper limit that may be used as a standard of comparison for practical antennas. The formula for this ideal is the ultimate in simplicity, and this power factor can nearly be realized in practice.

Fig. 6(b) shows another case, in which a spherical coil is used as a small antenna submerged in sea water. The water surrounds a spherical radome (of radius  $a'$ ) enclosing the coil. The radome is assumed to be much smaller than the radianlength or skin depth ( $\delta'$ ) in the water. Then the nearby conduction in the water is limited by its conductivity rather than the skin effect [18].

The currents induced in the water are computed for a continuous series of spherical shells. The resulting dis-

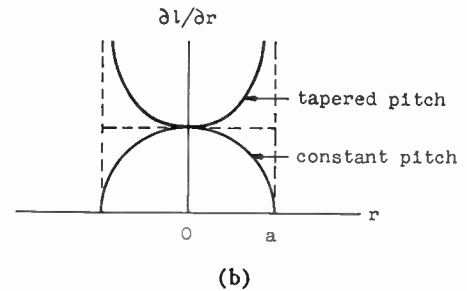
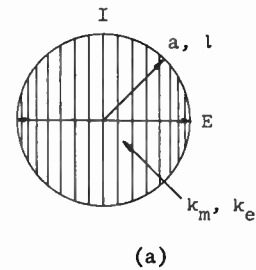


Fig. 7—Self-resonant spherical coil.

sipation in the water determines the radiation power factor, which is found to have the following value:

$$p = \frac{a^3}{a'\delta'^2} \frac{2}{1 + 2/k} \quad (30)$$

The principal factor is the ratio of the coil volume over another volume determined by the radome size and the skin depth in the water.

Submersion of this antenna reduces its interception area, as referred to the wave power density above the water. The free-space interception area is 3/2 of one radiancircle in free space. If this antenna is submerged to a depth several times the radome radius but much less than the skin depth in the water, its interception area is reduced to

$$\frac{3\pi}{2} a'\delta' \quad (31)$$

This depends not on the coil size, but on the radome size and the skin depth.

X. SELF-RESONANT COIL

A certain form of winding on a spherical coil leads to a self-resonant inductor with the same pattern of magnetic and electric fields. By this we mean that each field inside the sphere is uniform, and outside has the field pattern of a small dipole.

Fig. 7(a) shows such a spherical coil, with its core having magnetic and electric ratios  $k_m$  and  $k_e$ . All the current in the winding is the capacitive current in the inner and outer space. The middle turns carry maximum current, while the current tapers off toward the end turns in proportion to the decreasing area per turn. The uniform fields inside require that the current density be the same as in the simple spherical inductor with

constant current (and constant axial density of current). Therefore the pitch of winding must be reduced in the ratio of the area per turn. This rule leads to an indefinitely large number of turns but a finite length of wire.

Fig. 7(b) shows the basis for computing the total length of wire on a coil of tapered pitch. For reference, the lower curve gives the axial distribution of length of wire for constant pitch. In this case, the axial density ratio ( $\partial l/\partial r$ ) is proportional to the radius of the turns, hence the semicircular shape. For the self-resonant coil, the pitch is reduced in proportion to the area per turn, or the radius-squared, so the length of wire has an axial density inversely proportional to the radius of the turns; this is shown by the upper curve. The total length of wire is proportional to the area under these curves. Since the upper curve has twice the area of the lower curve, the self-resonant coil with tapered pitch has a total length of wire twice as great as the simple coil with constant pitch (assuming the same pitch in the middle).

As a measure of the varying pitch, we may write the formulas in terms of the pitch ( $c$ ) of the middle turns. The simple spherical coil of uniform axial pitch ( $c=2a/n$ ) has its inductance given by substituting this relation in (4), also changing symbols  $k$  to  $k_m$  and  $k'$  to 1.

$$n = 2a/c \tag{32}$$

$$L = \frac{2\pi}{9} \mu_0 a n^2 \frac{3}{1 + 2/k_m} = \frac{8\pi}{9} \mu_0 \frac{a^3}{c^2} \frac{3}{1 + 2/k_m} \tag{33}$$

In the modified spherical coil with tapered pitch of winding, the same maximum current in the middle turns is associated with the same magnetic field, so it sees the same amount of inductance.

In the simple spherical coil, the axial gradient of the voltage along the winding varies with the area per turn, in the manner of Fig. 1(c), so the average gradient is  $\frac{2}{3}$  of the middle gradient.

The tapered pitch changes the voltage distribution, making the axial gradient constant, because the smaller area per turn toward the ends is just compensated by the greater density of turns. Therefore the average gradient is equal to the middle gradient and the total voltage from pole to pole is  $3/2$  as great for the same maximum current in the middle turns. This voltage is

$$E = \frac{3}{2} I L \omega \tag{34}$$

in terms of  $L$  given by (33).

The capacitive current inside the coil has its maximum value ( $I$ ) in the middle turns, equal to that caused by the total voltage ( $E$ ) in a cylindrical condenser of area  $\pi a^2$  and spacing  $2a$ . This capacitance is

$$\text{cyl } C = k_e \epsilon_0 \frac{\pi a^2}{2a} = \frac{\pi}{2} k_e \epsilon_0 a. \tag{35}$$

The current in this internal capacitance is

$$I(\text{in}) = E\omega(\text{cyl } C) = E\omega\epsilon_0 \frac{\pi}{2} a k_e. \tag{36}$$

Just as the magnetic flux path outside the coil has an effective length  $\frac{1}{2}$  as great as inside, the same is true of the electric flux path. But the two electric flux paths are in parallel, not in series. Therefore the total capacitive current (in the middle turns) is

$$I = E\omega\epsilon_0 \frac{\pi}{2} a(k_e + 2). \tag{37}$$

In the tapered winding, as explained with reference to Fig. 7(b), the length of wire is found to be twice as great for the same middle pitch of winding. This length is

$$l = \frac{\pi}{2} 2\pi a \frac{2a}{c} = 2\pi^2 a^2/c \tag{38}$$

$$c = 2\pi^2 a^2/l. \tag{39}$$

Substituting in (33),

$$L = \frac{2}{9\pi^3} \mu_0 \frac{l^2}{a} \frac{3}{1 + 2/k_m}. \tag{40}$$

To determine the condition for resonance, eliminate  $E$  and  $I$  from (34) and (37), then express  $\omega$  in terms of  $\lambda$ , and finally substitute for  $L$  from (40):

$$1 = \frac{3}{2} L\omega^2\epsilon_0 \frac{\pi}{2} a(2 + k_e) = 3\pi^3 \frac{L a}{\mu_0 \lambda^2} (2 + k_e) \tag{41}$$

$$l = \frac{\lambda}{2} \sqrt{\frac{1 + 2/k_m}{1 + k_e/2}}. \tag{42}$$

This shows that a coiled length of wire is self-resonant at a frequency such that its length is about  $\frac{1}{2}$  wavelength, which is the well-known rule for a straight wire.

An ideal self-resonant spherical coil is conceived to be one having no energy stored inside ( $k_e=0, k_m=\infty$ ). Its resonance corresponds exactly to a wire length of  $\frac{1}{2}$  wavelength. Its external electric and magnetic fields store equal amounts of energy in the same pattern so they radiate equal amounts of power. They combine to radiate a wave that is circularly polarized [7].

The radiation power factors of the magnetic and electric fields, for any core properties, are

$$p_m = \frac{V/V_r}{1 + 2/k_m}; \quad p_e = \frac{V/V_r}{1 + k_e/2}. \tag{43}$$

For an air core ( $k_m=k_e=1$ ) it appears that the electric field radiates twice as much power as the magnetic field. However, if  $k_m k_e=4$ , the two fields radiate equal amounts of power; this is therefore a general condition for circular polarization of the radiation. This is realizable, for example, with a dielectric core such that  $k_e=4, k_m=1$ .

This same condition is one which causes the coil to resonate with a half-wavelength of wire, as indicated

by (42). In this type of coil with an air core, resonance corresponds to  $l = \lambda/\sqrt{2}$ .

In a self-resonant coil having  $l = \lambda/2$ , a dimensional relationship from (38) and (39) is

$$\lambda c = 4\pi^2 a^2 = (6\pi V)^{2/3}. \quad (44)$$

If such a coil has enough turns to be recognized as a current sheet ( $c \ll 2a$ ), its volume is much less than the radiansphere so its radiation power factor is very small.

### XI. EQUIVALENT SPHERICAL COIL

Any coil in a certain class has an equivalent spherical coil that may be specified on a logical basis. This class of coils includes every coil that has an air core and is made up of any number of turns wound in the same direction and located in parallel planes. The simpler cases include ordinary coils with coaxial circular turns, such as the helix of one or more layers.

A spherical coil is said to be equivalent to any coil in this class if it has the same inductance ( $L$ ) and the same far field, the latter requiring the same total area of turns ( $A$ ). In terms of these two properties, the equivalent spherical coil is formulated from (4) and (28) by solving for the following dimensions:

$$a = \left( \frac{\mu_0 A^2}{2\pi L} \right)^{1/3} \quad (45)$$

$$n = \left( \frac{6L^2}{\pi\mu_0^2 A} \right)^{1/3}. \quad (46)$$

The diameter ( $2a$ ) of this equivalent spherical coil will always be less than the maximum dimension of the space occupied by the nonspherical coil.

As an example, we may take the familiar case of a long solenoid. The equivalent sphere is found to be one that has a volume slightly greater than  $\frac{2}{3}$  of that of the solenoid. Therefore its diameter is greater than the solenoid diameter but much less than the solenoid length.

The equivalent spherical coil, as specified, has the same radiation power factor when regarded as a small antenna. In the case of two coils coupled in either coaxial or coplanar relationship, at a distance much greater than their radii, the two equivalent spherical coils have the same coefficient of coupling.

### XII. CONCLUSION

The spherical coil is an interesting idealized inductor whose properties can be expressed exactly by remarkably simple formulas. Its field configurations are the simplest conceivable, as are also its formulas for coeffi-

cient of coupling and power factor of radiation. It is a basis for computing the shielding effect of a closed conducting shell (nonmagnetic). A special winding yields a corresponding simple form of self-resonant coil, whose length of wire is near  $\frac{1}{2}$  wavelength at resonance. Referring to the spherical forms in general, the exact formulas for various properties yield simple rules that are approximately applicable to practical inductors such as short solenoids.

### XIII. REFERENCES

- [1] Maxwell, J. C. *Electricity and Magnetism*. New York: Oxford University Press, 3rd ed., Vol. 2, 1892. (Spherical coil, pp. 304-308.)
- [2] Wheeler, H. A., and MacDonald, W. A. "Theory and Operation of Tuned-Radio-Frequency Coupling Systems," *PROCEEDINGS OF THE IRE*, Vol. 19 (May, 1931), pp. 738-805. (Leakage inductance of 3-coil transformer.)
- [3] Wheeler, H. A. "The Properties of Spherical Coils and Objects," Hazeltine Electronics Corp., Little Neck, N. Y., Rep. No. 1230W, August 8, 1941.
- [4] ———. "Formulas for the Skin Effect," *PROCEEDINGS OF THE IRE*, Vol. 30 (September, 1942), pp. 412-424.
- [5] Burgess, R. E. "Iron-Cored Loop Receiving Aerial," *Wireless Engineer*, Vol. 23 (June, 1946), pp. 172-178. (Spherical coil and core.)
- [6] Wheeler, H. A. "Fundamental Limitations of Small Antennas," *PROCEEDINGS OF THE IRE*, Vol. 35 (December, 1947), pp. 1479-1484. (Radiation power factor.)
- [7] ———. "A Helical Antenna for Circular Polarization," *PROCEEDINGS OF THE IRE*, Vol. 35 (December, 1947), pp. 1484-1488.
- [8] Chu, L. J. "Physical Limitations of Omnidirectional Antennas," Research Laboratory of Electronics, Massachusetts Institute of Technology, Cambridge, Mass., Tech. Rep. No. 64, May 1, 1948. (Radiation  $Q$  of space outside of sphere around electric dipole.)
- [9] Harnwell, G. P. *Principles of Electricity and Electromagnetism*. New York: McGraw-Hill Book Co., Inc., 2nd ed., 1949. (Mutual inductance between coaxial coils, p. 329.)
- [10] Smythe, W. R. *Static and Dynamic Electricity*. New York: McGraw-Hill Book Co., Inc., 2nd ed., 1950. (Coils on spherical forms, pp. 314-315.)
- [11] Wait, J. R. "The Magnetic Dipole Antenna Immersed in a Conducting Medium," *PROCEEDINGS OF THE IRE*, Vol. 40 (October, 1952), pp. 1951-1952. (In a spherical cavity.)
- [12] Wheeler, H. A. "Universal Skin-Effect Chart for Conducting Materials," *Electronics*, Vol. 25 (November, 1952), pp. 152-154. (Including sea water.)
- [13] Wait, J. R. "The Receiving Loop with a Hollow Prolate Spheroidal Core," *Canadian Journal of Technology*, Vol. 31 (June, 1953), pp. 132-137. (Ratio of increase of induction by core.)
- [14] Wheeler, H. A. "The Radiansphere Around a Small Antenna," Wheeler Laboratories, Inc., Great Neck, N. Y., Rep. No. 670, March 8, 1955. Presented at The Johns Hopkins University, Baltimore, Md., December 2, 1954. (Radiation power factor of spherical coil.)
- [15] Rumsey, V. H., and Weeks, W. L. "Electrically Small, Ferrite-Loaded Loop Antennas," 1956 IRE CONVENTION RECORD, Part 1, pp. 165-170. (Radiation  $Q$  of prolate spheroid.)
- [16] Wheeler, H. A. "The Spherical Coil as an Inductor, Shield, or Antenna," presented at staff meeting, Wheeler Laboratories, Inc., Great Neck, N. Y., September 25, 1956.
- [17] Cruzan, O. R. "Radiation Properties of a Spherical Ferrite Antenna," Diamond Ordnance Fuze Laboratories, Washington, D. C., Tech. Rep. No. 387, October 15, 1956. (One-turn loop around spherical iron core.)
- [18] Wheeler, H. A. "Fundamental Limitations of a Small VLF Antenna for Submarines," presented at National Bureau of Standards VLF Symposium, Boulder, Colo., January 23-25, 1957. *IRE TRANSACTIONS ON ANTENNAS AND PROPAGATION*, Vol. AP-6 (January, 1958), pp. 123-125.



# Error Probabilities for Binary Symmetric Ideal Reception through Nonselective Slow Fading and Noise\*

G. L. TURIN†, MEMBER, IRE

**Summary**—One of two correlated, equal energy, equiprobable waveforms is transmitted through a channel during a given time interval. The signal is corrupted in the channel by slowly-varying, frequency-nonsselective fading and by additive, Gaussian noise. On reception, the corrupted signal is processed by an ideal receiver, which guesses that the transmitted waveform was the one which it computes to be *a posteriori* most probable. Expressions for the probability of committing an error in making such a guess are derived for both coherent and noncoherent receivers; these are studied in detail, and some general trends and system design considerations are noted. In an illustrative example, the results are applied to binary frequency-shift keyed (FSK) systems with various pulse shapes and frequency separations.

## I. INTRODUCTION

THE problem we consider here is of a restricted nature (*binary, symmetric system; nonselective, slow fading*); yet, despite this, the results of our analysis will have fairly wide application to practical systems. For instance, in an illustrative example, we use a special case of one of the results to determine the effects of pulse shape and frequency separation on the performance of an FSK teletype system working through a scatter-propagation link.

A block diagram of the communication system studied is shown in Fig. 1. We postpone a detailed description of the various blocks until the next section; a brief description will suffice to give a statement of the problem.

At the transmitter, a choice is made between two narrow-band signals,  $\xi_1(t)$  and  $\xi_2(t)$ , and one is transmitted into the channel. We assume that both signals are zero outside of some time interval, say  $0 \leq t \leq T$ . Within this interval, however, the waveshapes of the signals are essentially arbitrary: they may be simple sine wave pulses of different frequencies, or they may be of considerable complexity. The two signals may be uncorrelated or they may be highly correlated. In fact, the only restrictions we place on the signals, aside from requiring finite time durations, are that they have equal probabilities of transmittal, and that they have the same energy. These are the requirements of *symmetry*, for it turns out that when they are satisfied,

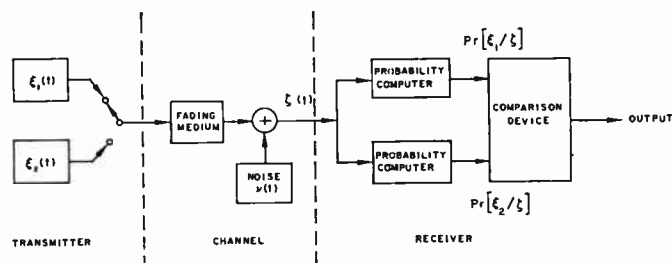


Fig. 1—The system under consideration.

the probability of mistaking signal 1 for signal 2 at the receiver is the same as that of mistaking signal 2 for signal 1.

The transmitted signal first passes through a linear medium which fades in a frequency-nonsselective way. That is to say, the whole band of frequencies occupied by the two signals is acted on uniformly by the medium; there is no possibility of simultaneous constructive interference at one frequency and destructive interference at another. Put another way, if there is more than one transmission path, the difference of delays of any pair of paths must be much less than the reciprocal of the width of the band of frequencies occupied by the signals.

The amount of fading at any instant is, of course, a random quantity. It is assumed, however, that it does not vary appreciably for the duration of the transmitted signal, and this is what we mean by *slow fading*.

After passing through the fading medium, the transmitted signal is further perturbed by additive noise, which we assume is white, stationary, Gaussian, and statistically independent of the fading medium. The resultant signal we call  $\zeta(t)$ ; it is the received signal.

The task of the receiver, which has available replicas of the two possible transmitted waveforms but does not know which was actually sent, is to guess, with minimum probability of error, which signal was transmitted. (We shall call a receiver which does this an *ideal receiver*.) It does this by operating on  $\zeta(t)$ , and it can be shown<sup>1</sup> that this operation consists of computing the *a posteriori* probabilities,  $Pr[\xi_1/\zeta]$  and  $Pr[\xi_2/\zeta]$ , of the two signals, and choosing the one with the larger probability. That is, the receiver always

\* Original manuscript received by the IRE, December 30, 1957; revised manuscript received, March 6, 1958. This paper is based heavily on previous work done by the author at Lincoln Lab., and at the Dept. of Elec. Eng., Mass. Inst. Tech., Cambridge, Mass., with the joint support of the U. S. Army, Navy, and Air Force. The new results presented here were obtained at Hughes Aircraft Co., Culver City, Calif., and were supported in small part by the U. S. Air Force.

† Hughes Res. Labs., Culver City, Calif.

<sup>1</sup> D. Van Meter and D. Middleton, "Modern approaches to reception in communication theory," IRE TRANS. ON INFORMATION THEORY, PGIT-4, pp. 119-145, sections 3.1 and 3.2; September, 1954.

guesses that the transmitted signal was the one which seems most probable on the basis of analysis of the received waveform.

We are mainly concerned with the evaluation of the probability of committing an error in making such a guess. In fact, the principal new result of this paper is (16), which is a general expression for this probability of error. The expression differs from previous results in that a broader class of fading phenomena (which includes, as extremes, the nonfading case and the Rayleigh-fading case) is postulated, and nonzero correlation between the two signals is allowed. The expression of course reduces to previous results in special cases, and these special cases will be pointed out.

A second goal we set is that of studying the general error probability expression in the hopes of extracting from it general trends and design rules. We shall, for example, find that the incidence even of what is normally only a moderate amount of fading markedly deteriorates the performance of the system and also makes inadvisable the use of such techniques as coherent reception and negative correlation between the two signals.

## II. DETAILED MODEL OF SYSTEM

Let us now, having stated the problem, go back and consider the various blocks in Fig. 1 in more detail.

### A. The Signals

We have assumed that the two signals are narrow-band waveforms which are zero outside the interval  $0 \leq t \leq T$ . A representation of these signals which is most convenient for our purposes is the complex representation described by Woodward.<sup>2</sup> We represent the two signals as products of complex low-pass modulation waveforms and cisoidal carriers:

$$\begin{aligned} \xi_1(t) &= x_1(t)e^{j2\pi f_0 t} \\ \xi_2(t) &= x_2(t)e^{j2\pi f_0 t} \end{aligned} \quad (1)$$

where  $f_0$  is a suitably defined carrier frequency. It is the real parts of the representations in (1) which correspond to the actual physical signals; these real parts are in the form of a more familiar representation of narrow-band signals:<sup>3</sup>

$$\begin{aligned} \hat{\xi}_m(t) &= \hat{x}_m(t) \cos 2\pi f_0 t - \hat{x}_m(t) \sin 2\pi f_0 t \\ &= |x_m(t)| \cos \left( 2\pi f_0 t + \tan^{-1} \frac{\hat{x}_m(t)}{\hat{x}_m(t)} \right) \quad (m = 1, 2) \end{aligned} \quad (2)$$

<sup>2</sup> P. M. Woodward, "Probability and Information Theory, with Applications to Radar," McGraw-Hill Book Co., Inc., New York, N. Y.; 1953.

<sup>3</sup> S. O. Rice, "Mathematical analysis of random noise," *Bell Sys. Tech. J.*, vol. 23, pp. 282-333; July, 1944, and vol. 24, pp. 46-157, January, 1945. [See section 3.7.] This paper also appears in "Selected Papers on Noise and Stochastic Processes," ed. N. Wax, Dover Publications, Inc., New York, N. Y.; 1954.

where we have used " $\hat{\cdot}$ " to denote "real part of" and " $\sim$ " to denote "imaginary part of." Note that the complex modulation waveforms,  $x_m(t)$ , contain both amplitude and phase modulations of the carrier in the form of  $|x_m(t)|$  and  $\tan^{-1}\hat{x}_m(t)/\hat{x}_m(t)$ , respectively. For an FSK system, as an example,

$$\begin{aligned} x_1(t) &= A(t)e^{j\pi\Delta f t}, \\ x_2(t) &= A(t)e^{-j\pi\Delta f t}, \end{aligned} \quad (3)$$

where  $A(t)$  is some (real) pulse envelope waveform and  $\Delta f$  is the frequency separation of the "mark" and "space" channels.

The energies of the two signals are assumed equal and may be related to the complex representations of (1) by<sup>4</sup>

$$E = \frac{1}{2} \int_0^T |\xi_1(t)|^2 dt = \frac{1}{2} \int_0^T |\xi_2(t)|^2 dt. \quad (4)$$

An important quantity which relates the two signals is the complex correlation coefficient. We define it as

$$\lambda = \frac{1}{2E} \int_0^T \xi_1^*(t)\xi_2(t) dt = \frac{1}{2E} \int_0^T x_1^*(t)x_2(t) dt. \quad (5)$$

The real part of this,  $\hat{\lambda}$ , is the value of the normalized cross-correlation function of the signals at the origin.<sup>4</sup> The magnitude,  $|\lambda|$ , is the value of the envelope of this function at the origin.<sup>4</sup> It is easily shown by means of the Schwarz inequality that  $|\lambda| \leq 1$ .

$\lambda$  is a key parameter in the expressions for error probability which we shall derive; it describes the amount of "sameness" of the signals, *i.e.*, the difficulty the receiver has in telling them apart. For example, for the FSK signals described by (3), we have from (4) and (5):

$$\lambda_{\text{FSK}} = \frac{\int_0^T A^2(t)e^{-j2\pi\Delta f t} dt}{\int_0^T A^2(t) dt}. \quad (6)$$

The cross-correlation coefficient is thus directly related to the frequency separation of the "mark" and "space" channels; for  $\Delta f = 0$  we have  $\lambda = 1$ , the case of indistinguishable signals.

### B. The Fading Medium

The model for the fading medium perhaps can be described best by indicating what happens to a signal which passes through it. Suppose  $\xi_m(t) = x_m(t)e^{j2\pi f_0 t}$  is transmitted. The output of the fading model we are considering may then be represented as

$$\eta_m(t) = ax_m(t - \tau)e^{j(2\pi f_0 t - \theta)}. \quad (7)$$

That is, the fading medium comprises a frequency non-selective path which is characterized by three quantities:  $a$ , the strength;  $\tau$ , the modulation delay; and  $\theta$ , the

<sup>4</sup> Cf. Appendix I, letting  $\tau = 0$ .

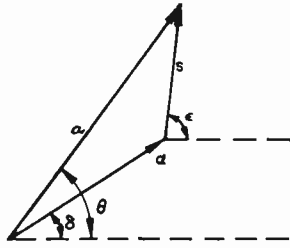


Fig. 2—Relationships among strengths and phase shifts of the fading medium.

carrier phase shift.<sup>5</sup> These quantities are random, and must therefore be described in terms of probability density distributions. Since we have assumed slow fading,  $a$ ,  $\theta$ , and  $\tau$  do not change appreciably during the transmission interval. Hence, the first-order joint density distribution,  $pr[a, \theta, \tau]$ , of the three path parameters will suffice to describe the fading medium.<sup>6</sup>

We assume here that  $\tau$  is known to the receiver, either *a priori* or as a result of measurements.<sup>7</sup> Then, assuming that  $a$  and  $\theta$  are statistically independent of  $\tau$ , only the distribution  $pr[a, \theta]$  is necessary to complete the description of the medium.

We further assume that the transmission path is composed of a *fixed* component and a *random* component, so that (7) may be written as

$$\eta_m(t) = x_m(t - \tau)[\alpha e^{-j\delta} + s e^{-j\epsilon}]e^{j2\pi f_0 t}; \quad (8)$$

$\alpha$  and  $\delta$  are the strength and phase shift of the fixed component, respectively, while  $s$  and  $\epsilon$  are the same quantities for the random component. The relationships among the quantities  $\alpha$ ,  $\delta$ ,  $s$ ,  $\epsilon$ ,  $a$ , and  $\theta$  are depicted vectorially in Fig. 2.

For the joint density distribution of  $s$  and  $\epsilon$  we postulate:

$$pr[s, \epsilon] = \begin{cases} \frac{s}{2\pi\sigma^2} \exp\left[-\frac{s^2}{2\sigma^2}\right] & \left\{ \begin{array}{l} 0 \leq s \leq \infty \\ 0 \leq \epsilon \leq 2\pi \end{array} \right\} \\ 0 & \text{elsewhere} \end{cases} \quad (9)$$

<sup>5</sup> Considering the modulation delay and carrier phase shift of the path as independent entities is a convenient device and is, moreover, justifiable on a physical basis: most nonselective transmission paths (e.g., nonselective scatter paths) which fluctuate randomly do so because of the alternate constructive and destructive interference of a large number of "subpaths" whose delays differ from one another by amounts which are small compared to the reciprocal of the transmission bandwidth. As far as the modulation is concerned, all of these subpaths have very nearly the same delay; this delay we call  $\tau$ . As far as the carrier is concerned, however, the subpaths have delays which are greatly different. Thus, small fluctuations in the subpath delays will not noticeably affect the modulation delay, but may greatly change the carrier phase. Therefore, we may speak of changes in  $\theta$  for a "fixed"  $\tau$ . For further discussion of this point, see footnotes 15 and 16.

<sup>6</sup> Fast fading has been considered in a special case (no fixed component) by R. Price, "Optimum detection of random signals in noise, with application to scatter-multipath communication," IRE TRANS. ON INFORMATION THEORY, vol. IT-2, pp. 125-135; December, 1956. Part II of Price's paper, to be published, contains error probability analyses of the ideal receiver in this special case. Also see R. Price and P. E. Green, Jr., "A communication technique for multipath channels," PROC. IRE, vol. 46, pp. 555-570; March, 1958.

<sup>7</sup> G. L. Turin, "On the estimation in the presence of noise of the impulse response of a random, linear filter," IRE TRANS. ON INFORMATION THEORY, vol. IT-3, pp. 5-10; March, 1957.

That is,  $s$  and  $\epsilon$  are independent quantities, the first being Rayleigh distributed with mean-square  $2\sigma^2$ , and the second uniformly distributed over the interval  $(0, 2\pi)$ . It is easily shown<sup>8</sup> that the joint distribution of the length and angle of the sum of the fixed vector ( $\alpha, \delta$ ) and the random vector ( $s, \epsilon$ ) described by (9) is

$$pr[a, \theta] = \begin{cases} \frac{a}{2\pi\sigma^2} \exp\left[-\frac{a^2 + \alpha^2 - 2\alpha a \cos(\theta - \delta)}{2\sigma^2}\right] & \left\{ \begin{array}{l} 0 \leq a \leq \infty \\ 0 \leq \theta - \delta \leq 2\pi \end{array} \right\} \\ 0 & \text{elsewhere} \end{cases} \quad (10)$$

The marginal distribution of the strength  $a$ , obtained by integrating (10) over  $\theta$ , is given by

$$pr[a] = \begin{cases} \frac{a}{\sigma^2} \exp\left[-\frac{a^2 + \alpha^2}{2\sigma^2}\right] I_0\left(\frac{\alpha a}{\sigma^2}\right) & 0 \leq a \leq \infty, \\ 0 & a < 0 \end{cases} \quad (11)$$

where  $I_0$  is the zeroth-order modified Bessel function of the first kind. Rice<sup>8</sup> gives (normalized) curves of this distribution with parameter  $\gamma = \alpha/\sigma$ ; these curves are reproduced in Fig. 3. Curves of the marginal distribution  $pr[\theta]$ , given by Middleton,<sup>9</sup> are reproduced with modifications<sup>9</sup> in Fig. 4. As is to be expected, the smaller the random component of the transmission path is compared to the fixed component ( $\sigma \rightarrow 0$ ), the more sharply the  $a$  and  $\theta$  distributions cluster around the values  $\alpha$  and  $\delta$ , respectively.

The joint distribution of (10) appears to be a good description of many "single"-path<sup>10</sup> propagation conditions which are encountered. For ionospheric radio links above the  $muf$ <sup>11</sup> and for tropospheric radio links,<sup>12</sup> experimental results indicate that the fading is Rayleigh distributed and quasi-stationary for time intervals of the order of minutes; this corresponds to letting  $\alpha = 0$  in (10), and considering that  $\sigma$  changes slowly over many minutes (*very* much longer than the transmission interval,  $T$ ). For ionospheric radio links below the  $muf$  there is evidence that both fixed and random components are present ( $\alpha \neq 0, \sigma \neq 0$ ),<sup>13,14</sup> although the physi-

<sup>8</sup> S. O. Rice, *op. cit.*, sec. 3.10.

<sup>9</sup> D. Middleton, "Some general results in the theory of noise through non-linear devices," *Quart. Appl. Math.*, vol. 5, pp. 445-498; Fig. 4(a); January, 1948. L. A. Rondinelli has called the author's attention to inaccuracies in Middleton's curves; these have been corrected in Fig. 4.

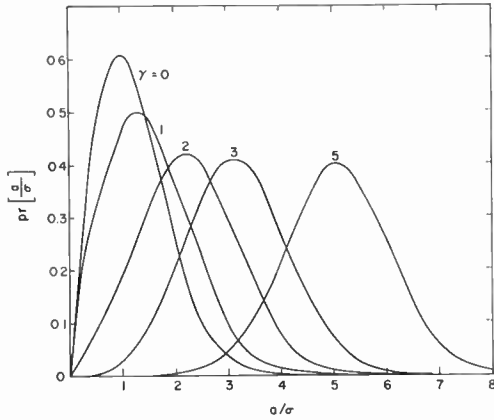
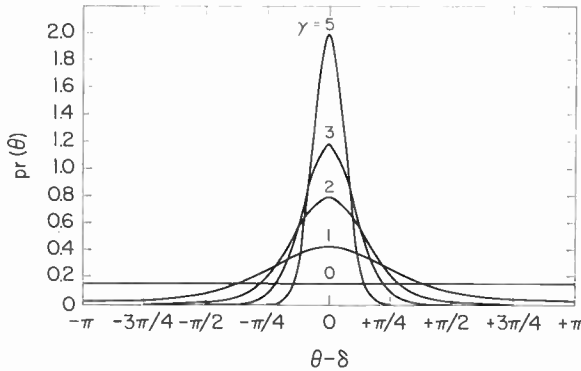
<sup>10</sup> However, a single path may consist of many subpaths (see footnote 5); hence, the quotation marks.

<sup>11</sup> R. A. Silverman and M. Balsler, "Statistics of electromagnetic radiation scattered by a turbulent medium," *Phys. Rev.*, vol. 96, pp. 560-563; November, 1954.

<sup>12</sup> K. Bullington, W. J. Inkster, and A. L. Durkee, "Results of propagation tests at 505 mc and 4090 mc on beyond-horizon paths," PROC. IRE, vol. 43, pp. 1306-1316; October, 1955.

<sup>13</sup> R. W. E. McNicol, "The fading of radio waves on medium and high frequencies," *Proc. IEE*, vol. 96, pt. 3, pp. 517-524; November, 1949. Also see D. G. Brennan and M. L. Phillips, "Phase and Amplitude Variability in Medium-Frequency Ionospheric Transmission," M.I.T., Lincoln Lab., Lexington, Mass., Tech. Rep. 93; September 16, 1957.

<sup>14</sup> R. Price, "The autocorrelogram of a complete carrier wave received over the ionosphere at oblique incidence," PROC. IRE, vol. 45, pp. 879-880; June, 1957.

Fig. 3—Normalized marginal distribution of  $a$ .Fig. 4—Marginal distribution of  $\theta$ .

cal nature of these is not completely clear at present; the two components are often called, respectively, the specular and the scatter components.

The three parameters,  $\alpha$ ,  $\sigma$ , and  $\delta$  of the distribution (10) have useful interpretations.  $\alpha$  is the strength of the fixed component and  $\sqrt{2}\sigma$  is the rms strength of the random component; if average power  $P$  is transmitted, the received average power is  $(\alpha^2 + 2\sigma^2)P$ .<sup>8</sup> We define the ratio  $\gamma = \alpha/\sigma$ ;  $\gamma^2$  is thus twice the ratio of the average power received via the fixed component to the average power received via the random component.  $\delta$  is the mean or expected phase shift of the path.

### C. The Additive Noise

We assume that the additive noise is Gaussian, statistically stationary, independent of the fading medium, and has a flat (single-ended) power density,  $N_0$  (watts/cps), at least over the transmission bandwidth.

### D. The Receiver

It is assumed that the receiver has a knowledge of the time base and, in the coherent case considered below, of the phase base of the transmitter. In previous work<sup>15,16</sup>

it was shown that the basic operation performed by the ideal receiver in computing the *a posteriori* probabilities,  $Pr[\xi_1/\zeta]$  and  $Pr[\xi_2/\zeta]$  is that of cross-correlation of the received signal with the stored replicas of each of the two transmitted signals. In complex notation, the basic cross-correlation functions are

$$\begin{aligned} \rho_m(u) &= \frac{1}{2} \int \xi^*(t) \zeta_m(t-u) dt \\ &= \left[ \frac{1}{2} \int z^*(t) x_m(t-u) dt \right] e^{-i2\pi f_0 u} \\ &= r_m(u) e^{-i2\pi f_0 u} \quad (m = 1, 2) \end{aligned} \quad (12)$$

where  $\zeta(t) = z(t)e^{i2\pi f_0 t}$  is the complex representation of the received signal, the asterisk denotes "complex conjugate," and the integral is taken over all intervals of nonzero integrand. Note that  $\rho_m(u)$  is, like  $\xi_1(t)$  and  $\xi_2(t)$  of (1), a product of a complex low-pass modulation function,

$$r_m(u) = \frac{1}{2} \int z^*(t) x_m(t-u) dt, \quad (13)$$

and a cisoidal carrier of frequency  $f_0$ . That is,  $\rho_m(u)$  is an amplitude and phase modulated waveform with carrier frequency  $f_0$ . It can be shown,<sup>17</sup> using the usual narrow-band approximations, that the real part of  $\rho_m(u)$  is the cross-correlation function of the physical signals,  $\tilde{\zeta}(t)$  and  $\tilde{\xi}_m(t)$ , and the magnitude of  $\rho_m(u)$  is the envelope of this physical cross-correlation function. That is,

$$\hat{\rho}_m(u) = \text{Re} \{ r_m(u) e^{-i2\pi f_0 u} \} = \int \tilde{\zeta}(t) \tilde{\xi}_m(t-u) dt \quad (14a)$$

and

$$|\rho_m(u)| = |r_m(u)| = \text{env} \left[ \int \tilde{\zeta}(t) \tilde{\xi}_m(t-u) dt \right]. \quad (14b)$$

In the previous work just referred to, it is shown that for the binary, symmetric, "single"-path case we are considering, the ideal receiver decides whether  $Pr[\xi_1/\zeta]$  or  $Pr[\xi_2/\zeta]$  is the larger by performing the following operations.

1) *Coherent Receiver*: When the mean path phase,  $\delta$ , is known to the receiver, it makes its decision according as<sup>18</sup>

$$\frac{\sigma^2}{N_0} |r_m(\tau)|^2 + \alpha \text{Re} \{ r_m(\tau) e^{-i\delta} \} \quad (15)$$

is larger for  $m=1$  or  $m=2$ . Notice from (14b) that the first term of (15) contains the envelope of the cross-

<sup>15</sup> See Appendix I.

<sup>16</sup> See (34) of footnote 15, in which let  $L=1$ ,  $E_1=E_2$  and then note that  $\Delta_m$  is a monotone increasing function of

$$\frac{\sigma_1^2}{N_0} |g_{m1}|^2 + 2\alpha_1 \text{Re} [g_{m1} e^{-i\delta_1}].$$

Identify  $\sigma_1$ ,  $\alpha_1$ ,  $\delta_1$  and  $g_{m1}$  with  $\sigma$ ,  $\alpha$ ,  $\delta$ , and  $2r_m(\tau)$  of the present paper.

<sup>8</sup> G. L. Turin, "Communication through noisy, random-multipath channels," 1956 IRE NATIONAL CONVENTION RECORD, pt. 4, pp. 154-166; March, 1956.

<sup>16</sup> G. L. Turin, "Communication Through Noisy, Random-Multipath Channels," M.I.T., Lincoln Lab., Lexington, Mass., Tech. Rep. 116; May 14, 1956. This is a more detailed report than footnote 15.

correlation of the received signal and the  $m$ th stored signal, evaluated at delay  $\tau$ . Similarly, by comparison with (14a), one can identify the factor  $\text{Re}\{r_m(\tau)e^{-j\delta}\}$  of the second term of (15) as the cross correlation of the received signal and the  $m$ th stored signal, evaluated at modulation delay  $\tau$ , in phase  $\delta$ .<sup>19</sup> Several methods of actually obtaining these quantities are reviewed in Appendix II.

Note from (15) that in addition to knowing  $\delta$ , the coherent receiver generally must know the channel-parameter ratio  $\sigma^2/\alpha N_0$ .

2) *Noncoherent Receiver*: If the receiver does not know the value of  $\delta$  (or equivalently does not know the transmitter phase), it makes its decision on the basis of samples of cross-correlation envelopes alone. That is, it decides that signal 1 or signal 2 has been sent according as  $|r_m(\tau)|$  is greater for  $m=1$  or  $m=2$ .<sup>20</sup> Note that in addition to not knowing  $\delta$ , a noncoherent receiver need not know  $\sigma^2/\alpha N_0$  either, in order to make a decision; this is a great practical advantage over a coherent receiver, which must know both quantities.

### III. PROBABILITY OF ERROR

We are now in a position to derive expressions for the probability that the receiver makes an error in its decision. The details of the derivations are left to the Appendices; here we merely set down the expressions and special cases of these, and then consider an illustrative application to a practical system.

The generic form of the probability of error,  $P_e$ , for both the coherent and noncoherent cases, is:<sup>21</sup>

$$P_e = Q(ac, bc)$$

$$= \frac{1}{2} \left[ 1 + \frac{\mu\sqrt{1-|\lambda|^2}}{\sqrt{1-\mu^2|\lambda|^2}} \right] e^{-(a^2+b^2)c^2/2} I_0(abc^2), \quad (16)$$

where we have

$$Q(x, y) = \int_0^\infty e^{-(x^2+y^2)t/2} I_0(xyt) dt, \quad (17)$$

$$\mu = \frac{\beta}{\beta + 2}, \quad (18)$$

$$\beta = \frac{2\sigma^2 E}{N_0}, \quad \gamma = \frac{\alpha}{\sigma}, \quad (19)$$

and  $\lambda$  is given by (5). The  $Q$ -function,  $Q(x, y)$ , has been tabulated by Marcum.<sup>22</sup> The quantities  $a$ ,  $b$ , and  $c$  of (16) differ for the coherent and noncoherent cases.

<sup>19</sup> Again we make use of the vast difference in the period of the highest modulation frequency in  $\xi_m(t)$  [and hence in  $\rho_m(u)$ ] and the carrier period to justify speaking of any carrier phase of  $\rho_m(u)$  for a given modulation delay.

<sup>20</sup> See (26) of footnote 15 in which let  $L=1$ ,  $E_1=E_2$ , and then note that  $\Lambda'_m$  is a monotone increasing function of  $|g_{m1}|$ .

<sup>21</sup> Note that the  $a$  in (16) is not the same as that in (7).

<sup>22</sup> J. I., Marcum, "Table of  $Q$  Functions," Rand Corp., Santa Monica, Calif., Rep. RM-339; January 1, 1950. Machine computation using a series representation for  $Q$  was used in the present paper, however.

#### A. Coherent Receiver

For this case we have<sup>23</sup>

$$a = 1 - \frac{\mu\sqrt{1-|\lambda|^2}}{\sqrt{1-\mu^2|\lambda|^2}}, \quad (20)$$

$$b = 1 + \frac{\mu\sqrt{1-|\lambda|^2}}{\sqrt{1-\mu^2|\lambda|^2}}, \quad (21)$$

$$c = \sqrt{\frac{\beta\gamma^2[\beta(1-|\lambda|^2) + 2(1-\hat{\lambda})]}{4\beta^2(1-|\lambda|^2)}}. \quad (22)$$

Two special cases of interest are worth noting. The first is for  $\sigma=0$  ( $\gamma=\infty$ ), or a fixed path of known phase. Here  $\beta=0$  and  $\mu=0$ , while

$$\beta\gamma^2 = \frac{2\sigma^2 E}{N_0} \cdot \frac{\alpha^2}{\sigma^2} = \frac{2\alpha^2 E}{N_0}$$

stays nonzero and finite. In order to evaluate  $P_e$  in this case, we note the following asymptotic expressions:

$$I_0(x) \sim \frac{e^x}{\sqrt{2\pi x}} \quad \text{for large } x, \quad (23)$$

$$Q(x, y) \sim \frac{1}{2} \left[ 1 - \text{erf} \left( \frac{y-x}{\sqrt{2}} \right) \right] \quad \text{for large } x \text{ and } y, \quad (24)$$

where

$$\text{erf}(z) = \frac{2}{\sqrt{\pi}} \int_0^z e^{-t^2} dt. \quad (25)$$

Hence for  $\sigma \rightarrow 0$ ,

$$P_e \sim \frac{1}{2} \left[ 1 - \text{erf} \left\{ \frac{(b-a)c}{\sqrt{2}} \right\} \right] - \frac{1}{2} \frac{e^{-(b-a)^2 c^2 / 2}}{\sqrt{2\pi abc^2}}. \quad (26)$$

But for  $\sigma \rightarrow 0$ ,

$$(b-a)c \rightarrow \sqrt{\frac{\beta\gamma^2(1-\hat{\lambda})}{2}} \quad \text{and} \quad c \rightarrow \infty. \quad (27)$$

So, finally,

$$P_e = \frac{1}{2} \left[ 1 - \text{erf} \left( \sqrt{\frac{\alpha^2 E(1-\hat{\lambda})}{2N_0}} \right) \right]. \quad (28)$$

This result agrees with previously derived expressions.<sup>25</sup>

The other special case of interest is that for  $\alpha=0$  ( $\gamma=0$ ), or Rayleigh-distributed fading [see (10) with  $\alpha=0$ ]. Here the criteria for coherent and noncoherent detection become the same, *i.e.*, a comparison of correlation envelopes. Putting  $c=0$  in (16) and noting that  $Q(x, 0)=1$ , we have for this case

<sup>23</sup> See Appendix III.

<sup>24</sup> C. W. Helstrom, "The resolution of signals in white, Gaussian noise," *Proc. IRE*, vol. 43, pp. 1111-1118, eq. (60); September, 1955.

<sup>25</sup> C. W. Helstrom, *op. cit.*, (13). Also see (55) of footnote 15.

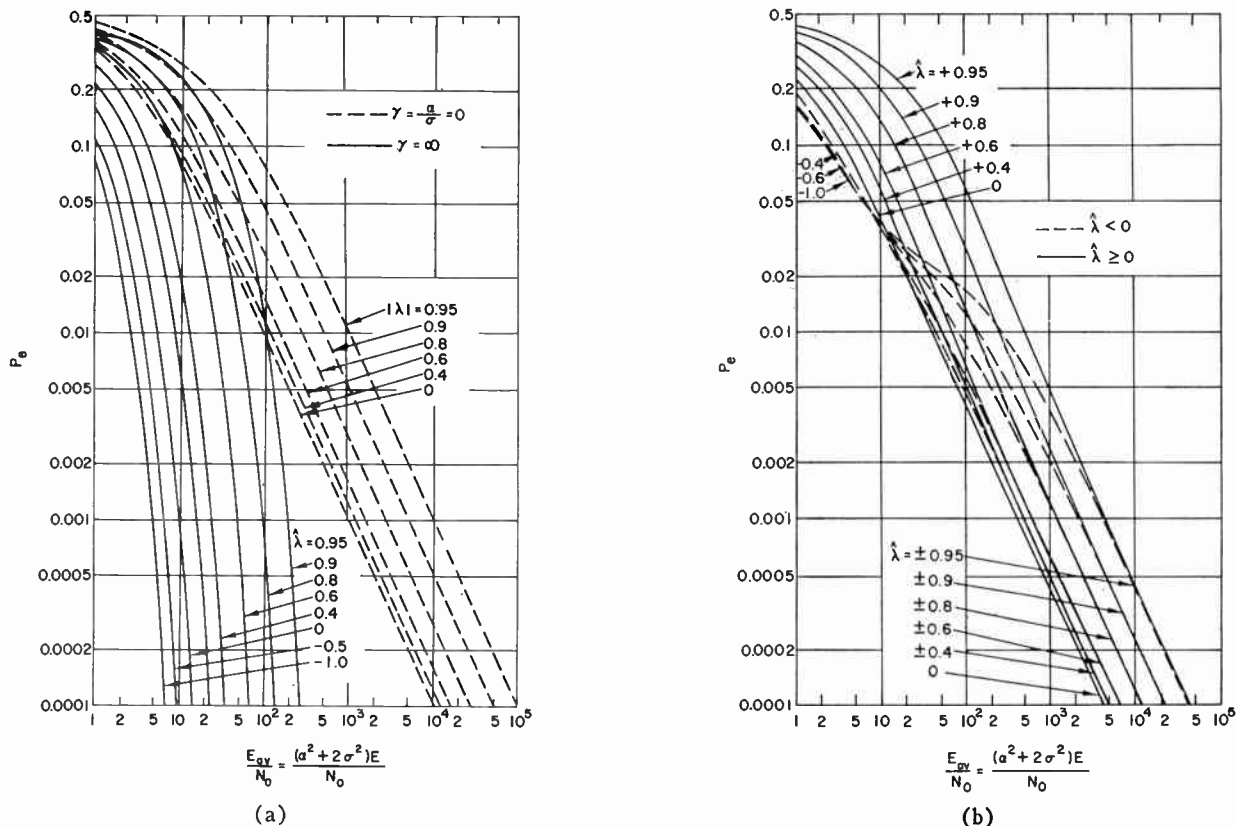


Fig. 5—Probability of error, coherent receiver (a)  $\gamma=0$  and  $\gamma = \infty$ , (b)  $\gamma=2$ .

$$P_e = \frac{1}{2} \left[ 1 - \frac{\mu \sqrt{1 - |\lambda|^2}}{\sqrt{1 - \mu^2 |\lambda|^2}} \right]. \quad (29)$$

This agrees with a previously given result.<sup>26</sup>

The difference of the performances with increasing signal-to-noise ratio of the two special cases of the ideal coherent receiver considered above is striking. Consider (28) as we let the ratio  $E/N_0$ , increase to large values. Then<sup>27</sup>

$$P_e \sim \frac{1}{\sqrt{2\pi} \frac{\alpha^2 E(1 - \tilde{\lambda})}{N_0}} e^{-\alpha^2 E(1 - \tilde{\lambda})/2N_0}. \quad (30)$$

Thus, when  $\sigma=0$ ,  $P_e$  decreases approximately exponentially with  $E/N_0$  for large  $E/N_0$ .

Now, as a comparison, let us consider the behavior of  $P_e$  for large  $E/N_0$  when  $\alpha=0$ . Using (18), let us first rewrite (29) as

$$P_e = \frac{\sqrt{1 + K} - 1}{2\sqrt{1 + K}}, \quad (31)$$

<sup>26</sup> See (57) and (58) of footnote 15. For the special case of  $|\lambda|=0$ , also see M. Masonson, "Binary transmission through noise and fading," 1957 IRE NATIONAL CONVENTION RECORD, pt. 2, pp. 69-82, (20), in which identify Masonson's  $2\mu$  with  $\beta$  of the present paper.

<sup>27</sup> W. Magnus and F. Oberhettinger, "Formulas and Theorems for the Functions of Mathematical Physics," Chelsea Publishing Co., New York, N. Y., p. 96; 1954.

where

$$K = \frac{4(\beta + 1)}{\beta^2(1 - |\lambda|^2)}. \quad (32)$$

As  $(E/N_0) \rightarrow \infty$ , we have  $\beta \rightarrow \infty$ , and

$$K \rightarrow \frac{4}{\beta(1 - |\lambda|^2)}.$$

Further,

$$P_e \rightarrow \frac{1}{4} K \rightarrow \frac{1}{\beta(1 - |\lambda|^2)} = \frac{1}{2\sigma^2 E(1 - |\lambda|^2) N_0}. \quad (33)$$

Thus, for  $\alpha=0$ ,  $P_e$  decreases only *inversely* with  $E/N_0$  for large  $E/N_0$ . This is a far cry from the exponential behavior shown by (30) for the fixed-path case!

$P_e$  is shown in Fig. 5 as a function of

$$\frac{E_{av}}{N_0} = \frac{(\alpha^2 + 2\sigma^2)E}{N_0},$$

which, as we have seen, is the ratio of the average received energy to the noise power density.<sup>28</sup> Three

<sup>28</sup> The quantity  $E_{av}/N_0$  is related to the average received signal-to-noise *power* ratio in the band of either signal in the following way. Let  $B_m$  be the *noise* bandwidth of the  $m$ th signal ( $m=1, 2$ ), or equivalently of its matched filter (see Appendix 11); then  $B_m N_0 = N_m$  is the noise power in the  $m$ th band.  $E_{av}/T = P_{av}$  is the average power of the received signal. Thus,  $P_{av}/N_m = (1/B_m T) (E_{av}/N_0)$  is the average received signal-to-noise power ratio *in the  $m$ th band* when signal  $m$  is transmitted.

sets of curves are given:  $\gamma=0(\alpha=0)$ ,  $\gamma=2(\alpha=2\sigma)$ , and  $\gamma=\infty(\sigma=0)$ . The family parameter in the first set is  $|\lambda|$ ;  $\hat{\lambda}$  does not appear explicitly [cf. (29)]. In the second set, we let  $\hat{\lambda}=0$  since it can be shown<sup>29</sup> that this value minimizes  $P_e$  with respect to  $\hat{\lambda}$ ; hence, for  $\gamma=2$  we set  $|\lambda|^2=\hat{\lambda}^2$ . The parameter of the third set is  $\hat{\lambda}$ , since  $\hat{\lambda}$  does not appear in (28).

We have seen how greatly deteriorated the large- $E_{av}/N_0$  performance of a Rayleigh-fading channel ( $\gamma=0$ ) is, compared to that of a nonfading channel; this is well illustrated in Fig. 5(a). Note from Fig. 5(b) that the deterioration is almost as bad for the case  $\gamma=2$ . Since  $r=2$  apparently does not correspond to an abnormally large amount of fading in actual physical cases when both fixed and random path components are present (e.g., in below-the-muf ionospheric transmission<sup>13</sup>), we may state as a rough general conclusion that the incidence of fading is accompanied by markedly deteriorated performance; that is, in those physical situations where fading is generally encountered, we may expect relatively high error rates. This conclusion is not so surprising when one considers the catastrophic effect of *deep* fades on the error probability. In a deep fade, the signal for all practical purposes disappears, so that the error probability in this condition is near 1/2. Thus, even if such deep fades are fairly improbable, the contribution of deep-fade errors to the over-all error probability still may well be considerable, and cause a very much larger error probability than if, as in the nonfading case, deep fades did not exist at all.

Note from Fig. 5 that for  $\gamma=\infty$ ,  $\lambda=-1$  yields the minimum value of  $P_e$  for all signal-to-noise ratios. Now,  $\lambda=-1$  obtains when  $\xi_1(t)=-\xi_2(t)$  [see (4) and (5)], that is, when the two signals are the same except for a 180° difference in carrier phase. Thus, as we should expect for a coherent receiver and a fixed path, we can make use of phase differences between the signals in the reception process.

At the opposite extreme, when  $\gamma=0$ ,  $\lambda=0$  is optimum for all  $E/N_0$ . In this case, the phase is completely randomized by the fading medium, so phase relationships between the two signals cannot be exploited in the reception process; uncorrelated signals are best.

For intermediate values of  $\gamma$  the optimum value of  $\hat{\lambda}$  is a function of signal-to-noise ratio. In general [see, e.g., Fig. 5(b)],  $\lambda_{opt}=-1$  for small  $E_{av}/N_0$  (roughly, when noise is the more important of the two channel disturbances), while  $\lambda_{opt}=0$  for large  $E_{av}/N_0$  (roughly, when fading is the more important disturbance). There is a transition region for which  $0 < \lambda_{opt} < -1$ .

Note, however, that even for  $\gamma=2$ , the optimum value of  $\lambda$  is essentially zero in the region of interest,  $P_e \leq 0.01$ . Now, for ionospheric and tropospheric scatter transmission ( $\gamma=0$ ), the fading is of course always more severe than that for  $\gamma=2$ . For below-the-muf ionospheric transmission, as we have noted, empirical data<sup>13</sup>

indicate that fading is usually more severe than that for  $\gamma=2$ . We are thus led to the following loose generalization: when fading does exist, uncorrelated signals are normally optimum in the operating region of interest. In this case, the phase coherence of the fixed component, even when dominant, cannot be exploited by making  $\hat{\lambda}$  negative; in particular, setting  $\hat{\lambda}=-1$  would be almost as bad as setting  $\lambda=+1$  (for which  $P_e \equiv \frac{1}{2}$ ).

**B. Noncoherent Receiver**

For this case we have<sup>30</sup>

$$a = \sqrt{1 - \frac{\sqrt{(1 - |\lambda|^2)(1 - \mu^2|\lambda|^2)}}{1 - \mu|\lambda|^2}}, \tag{34}$$

$$b = \sqrt{1 + \frac{\sqrt{(1 - |\lambda|^2)(1 - \mu^2|\lambda|^2)}}{1 - \mu|\lambda|^2}}, \tag{35}$$

$$c = \sqrt{\frac{\mu\gamma^2}{2} \cdot \frac{1 - \mu|\lambda|^2}{1 - \mu^2|\lambda|^2}}. \tag{36}$$

Note that here  $a^2 + b^2 = 2$ .

Again the two special cases  $\sigma=0$  and  $\alpha=0$  of interest. For the first of these, i.e., for a fixed path and phase-noncoherent receiver,  $P_e$  reduces to

$$P_e = Q \left( \sqrt{\frac{\beta\gamma^2}{4} (1 - \sqrt{1 - |\lambda|^2})}, \sqrt{\frac{\beta\gamma^2}{4} (1 + \sqrt{1 - |\lambda|^2})} \right) - \frac{1}{2} e^{-(\beta\gamma^2)/4} I_0 \left( \frac{\beta\gamma^2}{4} |\lambda| \right). \tag{37}$$

This expression checks with one derived by Helstrom.<sup>31</sup> On letting  $(E/N_0) \rightarrow \infty$  in (37), and using (24) and the asymptotic expression for erf(x), it is easy to show that for a noncoherent receiver, as for a coherent receiver,  $P_e$  drops off approximately exponentially with increasing  $E/N_0$  for  $\sigma=0$ .

When  $\alpha=0$ , the noncoherent receiver and the coherent receiver are identical, and as we should expect,  $P_e$  reduces to the coherent-receiver expression for the  $\alpha=0$  case, (29).

Another special case of interest is that for  $|\lambda|=0$ . In this limit, we have  $a=0$ ,  $b=\sqrt{2}$ , and  $c=\sqrt{\mu\gamma^2/2}$ . Since  $Q(0, y) = e^{-y^2/2}$ , then,

$$P_e = \frac{1}{\beta + 2} e^{-(\beta\gamma^2)/2(\beta+2)}. \tag{38}$$

This checks with a previous result.<sup>32</sup>

<sup>30</sup> See Appendix IV.

<sup>31</sup> C. W. Helstrom, *op. cit.*, (37). Note that Helstrom uses the symbol  $\lambda$  in two senses: in reference to a coherent receiver, it stands for our  $\hat{\lambda}$ ; in reference to a noncoherent receiver, it stands for our  $|\lambda|$ .

<sup>32</sup> See (36) of footnote 15.

<sup>29</sup> See chapter V of footnote 16.

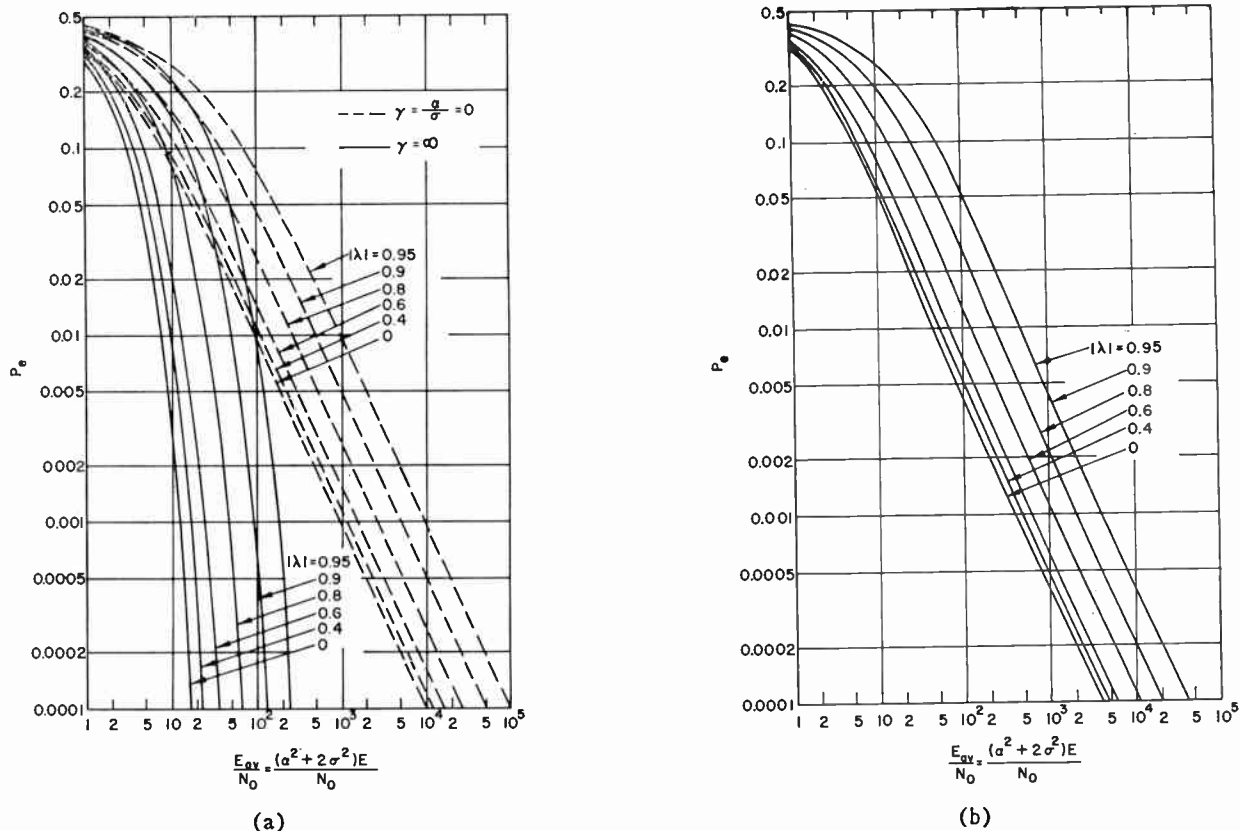


Fig. 6—Probability of error, noncoherent receiver (a)  $\gamma=0$  and  $\gamma = \infty$ , (b)  $\gamma=2$ .

Families of curves of  $P_e$  for noncoherent reception for  $\gamma=0, \gamma=2$ , and  $\gamma = \infty$  are given in Fig. 6, with  $|\lambda|$  as a parameter in each family. Note that  $|\lambda|=0$  (uncorrelated signals) is optimum for all  $\gamma$  and all  $E/N_0$ . A comparison of Fig. 6 with Fig. 5 will show that for each  $\gamma$  the curves of  $P_e$  for the coherent and noncoherent cases are approximately coincident for large  $E_{av}/N_0$ , with the approximation getting better for large  $|\lambda|$ .

For comparison purposes, various curves from Fig. 5 and Fig. 6 are replotted in Fig. 7. Inspection of Fig. 7 reveals a generalization which is corollary to our previous generalization about  $\lambda_{opt}$ : when fading does exist, normally little is gained by the use of a coherent receiver (see curves 1, 2, and 3 in Fig. 7). Of course, for a fixed path, the use of a coherent receiver can result in up to a 4-dB improvement over a noncoherent receiver (see curves 4, 5, and 6 in Fig. 7). But the performance of a noncoherent receiver for  $\gamma = \infty$  is already so excellent that the extra power advantage may not be needed.

One is led, on the basis of our discussions of Fig. 5–Fig. 7, to the practical conclusion that a system which is to operate through both fixed and nonselectively fading paths will be essentially optimal if it is designed to use uncorrelated signals and noncoherent reception exclusively. The use of noncoherent reception also has the benefit, as seen, of obviating the need for knowledge of the channel parameters  $\delta$  and  $\sigma^2/\alpha N_0$  at the receiver.

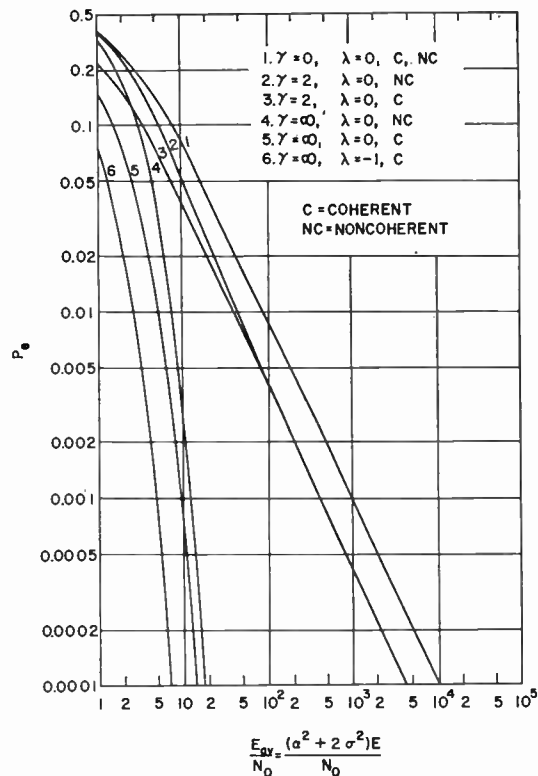


Fig. 7—Comparison of probability of error curves for several important cases.

IV. AN EXAMPLE

To illustrate the application of the previous results to a practical system, we consider the FSK system characterized by the modulation waveforms of (3). These waveforms are sine wave pulses, both having the pulse shape  $A(t)$ , but one having carrier frequency  $f_0 - (\Delta f/2)$  and the other having carrier frequency  $f_0 + (\Delta f/2)$ . The complex correlation coefficient of these waveforms is given by (6). We shall consider only the noncoherent case, so we require only  $|\lambda|$ . We now derive expressions for the functional dependence of  $|\lambda|$  on the frequency separation,  $\Delta f$ , for some particular pulse shapes.

A. Rectangular Pulses

For a rectangular pulse,  $A(t)$  is

$$A(t) = \begin{cases} 1 & 0 \leq t \leq T \\ 0 & \text{elsewhere,} \end{cases} \quad (39)$$

$|\lambda|$  is then, from (6),

$$|\lambda| = \left| \frac{\sin \pi \Delta f T}{\pi \Delta f T} \right|. \quad (40)$$

B. Gaussian Pulses

Here we take

$$A(t) = \begin{cases} e^{-a^2(t-T/2)^2} & 0 \leq t \leq T \\ 0 & \text{elsewhere.} \end{cases} \quad (41)$$

If a sufficient amount of the tails of the Gaussian pulse are included in the interval  $(0, T)$ , *i.e.*, if say  $(a^2 T^2/4) > 3$ , then the limits on the integrals in (6) and the tails of  $A(t)$  may for approximate computational purposes be extended to  $(-\infty, \infty)$ , and  $|\lambda|$  is easily evaluated as

$$|\lambda| = e^{-0.692(\Delta f/W)^2}. \quad (42)$$

Here  $W = 0.375a$  is the half-power bandwidth of the spectrum of the infinitely extended Gaussian pulse, and very nearly the half-power bandwidth of the finite duration pulse.

C. Exponential Pulses

Now we consider

$$A(t) = \begin{cases} e^{-\pi W t} & 0 \leq t \leq T \\ 0 & \text{elsewhere.} \end{cases} \quad (43)$$

Again, if a sufficient amount of the tail of  $A(t)$  is included in  $(0, T)$  [ $WT > 1$ , say] then we may infinitely extend the limits in (6) and the right tail of  $A(t)$  to obtain as a good approximation

$$|\lambda| = \frac{1}{\sqrt{1 + \left(\frac{\Delta f}{W}\right)^2}}. \quad (44)$$

$W$  is very nearly the half-power bandwidth of the spectrum of  $A(t)$ .

D. Rectangular Spectra

Finally let us evaluate  $|\lambda|$  for an  $A(t)$  of the form

$$A(t) = \begin{cases} \frac{\sin \pi W(t - T/2)}{\pi W(t - T/2)} & 0 \leq t \leq T/2. \\ 0 & \text{elsewhere} \end{cases} \quad (45)$$

If  $(WT/2) > 3$ , say, we may again extend the limits on the integrals of (6) and the tails of  $A(t)$ , and write

$$|\lambda| = \begin{cases} 1 - \frac{\Delta f}{W} & \Delta f \leq W \\ 0 & \Delta f > W. \end{cases} \quad (46)$$

The two signals,  $\hat{\xi}_1(t)$  and  $\hat{\xi}_2(t)$ , have very nearly rectangular spectra of bandwidth  $W$  centered on  $f_0 - (\Delta f/2)$  and  $f_0 + (\Delta f/2)$ , respectively. The spectra become more and more rectangular as  $TW \rightarrow \infty$ .

The four correlation coefficients derived above are plotted as functions of  $\Delta f$  in Fig. 8. Using these curves in conjunction with the curves of Fig. 5 and Fig. 6 one may answer such questions as, "How much must transmitter power be increased in order to keep the same error rate for a given reduction in frequency separation (or over-all bandwidth)?" For example, consider a system which operates through a scatter-propagation link ( $\gamma = 0$ ). From Fig. 5 or Fig. 6 and Fig. 8 one can plot the required  $E_{av}/N_0$  as a function of frequency separation for any given value of  $P_e$ . This is done in Fig. 9 for  $P_e = 0.01$ , where the reference value (0 db) of  $E_{av}/N_0$  is that for  $|\lambda| = 0$  ( $\Delta f = \infty$ ). From this figure we note, for instance, that in the case of rectangular spectra a change from adjacent but nonoverlapping bands ( $\Delta f/W = 1$ ) to bands which overlap each other by 50 per cent ( $\Delta f/W = \frac{1}{2}$ ), requires a 1.2 db increase in transmitter power to maintain a 1 per cent error probability; that is, a 25 per cent reduction in over-all bandwidth in this case requires a 30 per cent increase in power.

We may also compare the performances of systems with different pulse shapes. Suppose, for example, we wish to compare two FSK systems which are to work through a scatter link: one with rectangular pulses, the other with Gaussian pulses. For a fair comparison we assume equal time durations of the different pulses, so as to have equal information rates. That is, letting the Gaussian pulse duration,  $T_g$ , extend to say the 5 per cent points on the tails ( $a^2 T_g^2/4 = 3$  in (41)), and equating  $T_g$  to the duration of the rectangular pulse,  $T_r$ , we get

$$a^2 = 12 \cdot \frac{1}{T_r^2}. \quad (47)$$

In terms of the half-power bandwidths of the pulses

$$W_g = 0.375a, \quad W_r = \frac{0.88}{T_r},$$

we have

$$W_g \cong 1.47W_r. \quad (48)$$

We also equate the energies (and, hence, average powers) of the two types of pulses [*cf.* (4)]:

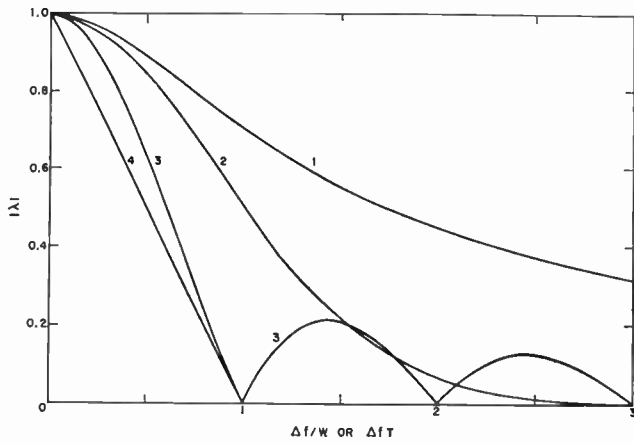


Fig. 8—The magnitude,  $|\lambda|$ , of FSK correlation coefficients for several pulse shapes. 1) Exponential pulses: half-power bandwidth,  $W$ . 2) Gaussian pulses: half-power bandwidth,  $W$ . 3) Rectangular pulses: duration,  $T$ . 4) Rectangular spectra: bandwidth,  $W$ .

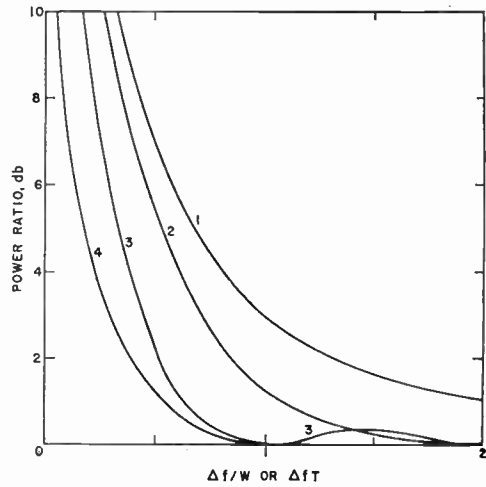


Fig. 9—The effect of FSK frequency separation,  $\Delta f$ , on power required for one per cent error probability,  $\gamma=0$  (0 db corresponds to  $\Delta f = \infty$ ). 1) Exponential pulses: half-power bandwidth,  $W$ . 2) Gaussian pulses: half-power bandwidth,  $W$ . 3) Rectangular pulses: duration,  $T$ . 4) Rectangular spectra: bandwidth,  $W$ .

$$\frac{1}{2} \int_{-T_g/2}^{T_g/2} k^2 e^{-2a^2 t^2} dt = \frac{1}{2} \int_{-T_r/2}^{T_r/2} dt. \quad (49)$$

Here  $k$  is the height of the peak of the Gaussian pulse relative to that of the rectangular pulse. Using the approximation of extending the limits of the left-hand integral to  $(-\infty, \infty)$ , and using (47), we get  $k^2 = 2.76$ ; that is, 2.76 times as much peak power must be used in the Gaussian case for the same average power. This situation is depicted in Fig. 10.

Now suppose that at the receiver  $2\sigma^2 E/N_0 = 130$ ,<sup>33</sup> and we require  $P_e \leq 0.01$ . From the  $\gamma = 0$  curves of Fig. 5 and Fig. 6 we have then the requirement  $|\lambda| \leq 0.5$ . Choosing  $|\lambda| = 0.5$ , we have from Fig. 8:  $\Delta f_g = W_g$  and

<sup>33</sup> This corresponds to an average received signal-to-noise power ratio of about 21 db *per band* for rectangular pulses and about 20 db *per band* for Gaussian pulses. (See footnote 28.)

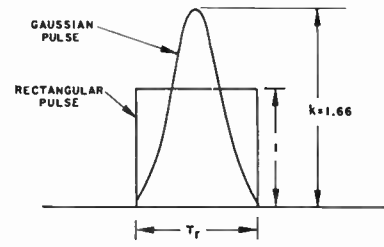


Fig. 10—The “equivalent” Gaussian and rectangular pulses of the example in the text.

$$\Delta f_r = \frac{0.6}{T_r} \cong 0.682 W_r.$$

If we define the over-all bandwidth of each system as the difference between the upper half-power frequency of the upper band and the lower half-power frequency of the lower band, we have the over-all bandwidths

$$\left. \begin{aligned} W_{g0} &= 2W_g \\ W_{r0} &= 1.682W_r \end{aligned} \right\}, \quad (50)$$

so, from (48),

$$W_{g0} \cong 1.75W_{r0}. \quad (51)$$

That is, under the conditions described above, the penalties attached to using the Gaussian pulse shape of Fig. 10 instead of the rectangular pulse shape are 4.4 db greater peak power and 75 per cent greater over-all half-power bandwidth.

### APPENDIX I. THE COMPLEX CORRELATION FUNCTION

Suppose we have two narrow-band complex transient waveforms  $\mu(t) = m(t)e^{j2\pi f_0 t}$  and  $\nu(t) = n(t)e^{j2\pi f_0 t}$ . Their complex cross-correlation function is defined as

$$\psi(\tau) = \frac{1}{2} \int \mu^*(t)\nu(t - \tau) dt \quad (52)$$

where the integration is over all intervals of nonzero integrand. The real part of  $\psi(\tau)$  is

$$\hat{\psi}(\tau) = \frac{1}{2} \int [\hat{\mu}(t)\hat{\nu}(t - \tau) + \tilde{\mu}(t)\tilde{\nu}(t - \tau)] dt \quad (53)$$

in which

$$\hat{\mu}(t) = \hat{m}(t) \cos 2\pi f_0 t - \hat{m}(t) \sin 2\pi f_0 t \quad (54a)$$

$$\tilde{\mu}(t) = \hat{m}(t) \sin 2\pi f_0 t + \hat{m}(t) \cos 2\pi f_0 t \quad (54b)$$

and similar expressions hold for  $\nu(t)$  and  $\tilde{\nu}(t)$ . From (54a)

$$\begin{aligned} \hat{\mu}\left(t - \frac{1}{4f_0}\right) &= \hat{m}\left(t - \frac{1}{4f_0}\right) \sin 2\pi f_0 t \\ &+ \hat{m}\left(t - \frac{1}{4f_0}\right) \cos 2\pi f_0 t \end{aligned} \quad (55)$$

Now, it has been assumed that  $\mu(t)$  represents a narrow-band waveform. This implies that  $m(t)$  remains essentially constant over many cycles of carrier, so we may write

$$m\left(t - \frac{1}{4f_0}\right) = m(t),$$

and hence from (55) and 54(b)

$$\hat{\mu}\left(t - \frac{1}{4f_0}\right) = \mu(t). \tag{56}$$

Similarly

$$\hat{\nu}\left(t - \frac{1}{4f_0}\right) = \nu(t). \tag{57}$$

Using (56) and (57) in (53), we notice that the integrals of both terms on the right are equal, so

$$\hat{\psi}(\tau) = \int \hat{\mu}(t)\hat{\nu}(t - \tau)dt. \tag{58}$$

That is, the real part of  $\psi(\tau)$  is the cross-correlation function of physical waveforms  $\hat{\mu}(t)$  and  $\hat{\nu}(t)$ .

By inserting expressions for  $\hat{\mu}(t)$  and  $\hat{\nu}(t)$  in the form of (54a) in (58) one obtains, after some trigonometric manipulations and the use of the narrow-band assumption to eliminate integrals of double-frequency terms,

$$\hat{\psi}(\tau) = A(\tau) \cos 2\pi f_0\tau + B(\tau) \sin 2\pi f_0\tau, \tag{59}$$

where

$$A(\tau) = \frac{1}{2} \int [\hat{m}(t)\hat{n}(t - \tau) + \tilde{m}(t)\tilde{n}(t - \tau)]dt, \tag{60a}$$

$$B(\tau) = \frac{1}{2} \int [\hat{m}(t)\tilde{n}(t - \tau) - \tilde{m}(t)\hat{n}(t - \tau)]dt. \tag{60b}$$

The envelope of  $\hat{\psi}(\tau)$  is just

$$\sqrt{A^2(\tau) + B^2(\tau)}.$$

But one can easily show from (52) that

$$|\psi(\tau)| \equiv \sqrt{\hat{\psi}^2(\tau) + \tilde{\psi}^2(\tau)} = \sqrt{A^2(\tau) + B^2(\tau)}$$

so we have

$$|\psi(\tau)| = \text{env } \hat{\psi}(\tau). \tag{61}$$

That is, the magnitude of the complex cross-correlation function is just the envelope of the physical cross-correlation function.

## APPENDIX II. CROSS-CORRELATION TECHNIQUES

Here we review methods of obtaining the terms in (15) by physical operations. In particular, we consider three techniques: multiplication and low-pass filter-

ing,<sup>34-37</sup> multiplication and band-pass filtering,<sup>37</sup> and matched filtering.<sup>38</sup>

### A. Multiplication and Low-Pass Filtering

In order to obtain  $\text{Re}[r_m(\tau)e^{-j\delta}]$ , one multiplies the received signal by the stored replica of the  $m$ th transmitted waveform, which has been delayed by such an amount that its modulation is delayed by  $\tau$  (within a fraction of a carrier period), and its carrier phase is shifted by  $\delta$ .<sup>39</sup> The multiplier output is fed into a low-pass short-time integrating filter whose output is then (cf. Appendix I):

$$\begin{aligned} e_0(t) &= \frac{1}{2} \text{Re} \int_{t-T}^t \xi_m^*(t)x_m(t - \tau)e^{j(2\pi f_0 t - \delta)}dt, \\ &= \frac{1}{2} \text{Re} \left\{ e^{-j\delta} \int_{t-T}^t z_m^*(t)x_m(t - \tau)dt \right\}. \end{aligned} \tag{62}$$

$T$ , the integrating time of the filter, is taken to be equal to the duration of  $\xi_m(t)$  [and hence  $x_m(t)$ ]. Thus, we have from (62) and (13),

$$e_0(\tau + T) = \text{Re} \{ r_m(\tau)e^{-j\delta} \}. \tag{63}$$

The required quantity is, therefore, the output of the integrating filter sampled at  $t = \tau + T$  (where  $t = 0$  corresponds to the start of the transmission interval<sup>39</sup>).

In order to obtain  $|r_m(\tau)|^2$ , it suffices to obtain  $\text{Im} \{ r_m(\tau)e^{-j\delta} \}$ , square it, and add this to the square of  $\text{Re} \{ r_m(\tau)e^{-j\delta} \}$  obtained above. To obtain  $\text{Im} \{ r_m(\tau)e^{-j\delta} \}$  physically, one gives to the delayed replica of  $\xi_m(t)$ , described above, an additional phase shift of  $90^\circ$ . This quadrature waveform is then multiplied by the received waveform, the product passed into a low-pass short-time integrating filter, and the output of the filter sampled at  $t = \tau + T$ . This sample value is, by direct analogy with the previous derivation,

$$e_0'(\tau + T) = \text{Re} \{ r_m(\tau)e^{-j(\delta + \pi/4)} \} = \text{Im} \{ r_m(\tau)e^{-j\delta} \} \tag{64}$$

which is what we require. The last equality in (64) is readily proven by expressing both sides in terms of the real and imaginary parts of  $r_m(\tau)$  and of the exponentials.

<sup>34</sup> Y. W. Lee, T. P. Cheatham, and J. B. Wiesner, "The Application of Correlation Functions in the Detection of Small Signals in Noise," M.I.T., Cambridge, Mass., Res. Lab. of Electronics, Tech. Rep. 141; October 13, 1949.

<sup>35</sup> R. M. Fano, "Signal-to-Noise Ratio in Correlation Detectors," M.I.T., Cambridge, Mass., Res. Lab. of Electronics, Tech. Rep. 186, February 19, 1951.

<sup>36</sup> W. B. Davenport, Jr., "Correlator Errors Due to Finite Observation Intervals," M.I.T., Cambridge, Mass., Res. Lab. of Electronics, Tech. Rep. 191; March 8, 1951.

<sup>37</sup> P. E. Green, Jr., "The output signal-to-noise ratio of correlation detectors," IRE TRANS. ON INFORMATION THEORY, vol. IT-3, pp. 10-18; March, 1957.

<sup>38</sup> R. M. Fano, "Communication in the presence of noise," M.I.T., Cambridge, Mass., unpublished lecture notes; 1951.

<sup>39</sup> It is to be remembered that the (coherent) receiver is assumed to know  $\tau$  and  $\delta$ , and to have time and phase bases which are synchronous with those in the transmitter.

*B. Multiplication and Band-Pass Filtering*

In order to eliminate the additional multiplier and integrator needed to obtain  $|r_m(\tau)|^2$  with low-pass filtering, the following method may be used.

The  $m$ th stored waveform is delayed by such an amount that its modulation is delayed by  $\tau$  (within a fraction of a carrier period), and its carrier is in phase with that of the undelayed waveform. Before multiplication of the delayed stored waveform and the received waveform, one or the other is shifted in frequency by an amount  $\Delta$  cps. If the product waveform, whose spectrum is centered at  $\Delta$  cps, is integrated by a short-time *band-pass* integrator with impulse response

$$k(t) = \begin{cases} \text{Re} \{ e^{j2\pi\Delta t} \} & 0 \leq t \leq T \\ 0 & \text{elsewhere} \end{cases} \quad (65)$$

the integrator output is

$$e_0(t) = \frac{1}{2} \text{Re} \left\{ e^{\pm j2\pi\Delta t} \int_{t-T}^t z^*(l)x_m(t-\tau)dl \right\}. \quad (66)$$

The sign of the exponent is positive if the received signal is shifted down by  $\Delta$  or the stored signal shifted up, and negative if the received signal is shifted up or the stored signal down. If we sample  $e_0(t)$ , which is a band-pass waveform centered on  $\Delta$  cps, at (modulation) time  $t = \tau + T$ , in phase  $\mp \delta$ , we then get the required  $\text{Re} \{ r_m(\tau)e^{-j\delta} \}$ ; the phase is of course measured here with respect to that of the shifting oscillator, which goes through zero phase at  $t = 0$ . Note that the envelope of the waveform  $e_0(t)$  is just

$$\left| \frac{1}{2} \int_{t-T}^t z^*(l)x_m(t-\tau)dl \right|,$$

so  $|r_m(\tau)|$  is just the envelope of  $e_0$  at  $t = \tau + T$ .

*C. Matched Filtering*

If we have a filter with impulse response

$$h_m(t) = \text{Re} \xi_m(-t) \quad (67)$$

the response of this filter to the received signal is just

$$e_0(t) = \frac{1}{2} \text{Re} \left\{ e^{-j2\pi f t} \int z^*(\sigma)x_m(\sigma-t)d\sigma \right\} \quad (68)$$

where the integral is taken over all intervals of nonzero integrand. Thus

$$e_0(t) = \text{Re} \{ r_m(t)e^{-j2\pi f t} \}, \quad (69)$$

so  $\text{Re} \{ r_m(\tau)e^{-j\delta} \}$  is  $e_0(t)$ , sampled at (modulation) time  $\tau$ , in phase  $\delta$ . Similarly,  $|r_m(\tau)|$  is the envelope of  $e_0$ , sampled at  $t = \tau$ .

The filter of (67) is called the filter which is "matched"<sup>40</sup> to  $\text{Re} \xi(t)$ ; its transfer function is the com-

plex conjugate of the signal spectrum. As written in (67) it is unrealizable, since  $h_m(t)$  is not zero for  $t < 0$ . However, by inserting a delay  $T$ , *i.e.*, by letting  $h_m(t) = \text{Re} \xi_m(T-t)$ , the filter is made realizable; the output samples are now taken exactly  $T$  seconds later than indicated above.

Note from (69) that the matched filter output is the *complete* crosscorrelation function of the received signal and the  $m$ th stored waveform as a function of time; introduction of the parameter  $\tau$  does not take place until after the matched-filter processing of the received signal. On the other hand, the correlation techniques described by (62) and (66) give the required crosscorrelation function evaluated only for a *particular* value of the parameter  $\tau$ , which is introduced before the processing of the received signal.

APPENDIX III. PROBABILITY OF ERROR, COHERENT CASE

We may assume, without loss of generality, that  $\tau = 0$  and  $\delta = 0$  since in any case these are both known to the receiver. Then, letting

$$D = \left[ \frac{\sigma^2}{N_0} |r_1(0)|^2 + \alpha r_1(0) \right] - \left[ \frac{\sigma^2}{N_0} |r_2(0)|^2 + \alpha r_2(0) \right] \quad (70)$$

we see from (15) that the receiver guesses signal 1 as the transmitted signal if  $D > 0$  and signal 2 if  $D < 0$ . Because of the symmetry of the system, there will be the same probability of error when signal 1 is sent as when signal 2 is sent. Thus we can compute the over-all probability of error by assuming that signal 1 was sent, and finding the probability that  $D < 0$ .

We first define four new variables:

$$\begin{aligned} w_1 &= \frac{\sigma}{N_0} \text{Re} \int z^*(l)x_1(l)dl + \frac{\alpha}{\sigma} \\ w_2 &= \frac{\sigma}{N_0} \text{Im} \int z^*(l)x_1(l)dl \\ w_3 &= \frac{\sigma}{N_0} \text{Re} \int z^*(l)x_2(l)dl + \frac{\alpha}{\sigma} \\ w_4 &= \frac{\sigma}{N_0} \text{Im} \int z^*(l)x_2(l)dl. \end{aligned} \quad (71)$$

Then, from (13) and (71),  $D < 0$  implies

$$w_1^2 + w_2^2 - w_3^2 - w_4^2 < 0. \quad (72)$$

Now, the hypothesized received signal is the sum of a Gaussian noise waveform and the output of the fading medium assuming signal 1 was sent. Thus in terms of modulation waveforms [*cf.* (7)],

<sup>40</sup> J. H. Van Vleck and D. Middleton, "A theoretical comparison of the visual, aural, and meter reception of pulsed signals in the presence of noise," *J. Appl. Phys.*, vol. 17, pp. 940-971; November, 1946.

$$z(t) = \alpha x_1(t)e^{-i\theta} + n(t), \tag{73}$$

where  $n(t)$  is the modulation waveform of the noise.  $a$  and  $\theta$  share the joint distribution of (10); using this it is easy to show that the real and imaginary parts of the first term in (73) are Gaussianly distributed.<sup>8</sup> The real and imaginary parts of  $n(t)$  are also Gaussianly distributed.<sup>3</sup> Hence the two parts of  $z(t)$  are Gaussianly distributed. It then follows that the real and imaginary parts of  $\int z^*(t)x_i(t)dt$  ( $i=1, 2$ ), and hence  $w_1, w_2, w_3$ , and  $w_4$ , share joint Gaussian distributions.<sup>41</sup> Thus  $R = w_1^2 + w_2^2 - w_3^2 - w_4^2$  is a quadratic form of correlated Gaussian variables.

It is easily shown that the characteristic function of a quadratic form,  $R$ , of Gaussian variables is given by<sup>42</sup>

$$F_R(ju) = e^{i\overline{uR}} = \frac{\exp[-\frac{1}{2}\overline{W}M^{-1}\{I - (I - 2juM\mathcal{Q})^{-1}\}\overline{W}]}{|I - 2juM\mathcal{Q}|^{1/2}} \tag{74}$$

where  $I$  is the unit matrix,  $\mathcal{Q}$  is the matrix of the quadratic form,  $M$  is the moment matrix of the variables,<sup>43</sup>  $\overline{W}$  is the (column) matrix of the means of the variables,<sup>44</sup> “ $t$ ” denotes “transpose of,” and  $|\dots|$  denotes “determinant of.” The probability density distribution of  $R$  is the Fourier transform of  $F_R$ :

$$p_R[R] = \frac{1}{2\pi j} \int_{-j\infty}^{j\infty} F_R(s)e^{-sR} ds. \tag{75}$$

Hence, the probability of error is

$$\begin{aligned} P_e &= Pr[R < 0] = \int_{-\infty}^0 p_R[R] dR \\ &= -\frac{1}{2\pi j} \int_{-j\infty}^{j\infty} \frac{F_R(s)}{s} ds. \end{aligned} \tag{76}$$

The path of integration of the last integral in (76) is taken to be indented to the left at all  $j$ -axis singularities.

In order to evaluate (76), we must know  $F_R(s)$ , and this entails finding the matrices of means and second moments of the  $w$  variables, (71). Using (73), and then (4) and (5), we have

$$\begin{aligned} \int z^*(t)x_1(t)dt &= 2aEe^{i\theta} + \int n^*(t)x_1(t)dt, \\ \int z^*(t)x_2(t)dt &= 2aE\lambda e^{i\theta} + \int n^*(t)x_2(t)dt. \end{aligned} \tag{77}$$

Once we have found the matrices of means and second moments of the real and imaginary parts of the random variables in (77), we can easily obtain these matrices for the  $w$  variables of (71). Let

<sup>41</sup> H. Cramér, “Mathematical Methods of Statistics,” Princeton University Press, Princeton, N.J., sec. 24.4; 1951.

<sup>42</sup> See footnote 16, Appendix V. For  $\overline{W}=0$  this result also appears in P. Whittle, “Hypothesis Testing in Time Series Analysis,” Almqvist and Wiksells AB, Uppsala, Sweden; 1951.

<sup>43</sup> The elements of  $M$  are  $m_{ij} = \overline{w_i w_j - w_i w_j}$ .

<sup>44</sup> The elements of  $\overline{W}$  are  $\overline{w_i}$ .

$$\hat{p} = 2aEe^{i\theta},$$

$$q_i = \int n^*(t)x_i(t)dt \quad i = 1, 2. \tag{78}$$

Then

$$\begin{aligned} \text{Re} \int z^*(t)x_1(t)dt &= \hat{p} + \hat{q}_1, \\ \text{Im} \int z^*(t)x_1(t)dt &= \hat{p} + \hat{q}_1, \\ \text{Re} \int z^*(t)x_2(t)dt &= \hat{p}\hat{\lambda} - \hat{p}\hat{\lambda} + \hat{q}_2, \\ \text{Im} \int z^*(t)x_2(t)dt &= \hat{p}\lambda + \hat{p}\hat{\lambda} + \hat{q}_2. \end{aligned} \tag{79}$$

Since we have assumed that  $a$  and  $\theta$  share the joint distribution of (10) with  $\delta=0$  we get easily<sup>45</sup>

$$\begin{aligned} \overline{\hat{p}} &= 2\alpha E, \\ \overline{\hat{p}} &= 0, \\ \overline{\hat{p}^2} &= 4(\alpha^2 + \sigma^2)E^2, \\ \overline{\hat{p}^2} &= 4\sigma^2 E^2, \\ \overline{\hat{p}\hat{p}} &= 0. \end{aligned} \tag{80}$$

From (78) we have

$$\begin{aligned} \hat{q}_i &= \int [\hat{n}(t)\hat{x}_i(t) + \tilde{n}(t)\tilde{x}_i(t)]dt \\ \tilde{q}_i &= \int [\hat{n}(t)\tilde{x}_i(t) - \tilde{n}(t)\hat{x}_i(t)]dt \end{aligned} \quad i = 1, 2. \tag{81}$$

Noting that  $\overline{\hat{n}(t)} = \overline{\tilde{n}(t)} = 0$  (the noise has zero mean), we have

$$\overline{\hat{q}_i} = \overline{\tilde{q}_i} = 0 \quad i = 1, 2. \tag{82}$$

Since the noise has been assumed white, we have for the two quadrature components:

$$\begin{aligned} \overline{\hat{n}(t)\hat{n}(s)} &= \overline{\tilde{n}(t)\tilde{n}(s)} = N_0\delta(t-s), \\ \overline{\hat{n}(t)\tilde{n}(s)} &= 0, \end{aligned} \tag{83}$$

where  $N_0$  is the noise power density and  $\delta(x)$  is the Dirac delta-function. Using (4), (5), (82), and (83), we obtain

$$\begin{aligned} \overline{\hat{q}_1^2} &= \overline{\tilde{q}_1^2} = \overline{\hat{q}_2^2} = \overline{\tilde{q}_2^2} = 2EN_0, \\ \overline{\hat{q}_1\tilde{q}_1} &= \overline{\hat{q}_2\tilde{q}_2} = 0, \\ \overline{\hat{q}_1\hat{q}_2} &= \overline{\tilde{q}_1\tilde{q}_2} = 2\hat{\lambda}EN_0, \\ \overline{\hat{q}_1\tilde{q}_2} &= -\overline{\tilde{q}_1\hat{q}_2} = 2\hat{\lambda}EN_0. \end{aligned} \tag{84}$$

Finally, because of the assumed independence of the noise and the multipath medium, we find

<sup>45</sup> See Fig. 2, in which let  $\delta=0$ , and multiply all vectors by  $2E$ .

$$\begin{aligned} \overline{\dot{p}\dot{q}_i} &= \overline{\dot{p}} \overline{\dot{q}_i} = 0, \\ \overline{\dot{p}\ddot{q}_i} &= \overline{\dot{p}} \overline{\ddot{q}_i} = 0, \\ \overline{\ddot{p}\dot{q}_i} &= \overline{\ddot{p}} \overline{\dot{q}_i} = 0, \\ \overline{\ddot{p}\ddot{q}_i} &= \overline{\ddot{p}} \overline{\ddot{q}_i} = 0. \end{aligned} \tag{85}$$

The moments in (80), (82), (84), and (85) suffice for the evaluation of the means and the various second self- and cross-moments of the four variables on the left of (79). Using these latter, it is an easy step to compute the matrices of the means and second moments of the  $w$  variables, (71). These are

$$\overline{W} = \begin{bmatrix} \gamma(\beta + 1) \\ 0 \\ \gamma(\beta\hat{\lambda} + \mathbb{1}) \\ \gamma\beta\hat{\lambda} \end{bmatrix} \tag{86}$$

and

$$M = \beta \begin{bmatrix} (\beta+1) & 0 & \hat{\lambda}(\beta+1) & \hat{\lambda}(\beta+1) \\ 0 & (\beta+1) & -\hat{\lambda}(\beta+1) & \hat{\lambda}(\beta+1) \\ \hat{\lambda}(\beta+1) & -\hat{\lambda}(\beta+1) & \beta|\lambda|^2+1 & 0 \\ \lambda(\beta+1) & \hat{\lambda}(\beta+1) & 0 & \beta|\lambda|^2+1 \end{bmatrix}. \tag{87}$$

The matrix of the quadratic form  $R = w_1^2 + w_2^2 - w_3^2 - w_4^2$  is

$$Q = \begin{bmatrix} 1 & 0 & 0 & 0 \\ 0 & 1 & 0 & 0 \\ 0 & 0 & -1 & 0 \\ 0 & 0 & 0 & -1 \end{bmatrix}. \tag{88}$$

Using (86) through (88) we may evaluate the characteristic function,  $F_R(j\mathbf{u})$ , of (74). The two matrices,  $M$  and  $(I - 2j\mathbf{u}M\mathbf{Q})$ , in (74) which must be inverted are both of the form

$$\begin{bmatrix} a & 0 & b & c \\ 0 & a & -c & b \\ b & -c & d & 0 \\ c & b & 0 & d \end{bmatrix}, \tag{89}$$

which has the inverse

$$\frac{1}{ad - b^2 - c^2} \begin{bmatrix} d & 0 & -b & -c \\ 0 & d & c & -b \\ -b & c & a & 0 \\ -c & -b & 0 & a \end{bmatrix}. \tag{90}$$

The determinant of the matrix of (89) is  $(ad - b^2 - c^2)^2$ . After some matrix manipulations, we obtain, replacing  $j\mathbf{u}$  by  $s$ ,

$$F_R(s) = \frac{\exp \left[ \frac{k_1 s (1 + k_2 s)}{1 - k_3 s (1 + k_2 s)} \right]}{1 - k_3 s (1 + k_2 s)} \tag{91}$$

where

$$\begin{aligned} k_1 &= \beta\gamma^2[\beta(1 - |\lambda|^2) + 2(1 - \hat{\lambda})], \\ k_2 &= 2(\beta + 1), \\ k_3 &= 2\beta^2(1 - |\lambda|^2). \end{aligned} \tag{92}$$

On placing (91) in (76), we note that the resulting integrand has singularities at the origin and at

$$\frac{1}{2k_2} \left( -1 \pm \sqrt{1 + \frac{4k_2}{k_3}} \right).$$

The path of integration is along the  $j$  axis, indented to the left at the origin. We may simplify the integral in the following way. First we move the path of integration to the left by  $1/2k_2$ ; no singularities are crossed by the path in this process, so the value of the integral remains the same. The new limits of integration are

$$\left( -j\infty - \frac{1}{2k_2}, +j\infty - \frac{1}{2k_2} \right).$$

Next we make the change of variable  $s = (1/2k_2)(jz - 1)$ ; the limits on the  $z$  integral are then  $(-\infty, +\infty)$ . On separating the new integrand in the  $z$  variable into its real and imaginary parts, we note that the real part is even and the imaginary part odd about  $z=0$ . The integral of the imaginary part thus disappears, and the integral of the real part can be evaluated by doubling its integral over  $(0, \infty)$ . After a little algebra, we obtain

$$P_e = \frac{k_4^2 - 1}{\pi} \int_0^\infty \frac{\exp \left[ -\frac{k_5(z^2 + 1)}{z^2 + k_4^2} \right]}{(z^2 + 1)(z^2 + k_4^2)} dz, \tag{93}$$

where

$$\begin{aligned} k_4 &= \sqrt{1 + \frac{4k_2}{k_3}} \\ k_5 &= \frac{k_1}{k_3}. \end{aligned} \tag{94}$$

We next change the integral into trigonometric form by letting

$$z^2 = k_4^2 \frac{1 - \cos \phi}{1 + \cos \phi}.$$

Using this in (93) and noting that  $z$  can be expressed as

$$z = k_4 \tan \frac{\phi}{2} = k_4 \frac{\sin \phi}{1 + \cos \phi},$$

we obtain

$$P_e = \frac{A}{\pi} \int_0^\pi f(\phi) e^{B \cos \phi} d\phi, \tag{95}$$

where

$$A = \frac{k_4^2 - 1}{2k_4} \exp \left[ -\frac{k_5(1 + k_4^2)}{2k_4^2} \right]$$

$$B = \frac{k_5}{2k_4^2} (k_4^2 - 1) \tag{96}$$

$$a = \frac{k_4 - 1}{k_4},$$

$$b = \frac{k_4 + 1}{k_4},$$

$$c = \sqrt{\frac{k_5}{2}}, \tag{105}$$

and

$$f(\phi) = \frac{1 + \cos \phi}{(k_4^2 + 1) - (k_4^2 - 1) \cos \phi} \tag{97}$$

The integral in (95) may be evaluated by first expanding  $f(\phi)$  in a Fourier cosine series:<sup>46</sup>

$$f(\phi) = \frac{a_0}{2} + \sum_{n=1}^{\infty} a_n \cos n\phi, \tag{98}$$

where

$$a_n = \frac{1}{\pi} \int_{-\pi}^{\pi} f(\phi) \cos n\phi d\phi. \tag{99}$$

Then, noting that

$$\frac{1}{\pi} \int_0^{\pi} e^{B \cos \phi} \cos n\phi d\phi = I_n(B), \tag{100}$$

where  $I_n$  is the  $n$ th-order modified Bessel function of the first kind, we have from (95) and (98)

$$P_e = A \left[ \frac{a_0}{2} I_0(B) + \sum_{n=1}^{\infty} a_n I_n(B) \right]. \tag{101}$$

From (97) and (99) we can evaluate the  $a_n$ 's; they turn out to be:<sup>47</sup>

$$a_n = \begin{cases} \frac{2}{k_4 + 1} & n = 0 \\ \frac{2k_4}{k_4^2 - 1} \left( \frac{k_4 - 1}{k_4 + 1} \right)^n & n > 0. \end{cases} \tag{102}$$

In order to put (101) into the form of (16) we use the following identity:<sup>48</sup>

$$\sum_{n=0}^{\infty} \left( \frac{x}{y} \right)^n I_n(xy) = e^{(x+y)/2} Q(x, y), \tag{103}$$

where  $Q(x, y)$  is given by (17). Putting (102) and (103) into (101), we get

$$P_e = A \left[ -\frac{1}{k_4 - 1} I_0(B) + \frac{1}{A} Q \left( \frac{k_4 - 1}{k_4} \sqrt{\frac{k_5}{2}}, \frac{k_4 + 1}{k_4} \sqrt{\frac{k_5}{2}} \right) \right]. \tag{104}$$

If we let

(104) reduces immediately to (16). The expressions for  $a$ ,  $b$ , and  $c$  in (105) may easily be shown to be identical with those in (20), (21), and (22), respectively, through the use of (92) and (94).

#### APPENDIX IV. PROBABILITY OF ERROR, NON-COHERENT CASE

We may start our derivation of  $P_e$  for the noncoherent case at a fairly advanced point by making use of a result of Helstrom.<sup>24</sup> The result gives  $P_e$  for the noncoherent case for a fixed path [cf. (37)]. Now since in the noncoherent case the form of the ideal receiver for a fading path is the same as that for a fixed path<sup>49</sup>—comparison of the two correlation envelopes at a sampling instant—Helstrom's result may alternatively be considered as the conditional probability of error for a fading path for a given path strength. If we then average this conditional probability of error over all path strengths using the path strength distribution of (11), the result will be  $P_e$  for the noncoherent fading case.

Our starting point is Helstrom's (54). This is, in our terminology,

$$P_e(a) = \frac{\sqrt{1 - |\lambda|^2}}{4\pi} \cdot e^{-\beta a / 4\sigma^2} \int_0^{2\pi} \frac{\exp \left[ \frac{\beta a^2 |\lambda| \cos \phi}{4\sigma^2} \right]}{1 - |\lambda| \cos \phi} d\phi. \tag{106}$$

$P_e(a)$  is the probability of error on condition that path strength is  $a$ . The over-all probability of error is then

$$P_e = \int_0^{\infty} p_r[a] P_e(a) da \tag{107}$$

where  $p_r[a]$  is given by (11).

On placing (106) and (11) in (107), and integrating first on  $a$ ,<sup>50</sup> we arrive, after some algebraic manipulation, at

$$P_e = \frac{\sqrt{1 - |\lambda|^2}}{4\pi} \cdot e^{-\gamma^2/2} \int_0^{2\pi} \left[ \frac{1}{1 - |\lambda| \cos \phi} - \frac{\mu}{1 - \mu |\lambda| \cos \phi} \right] \cdot \exp \left[ \frac{\mu \gamma^2}{\beta(1 - \mu |\lambda| \cos \phi)} \right] d\phi, \tag{108}$$

where  $\mu$ ,  $\beta$ , and  $\gamma$  are given by (18) and (19).

<sup>46</sup> I am indebted to Dr. W. L. Doyle for this suggestion.  
<sup>47</sup> W. Gröbner and N. Hofreiter, "Integraltafel," Springer-Verlag, Vienna, pt. II, p. 112; 1950. See eq. 24.  
<sup>48</sup> J. I. Marcum, "A Statistical Theory of Target Detection by Pulsed Radar," "Mathematical Appendix," Rand Corp., Santa Monica, Calif., Rep. RM-753, p. 5; July 1, 1948.

<sup>49</sup> Note from (15) that this is not true in the coherent case.  
<sup>50</sup> Magnus and Oberhettinger, *op. cit.*, p. 35.

In order to evaluate (108), we must evaluate integrals of the form

$$y(A, B, C) = \int_0^{2\pi} \frac{\exp\left[\frac{A}{1 - B \cos \phi}\right]}{1 - C \cos \phi} d\phi, \quad (109)$$

where  $0 \leq B \leq C \leq 1$ . This may be done as follows.<sup>51</sup> The derivative of  $y$  with respect to  $A$  is

$$\frac{\partial y(A, B, C)}{\partial A} = \int_0^{2\pi} \frac{\exp\left[\frac{A}{1 - B \cos \phi}\right]}{(1 - B \cos \phi)(1 - C \cos \phi)} d\phi. \quad (110)$$

Noting that

$$\frac{1}{(1 - B \cos \phi)(1 - C \cos \phi)} = -\frac{B}{C - B} \frac{1}{1 - B \cos \phi} + \frac{C}{C - B} \frac{1}{1 - C \cos \phi}, \quad (111)$$

we may write (110) as

$$\frac{\partial y(A, B, C)}{\partial A} = \frac{C}{C - B} y(A, B, C) - \frac{B}{C - B} y(A, B, B). \quad (112)$$

The integral

$$y(A, B, B) = \int_0^{2\pi} \frac{\exp\left[\frac{A}{1 - B \cos \phi}\right]}{1 - B \cos \phi} d\phi, \quad (113)$$

may be put in a recognizable form by making the change of variable

$$t = \frac{1 - B^2}{B(1 - B \cos \phi)} - \frac{1}{B}. \quad (114)$$

Doing this, we obtain<sup>52</sup>

$$y(A, B, B) = \frac{2\pi}{\sqrt{1 - B^2}} I_0\left(\frac{BA}{1 - B^2}\right) \exp\left[\frac{A}{1 - B^2}\right]. \quad (115)$$

$$g(A) = \frac{1}{\sqrt{K_1^2 - K_2^2}}$$

$$\cdot \left[ 2e^{K_1 A} Q\left(\sqrt{K_1 A \left(1 - \sqrt{1 - \left(\frac{K_2}{K_1}\right)^2}\right)}\right), \right.$$

$$y(A, B, C) = \exp\left[\frac{CA}{C - B}\right] \left[ \frac{2\pi}{\sqrt{1 - C^2}} - \frac{B}{C - B} \int_0^A y(x, B, B) \exp\left[-\frac{Cx}{C - B}\right] dx \right]. \quad (116)$$

The evaluation of  $y(A, B, C)$  is thus reduced to the evaluation of

$$Z = \int_0^A e^{-K_1 x} I_0(K_2 x) dx, \quad (117)$$

where

$$K_1 = \frac{C}{C - B} - \frac{1}{1 - B^2} = \frac{B(1 - BC)}{(C - B)(1 - B^2)}$$

$$K_2 = \frac{1}{1 - B^2}. \quad (118)$$

On using in (117) the integral representation of  $I_0(K_2 x)$  afforded by (100), and integrating on  $x$  first, one obtains

$$Z = g(0) - g(A)e^{-K_1 A}, \quad (119)$$

where

$$g(A) = \frac{1}{\pi} \int_0^\pi \frac{e^{K_1 A} \cos \phi}{K_1 - K_2 \cos \phi} d\phi. \quad (120)$$

From (118) and the fact that  $0 \leq B \leq C \leq 1$ , it is easily shown that  $K_1 \geq K_2$ .

On placing the Fourier series expansion

$$\frac{1}{K_1 - K_2 \cos \phi} = \frac{a_0}{2} + \sum_{n=1}^\infty a_n \cos n\theta \quad (121)$$

where<sup>47</sup>

$$a_n = \frac{2}{\sqrt{K_1^2 - K_2^2}} \left[ \frac{K_1}{K_2} \left( 1 - \sqrt{1 - \left(\frac{K_2}{K_1}\right)^2} \right) \right]^n \quad (122)$$

in (120), one obtains, using (100),

$$g(A) = \frac{a_0}{2} I_0(K_2 A) + \sum_{n=1}^\infty a_n I_n(K_2 A). \quad (123)$$

Then, on using (103), (123) becomes

$$\left[ \sqrt{K_1 A \left( 1 + \sqrt{1 - \left(\frac{K_2}{K_1}\right)^2} \right)} - I_0(K_2 A) \right]. \quad (124)$$

Now (112) is a differential equation in  $y(A, B, C)$  which may be solved in terms of  $y(A, B, B)$ :

Note that

$$g(0) = \frac{1}{\sqrt{K_1^2 - K_2^2}} = \frac{C - B}{B} \sqrt{\frac{1 - B^2}{1 - C^2}}. \quad (125)$$

Using (124) and (125) in (119), and the result in (116), we obtain for the desired integral

<sup>51</sup> I am indebted to Dr. M. A. Steinberg for the following derivation, culminating in (116).

<sup>52</sup> Bateman Manuscript Project, "Higher Transcendental Functions," McGraw-Hill Book Co., Inc., New York, N. Y., vol. II, p. 81; 1953. See eq. (10).

$$y(A, B, C) = \frac{2\pi \exp\left[\frac{CA}{C-B}\right]}{\sqrt{1-C^2}} \cdot \left[ 2Q\left(\sqrt{K_1 A \left(1 - \sqrt{1 - \left(\frac{K_2}{K_1}\right)^2}\right)}, \sqrt{K_1 A \left(1 + \sqrt{1 - \left(\frac{K_2}{K_1}\right)^2}\right)}\right) - I_0(K_2 A) e^{-K_1 A} \right], \quad (126)$$

where  $K_1(B, C)$  and  $K_2(B, C)$  are given by (118). It can be shown that (126) indeed reduces to (115) in the limit  $B = C$ .

From (108), we have

$$P_s = \frac{\sqrt{1-|\lambda|^2}}{4\pi} e^{-\gamma^2/2} \left[ y\left(\frac{\mu\gamma^2}{\beta}, \mu|\lambda|, |\lambda|\right) - \mu y\left(\frac{\mu\gamma^2}{\beta}, \mu|\lambda|, \mu|\lambda|\right) \right]. \quad (127)$$

Eq. (16), with  $a$ ,  $b$ , and  $c$  as defined in (34), (35) and (36), follows directly on substitution of (115) and (126) into (127).

#### ACKNOWLEDGMENT

The present work is based heavily on the author's M.I.T. doctoral thesis,<sup>16</sup> the value of which was greatly augmented by the suggestions of Dr. W. B. Davenport, Jr., Prof. R. M. Fano, and Dr. R. Price. It is a pleasure to acknowledge indebtedness to them, as well as to Drs. W. L. Doyle, M. A. Steinberg and P. Slepian, without whose aid at certain points in the derivations, the new results reported here would not have been obtained. The author also extends his thanks to Drs. R. Price and L. Weinberg for reading this manuscript and making suggestions for improvement; and to the Mathematics Section, Systems Analysis Laboratory, Hughes Aircraft Company, and in particular, H. I. Fleischer, for programming (16) for machine computation.

## Diffraction by Smooth Cylindrical Mountains\*

H. E. J. NEUGEBAUER† AND M. P. BACHYNSKI†, MEMBER, IRE

**Summary**—This paper is a contribution to the problem of diffraction of EM waves by the smooth crest of a perfectly reflecting mountain. Model experiments at K-band frequencies with mountains of various radii of curvature have been made. The results are compared to an improved Fresnel theory where the reflections of the waves at the surface of the cylinder near its crest are taken into consideration and a correction factor from Fock's theory of grazing incidence is used. The results are also compared to Artmann's and Rice's theories.

### I. INTRODUCTION

A SITUATION sometimes encountered when electromagnetic waves propagate over the surface of the earth is that a mountain range separates a receiving station from the transmitter, causing a diffracted field which may be stronger than one without the mountain. This effect is known as obstacle gain.

In the usual theoretical treatment the mountain has been replaced by a vertical half-plane, and the predictions of this knife edge theory have been found to agree

reasonably well with experimental results obtained in different mountainous areas.<sup>1,2</sup> However, agreement has not been good enough in several other experiments to consider them a justification of the theory. Reference is made to a paper by Crysdale, *et al.*<sup>3</sup> One reason for such discrepancies may be that the knife edge approximation is not adequate and should be replaced by a theory for mountains with a smooth cylindrical crest. Rice<sup>4</sup> has derived a theory for a parabolic cylinder, but it has the disadvantage that its numerical evaluation is difficult in many cases, for instance in the one encountered by Crysdale.

It is obvious that this problem is closely related to the scattering of electromagnetic waves by circular

<sup>1</sup> F. H. Dickson, J. J. Egli, J. W. Herbstreit, and G. S. Wickizer, "Large reductions of vhf transmission loss and fading by the presence of a mountain obstacle in beyond-line-of-sight paths," *Proc. IRE*, vol. 41, pp. 967-969; August, 1953.

<sup>2</sup> R. S. Kirby, H. T. Dougherty, and P. L. McQuate, "Obstacle gain measurements over Pikes Peak at 60 to 1046 mc," *Proc. IRE*, vol. 43, pp. 1467-1472; October, 1955.

<sup>3</sup> J. Crysdale, J. W. B. Day, W. S. Cook, M. E. Psutka, and P. E. Robillard, "An experimental investigation of the diffraction of electromagnetic waves by a dominating ridge," *IRE TRANS. ON ANTENNAS AND PROPAGATION*, vol. AP-5, pp. 203-210; April, 1957.

<sup>4</sup> S. O. Rice, "Diffraction of plane radio waves by a parabolic cylinder," *Bell Sys. Tech. J.*, vol. 33, pp. 417-504; March, 1954.

\* Original manuscript received by the IRE, November 25, 1957. Some of the material contained in this paper was presented at the General Assembly of URSI in Boulder, Colo., August-September, 1957.

† Res. Labs., RCA Victor Co., Ltd., Montreal, Quebec, Can.

cylinders. For good surveys of the existing literature, reference is made to papers by Wait<sup>5</sup> and Adey.<sup>6</sup> For large  $ka = 2\pi a/\lambda$  the mathematical difficulties of evaluating existing theoretical solutions are still great ( $a =$  radius,  $\lambda =$  free space wavelength).

One of the best theoretical approaches has been made by Fock.<sup>7</sup> His very general theory and its recent extensions by Logan<sup>8</sup> require a considerable amount of mathematical manipulations which, in many cases, is prohibitive. Due to these difficulties, a new approach to the problem was made by model experiments in the laboratory and by the derivation of an improved Fresnel theory. Both approaches lead to some interesting results which are in satisfactory mutual agreement.

## II. THEORY

### A. Knife Edge Diffraction

The scalar theory of knife edge diffraction, or diffraction by a conducting half-plane, is based on (1).<sup>9</sup>

$$E = (jk/2\pi) \int_{y=0}^{+\infty} \int_{z=-\infty}^{+\infty} (1/R_1 R_2) \cdot \exp[-jk(R_1 + R_2)] \cos \theta dz dy. \quad (1)$$

$E$  is the field at receiver  $T_2$  (see Fig. 1) when a spherical wave  $(1/R_1) \exp[-jk(R_1 - ct)]$  is transmitted from  $T_1$ . The time dependent factor  $e^{jkc t}$  is omitted in (1). The present treatment differs slightly from the usual one in that the integration is carried out over the half plane  $AC$  which is not in general the continuation of the plane  $AB$  of the obstacle. The plane  $B'AC$  goes through the edge  $A$  of the obstacle and divides angle  $T_1 A T_2$  into equal parts. This "symmetrical" method of evaluating (1) simplifies the formulas when the more general case of a mountain with a smooth cylindrical crest will be treated.

The meaning of most of the symbols and notations is obvious from Fig. 1. It may be added that  $y, z$  is a rectangular coordinate system in the plane  $AC$ , edge  $A$  being the  $z$  axis. The origin and the points  $T_1, T_2$  lie in one plane perpendicular to edge  $A$ . Since the theory will be confined to small scattering angles,  $\Psi_1$  and  $\Psi_2$ , the angle  $2\psi_0 = \Psi_1 + \Psi_2$  is also small, and the distances of the stations from the mountain are nearly the same whether they are referred to the plane  $AB$  or to the plane of integration  $B'AC$  ( $d_1 \approx D_1, d_2 \approx D_2$ ).

<sup>5</sup> J. R. Wait, "Scattering of a plane wave from a circular dielectric cylinder at oblique incidence," *Can. J. Physics*, vol. 33, pp. 189-195; May, 1955.

<sup>6</sup> A. W. Adey, "Diffraction of microwaves by long metal cylinders," *Can. J. Physics*, vol. 33, pp. 407-419; August, 1955.

<sup>7</sup> V. Fock, "The distribution of currents induced by a plane wave on the surface of a conductor," *J. Phys. (USSR)*, vol. 10, pp. 130-136; February, 1946.

"The field of a plane wave near the surface of a conducting body," *J. Phys. (USSR)*, vol. 10, pp. 399-409; May, 1946.

<sup>8</sup> The authors are indebted to N. Logan for making available to them extensive tables of the Fock functions for positive values of the independent variable and for discussions of his improved derivations of more general formulas before publication.

<sup>9</sup> See, e.g., M. Born, "Optik," Julius Springer, Berlin, Ger., p. 153; 1933.

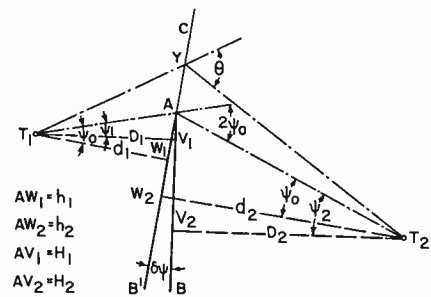


Fig. 1—Knife edge theory.

Another consequence of the assumption of small scattering angles is that the directional beam patterns of the transmitter and receiver could be neglected in (1).

The integration with respect to  $z$  is carried out in the usual manner leading to

$$E = \frac{e^{j\pi/4}}{2d_1 d_2} \sqrt{\frac{kd}{\pi}} \int_0^\infty e^{-jk[R_1 + R_2]} \cos \theta dy \quad (2)$$

where

$$2/d = 1/d_1 + 1/d_2. \quad (3)$$

For a knife edge mountain the integration with respect to  $y$  can also be carried out. The result is denoted by  $E_k(2\psi_0)$  to indicate that it is the field produced by a knife edge when the scattering angle is  $2\psi_0$ .

It is

$$E_k(2\psi_0) = E_k(0) [1 - (C + S) + j(S - C)] \cdot \exp[-jk\psi_0^2(d_1 + d_2 - 2d)/2] \quad (4)$$

where

$$E_k(0) = \frac{\exp[-jk(d_1 + d_2)]}{2(d_1 + d_2)} \quad (5)$$

$$C = C\left(\psi_0 \sqrt{\frac{2kd}{\pi}}\right), \quad S = S\left(\psi_0 \sqrt{\frac{2kd}{\pi}}\right)$$

are the well-known Fresnel integrals.

### B. Diffraction by Cylindrical Mountain

The case of diffraction by a mountain with a smooth crest is illustrated by Fig. 2. It is assumed that the mountain (which is drawn like a wall of thickness  $2a$  with parallel sides) is topped by a half cylinder of radius  $a$  with its axis through point  $M$ . The tangents to the cylinder through  $T_1$  and  $T_2$  intersect at  $N$ ;  $MANC$  is the plane of reference and of integration in the same sense as in the knife edge case. The scattering angle,  $2\psi_0 = \Psi_1 + \Psi_2$  is assumed small and  $d_1 \approx D_1, d_2 \approx D_2$ .

The effects taking place in the case of Fig. 2 are the following:

- 1) Radiation travels from  $T_1$  to  $Y$  where it acts as a source of a secondary wavelet which irradiates  $T_2$ . This scattered radiation is exactly the same as in the case of a knife edge mountain.

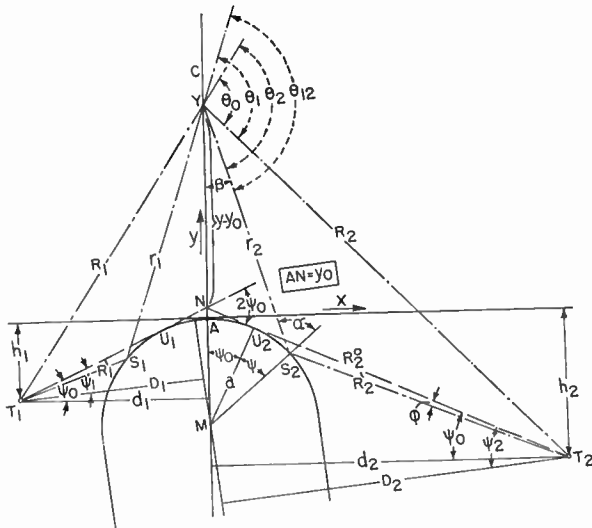


Fig. 2—Four ray theory for mountain with smooth crest.

- 2) Radiation travels from  $T_1$  to  $S_1$  and is reflected towards point  $Y$  where it causes another secondary wavelet which also irradiates  $T_2$ .
- 3) The radiation from both secondary wavelets mentioned in 1 and 2 is reflected at  $S_2$  to reach  $T_2$  via path  $YS_2T_2$ .

Hence, there are four different paths along which radiation can travel from  $T_1$  to  $T_2$ , viz.,  $T_1YT_2$ ,  $T_1S_1YT_2$ ,  $T_1YS_2T_2$ , and  $T_1S_1YS_2T_2$ . The total scattering field at  $T_2$  can be obtained when the integral in (2) is replaced by the four integrals of (6).

$$E = \frac{e^{i\pi/4}}{2d_1d_2} \sqrt{\frac{kd}{\pi}} \left\{ \int_{y_0}^{\infty} \exp[-jk(R_1 + R_2)] \cos \theta_0 dy \right. \\ + \rho \int_{y_0}^{\infty} \text{Div}(S_1) \exp[-jk(R_1' + r_1 + R_2)] \cos \theta_1 dy \\ + \rho \int_{y_0}^{\infty} \text{Div}(S_2) \exp[-jk(R_1 + r_2 + R_2')] \cos \theta_2 dy \\ + \rho^2 \int_{y_0}^{\infty} \text{Div}(S_1) \text{Div}(S_2) \\ \cdot \exp[-jk(R_1' + r_1 + r_2 + R_2')] \cos \theta_{12} dy \left. \right\}. \quad (6)$$

This equation requires two explanations.

- 1) The factor  $\rho$  indicates change of phase and/or intensity on reflection. In Section II-C it will be shown that, for a perfect conductor,  $\rho = +0.7$  for vertical polarization (electric vector perpendicular to cylinder axis) and  $\rho = -1.0$  for horizontal polarization (electric vector parallel to cylinder axis.)
- 2) The intensity of a beam which is reflected by a curved surface is reduced due to its energy being spread over a wider angle. The divergence factors  $\text{Div}(S_1)$  and  $\text{Div}(S_2)$  representing these intensity losses for reflections at  $S_1$  or  $S_2$  are given by

$$\text{Div}(S_i) = 1 / \sqrt{1 + \frac{2 \sec \alpha_i}{a(1/R_i' + 1/r_i)}} \quad (i = 1, 2) \quad (7)$$

where  $\alpha_1$  and  $\alpha_2$  are the angles of incidence. Eq. (7) is easily obtained from (22) of a paper by Riblet and Barker.<sup>10</sup>

The first integral of (6) is evaluated as in the knife edge case; the only difference is that  $y_0$  (distance between  $A$  and  $N$ ) should be added to  $h_1$  and  $h_2$ . However,  $y_0 \ll h_1, h_2$  for small scattering angles  $2\psi_0$  and large distances  $d_1, d_2$  so that, with these restrictions, the first term is the same as in the knife edge case. The evaluation of the third integral of (6) may be discussed as an example. The second integral can be treated in exactly the same, and the fourth integral in a very similar manner.

The evaluation depends on the behavior of the exponent  $R_1 + r_2 + R_2'$  and of the factors  $\text{Div}(S_2)$  and  $\cos \theta_2$  for increasing  $y$ . It is seen from Fig. 2 that point  $S_2$  does not move much when point  $Y$  goes to infinity. Hence,  $R_2'$  remains almost constant while  $r_2$  increases approximately as fast as  $y$ .  $R_1$  increases at the same rate as in the knife edge case  $(y + h_1)^2/d_1$ . It can therefore be expected that large values of  $y$  do not contribute much to the value of the integral because the exponent oscillates too rapidly. In addition it is seen that the angle  $\theta_2$  grows rapidly when  $Y$  moves away from  $N$  so that  $\cos \theta_2 \rightarrow 0$ . Also the divergence factor  $\text{Div}(S_2)$  becomes small for large  $y$  as  $\sec \alpha_2 \approx \sqrt{2}$ ,  $a/R_2' \ll 1$  and  $a/r_2 \rightarrow 0$ .

These considerations make it appear likely that the main contribution to the integral comes from points  $Y$  near  $N$ . To justify this assumption and to calculate the integral it is convenient to express all the variables as functions of the angle  $\psi$  between the two radii  $MU_2$  and  $MS_2$ .

$$y = a[\sin(\psi + \psi_0) \tan(2\psi + \phi + \psi_0) + \cos(\psi + \psi_0) - 1] \quad (8a)$$

$$R_1 = d_1 + (y + h_1)^2/2d_1 \quad (8b)$$

$$r_2 = a \sin(\psi + \psi_0) / \cos(2\psi + \phi + \psi_0) \quad (8c)$$

$$R_2' = \sqrt{4a^2 \sin^4 \frac{\psi}{2} + (R_2^0 - a \sin \psi)^2} \quad (8d)$$

$$\phi \text{ follows from } R_2^0 \sin \phi = 2a \sin \frac{\psi}{2} \sin(\phi + \psi/2) \quad (8e)$$

$$\theta_2 = 2\psi + \psi_0 + \phi + \tan^{-1}[(y + h_1)/d_1] \quad (8f)$$

$$\text{Div}(S_2) = 1 / \sqrt{1 + \frac{2r_2d_2}{a(r_2 + d_2) \sin(\psi + \phi)}} \quad (8g)$$

It may be recalled that  $\psi_0$  has been assumed to be small. Hence, in the following series expansions obtained from (8)  $\psi$  and  $\psi_0$  are treated as small angles.

<sup>10</sup> H. J. Riblet and C. B. Baker, "A general divergence formula," *J. Appl. Phys.*, vol. 19, pp. 63-70; January, 1948.

work is particularly simple when the distances  $d_1$  and  $d_2$  are big enough so that  $d_{1,2} \gg 5a\psi_0$ . Then (17) and (22) can be replaced by  $F_1 = F_2 = F = 2$ , and the only parameter on which the integral for  $E_1$  depends is  $x_0 = \psi_0 \sqrt{2ka}$ . Since this holds true also for the other integrals  $E_2$  and  $E_{12}$ , some simple algebraic operations are sufficient to calculate the diffraction curve for any  $ka$  after the integrals have been evaluated for a series of values of only one parameter,  $x_0$ . The calculated results quoted in Section III have been obtained under these simplifying assumptions.

*E. Artmann Shift*

Both Artmann<sup>13</sup> and Rice<sup>4</sup> predict that the power measured behind a cylinder as a function of scattering angle varies in the same manner as behind a knife edge, except that the edge appears higher or lower depending upon the polarization and radius of curvature of the cylinder. This virtual displacement in height ( $\delta$ ) is given by:

$$\delta = \kappa_{\perp, \parallel} \lambda \left( \frac{a}{\lambda} \right)^{1/3} \tag{32}$$

where  $\kappa_{\perp, \parallel}$  is a constant depending upon polarization.

For a comparison of this theory with the theories of Artmann and Rice, it must be kept in mind that these two authors obtain their results under the assumption of an incident plane wave and of a receiver that tends towards infinity. In the notations of this paper

$$d_2 \rightarrow \infty \tag{33}$$

$$d_1 \gg d_2. \tag{34}$$

When the two conditions (33) and (34) are observed, a similar result can be obtained from this theory.

It follows from (33) that the diffraction curves are straight and parallel for the intervals of  $\psi_0$  and  $ka$  considered in the following derivation.

Curve 1 of Fig. 4 shows power  $P$  against the half scattering angle  $\psi_0$  for knife edge diffraction. The slope ( $\tan \alpha$ ) of this curve can be calculated by differentiation of  $P = E_k(\psi_0)E_k^*(\psi_0)$  with respect to  $\psi_0$ . With the expression (4) for  $E_k(\psi_0)$  it is found

$$\tan \alpha = - \frac{1}{2(d_1 + d_2)^2} \sqrt{\frac{2kd}{\pi}}. \tag{35}$$

Curve 2 shows diffraction for a cylindrical mountain. The distance  $\sigma$  between the two curves for  $\psi_0 = 0$  is obtained from (38). Assume that  $d$  is large enough for the third term in the square bracket of (38) to be neglected, then

$$\sigma = \frac{A_{\perp, \parallel}}{4(d_1 + d_2)^2} \cdot \frac{\sqrt[3]{ka}}{\sqrt{\pi kd}}. \tag{36}$$

The Artmann shift  $\delta = -2\psi_0 d_2$  is obtained from (35), (36) and  $\psi_0 = \sigma / \tan \alpha$ .

<sup>13</sup> K. Artmann, "Beugung polarisierten Lichtes an Blenden endlicher Dicke im Gebiet der Schattengrenze," *Z. für Phys.*, vol. 127, pp. 468-494; May, 1950.

$$\delta = \frac{A_{\perp, \parallel} \sqrt[3]{2\pi}}{2\sqrt{2\pi}} \lambda \sqrt[3]{\frac{a}{\lambda}} \frac{d_2}{d}. \tag{37}$$

From (3) and (34),

$$d = 2d_2$$

which is substituted into (37). Comparing (32) and (37).

$$\kappa_{\perp, \parallel} = \frac{\sqrt[3]{2\pi}}{\sqrt{2\pi}} A_{\perp, \parallel}.$$

With the numerical values for  $A_{\perp, \parallel}$  given in (38)

$$\kappa_{\perp} = + 0.316; \quad \kappa_{\parallel} = - 0.333.$$

If, however, condition (34) is dropped,

$$\kappa_{\perp} = + 0.316(1 + d_2/d_1); \quad \kappa_{\parallel} = - 0.333(1 + d_2/d_1).$$

Hence, the constants  $\kappa$  assume about twice the values calculated above when  $d_1$  and  $d_2$  are of the same order of magnitude.

A table of the values calculated by different authors for  $\kappa$  will be given in Section III in connection with the experimental determinations.

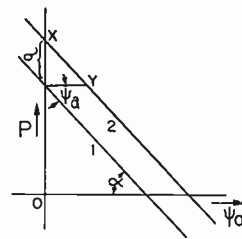


Fig. 4—Derivation of Artmann shift.

III. EXPERIMENT

*A. Apparatus and Technique*

Investigation of diffraction by smooth half-cylindrical mountains and comparison of these results with those of knife edge diffraction have been made by taking measurements on models in the *K*-band frequency range. The experimental arrangement is shown in Fig. 5. A 2K33 klystron was used as a source of energy, and the oscillator was sufficiently isolated from the transmitting horn by means of a uniline. The transmitted signal, modulated at 1000 cps, was detected by a 1N26 crystal and the rectified signal was fed directly into a Scientific Instruments Automatic Pattern Recorder Model 121. The motion of the receiving probe was directly coupled to the selsyn drive of the recorder so that scans of received power against probe position could be directly obtained. Small horns with very similar patterns in both the *E* and *H* planes were used for the transmitting and receiving antennas. The measurements obtained with the receiving horn were checked against those obtained with a dipole and found to be identical for the range of scattering angles investigated in these experiments.

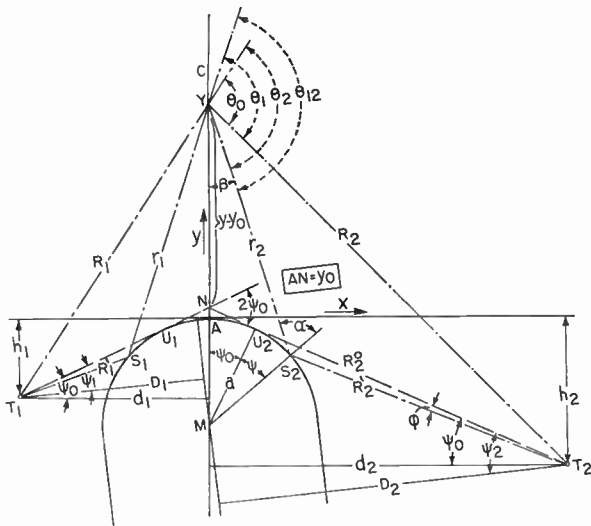


Fig. 2—Four ray theory for mountain with smooth crest.

- 2) Radiation travels from  $T_1$  to  $S_1$  and is reflected towards point  $Y$  where it causes another secondary wavelet which also irradiates  $T_2$ .
- 3) The radiation from both secondary wavelets mentioned in 1 and 2 is reflected at  $S_2$  to reach  $T_2$  via path  $YS_2T_2$ .

Hence, there are four different paths along which radiation can travel from  $T_1$  to  $T_2$ , viz.,  $T_1YT_2$ ,  $T_1S_1YT_2$ ,  $T_1YS_2T_2$ , and  $T_1S_1YS_2T_2$ . The total scattering field at  $T_2$  can be obtained when the integral in (2) is replaced by the four integrals of (6).

$$\begin{aligned}
 E = & \frac{e^{i\pi/4}}{2d_1d_2} \sqrt{\frac{kd}{\pi}} \left\{ \int_{y_0}^{\infty} \exp[-jk(R_1 + R_2)] \cos \theta_0 dy \right. \\
 & + \rho \int_{y_0}^{\infty} \text{Div}(S_1) \exp[-jk(R_1' + r_1 + R_2)] \cos \theta_1 dy \\
 & + \rho \int_{y_0}^{\infty} \text{Div}(S_2) \exp[-jk(R_1 + r_2 + R_2')] \cos \theta_2 dy \\
 & + \rho^2 \int_{y_0}^{\infty} \text{Div}(S_1) \text{Div}(S_2) \\
 & \left. \cdot \exp[-jk(R_1' + r_1 + r_2 + R_2')] \cos \theta_{12} dy \right\}. \quad (6)
 \end{aligned}$$

This equation requires two explanations.

- 1) The factor  $\rho$  indicates change of phase and/or intensity on reflection. In Section II-C it will be shown that, for a perfect conductor,  $\rho = +0.7$  for vertical polarization (electric vector perpendicular to cylinder axis) and  $\rho = -1.0$  for horizontal polarization (electric vector parallel to cylinder axis.)
- 2) The intensity of a beam which is reflected by a curved surface is reduced due to its energy being spread over a wider angle. The divergence factors  $\text{Div}(S_1)$  and  $\text{Div}(S_2)$  representing these intensity losses for reflections at  $S_1$  or  $S_2$  are given by

$$\text{Div}(S_i) = 1 / \sqrt{1 + \frac{2 \sec \alpha_i}{a(1/R_i' + 1/r_i)}} \quad (i = 1, 2) \quad (7)$$

where  $\alpha_1$  and  $\alpha_2$  are the angles of incidence. Eq. (7) is easily obtained from (22) of a paper by Riblet and Barker.<sup>10</sup>

The first integral of (6) is evaluated as in the knife edge case; the only difference is that  $y_0$  (distance between  $A$  and  $N$ ) should be added to  $h_1$  and  $h_2$ . However,  $y_0 \ll h_1, h_2$  for small scattering angles  $2\psi_0$  and large distances  $d_1, d_2$  so that, with these restrictions, the first term is the same as in the knife edge case. The evaluation of the third integral of (6) may be discussed as an example. The second integral can be treated in exactly the same, and the fourth integral in a very similar manner.

The evaluation depends on the behavior of the exponent  $R_1 + r_2 + R_2'$  and of the factors  $\text{Div}(S_2)$  and  $\cos \theta_2$  for increasing  $y$ . It is seen from Fig. 2 that point  $S_2$  does not move much when point  $Y$  goes to infinity. Hence,  $R_2'$  remains almost constant while  $r_2$  increases approximately as fast as  $y$ .  $R_1$  increases at the same rate as in the knife edge case  $(y + h_1)^2/d_1$ . It can therefore be expected that large values of  $y$  do not contribute much to the value of the integral because the exponent oscillates too rapidly. In addition it is seen that the angle  $\theta_2$  grows rapidly when  $Y$  moves away from  $N$  so that  $\cos \theta_2 \rightarrow 0$ . Also the divergence factor  $\text{Div}(S_2)$  becomes small for large  $y$  as  $\sec \alpha_2 \approx \sqrt{2}$ ,  $a/R_2' \ll 1$  and  $a/r_2 \rightarrow 0$ .

These considerations make it appear likely that the main contribution to the integral comes from points  $Y$  near  $N$ . To justify this assumption and to calculate the integral it is convenient to express all the variables as functions of the angle  $\psi$  between the two radii  $MU_2$  and  $MS_2$ .

$$y = a[\sin(\psi + \psi_0) \tan(2\psi + \phi + \psi_0) + \cos(\psi + \psi_0) - 1] \quad (8a)$$

$$R_1 = d_1 + (y + h_1)^2/2d_1 \quad (8b)$$

$$r_2 = a \sin(\psi + \psi_0) / \cos(2\psi + \phi + \psi_0) \quad (8c)$$

$$R_2' = \sqrt{4a^2 \sin^4 \frac{\psi}{2} + (R_2^0 - a \sin \psi)^2} \quad (8d)$$

$$\phi \text{ follows from } R_2^0 \sin \phi = 2a \sin \frac{\psi}{2} \sin(\phi + \psi/2) \quad (8e)$$

$$\theta_2 = 2\psi + \psi_0 + \phi + \tan^{-1}[(y + h_1)/d_1] \quad (8f)$$

$$\text{Div}(S_2) = 1 / \sqrt{1 + \frac{2r_2d_2}{a(r_2 + d_2) \sin(\psi + \phi)}} \quad (8g)$$

It may be recalled that  $\psi_0$  has been assumed to be small. Hence, in the following series expansions obtained from (8)  $\psi$  and  $\psi_0$  are treated as small angles.

<sup>10</sup> H. J. Riblet and C. B. Baker, "A general divergence formula," *J. Appl. Phys.*, vol. 19, pp. 63-70; January, 1948.

$$y = 2a\psi_0\psi + (3a + a^2\psi_0/d_2)\psi^2/2 + \psi^3 a^2/(2d_2) \quad (9a)$$

$$R_1 = d_1(1 + \psi_0^2/2) + 2a\psi_0^2\psi + 3a\psi_0\psi^2/2 + [3/d_1 + 1/(2d_2)]a^2\psi_0\psi^3 \quad (9b)$$

$$r_2 = a\psi_0 + a\psi(1 + 2\psi_0^2) + 7a\psi_0\psi^2/2 + [11/6 + 3a\psi_0/(2d_2)]a\psi^3 \quad (9c)$$

$$R_2' = d_2(1 + \psi_0^2/2) - a\psi_0 - a\psi + a\psi^3/6 \quad (9d)$$

$$\phi = a\psi^2/(2d_2) + a^2\psi^3/(2d_2^2) \quad (9e)$$

$$\cos \theta_2 = 1 \quad (9f)$$

$$\text{Div}(S_2) = \sqrt{\psi/(3\psi + 2\psi_0)} \quad (9g)$$

and

$$R_1 + r_2 + R_2' = (d_1 + d_2)(1 + \psi_0^2/2) + 4a\psi_0^2\psi + [5 + \psi_0\{a/d_2 + 11a/(4d_1)\}]a\psi_0\psi^2 + [2 + a\psi_0\{2/d_2 + 3/d_1\}]a\psi^3 + \dots \quad (10)$$

From (10) and (9a) one can see that, for  $\psi_0=0$  and small  $y$ , the exponent  $R_1+r_2+R_2'$  behaves as  $y^{2/3}$  (or  $\psi^3$ ) although it has been shown to grow at least as fast as  $y$  for larger values of  $y$ . Hence, the main contribution to the integral comes from small  $\psi$ . If  $\psi_0 \neq 0$ , terms of lower order in  $\psi$  appear at the right side of (10). Since the linear term contains the factor  $\psi_0^2$ , small values of  $\psi$  are still decisive for the integration providing that  $\psi_0$  is small enough. The linear term in  $\psi$  will be omitted in the sequel.

C. Fock Correction

In the preceding part it has been established that only points  $Y$  near the surface of the mountain contribute essentially to the integral. This fact makes the approximate calculation of the integral possible. Another consequence is that the factor  $\rho$  can be specified. The derivation of (6) has been based on Huygen's principle and on the application of *geometric optics* to the rays coming from the transmitter or from secondary sources. According to geometric optics the total field near the surface is twice the incident field for vertical polarization, and no phase change takes place. It is zero for horizontal polarization, and the phase change is  $\pi$ .

According to the theory of Fock<sup>7</sup> which has been experimentally confirmed by Wetzel and Brick<sup>11</sup> the geometric optics field must be multiplied with a slowly varying factor to obtain the real field in the penumbra zone for large  $ka$ . No correction is required for horizontal polarization because geometric optics and Fock's theory predict a vanishing field near the surface. For vertical polarization, geometric optics predicts twice the incident field whereas Fock's theory predicts 1.4 times the incident field. Hence, this theory is brought into agreement with Fock's results by putting

$$\rho_{\parallel} = -1.0; \quad \rho_{\perp} = +0.7. \quad (11)$$

<sup>11</sup> L. Wetzel and D. B. Brick, "An Experimental Investigation of High-Frequency Current Distributions on Conducting Cylinders," *Cruft Lab., Harvard University, Cambridge, Mass., Sci. Rep. No. 4; December 12, 1955.*

D. Evaluation of Integrals

Eq. (6) may be written

$$E_{1,\parallel} = E_k + \rho_{\perp,\parallel}E_1 + \rho_{\perp,\parallel}E_2 + \rho_{\perp,\parallel}^2E_{12} \quad (12)$$

where

$$E_k = \frac{e^{i\pi/4}}{2d_1d_2} \sqrt{\frac{kd}{\pi}} \int \exp[-jk(R_1 + R_2)]dy \quad (13a)$$

$$E_1 = \frac{e^{i\pi/4}}{2d_1d_2} \sqrt{\frac{kd}{\pi}} \int \text{Div}(S_1) \cdot \exp[-jk(R_1' + r_1 + R_2)]dy \quad (13b)$$

$$E_2 = \frac{e^{i\pi/4}}{2d_1d_2} \sqrt{\frac{kd}{\pi}} \int \text{Div}(S_2) \cdot \exp[-jk(R_1 + r_2 + R_2')]dy \quad (13c)$$

$$E_{12} = \frac{e^{i\pi/4}}{2d_1d_2} \sqrt{\frac{kd}{\pi}} \int \text{Div}(S_1) \text{Div}(S_2) \cdot \exp[-jk(R_1' + r_1 + r_2 + R_2')]dy. \quad (13d)$$

On substitution from (9) and (10) into (13c) and by some elementary manipulations (14) is obtained.

$$E_2 = E_k(0) \frac{2ka}{\sqrt{\pi kd}} e^{i[\pi/4 - \psi_0(d_1+d_2)/2]} \int_0^\infty L_2 \cdot \exp[-jka(G\psi^2 + F_2\psi^3)]d\psi \quad (14)$$

with

$$L_2 = \sqrt{\psi/(3\psi + 2\psi_0)} [2\psi_0 + (3 + a\psi_0/d_2)\psi] \quad (15)$$

$$G = 5\psi_0, \quad F_2 = 2 + a\psi_0(2/d_2 + 3/d_1). \quad (16)$$

The corresponding expression for  $E_1$  is obtained by replacing subscript 2 by subscript 1. In most cases  $L_1$  differs so little from  $L_2$  and  $F_1$  from  $F_2$  that  $E_1 = E_2$ . Usually

$$L_1 = L_2 = \sqrt{\psi(3\psi + 2\psi_0)} \\ F_1 = F_2 = 2 + 5a\psi_0/d \quad \text{or even } F_1 = F_2 = 2 \quad (17)$$

are sufficiently accurate approximations. When the corresponding substitutions are made in (13d), a slight complication arises from the fact that the two angles  $\psi$  on the side of transmitter  $T_1$  and receiver  $T_2$ , which belong to the same point  $Y$ , are not equal unless  $d_1 = d_2$ . The two angles may be denoted  $\psi_1$  and  $\psi_2$ . The result of the substitution of (9) into (13d) is

$$E_{12} = E_k(0) \frac{2k}{\sqrt{\pi kd}} e^{i[\pi/4 - \psi_0(d_1+d_2)/2]} \int_0^\infty \text{Div}(S_1) \text{Div}(S_2) \cdot \exp[-jka\{G'(\psi_1^2 + \psi_2^2) + F_1'\psi_1^3 + F_2'\psi_2^3\}]dy, \quad (18)$$

where

$$G' = 7\psi_0/2, \quad F_1' = 2 + 3a\psi_0/(2d_1), \quad F_2' = 2 + 3a\psi_0/(2d_2).$$

The angles  $\psi_1$  and  $\psi_2$  are related to  $y$  by means of

$$y = 2a\psi_0\psi_1 + (3a + a^2\psi_0/d_1)\psi_1^2/2 \\ = 2a\psi_0\psi_2 + (3a + a^2\psi_0/d_2)\psi_2^2/2. \quad (19)$$

In most practical cases (18) can be simplified by setting

$$1/d_1 = 1/d + \Delta, \quad 1/d_2 = 1/d - \Delta$$

and by introducing a new variable  $\psi$  by means of

$$y = 2a\psi_0\psi + (3a + a^2\psi_0/d)\psi^2/2. \quad (20)$$

When correction terms of second or higher order are neglected, (18) can be written:

$$E_{12} = E_k(0) \frac{2ka}{\sqrt{\pi kd}} e^{j[\pi/4 - \psi_0^2(d_1+d_2)/2]} \int_0^\infty L \cdot \exp[-2jka(G'\psi^2 + F'\psi^3)] d\psi \quad (21)$$

where

$$2F' = F_1' + F_2' = 2(2 + 3a\psi_0/[2d])$$

and

$$L = [\psi/(2\psi_0 + 3\psi)][2\psi_0 + 3\psi + a\psi_0\psi/d] \approx \psi. \quad (22)$$

Collecting the results for the four integrals occurring in (12),

$$E = E_k(0)e^{-jk\psi_0^2(d_1+d_2)/2} \left\{ [1 - (1+j)(C-jS)]e^{jk\psi_0 d} + \frac{2ka}{\sqrt{\pi kd}} e^{j\pi/4} \left[ \rho \int_0^\infty L_1 \exp[-jka(G\psi^2 + F_1\psi^3)] d\psi + \rho \int_0^\infty L_2 \exp[-jka(G\psi^2 + F_2\psi^3)] d\psi + \rho^2 \int_0^\infty \psi \exp[-2jka(G'\psi^2 + F'\psi^3)] d\psi \right] \right\}. \quad (23)$$

Concerning the numerical evaluation of these integrals it is advantageous to introduce a new variable  $x$  which, in the case of the first integral of (23), is defined by

$$x = \beta_1 e^{j\pi/6} \psi \quad (24)$$

with

$$\beta_1 = \sqrt[3]{kaF_1}. \quad (25)$$

In addition

$$x_0 = \beta_1 \psi_0. \quad (26)$$

As a result of transformation (24) the path of integration is from zero to  $\infty e^{j\pi/6}$  but can be replaced by the real axis from zero to infinity. The justification is the same as for the evaluation of Fresnel's integrals.<sup>12</sup>

The complete expression for  $E_1$  can finally be written

$$E_1 = E_k(0) \frac{2\beta_1\rho}{F_1\sqrt{\pi kd}} \cdot e^{-jk\psi_0^2(d_1+d_2)/2} \cdot \int_0^\infty \sqrt{xM} \{ \cos P - j \sin P \} \cdot \exp \left[ - \left( \frac{5\sqrt{3}x_0}{2F_1} x^2 + x^3 \right) \right] dx \quad (27)$$

where the real quantities  $M$ ,  $P$ , and  $\mu$  are defined by

$$Me^{j\mu} = 3x + 2x_0e^{j\pi/6}$$

$$P = \pi/12 - \mu/2 + \frac{5x_0}{2F_1} x^2.$$

It is easy to calculate (27), for example by Simpson's rule, as the exponential tends rapidly towards zero. The other integrals are calculated correspondingly.

A slight change in (23) and the similar equations of the preceding sections is required when the stations are higher than the mountain. This case is illustrated in Fig. 3. With the convention chosen in this paper the station "heights"  $h_1$ ,  $h_2$  and the scattering angle  $2\psi_0$  are negative. It is seen from Fig. 3 that nothing has to be changed except the lower limit of the integrals, which is  $-\psi_0$  instead of zero;  $S_1$  must always lie on the left and  $S_2$  on the right of plane  $MAC$ .

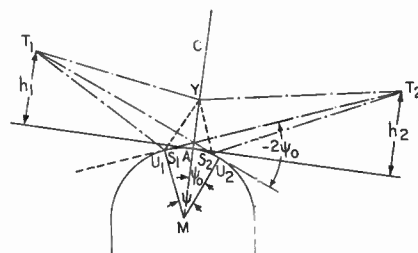


Fig. 3—Stations above the mountain.

Term  $E_1$  may be treated as example.

The substitution

$$\psi = -\psi_0 + \psi'$$

brings the expression  $G\psi^2 + F_1\psi^3$  into the form

$$-(F_1\psi_0^3 - G\psi_0^2) + (3F_1\psi_0^2 - 2G\psi_0)\psi' - (3F_1\psi_0 - G)\psi'^2 + F_1\psi'^3. \quad (28)$$

The order of magnitude of the terms of (28) can be estimated by putting  $F_1 = 2$  and  $G = 5\psi_0$  leading to

$$3\psi_0^3 - 4\psi_0^2\psi' - \psi_0\psi'^2 + 2\psi'^3.$$

For small scattering angles it appears justified to neglect the first two terms in (28) so that the integral reduces to

$$\int_{-\psi_0}^\infty L_1 \exp[-jka(G\psi^2 + F_1\psi^3)] d\psi = \int_0^\infty L_1 \exp[-jka(-H_1\psi_0\psi'^2 + F_1\psi'^3)] d\psi \quad (29)$$

with

$$L_1 = \sqrt{(\psi' - \psi_0)(3\psi' - \psi_0)} \quad (30)$$

and

$$H_1 = 3F_1 - 5. \quad (31)$$

To find the complete diffraction curve for a certain radius of curvature it is necessary to calculate the received power  $P = EE^*$  for different values of  $2\psi_0$ . This

<sup>12</sup> Born, *op. cit.*, p. 193.

work is particularly simple when the distances  $d_1$  and  $d_2$  are big enough so that  $d_{1,2} \gg 5a\psi_0$ . Then (17) and (22) can be replaced by  $F_1 = F_2 = F = 2$ , and the only parameter on which the integral for  $E_1$  depends is  $x_0 = \psi_0 \sqrt{2ka}$ . Since this holds true also for the other integrals  $E_2$  and  $E_{12}$ , some simple algebraic operations are sufficient to calculate the diffraction curve for any  $ka$  after the integrals have been evaluated for a series of values of only one parameter,  $x_0$ . The calculated results quoted in Section III have been obtained under these simplifying assumptions.

*E. Artmann Shift*

Both Artmann<sup>13</sup> and Rice<sup>4</sup> predict that the power measured behind a cylinder as a function of scattering angle varies in the same manner as behind a knife edge, except that the edge appears higher or lower depending upon the polarization and radius of curvature of the cylinder. This virtual displacement in height ( $\delta$ ) is given by:

$$\delta = \kappa_{\perp, \parallel} \lambda \left( \frac{a}{\lambda} \right)^{1/3} \tag{32}$$

where  $\kappa_{\perp, \parallel}$  is a constant depending upon polarization.

For a comparison of this theory with the theories of Artmann and Rice, it must be kept in mind that these two authors obtain their results under the assumption of an incident plane wave and of a receiver that tends towards infinity. In the notations of this paper

$$d_2 \rightarrow \infty \tag{33}$$

$$d_1 \gg d_2. \tag{34}$$

When the two conditions (33) and (34) are observed, a similar result can be obtained from this theory.

It follows from (33) that the diffraction curves are straight and parallel for the intervals of  $\psi_0$  and  $ka$  considered in the following derivation.

Curve 1 of Fig. 4 shows power  $P$  against the half scattering angle  $\psi_0$  for knife edge diffraction. The slope ( $\tan \alpha$ ) of this curve can be calculated by differentiation of  $P = E_k(\psi_0)E_k^*(\psi_0)$  with respect to  $\psi_0$ . With the expression (4) for  $E_k(\psi_0)$  it is found

$$\tan \alpha = - \frac{1}{2(d_1 + d_2)^2} \sqrt{\frac{2kd}{\pi}}. \tag{35}$$

Curve 2 shows diffraction for a cylindrical mountain. The distance  $\sigma$  between the two curves for  $\psi_0 = 0$  is obtained from (38). Assume that  $d$  is large enough for the third term in the square bracket of (38) to be neglected, then

$$\sigma = \frac{A_{\perp, \parallel}}{4(d_1 + d_2)^2} \cdot \frac{\sqrt[3]{ka}}{\sqrt{\pi kd}}. \tag{36}$$

The Artmann shift  $\delta = -2\psi_0 d_2$  is obtained from (35), (36) and  $\psi_0 = \sigma / \tan \alpha$ .

<sup>13</sup> K. Artmann, "Beugung polarisierten Lichtes an Blenden endlicher Dicke im Gebiet der Schattengrenze," *Z. für Phys.*, vol. 127, pp. 468-494; May, 1950.

$$\delta = \frac{A_{\perp, \parallel} \sqrt[3]{2\pi}}{2\sqrt{2\pi}} \lambda \sqrt[3]{\frac{a}{\lambda}} \frac{d_2}{d}. \tag{37}$$

From (3) and (34),

$$d = 2d_2$$

which is substituted into (37). Comparing (32) and (37).

$$\kappa_{\perp, \parallel} = \frac{\sqrt[3]{2\pi}}{\sqrt{2\pi}} A_{\perp, \parallel}.$$

With the numerical values for  $A_{\perp, \parallel}$  given in (38)

$$\kappa_{\perp} = + 0.316; \quad \kappa_{\parallel} = - 0.333.$$

If, however, condition (34) is dropped,

$$\kappa_{\perp} = + 0.316(1 + d_2/d_1); \quad \kappa_{\parallel} = - 0.333(1 + d_2/d_1).$$

Hence, the constants  $\kappa$  assume about twice the values calculated above when  $d_1$  and  $d_2$  are of the same order of magnitude.

A table of the values calculated by different authors for  $\kappa$  will be given in Section III in connection with the experimental determinations.

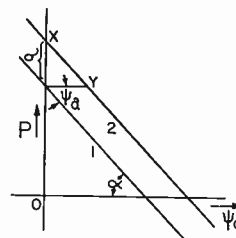


Fig. 4—Derivation of Artmann shift.

III. EXPERIMENT

A. Apparatus and Technique

Investigation of diffraction by smooth half-cylindrical mountains and comparison of these results with those of knife edge diffraction have been made by taking measurements on models in the *K*-band frequency range. The experimental arrangement is shown in Fig. 5. A 2K33 klystron was used as a source of energy, and the oscillator was sufficiently isolated from the transmitting horn by means of a uniline. The transmitted signal, modulated at 1000 cps, was detected by a 1N26 crystal and the rectified signal was fed directly into a Scientific Instruments Automatic Pattern Recorder Model 121. The motion of the receiving probe was directly coupled to the selsyn drive of the recorder so that scans of received power against probe position could be directly obtained. Small horns with very similar patterns in both the *E* and *H* planes were used for the transmitting and receiving antennas. The measurements obtained with the receiving horn were checked against those obtained with a dipole and found to be identical for the range of scattering angles investigated in these experiments.

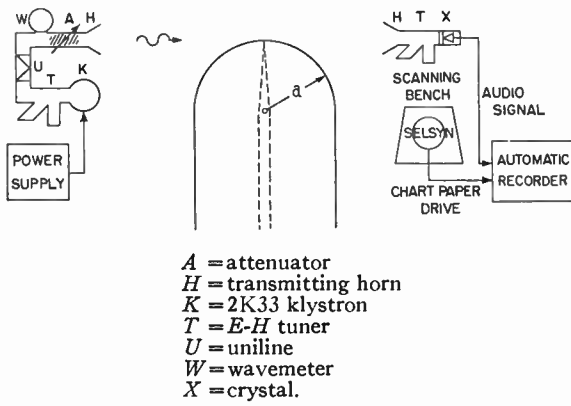


Fig. 5—Schematic diagram of the experimental arrangement.

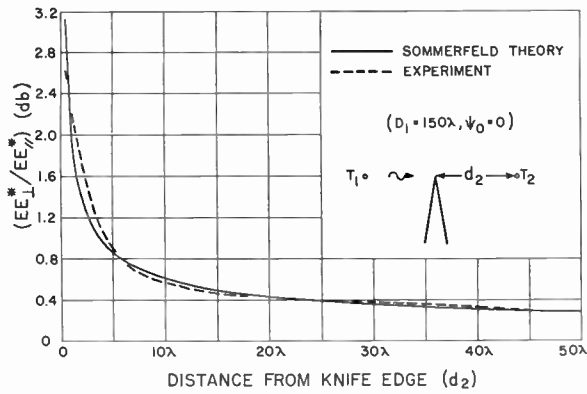


Fig. 6—Ratio of power behind a knife edge at grazing incidence when the electric field is perpendicular to the edge to power behind knife edge when the electric field is parallel to the edge.

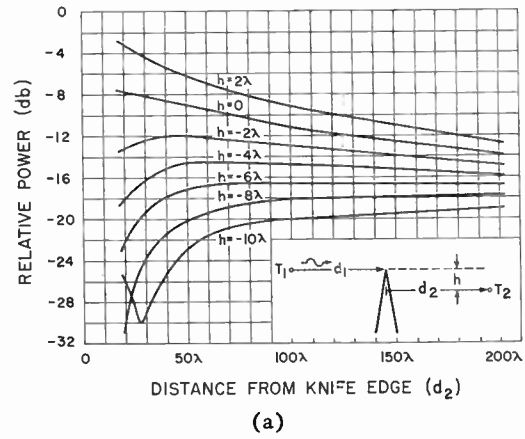
The knife edge consisted of aluminum sheet, 1/16-inch thick while the half-cylinders were constructed from thin, conducting aluminum foil, sufficiently reinforced to form smooth, cylindrical surfaces. Care was taken to make the knife-edge and cylinders sufficiently long so that end effects were completely negligible.

**B. Knife Edge**

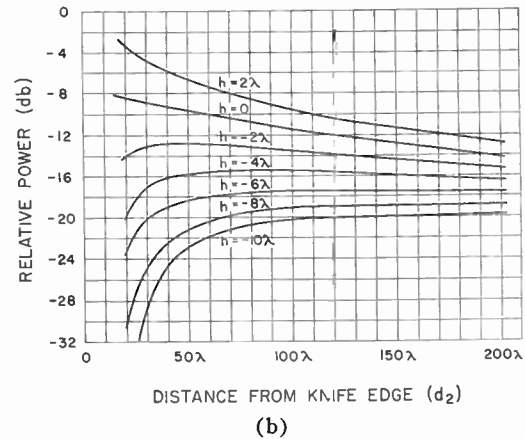
Measurements on a diffracting knife edge served as a comparison for the results obtained experimentally for the cylindrical mountains.

Knife edge diffraction was solved rigorously many years ago by Sommerfeld.<sup>14</sup> Polarization effects predominate only at relatively short distances (measured in wavelength) from the diffracting edge. Hence, in optics, due to the extremely short wavelengths, experimental confirmation of Sommerfeld's theory is rare. At microwave frequencies, the measurement of the polarization effects is entirely feasible. Since to the author's knowledge no such measurements have been published, they are included for general interest despite the fact that they have little bearing on the main problem of this paper.

Fig. 6 shows the ratio of received power for vertical polarization to the received power with horizontal



(a)



(b)

Fig. 7—(a) Power distribution behind a knife edge ( $ka=0, d_1=150\lambda$ ) for vertical polarization. (b) Power distribution behind a knife edge ( $ka=0, d_1=150\lambda$ ) for horizontal polarization.

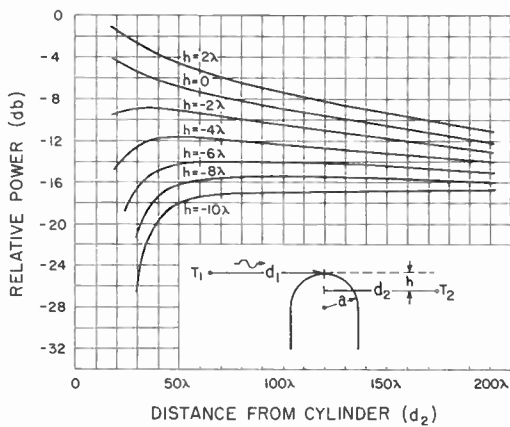
polarization as a function of the distance from the diffracting edge. Comparison with Sommerfeld's theory is in good agreement. At a distance of  $50\lambda$  from the edge the difference between the two polarizations is only 0.4 db in power. In addition, the power measured behind a knife edge as function of probe height is shown in Fig. 7(a) and 7(b). Both planes of polarization give similar results when the edge is not approached too closely.

**C. Cylindrical Mountains**

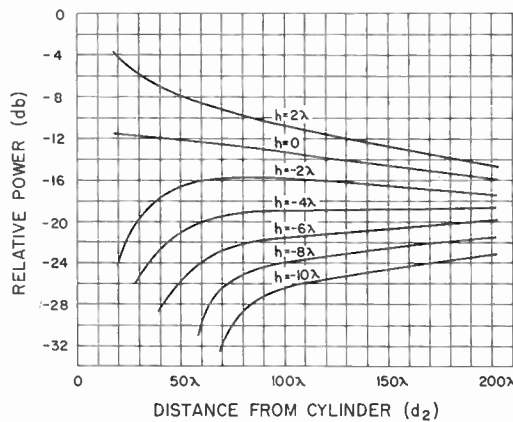
The power measured behind a conducting cylindrical mountain of  $ka=239$  ( $k=2\pi/\lambda, a$  = crest radius) is shown in Fig. 8(a) and 8(b). A large difference exists between the two polarizations, particularly when the mountain is approached. For vertical polarization the field is much stronger than for horizontal polarization.

The halo effect is a function of the radius of curvature of the crest (in terms of  $\lambda$ ) and of polarization as is shown in the measurements of Fig. 9 which were performed with a series of cylindrical mountains of different radii. For vertical polarization the received power increases with  $ka$ , while the reverse is true for horizontal polarization. In addition, the slope of the power variation with scattering (diffraction) angle is essentially the same as for a knife edge in the case of vertical polarization, but becomes steeper with increasing  $ka$  for horizontal polari-

<sup>14</sup> Born, *op. cit.*, pp. 212-215.



(a)



(b)

Fig. 8—(a) Power distribution behind a cylindrical mountain ( $ka = 239, d_1 = 150\lambda$ ) for vertical polarization. (b) Power distribution behind a cylindrical mountain ( $ka = 239, d_1 = 150\lambda$ ) for horizontal polarization.

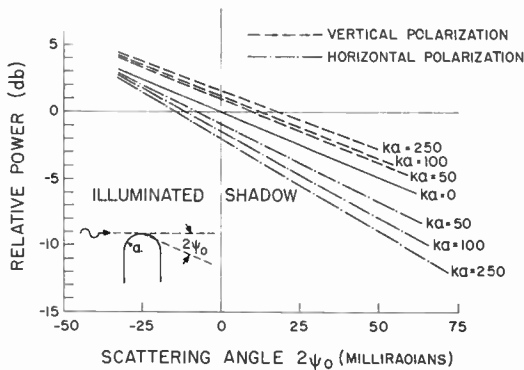


Fig. 9—Variation of power behind a cylindrical mountain with scattering angle as a function of radius of curvature (far field).

zation. Thus in the case of vertical polarization the region behind the mountain is “brighter” than that behind a knife edge; for horizontal polarization, it is “darker.”

The power at grazing incidence as the receiver moves away from the cylindrical mountain is shown in Fig. 10 for a crest of  $ka = 239$ . The effect of polarization de-

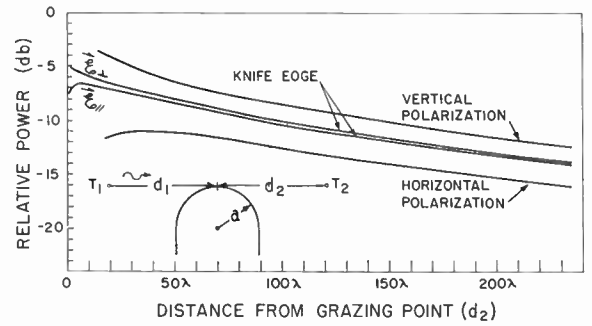


Fig. 10—Power measured at grazing incidence behind a cylindrical mountain ( $ka = 239, d_1 = 150\lambda, \psi_0 = 0$ ). Similar measurements behind a knife edge ( $ka = 0, d_1 = 150\lambda, \psi_0 = 0$ ) are shown for comparison.

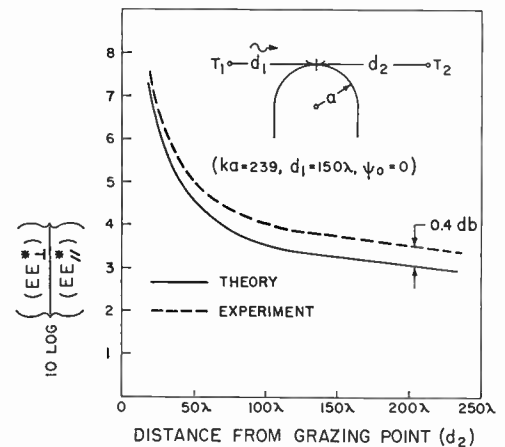


Fig. 11—Comparison of measured and calculated “halo” effects.

creases with distance from the mountain, but is still appreciable, even at  $250 \lambda$  from the mountain. In comparison the power variation for a knife edge is also shown. For a knife edge the polarization effect is small except near the edge itself.

If  $\psi_0 = 0$  the integrals of (23) reduce to Euler's integrals for the gamma function, and a simple expression for the received power,  $P$ , can be obtained.

$$P = (EE^*)_{\perp, \parallel} = \frac{1}{4(d_1 + d_2)^2} [1 + A_{\perp, \parallel} u + B_{\perp, \parallel} u^2] \quad (38)$$

with

$$u = \sqrt[3]{ka} / \sqrt{\pi kd},$$

$$A_{\perp} = 3.00; \quad B_{\perp} = 2.39; \quad A_{\parallel} = -3.10; \quad B_{\parallel} = 2.58.$$

Comparison of experiment with theory is shown in Fig. 11 where the ratio

$$10 \log \left\{ \frac{(EE^*)_{\perp}}{(EE^*)_{\parallel}} \right\}$$

is plotted against  $d_2$ . Good agreement with theory is obtained, and the spread between the predicted and

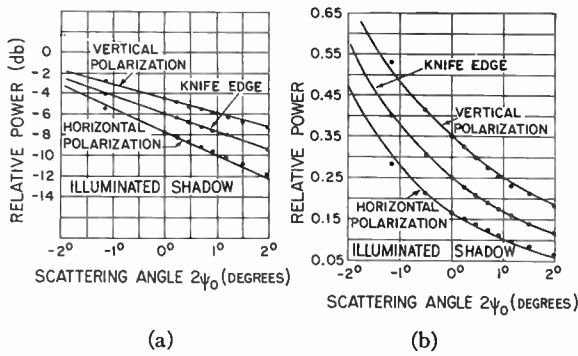


Fig. 12—Received power as a function of scattering angle plotted on (a) logarithmic scale and (b) linear scale ( $ka=239$ ,  $d_1=150\lambda$ ,  $d_2=113\lambda$ ). The points (...) are theoretical.

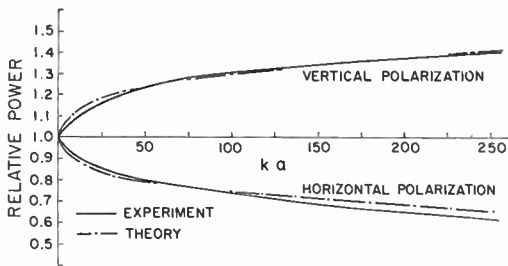


Fig. 13—Variation of power behind a cylindrical mountain at grazing incidence with radius of curvature of the crest ( $d_2=113\lambda$ ,  $d_1=150\lambda$ ,  $\psi_0=0$ ).

experimental results is within the limitations of the measuring equipment. If the received power is plotted as a function of scattering angle, the theory satisfactorily predicts the result over the range of small scattering angles encountered in practice (Fig. 12). It is evident that the variation of the power with diffracting angle is more rapid for horizontal polarization than for vertical polarization.

The power at grazing incidence as determined for a series of cylindrical mountains ( $ka$  values) for the two polarizations is shown in Fig. 13. For vertical polarization, the received power at grazing increases with  $ka$ ; for horizontal polarization, the power at grazing incidence decreases with  $ka$ . Agreement with theory is satisfactory along the coordinate for  $\psi_0=0$  as well as for small scattering angle (Fig. 12).

D. Artmann Shift

A comparison of the constants  $\kappa_{\perp}$  and  $\kappa_{\parallel}$  predicted by various authors is shown in Table I. The results derived here are approximately in agreement with those of Rice who considered the special case  $d_1 \gg d_2$ .

Experimental determinations of these constants have been attempted by: 1) measuring the power behind various cylindrical mountains by vertically scanning with the receiver, and 2) fixing the transmitter and receiver and varying the height of the mountain relative to the transmitter-receiver arrangement. Both of these techniques yielded the same results.

TABLE I  
THEORETICAL

Author	$\kappa_{\perp}$	$\kappa_{\parallel}$
Artmann	0.20	-0.39
Rice	0.346	-0.399
Theory ( $d_1 \approx d_2$ )	$0.316 (1 + d_2/d_1)$	$-0.333 (1 + d_2/d_1)$
Theory ( $d_1 \gg d_2$ )	0.316	-0.333

TABLE II  
EXPERIMENTAL ( $d_1=120\lambda$ ,  $d_2=80\lambda$ )

$ka$	$\kappa_{\perp}$	$\kappa_{\parallel}$
240	0.54	-0.57
192	0.53	-0.54
144	0.52	-0.52
96	0.51	-0.49
48	0.49	-0.44

The experimental values are listed in Table II. The calculated values for these measurements are  $\kappa_{\perp}=0.55$  and  $\kappa_{\parallel}=-0.58$ . The experiments show that  $\kappa_{\perp}$  and  $\kappa_{\parallel}$  are not constant for various  $ka$  values and the more accurate expression (38) should be used. This is a consequence of the fact that for finite distances, the slopes of the diffraction curves are different for each polarization and different from that for a knife edge.

IV. ACKNOWLEDGMENT

The authors' thanks are due to R. Cajka for his help with the calculations and to Dr. I. Shkarofsky for a critical perusal of the manuscript which led to a number of corrections and improvements.



# Refraction Anomalies in Airborne Propagation\*

MING S. WONG†, SENIOR MEMBER, IRE

**Summary**—Propagation at 250–10,000 mc often encounters: 1) dense fadings where the radio signal fluctuates spatially with large amplitudes and small spacings from maxima to minima, *e.g.* amplitudes of up to 40 db and spacings at 3000 mc of 1 mile; 2) radio holes, where the signal falls spatially to a level often 15 db or more below the levels outside; 3) antiholes, where the signal fluctuates spatially with large amplitudes and irregular spacings; 4) radio ducting, including cases where the transmitter or receiver is far above a ducting layer in the air.

The anomalies (1–4) are portrayed by ray tracings using a differential analyzer which solves the simplified ray equation

$$\frac{d^2h}{dx^2} \cong \frac{\partial n(h, x)}{\partial h} + \frac{1}{a}$$

Both hypothetical-prototype and complex-measured refractive index profiles of the atmosphere are used for the analog computation of the ray tracings which are interpreted to explain refraction anomalies in radio-wave propagation and are compared with signal-strength measurements. They involve divergence of rays, and concentration and crossing of direct rays in multipath transmission. Resulting radar angular and range errors are shown where the radar sights a target at a) multiple elevation angles, of under 1 degree, which deviate by up to few tenths of a degree from the angle obtained if the atmosphere were standard, and b) multiple range corrections, for a 200-mile range, which deviate by few tens of feet from the standard correction. Also shown are spatial variations of elevation angles of arrival of interfering rays at the points where they cross—variations showing differences of 0.15 degree between the envelopes of angle-of-arrival maxima and minima, at small angles; this corroborates radio-astronomical data on angular deviations of stars.

## I. INTRODUCTION

MEASUREMENTS with refractometers often show layers and smaller refractive-index inhomogeneities in the air.<sup>1</sup> These are due usually to water-vapor variations, and found mostly in the lowest 10,000 feet of air. Radiosonde-weather data show that in Ohio, layers occur from 20 per cent of the time for January to 60 per cent for July.

Anomalies which result from atmospheric refraction of radio waves have been extensively observed in airborne propagation at 250–10,000 mc. WADC has studied their correlations with atmospheric refractive-index conditions, on a prevailing cause-and-effect basis, in more than 50 air-to-air propagation flights in Ohio and in some ground-to-air flights in Florida. Radio holes and concomitant antiholes, occurring from anywhere far within to far beyond the standard (4/3)-earth horizon, are the prominent and frequently occurring anomalies air-to-air. Dense-radio fadings and extended

ducting effects are the important ones ground-to-air; holes far within the standard horizon have been observed (by W. M. Browne<sup>2</sup>) in ground-to-air propagation also, but these require rather special conditions as shown in Section VI.

Observations on the anomalies have been made also in point-to-point propagation links.<sup>3–6</sup> Thus, aside from data on spatial variations of radio-field intensity in airborne propagation, there are extensive data measured as functions of time on signal fadings, frequency selectivity of fadings, multiple angles of arrival and path delays of interfering signals. Bean observed “prolonged space-wave fadeouts”;<sup>6</sup> these represent the first report of radio holes within the standard horizon in propagation between low- and high-altitude points (between ground and mountain top), corresponding to the airborne radio holes. The anomalies occur in propagation over land and sea. They are not (at least they have not been observed to be) dependent on radio-wave polarization.

First explanations for radio holes were given by Doherty<sup>7</sup> and Price.<sup>8</sup> Ray theory, especially ray tracing,<sup>9</sup> is well adapted to handle this problem.

The categories of anomalies so far observed in propagation are portrayed by ray tracings in Section VI. Current ray-tracing techniques—using electronic differential analyzers, and building on techniques of Hartree, *et al.*<sup>10</sup> are well able to handle atmospheres where the refractive index varies with distance as well as height. Atmospheres which vary only with height suffice to cause serious anomalies air-to-air; only atmospheres which vary with both height and distance can cause any anomaly at all ground-to-air.

The ray tracings in Section VI comprise ray patterns, and results on initial angles, angles of arrival, relative

\* C. H. Duerfeldt, “Propagation in the 328–2300 Mc Frequency Band,” Naval Air Test Center, Patuxent River, Md., Rep. No. EL 44012.3, pp. 10–17; October, 1954.

† A. B. Crawford and W. C. Jakes, “Selective fading of microwaves,” *Bell Sys. Tech. J.*, vol. 31, pp. 68–90; January, 1952.

‡ O. E. De Lange, “Propagation of very short microwave pulses,” *Bell Sys. Tech. J.*, vol. 31, pp. 91–103; January, 1952.

§ J. P. Day, R. U. F. Hopkins, and L. G. Trolese, “Symposium on Tropospheric Radio Propagation within the Horizon,” Navy Electronics Lab., San Diego, Calif., Rep. No. 409, pp. 43–50; September, 1953.

¶ B. R. Bean, “Prolonged space-wave fadeouts at 1046 mc,” *Proc. IRE*, vol. 42, pp. 848–853; May, 1954.

‡ L. H. Doherty, “Geometrical Optics and the Field at a Caustic,” Ph.D. Dissertation, Elec. Eng., Cornell Univ., Ithaca, N. Y.; 1952.

§ W. L. Price, “Radio shadow effects produced in the atmosphere by inversions,” *Proc. Phys. Soc. London*, vol. 61, pp. 59–78; July, 1948.

¶ C. R. Burrows and S. S. Attwood, “Radio Wave Propagation,” Academic Press, New York, N. Y., pp. 138–150; 1949.

‡ D. R. Hartree, J. G. L. Michel, and P. Nicoloson, “Meteorological factors in radio propagation,” *Proc. Phys. Soc. London*, pp. 127–169; 1946.

\* Original manuscript received by the IRE, July 18, 1957; revised, manuscript received April 24, 1958.

† Propagation Lab., Air Force Cambridge Res. Center, Bedford, Mass. Formerly with Aerial Reconnaissance Lab., Wright Air Dev. Center, Dayton, Ohio.

‡ C. M. Crain, “Survey of airborne microwave refractometer measurements,” *Proc. IRE*, vol. 43, pp. 1405–1412; October, 1955.

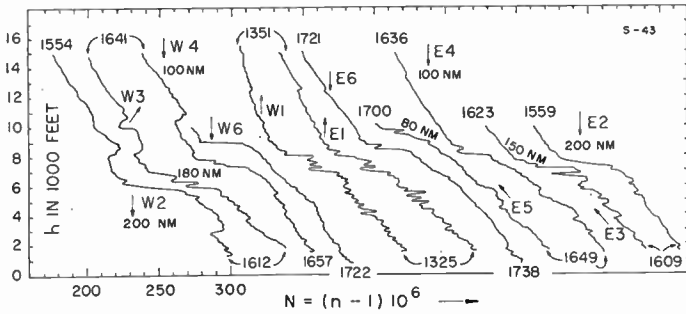


Fig. 1—Refractivity vs altitude profiles: W6, W1, E1, E6 are for Dayton, Ohio; W2-W4 for distances given in nautical miles (NM) to the west; E2-E5 for distances to the east. (May 20, 1953.)

phases, and ray-path corrections of the rays in these patterns. The patterns show spatial distribution of rays being refracted in various prototype and complex atmospheres. Though representing only time-stationary or “snap-shot” views of changing events, the patterns successfully correlate with radio field-intensity variations in airborne propagation; they consistently identify the occurrences, types, and locations of the anomalies. The other results are relevant to and corroborate radar angular and range errors, radio-astronomical data on angular deviations of stars, atmospheric corrections for velocity-of-radio-wave measurements, and appearances of multiple pulses on the output scope in air-to-air operation of Shoran.

With ray tracings, interpretations for the anomalous effects of atmospheric refraction observed in the point-to-point propagation links<sup>3-6</sup> are also apparent.

### II. REFRACTIVE-INDEX PROFILES

Fig. 1 shows an example of  $N$  vs  $h$  profiles at different times and places;  $N = (n - 1)10^6$  is the refractivity,  $n$  the index of refraction, and  $h$  the altitude above sea level. Appearing in west-east order, the profiles were measured by refractometers in two airplanes—one flying vertical spirals and slanting paths (shown by the vertical and slanting arrows) to measure the profiles west of Dayton, the other doing the same east of Dayton. The 4-digit numbers on the profiles denote times.

An extensive layer is seen where  $N$  decreases rapidly with  $h$  for large net changes of about 40  $N$  units. This layer is a few hundred feet thick, and lies between 6000 and 9000 feet. Though the altitude, thickness, and net change in  $N$  all vary with distance and time, the layer has a recognizable identity throughout the 400-mile path and 4-hour duration of the flight. The profiles for Dayton show strong wiggles at the beginning of the flight—wiggles which prevailed at heights below the layer, which later cleared away, and which represent small-size refractive-index inhomogeneities with changes in  $N$  of up to 10  $N$  units or more.

Fig. 1 illustrates some of the atmospheric situations treated in Section VI.

### III. DENSE FADINGS

Dense fadings are shown in Fig. 2 (due to Browne<sup>2</sup>).

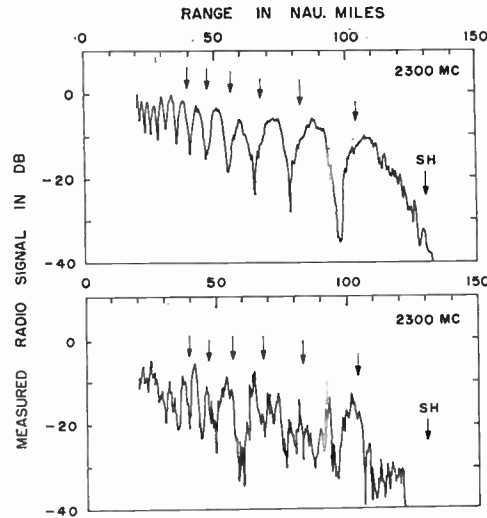


Fig. 2—Signal vs range curves on different days at 10,000-foot altitude in ground-to-air propagation over Chesapeake Bay. Top curve nearly standard, bottom shows mild case of dense fadings. (W. M. Browne data.<sup>2</sup>)

They are rather common in ground-to-air propagation, but are likely to be obscured by commonly occurring antiholes in air-to-air propagation.

In Fig. 2 the curves were measured on separate days—both at 2300 mc, with CW transmission, vertical polarization, 35-foot transmitting height, and 10,000-foot receiving-airplane height over Chesapeake Bay. The arrows denote locations of signal minima in the standard lobing curve for interference between direct and reflected signals in the standard atmosphere over spherical earth. The top curve is nearly standard. The bottom curve shows a mild case of dense fadings—where the signal fluctuates spatially with considerable amplitudes, and with the minima more closely spaced than in the standard curve. Curves measured at 328 and 1186 mc, simultaneously with 2300 mc and omitted here, show comparable fading amplitudes.

Dense fadings more severe than in Fig. 2 have been observed—with fading amplitudes of up to 40 db from signal maxima to minima, in distance spacings of 1 mile at 3000 mc.

Figs. 9 and 10 will show that horizontally varying layers and smaller refractive-index inhomogeneities provide atmospheric causes for dense fadings. Non-specular reflections at the earth’s surface provide another type of cause.

### IV. RADIO HOLES AND ANTIHOLES

Radio holes and antiholes occurring far from within to far beyond the standard horizon ( $SH$ ) are very common air-to-air. All of the 50 air-to-air propagation flights made by WADC encountered radio holes; these flights were all made under fair weather during May-October in a three-year period in Ohio. Holes far within the  $SH$  are not so common ground-to-air. Until they were first observed by Browne (Fig. 4), it was reasoned that holes could not occur far within the  $SH$  in ground-to-air propagation.

In Fig. 3, the signal vs range curve was measured air-to-air at 3296 mc, with horizontal polarization, pulse modulation, and with the transmitting and receiving airplanes flying opposite headings at 10,000 feet above sea level on a west-east path. The center of separation between the airplanes remained within a few miles of Bellefontaine, Ohio, where ground is near 1250 feet above sea level. The dashed curve represents inverse-distance ( $D^{-1}$ ) field intensity. There is a pair of hole (where the signal falls below the signal levels outside) and antihole (where the signal is enhanced and fluctuates spatially) within the standard horizon  $SH$ , and a second pair far beyond the  $SH$ . The signal in the second antihole rises to within few decibels of inverse-distance field intensity, and is several tens of decibels above the signal level due to atmospheric scattering or reflection.

The ray-density curve in Fig. 3 is given by ray tracings in Figs. 11(a), (b), and is based on in-flight measurements of refractive index vs height profiles. Good correlation is shown with the radio-signal curve; the circumstances were favorable in that the index profiles showed good stability with respect to time and distance along the propagation path.

Holes wider and deeper than those in Fig. 3 have been observed, sometimes with signal losses of 30 db or more.

In Fig. 4 the curves were measured ground-to-air simultaneously—at 328 mc with CW transmission from 70-foot transmitting height, 1186 mc with pulse modulation from 70-foot height, and 2300 mc with CW from 35-foot height. All three frequencies used vertical polarization; the receiving airplane flew at 10,000 feet over Chesapeake Bay. A deep radio hole, 30 miles wide, is seen far within the standard horizon  $SH$  at 1186 and 2300 mc. The hole is hardly noticeable at 328 mc. This presumably is because reflections by the Bay were specular, and thus gave considerable reflected signal in the hole, at 328 mc but were nonspecular and diffusely scattered at the two higher frequencies.

Fig. 12 will show that a wide radio hole can be produced far within the standard horizon, ground-to-air, by a strong layer which rises steeply from near the transmitter for several hundred feet of height and then levels off with distance. Such a layer occurs with incoming sea breeze.

In a radio hole, both the direct and earth-reflected signals must be weak. Thus reflections by land must often, and by sea must sometimes, be nonspecular and diffusely scattered such as to give only weak signals in the holes.

Propagation measurements at spot frequencies in the 250–10,000 mc band show that, except when affected by reflections from the earth's surface, the occurrences and locations of radio holes and antiholes do not in gross features depend on frequency in the band concerned. On entering and leaving a hole, the signal falls and rises at spatial rates which increase with frequency. In antiholes, the distance spacings between signal minima decrease with frequency.

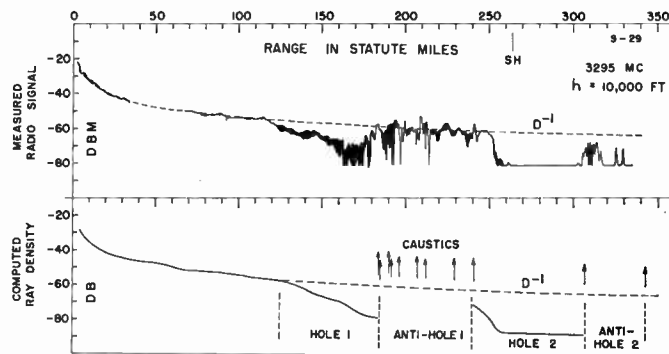


Fig. 3—Signal vs range curve at 10,000-foot altitude in air-to-air propagation, and ray-density curve computed from  $N$ -profile data. Holes and antiholes occur within and far beyond standard horizon. (Ohio, May 15, 1951.)

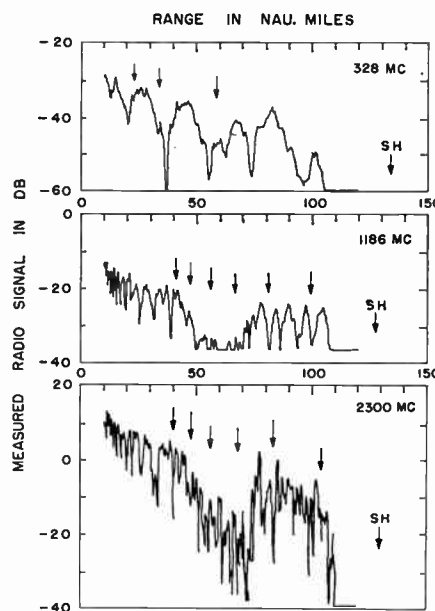


Fig. 4—Simultaneous signal vs range curves at 10,000-foot altitude in ground-to-air propagation over Chesapeake Bay. The hole so far within the standard horizon is unusual ground-to-air. (W. M. Browne data.<sup>2</sup>)

## V. DUCTING

Figs. 5 and 6 show the spatial variations of radio-field intensity, respectively, within a horizontally varying duct, and at a great height above a leaking duct.

In Fig. 5 the signal vs range curve was measured at 250 mc, with vertical polarization, square-wave modulation, and with the transmitting and receiving airplanes flying opposite headings at 10,000 feet above sea level on a west-east path. The center of separation between the airplanes remained within a few miles of Dayton, where ground is near 1000 feet above sea level. There are two wide-distance intervals where the signal falls deeply below inverse-distance ( $D^{-1}$ ) field intensity, where the signal envelopes are cusp-shaped with pointed minima. These intervals are not accompanied by antiholes. Outside these intervals, where the signal is high and near inverse-distance field intensity, only small-

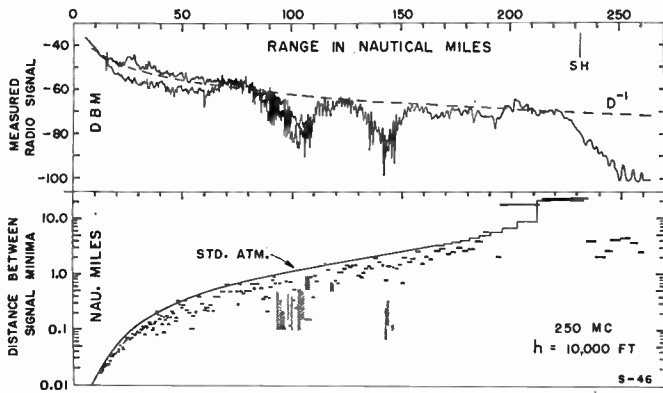


Fig. 5—Signal vs range curve at 10,000-foot altitude in air-to-air propagation, and curve of distance spacings between signal minima. The wide, cusp-shaped minima are due to interference of trapped and nontrapped rays in a radio duct. (Ohio, July 29, 1953.)

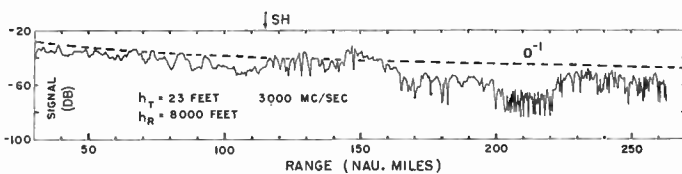


Fig. 6—Signal vs range curve at 8000-foot altitude in ground-to-air propagation over the Atlantic from Florida. Signal continuing on beyond *SH* is due to rays escaping from a thin duct at ocean surface. (May 23, 1956.)

amplitude fadings occur—instead of large-amplitude fadings which characterize antiholes. Fig. 13 will show that the transmitting and receiving airplanes were within a duct.

In the lower half of Fig. 5, the solid curve, superposed on the measured values of distance spacings between signal minima, represents interference between direct and reflected signals in the standard atmosphere over spherical earth. The decreased distance spacings between signal minima, in the figure, include effects of interference between rays which are trapped in the duct and rays which are not trapped.

Fig. 6 was measured at 3000 mc, with pulse modulation, vertical polarization, 23-foot transmitting height in Cape Canaveral, Fla., and 8000-foot receiving height over the Atlantic. The curve is very notable in its extended range. The signal is up to inverse-distance field intensity in a 45-mile interval beginning at the standard horizon *SH*, and is within several decibels of inverse-distance field intensity in a second 45-mile interval beginning 105 miles beyond the *SH*. Fig. 14 will explain this with rays initially trapped in a thin layer just above the ocean surface, and then progressively escaping at various distances through the top of the layer.

## VI. RAY TRACINGS

Fig. 7 through Fig. 15 show ray tracings under various atmospheric conditions, under Cases A-H below.

In each ray pattern,  $h$  is height above an arbitrary level, and  $x$  is spherical-earth distance. The  $dN/dh$  vs  $h$

profile shown is for  $x = 0$ , and varies with  $x$  in most cases; the scale for  $dN/dh$ , the vertical gradient of  $N = (n-1)10^6$ , is in  $N$ -units per foot (in units of  $10^{-6}$ /foot for  $dn/dh$ ). The transmitter emits rays in various directions within a beamwidth of initial elevation angles labeled on the rays. The rays are continually being refracted (bent) in the air; they may be viewed as trajectories of the normals to radio-wave fronts, *i.e.*, as paths followed by radio waves in the plane of propagation concerned.

The equation for tracing rays in an atmosphere where the index of refraction,  $n$ , varies with height and distance is

$$\frac{d^2h}{dx^2} \simeq \frac{\partial n}{\partial h}(h, x) + \frac{1}{a} \quad (1)$$

Here  $a$  is the earth's radius ( $1/a = 0.048 \times 10^{-6}$ /foot); the standard atmosphere has  $dN/dh = -0.012 \times 10^{-6}$ /foot. Eq. (1) is derived from Fermat's principle, and simplified for rays with elevation angles within  $\pm 6$  degrees. Each ray is a solution of (1) for given initial values of  $h$  (transmitter height) and  $dh/dx$  (angle of the ray at transmitter). For each ray pattern, (1) is solved and the rays are traced by electronic differential analyzers. The method of doing this is described in the Appendix.

Plotting  $h$  and  $x$  on rectangular axes, for convenience, causes the rays in the patterns to have an apparent curvature which is given, according to (1), approximately by  $(\partial n/\partial h + 1/a)$ , and which differs from the true curvature. For example, consider the rays in the standard atmosphere: physically, these rays have a slight, negative true curvature; in a pattern, these rays would appear as parabolas with a positive apparent curvature (see the standard rays in parts of Fig. 7(a)). The transformation of curvature does not matter in the correlations, below, between ray tracings and the propagation effects they portray.

### A. Horizontal Layer

Fig. 7(a): The  $dN/dh$  vs  $h$  profiles do not vary with  $x$ ;  $dN/dh$  has a positive peak for the layer in the top pattern, and a negative peak in the bottom.

The rays lying entirely above either layer are standard. In the top pattern the rays which graze the layer—those which travel down to the layer, and then turn upward with turning points inside the layer—are bent backward with respect to the up-going trajectories of the standard rays. In the bottom pattern the layer-grazing rays are bent forward. The rays which turn upward with turning points below either layer become progressively less affected.

In general, the ray-scarce areas in the ray patterns—which show only direct rays, and which (except Fig. 15) omit reflections of rays by the earth's surface—would give rise to radio holes provided the reflections do not give appreciable signals in the areas concerned. This has been found to be true in propagation over land many times, and over the ocean sometimes. The ray-crossing

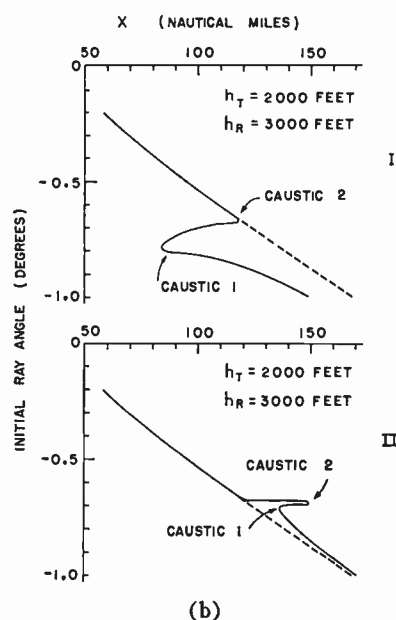
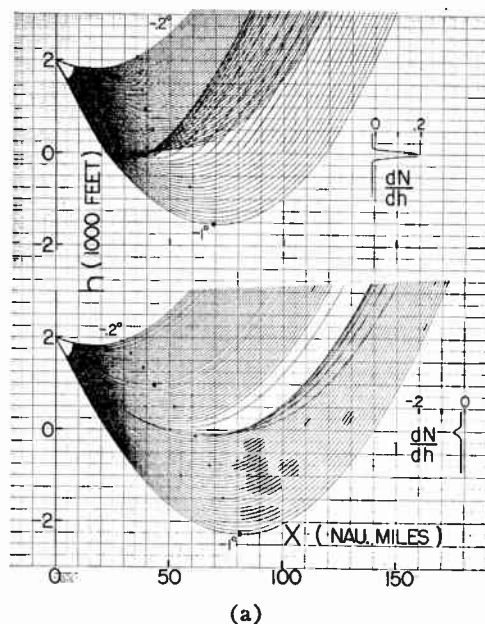


Fig. 7—(a) Ray patterns each with a ray-scarce and ray-crossing area (radio hole and antihole). Transmitter is above horizontal layer with positive  $dN/dh$  peak at top, negative  $dN/dh$  peak at bottom. (b) Diagrams of initial angles of rays vs their intercept distances at  $h = 3000$  feet in (a).

areas give rise to antiholes regardless of reflections, as a result of interference of the crossing rays.

Depending on the position of the transmitter, the effects of a horizontal layer are as follows: If the  $dN/dh$  peak is negative, and when the transmitter is anywhere above the layer, there occurs a hole followed by an antihole; when it is within or just slightly below the layer, there occur a horizontal duct along the layer, and a hole and antihole above the layer; when it is farther below the layer, no hole, antihole, or duct occurs. If the  $dN/dh$  peak is positive, there occurs an antihole followed by a hole—provided the transmitter is anywhere above, or within the layer.

The holes and antiholes curve upward without ending. To cause them, a layer need not extend more than a few tens of miles in distance.

From the above it is clear that horizontal layers can cause serious anomalies in air-to-air propagation (where the layers are apt to prevail below the transmitter); they can cause only subdued effects ground-to-air (layers above transmitter).

In Fig. 7(b) each diagram plots the initial angles of individual rays vs the distances,  $X$ , where the rays intercept a chosen horizontal path at the height  $h_R = 3000$  feet in one pattern of Fig. 7(a). The dashed curves are for the standard atmosphere.

The slope of a diagram of initial angles  $A_T$  of rays vs their intercept distances  $X$ , for a chosen path at height  $h_R$ , gives a measure of ray density. Consider two  $A_T$  vs  $X$  diagrams—one for an actual atmosphere, the second for the standard atmosphere, both for the same chosen path at height  $h_R$  and the same transmitting height. Then the square root of the ray-density ratio,

$$R(X; h_R) = \frac{\text{slope at distance } X \text{ of first diagram}}{\text{slope at distance } X \text{ of second diagram}}, \quad (2)$$

corresponds with the ratio of actual radio-field intensity to inverse-distance field intensity. This is valid at all points not too close to caustics where ray density is infinite.

The caustics appear in ray patterns as loci of dense-ray concentration; they are envelopes formed by intersections of consecutive rays.

Fig. 7(b) shows that each caustic is tangent to a serpentine  $U$  turn in the  $A_T$  vs  $X$  diagrams. The two arms of each  $U$  turn represent two groups of direct rays, one group crossing and interfering with the other. The space on one side of the caustic (the visibility side, where the  $U$  lies) is doubly traversed by the rays of the  $U$  concerned; the space on the other side of the caustic (the shadow side, where the  $U$  points away from) does not contain any rays of the  $U$ . Thus the resultant ray density, due to the rays of the  $U$  concerned, is zero on the shadow side, jumps to infinity at the caustic, then oscillates spatially with decreasing amplitude on the visibility side. This ray-theory picture is subject to a slight modification by wave theory, which gives the Airy type of result for caustics.<sup>7,11</sup> This modification—which can be obtained also by combining the ray tracings here with the known theory for caustics in *homogeneous* media—consists in giving a finite maximum of radio-field intensity near the caustic, and in giving an exponentially attenuated field intensity in place of the zero-ray density at the shadow side.

On the view that radio waves are propagated along rays, the apparent elevation angle of a target observed by radar is given by the initial angle of the ray which intercepts the target. Thus deviations and multiplicities

<sup>11</sup> G. B. Airy, "Intensity of light in the neighborhood of a caustic," *Proc. Cambridge Phil. Soc.*, vol. 6, pp. 379-401; May, 1838.

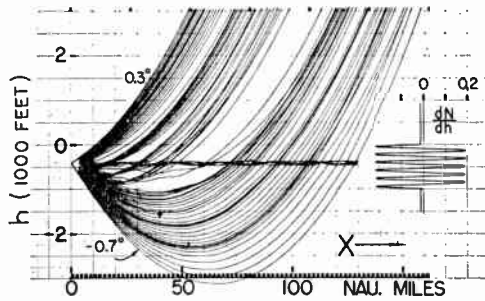


Fig. 8—Pattern with holes, antiholes, and horizontal duct. Transmitter is at a negative  $dN/dh$  peak in 1000-foot stratum of layer fragments.

of radar-elevation angles are involved in antiholes. In the upper diagram of Fig. 7(b), an airborne radar would sight a target at two elevation angles,  $-0.45$  and  $-0.8$  degree, when the target is at the range of the first caustic. The second angle, of  $-0.8$  degree, occurs at a range which departs from the standard range by 60 miles.

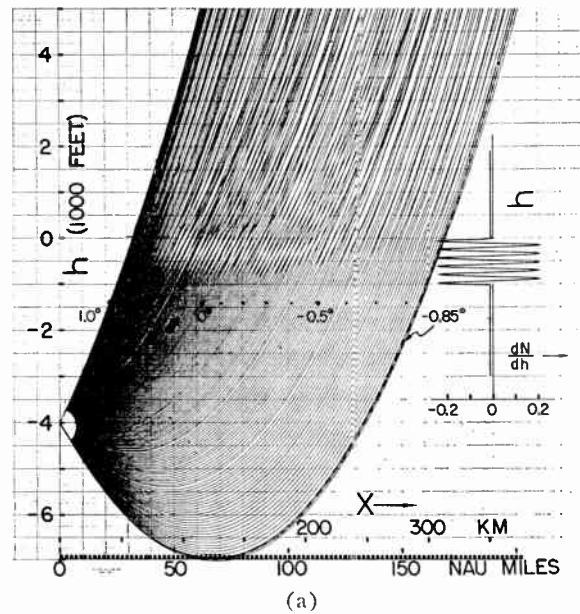
### B. Stratum of Layer Fragments

In Figs. 8 and 9,  $dN/dh$  varies as a function of  $h$  with negative and positive peaks inside a stratum 1000 feet thick. The  $dN/dh$  vs  $h$  profile applies over alternate 1-mile intervals of distance marked by shadings near the  $x$ -axis of each ray pattern;  $dN/dh$  is standard in the intervening miles of the stratum, and also above and below the stratum. The change in  $N$  under each  $dN/dh$  peak is 10  $N$  units. A layer fragment is obtained with each  $dN/dh$  peak in the stratum. The fragments thus obtained—each 91 feet thick, and extending 1 mile horizontally—have discontinuous changes of  $dN/dh$  across their vertical boundaries, and simulate refractive-index inhomogeneities in the air.

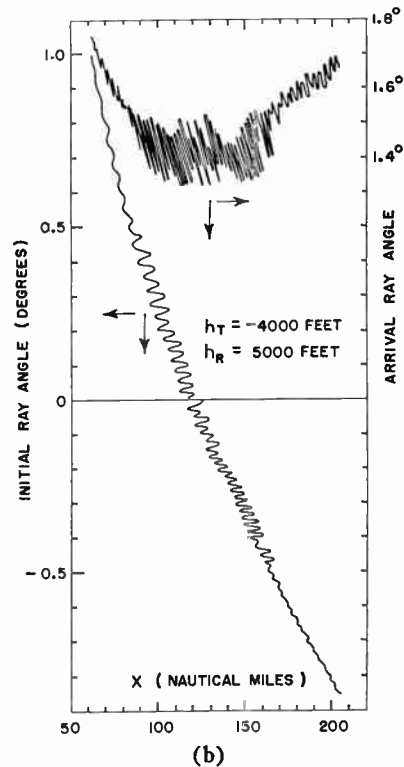
In Fig. 8 the  $dN/dh$  peaks above the transmitter do not produce any holes. The negative peak where the transmitter is located (the fifth peak from the top)—though the  $dN/dh$  profile is interrupted at 1-mile intervals—traps some rays in a duct; it, together with the 6th peak, causes the first narrow pair of hole and antihole above the duct. The 7th and 8th peaks act in unison, and give the second narrow pair of hole and antihole; the 9th and 10th peaks give the third narrow pair. The 11th peak, not counteracted by a lower positive peak, gives the fourth and wide hole which is followed by the wide (last) antihole.

In Fig. 9(a) dense-ray crossings—with closely spaced alternations of ray scarcity and concentration, and closely spaced caustics—take the place of radio holes and antiholes as soon as the transmitter is far enough below the layer fragments for ducting to cease. The dense crossings occur even when the transmitter is thousands of feet below the layer fragments. If the  $dN/dh$  vs  $h$  profile were to remain constant with  $x$ , no ray crossings would occur whenever the transmitter is below the  $dN/dh$  peaks.

Fig. 9(b) shows diagrams of initial angles and angles



(a)



(b)

Fig. 9—(a) Pattern with dense-ray crossings associated with dense-radio fadings (Fig. 2). Transmitter is far below 1000-foot stratum of layer fragments. (b) Diagrams of initial angles and angles of arrival of rays vs their intercept distances at  $h = 5000$  feet in (a).

of arrival of individual rays vs the distances,  $X$ , where the rays intercept a chosen horizontal path at the height  $h_R = 5000$  feet in Fig. 9(a). The initial-angle diagram makes serpentine  $U$  turns with closely spaced caustics; it shows that a radar, even when situated thousands of feet below the stratum, may sight a target above the stratum at multiple elevation angles with differences of up to 0.1 degree. The angle-of-arrival diagram shows multiple-valued branches which fluctuate spatially with differences of up to 0.15 degree between the envelopes

of angle-of-arrival maxima and minima; this corroborates the deviations due to atmospheric refraction, observed in the elevation angles of arrival of radio stars.<sup>12</sup>

The angles of arrival,  $A_R$ , of individual rays serve also to determine their relative path delays, and thus their relative phases. With Fermat's principle it can be shown that the relative phases of individual rays, as a function of the distances  $X$  where the rays intercept a chosen horizontal path at the height  $h_R$  is given by

$$\phi(X; h_R) = \frac{2\pi}{\lambda} \left( 1 + \frac{h_R}{a} \right) \int_{X_1}^X n(X; h_R) \cdot \cos A_R(X; h_R) dX. \quad (3)$$

Here  $A_R(X; h_R)$  denotes a single-valued branch of the  $A_R$  vs  $X$  diagram for the chosen path;  $\lambda$  is the wavelength;  $a$  the earth's radius;  $n$  the index of refraction;  $X_1$  is a distance chosen as the reference for zero phase. By taking  $X_1$  near the values of  $X$  concerned, (3) gives accurately the relative phases of the rays in each single-valued branch of an  $A_R$  vs  $X$  diagram. Eq. (3) is important in that the alternative procedure of computing first the enormously large path lengths of the rays concerned, and then their small differences to obtain the phases, is inaccurate.

The dense-ray crossings in Fig. 9(a) cause dense-radio fadings—as a result of the closely spaced caustics, and attendant interference of groups of rays. Each of these groups of rays corresponds to, and has a ray density determined by, a single-valued branch of an  $A_T$  vs  $X$  diagram; the rays of one group interfere with those of the other groups. The phases of the interfering rays at a ray-crossing point are given by (3).

Dense-ray crossings can be caused even with just a single layer where the peak of the  $dN/dh$  vs  $h$  profile varies continuously and gradually as a function of  $x$ ; this is shown in the next case.

### C. Layer Varying Sinusoidally with Distance

In Fig. 10 the height,  $h_c$ , of the layer varies sinusoidally with  $x$ ; the maxima of  $h_c$  depart only 100 feet from the mean, in distance of 1.25 miles. This variation of  $h_c$  is moderate for layers over an ocean.<sup>13</sup> The amplitude,  $P$ , and the shape of the  $dN/dh$  vs  $h$  peak does not vary with  $x$ ; the change in  $N$  through the layer is 40  $N$  units. The dense-ray crossings shown can be produced also by causing only the amplitude of the  $dN/dh$  peak to vary sinusoidally with  $x$ .

With the atmospheric situations in Figs. 9 and 10, the dense-ray crossings occur when the transmitter is anywhere above, within, or even far below the layer fragments or the horizontally varying layer. For any of these transmitter positions, the rays which intercept the layer fragments or the layer at sufficiently small elevation

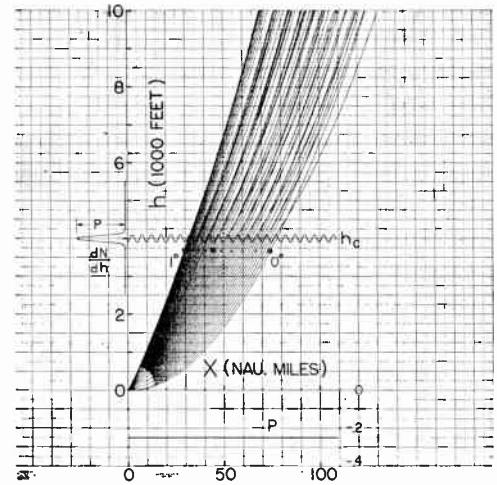


Fig. 10—Pattern with dense-ray crossings associated with dense-radio fadings (Fig. 2). Transmitter is far below layer which varies sinusoidally with distance.

angles, all have their up-going trajectories involved in ray crossings; these crossings extend from, and to all heights above, the layer fragments or layer.

### D. A $dN/dh$ Profile Measured with Propagation

In Fig. 11(a) the  $dN/dh$  vs  $h$  profile is computed from one of the three  $N$  profiles, all essentially alike, which were measured at different times and places along the air-to-air propagation path in Fig. 3; the  $dN/dh$  profile is presumed not to vary with  $x$ .

If the atmosphere were standard, the tangent ray (the ray which grazes the earth's surface from the transmitter) constitutes the farthest-reaching ray; in Fig. 11(a) it would reach 264 miles at  $h=10,000$  feet, with the ground at  $h=1250$  feet. With the  $dN/dh$  profile shown, the actual tangent ray reaches 307 miles; yet, it does not reach as far as other rays in the last antihole. This antihole, which has appreciable ray densities between 306 and 346 miles at  $h=10,000$  feet, is due to the layer near  $h=2000$  feet. The rays which graze this layer, because its  $dN/dh$  peak has values near  $-1/a$ , pursue nearly horizontal trajectories for large distances—with "flat bottoms" near the layer—before turning upward and intersecting one another to form the last antihole; hence the very wide hole preceding it.

The densities of rays along the horizontal path at  $h=10,000$  feet in Fig. 11(a)—as determined by (2), and the slope of the initial-angle diagram in Fig. 11(b)—give the ray-density curve in Fig. 3, the curve in favorable correlation with the measured radio-field intensity.

In Fig. 11(b), the diagrams show the initial angles and range corrections of individual rays vs the distances,  $X$ , where the rays intercept a chosen horizontal path at the height  $h_R=10,000$  feet in Fig. 11(a). (The initial-angle diagram in this case represents also the negative of the angle-of-arrival diagram of the rays, for the same intercepting height.) The range correction for each ray is computed as

<sup>12</sup> J. L. Pawsey and R. N. Bracewell, "Radio Astronomy," Oxford University Press, New York, N. Y., pp. 342-344; 1955.

<sup>13</sup> E. Gossard and W. Munk, "Gravity waves in the atmosphere," *J. Meteorology*, vol. 11, pp. 259-269; August, 1954.

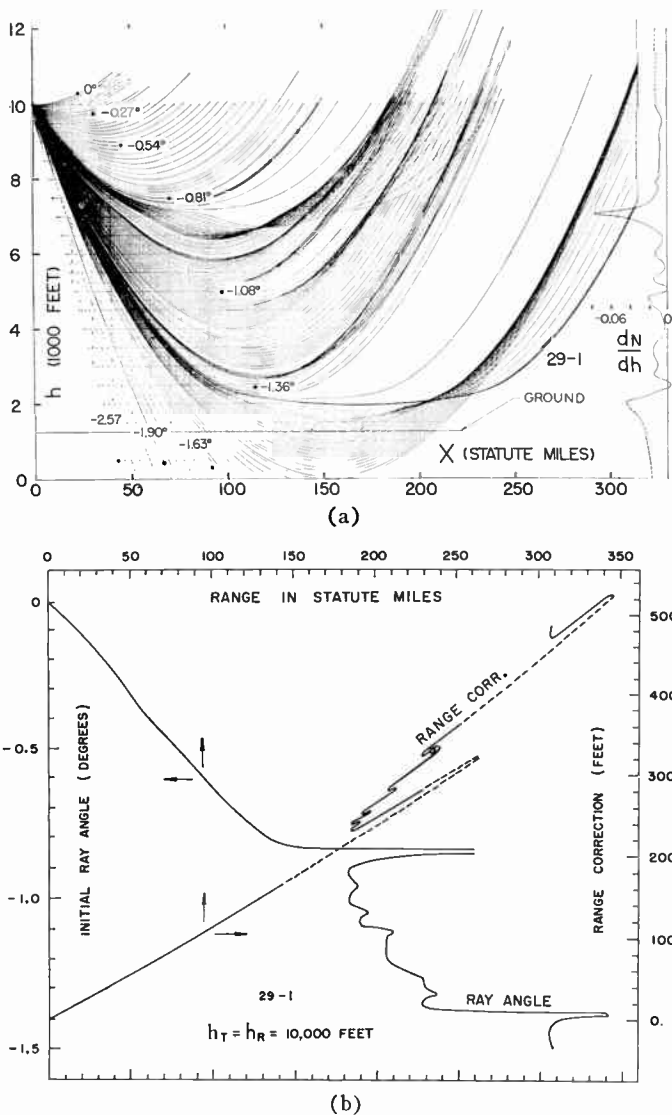


Fig. 11—(a) Pattern with holes and antiholes which correlate with Fig. 3.  $dN/dh$  profile is based on measurements during propagation. (b) Diagrams of initial angles and range corrections of rays vs their intercept distances at  $h = 10,000$  feet in (a).

$$\Delta S(X; h_R) = \int_{(0; h_T)}^{(X; h_R)} (n - 1) dS \quad (4)$$

where the integration is along the ray from transmitter to the point  $(X, h_R)$ ,  $n(x, h)$  is the index of refraction, and  $dS$  is an element of arc length. Eq. (4) gives the difference between the ray path traversed by radio waves in vacuum and the path traversed in the actual atmosphere concerned—for the same time duration, and same initial angle of the ray; it gives accurately the corrections for atmospheric effects in measurements on the velocity of radio waves.<sup>14</sup>

The diagrams in Fig. 11(b) show multiple-valued branches in the antiholes, each branch corresponding to a group of rays intersecting with other groups; as many as four groups, each with high ray density, intersect one

another near  $X = 190$  miles. Thus a radar sights a single target at multiple elevation angles, and multiple ranges; and interfering rays reach a receiving point at multiple angles of arrival. At a ray-crossing point, counting only rays of high density, the multiple angles have mutual differences of up to 0.15 degree; the multiple range corrections show ray-path differences of up to 10 feet or more. The initial-angle diagram deviates from the corresponding diagram for the standard atmosphere (given approximately by linear extension of the beginning segment of the diagram shown) by up to few tenths of a degree; the range-correction diagram deviates, from the standard, by 50 feet near  $X = 230$  miles, and by 80 feet near 340 miles.

*E. Steeply-Rising-and-Then-Level Layer*

In Fig. 12 the transmitter is at the bottom of a layer with a single  $dN/dh$  vs  $h$  peak shown; the layer rises at a 2-degree elevation angle for 750 feet of height and then levels horizontally. (After leveling off, the top of the layer lies along the top of the trapped rays shown.) The shape and the amplitude of the  $dN/dh$  peak does not vary with  $x$ . The change in  $N$  through the layer is 80  $N$  units.

The beginning, rising segment of the layer bends rays away from the hole. This rising segment—which covers only a small height interval, but which is strategically placed and has a properly sloping alignment relative to the trajectories of the rays intercepting the segment—causes the extensive ray-scarce area in agreement with the unusual and wide radio hole observed far within the standard horizon in ground-to-air propagation in Fig. 4. The level segment of the layer traps the rays with initial angles smaller than 1 degree. The resulting duct keeps the rays outside the duct from reaching as far as the standard tangent ray; this checks the fact that in Fig. 4 the radio field intensity dies out exponentially at a range short of the standard horizon.

In Fig. 12 the trapped rays reach as far downward as 1300 feet below the transmitter. If the surface of a bay intervenes at 35 feet below the transmitter (which is the case in Fig. 4), the rays which are shown trapped would all be reflected at the surface, but would still be trapped in a duct (with successive reflections at the surface).

*F. Horizontally Varying Layer Measured with Propagation*

In Fig. 13 the  $dN/dh$  vs  $h$  profile shown, consisting of a single  $dN/dh$  peak for the layer, is simplified from several  $N$  profiles measured during the air-to-air propagation flight in Fig. 5. The height of the layer varies with  $x$  in sloping-line sections; this is shown by the diagram II which, to avoid confusion, is displaced 2000 feet upward from the actual height of the layer. The amplitude,  $P$ , of the  $dN/dh$  peaks is constant from 0 to 210 miles, falls to zero from 210 to 250 miles, and is zero beyond 250 miles. With the transmitter inside the layer at  $x = 0$ , some rays are trapped in a leaking duct. At

<sup>14</sup> C. I. Aslakson, "New determinations of the velocity of radio waves," *Trans. Amer. Geophys. Union*, vol. 32, pp. 813-821; December, 1951.

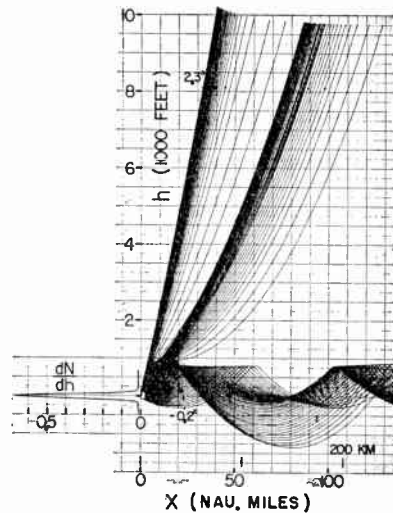


Fig. 12—Pattern with hole which correlates with unusual ground-to-air radio hole in Fig. 4. Transmitter is at bottom of a rising-and-then-level layer.

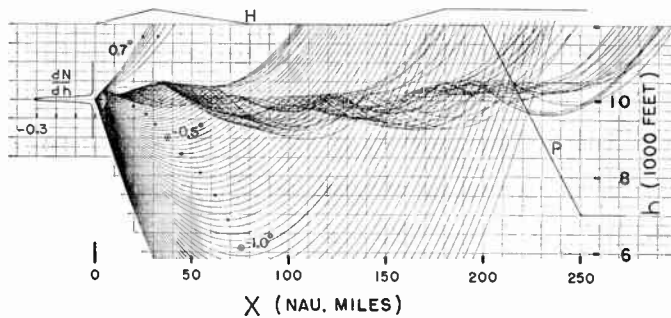


Fig. 13—Pattern with leaking elevated duct; interference between trapped and nontrapped rays explains Fig. 5. Height  $H$  and amplitude  $P$  of  $dN/dh$  peak varies with  $x$ .

$h = 10,000$  feet, the trapped rays have only small densities for distances greater than 165 miles; the nontrapped rays have an essentially standard density from  $x = 0$  to 224 miles.

In Fig. 13 the transmitter and layer are in fixed relative positions; in Fig. 5 the transmitting and receiving airplanes flew opposite headings at  $h = 10,000$  feet, while the layer varied with time and distance along the propagation path. However, the airplanes were within the layer a part of the time during propagation.

The lower half of Fig. 5 shows that the observed distances between successive signal minima mostly follow the solid curve, which is for interference between direct and reflected signals in the standard atmosphere over spherical earth; deviations from the standard curve occur near the two, cusp-shaped signal minima.

The upper half of Fig. 5 may be explained as follows: From 0 to 80 miles, the signal shows some interference between direct and ground-reflected signals; the transmitting and receiving airplanes were not yet within the layer for ducting to occur. From 80 to 160 miles, the two wide and cusp-shaped signal minima are due to interference of the trapped rays vs the nontrapped rays

in Fig. 13. The phase differences between the trapped and the nontrapped rays vary only slowly with distance in the duct; this can be verified with (3), and explains the large separation in range between the two cusp-shaped minima. The closely-spaced signal fluctuations, in the interval from 80 to 160 miles, are due to interference of the trapped and nontrapped direct rays on one hand vs the ground-reflected rays on the other. Beyond 160 miles, the signal is due chiefly to the nontrapped direct rays in Fig. 13, where the tangent ray reaches 224 miles at  $h = 10,000$  feet, in good agreement with the airplane separation at which the signal dies out exponentially in Fig. 5.

#### G. Intense Thin Layer at Ocean Surface

In Fig. 14  $dN/dh$  varies with  $h$  in the first 30 feet above the surface, with intense negative and positive  $dN/dh$  peaks of 3  $N$  units per foot; the refractive-index change through each peak is 9  $N$  units. The  $dN/dh$  vs  $h$  profile shown does not vary with  $x$ . In the ray pattern at the left, the transmitter is at  $h = 23$  feet, and the rays which have initial angles within  $-0.25$  to  $0.25$  degree are trapped in a thin duct. The rays with initial angles more negative than  $-0.25$  degree strike, and are reflected by, the earth; their up-going trajectories are not trapped. In the right-hand half of the figure, the rays all start at  $h = 0$ ; they are shown to start, separately, at different distances merely to avoid confusion. It is clear that any ray which strikes the ocean surface, from a transmitter above the surface, and is thence reflected at an elevation angle under 0.25 degree, would be trapped in a duct; this duct is only 6 feet thick, as shown.

When the signal was observed in Fig. 6, measurements were made also with a refractometer above the ocean surface. The refractivity  $N$ , recorded as a function of time at fixed points within 30 feet above the surface, showed large fluctuations of up to 30  $N$  units in time intervals of the order of one second. The  $N$  vs  $h$  profiles measured above 30 feet, at the same time, were very smooth. With this in mind, and to explain Fig. 6, an assumption is made: 1) there is a thin layer which lies immediately above the ocean surface, which extends for 160 miles, and in which  $dN/dh$  is intensely negative everywhere for long time durations. The intense values of  $dN/dh$ , and their rapid changes with time and distance, actually observed above this thin layer, are irrelevant in what follows.

The signal within the standard horizon  $SH$  in Fig. 6 fluctuates spatially with only small amplitudes; the radiation patterns of the transmitting and receiving antennas are not the cause of this. Thus an assumption is warranted: 2) on reflection by the ocean surface in Fig. 6, the elevation angle of a ray at reflection becomes smaller than its elevation angle at incidence. In this assumption, the angles are measured from the horizontal direction—the  $x$  direction, concentric with the spherical earth. The assumption does not preclude the validity

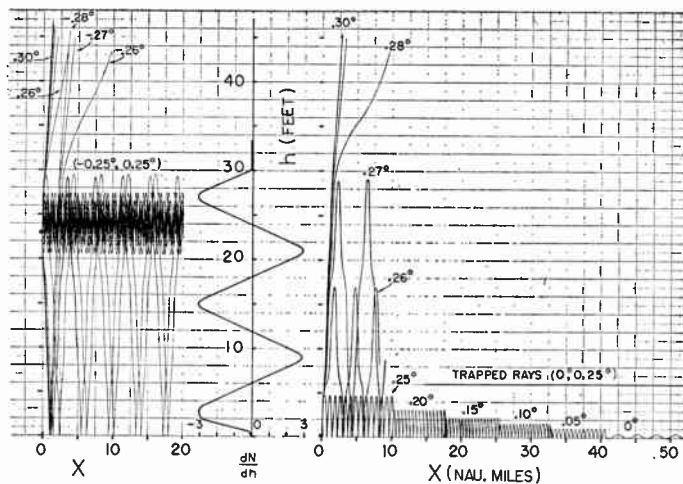


Fig. 14—Patterns each showing trapping of rays by a thin, negative  $dN/dh$  peak. Rays escaping from surface duct at right explains Fig. 6.

of Fresnel's law, that the angles of incidence and reflection are equal, in reflections by an irregular surface—provided the angles are measured with reference to the locally-tangential planes of that surface. The assumption finds support also in the observed occurrences of radio holes in airborne propagation over water.

With the assumptions 1) and 2), the observed signal extending so far beyond the standard horizon in Fig. 6 can be explained by rays leaking from a duct at the ocean surface. For illustration suppose that, with the transmitter at  $h=23$  feet, all the rays with initial angles more negative than  $-0.07$  degree strike the ocean, and that the rays with initial angles between  $-0.78$  and  $-0.07$  degree are reflected at elevation angles between  $0.25$  and  $0.02$  degree respectively. Then these rays are all trapped in a duct, only 6 feet thick as in Fig. 14. It can be shown (with ray tracings omitted here) that the rays within initial angles from  $-0.78$  to  $-0.28$  degree can escape from the duct, for example at ranges of between 25 and 65 miles from the transmitter, and then give the strong signal (which is up to and slightly above the inverse-distance field intensity) in the interval from 115 to 160 miles in Fig. 6. The rays with initial angles from  $-0.28$  to  $-0.27$  degree can escape at ranges between 65 and 125 miles, and give the weak signal observed from 160 to 220 miles. The rays with initial angles from  $-0.27$  to  $-0.07$  degree can escape at ranges between 125 and 160 miles, and give the observed strong signal from 220 to more than 265 miles.

#### H. Layer with Shaped Top at Ocean Surface

In Fig. 15 the thickness of the layer is 200 feet from  $x=0$  to 20 miles; it increases to 300 feet between  $x=20$  and 30 miles, and remains 300 feet beyond 30 miles. With just this localized and minor shaping in the top of an otherwise usual layer, an unusual effect is obtained: a duct is formed at the ocean surface with the transmitter 900 feet above the layer. The duct consists of rays which become trapped after being reflected at the

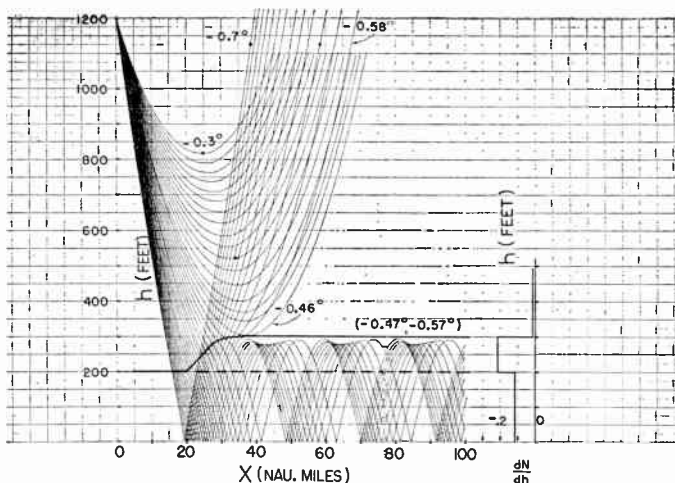


Fig. 15—Pattern showing trapping of rays with transmitter far above duct. Top of layer rises slightly between  $x=20$  and 30 miles.

ocean surface (at  $h=0$ ); these trapped rays lie within an 0.1 degree beamwidth of initial elevation angles at the transmitter. Rays lying within a comparable beamwidth of initial angles can be trapped in a surface duct even with the transmitter much higher than in Fig. 15, provided the conditions of radio-wave reflections at the ocean surface are such that the elevation angle of a ray is smaller at reflection than at incidence (see discussion of Fig. 14). This explains the occasional detections by airborne radars of surface targets at ranges up to hundreds of miles beyond the standard horizon; such detections have been made by radars flying reportedly as high as 15,000 feet.

#### VII. REMARKS

Radio holes far within the standard horizon, antiholes with fluctuating-enhanced signals far beyond the standard horizon, and ducting effects extending to great distances are all possible in both air-to-air and ground-to-air propagation, as the above ray tracings show. However, to account for them, considerations of rather gross and simple features of atmospheric layers suffice in the air-to-air case; localized details of the layers, or strategically deployed variations of the layers with distance, are crucial in the ground-to-air case. Dense-radio fadings are accounted for by horizontally varying layers or smaller refractive index inhomogeneities, both air-to-air and ground-to-air.

The rays from a transmitter, such as in each ray pattern, delineate the domain, in space, of atmospheric refraction—the domain of primary radio-wave illumination and visibility of the transmitter. As the rays often extend far beyond the standard horizon of the transmitter, it is convenient to speak of a "refraction horizon"—a horizon which is determined by the farthest distances reached by appreciable densities of rays from the transmitter, a horizon which depends on prevailing layers in the air and on the transmitter's position relative to the layers. Within this refraction horizon, there

may occur large gaps which are not reached by rays from the transmitter.

#### APPENDIX

##### Use of Differential Analyzer for Ray Tracing

The ray tracings in Section VI were obtained with either a REAC (Reeves Electronic Analog Computer, Reeves Instrument Company, New York) or a GEDA (Goodyear Electronic Differential Analyzer, Goodyear Company, Ohio). The REAC and GEDA have comparable capabilities; there is a large literature on analog computers such as these.<sup>15</sup> The following is a guide for nonspecialists.

In solving (1) with an analog computer, the independent variable  $x$  is represented by a voltage varying linearly with time  $t$  in the computation; the dependent variables  $h$ ,  $dh/dx$ , and  $d^2h/dx^2$  are represented by voltages varying nonlinearly with  $t$ . Thus, leaving aside scaling (multiplying) factors for simplicity, (1) becomes

$$h'' = \frac{d^2h}{dt^2} = \frac{\partial n}{\partial h} + \frac{1}{a}. \quad (5)$$

A given  $\partial n/\partial h$  vs  $h$  profile constitutes the "input function" in the computation.

To trace a single ray let us assume for the moment, that a voltage representing  $dn/dh$  as a function  $h(t)$  is available at the input to the integrator  $I_1$  in Fig. 16. Here  $h' = dh/dt$ , and for the moment we take  $dn/dh$  to depend only on  $h$ . With a constant voltage  $1/a$  in parallel with  $dn/dh$  at the input,  $I_1$  integrates the sum  $(dn/dh + 1/a)$ ; the output of  $I_1$ , according to (5), is  $-h'$ . The initial value  $h'_0$  of  $h'$  for the ray concerned is introduced as a constant voltage  $h'_0$  at the "initial condition" terminal of  $I_1$ . The output of  $I_1$  is then integrated by the integrator  $I_2$ , where the initial value of  $h$  for the ray is introduced as a constant voltage  $h_0$ . The output of  $I_2$ , after passing through potentiometer  $P$  and amplifier  $A$ , gives a voltage  $Kh$  which is proportional to  $h$  and varies as function of time in the computation of the ray.

The voltage  $Kh$  provides the  $h$ -axis variations of the input function generator, in the course of tracing the ray. This generator may consist of a rotating drum (6-inch diameter or larger) which is driven through servomechanisms by  $Kh$ . Wrapped around this drum is a graph paper on which a wire curve, representing the  $dn/dh$  vs  $h$  profile, is glued. A potentiometer  $PP$ —perpendicular to the  $h$ -axis, and consisting of a knife-edge ridge of plastic (unbreakable) material—makes continuous contact with the wire as the drum rotates. With a proper constant voltage across the potentiometer, the voltage on the wire goes through the variation of  $dn/dh$  with  $h$  while  $h$  is being varied in the course of tracing the ray. Thus the voltage on the wire curve,

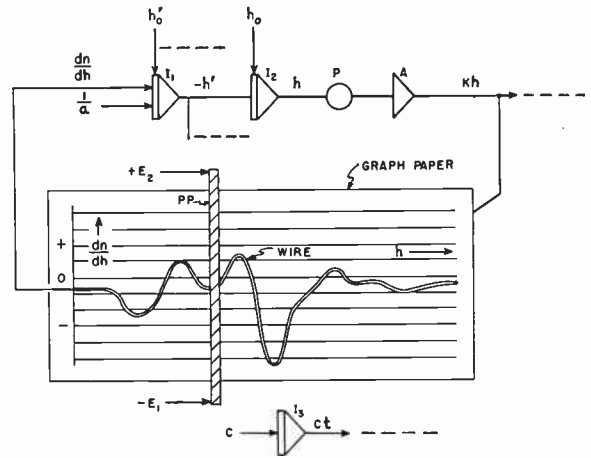


Fig. 16—Schematic diagram of ray tracing with analogue computer. Dashed lines denote voltages taken to output-plotting boards.

connected to the input of  $I_1$ , fulfills the assumption made above.

In place of the above type of function generator, a diode and relay arrangement can be used for generating a function in sloping-line segments. This latter arrangement has an advantage of fast response. A typical diode-function generating unit has twelve sloping-line segments available, and multiple units can be used in series. With a diode-function generator, it is simple to arrange for the intensity and the center height of each  $dn/dh$  vs  $h$  peak in a profile to vary with distance  $x$ ; this is done by use of additional diode-function generators for accommodating the variations of the intensity and the center height with  $x$  in sloping-line segments.

The computers (REAC or GEDA) used have rated tolerances of 0.1 per cent in the quality of the computing components. In practice this means that our ray-tracing results are accurate to within a fraction of 1 per cent of the plotted values wherever the rays are reproducible in the time duration of plotting one ray pattern (about half an hour). The rays which graze a layer at nearly zero values of elevation angles are not individually reproducible to within 1 per cent; however, these rays as a group are highly consistent, in the sense that they collectively cover the same area and the same ranges of initial and arrival angles in a given ray pattern, from one trial to the next.

The latest, and most advanced, analog computers manufactured have rated tolerances of 0.01 per cent; the best diode-function generators are capable of generating a reproducible, sharp peak (spike) occurring over a height interval as small as a thousandth of the total height concerned in a  $dn/dh$  vs  $h$  profile.

#### ACKNOWLEDGMENT

The writer is greatly indebted to G. B. Fanning and F. P. Miller who led the Wave Propagation Section in WADC; F. T. Sansom, R. T. Harnett, and H. R. McCarter for ray tracing; S. B. White, F. Overcash, and C. Hines for propagation; P. Springer for support.

<sup>15</sup> C. L. Johnson, "Analog Computer Techniques," McGraw-Hill Book Co., Inc., New York, N. Y.; 1956.

# A Cathode Test Utilizing Noise Measurements\*

W. DAHLKE† AND F. DLOUHY†

**Summary**—The well-known effect of full shot noise of current saturated parts of a cathode and shot-noise suppression under space-charge-limited conditions is shown to be very useful for evaluation of cathode quality. A test equipment and a practical test performance are described. Test results and their comparison to other methods of cathode evaluation demonstrate the high sensitivity of the proposed test. Alterations of the cathode quality by the method itself are very small. The test has been used in the laboratory for activation studies and cathode life tests during the past three years.

## I. INTRODUCTION

SEVERAL methods are available for measuring the electron emissive power of cathodes [1], [3], [4], [8], [11]. In manufacturing, the method of so-called under-heating curves is frequently used during which the emission current is measured as a function of the heater voltage. This often produces only qualitative results.

The method of measuring the saturation current with pulses is well known. This procedure is especially helpful with those tubes which are to be pulse operated during their lives. However, it must be borne in mind that the amplitude of the peak currents is dependent both upon cathode activity and the magnitude of interface layers of the oxide coating. Further, the barium-oxide layer, normally present on the grid wires, is easily decomposed during pulse operation when there is positive grid voltage. The resulting decomposition products can damage the cathode by poisoning.

This undesirable influencing of cathode activity by the measuring procedure does not appear when a diode-emission test [9] is used. At cathode temperatures of approximately 700°K and an anode voltage limited to 5 volts, such diode-current measurements  $I_d$  made during the life-time of a single tube of a definite type provide a clear picture of the changes of saturation current with life. Obviously, the temperature or the heater input of the cathode must be controlled very accurately because, as a result of the exponential dependence of the saturation current upon temperature, even small temperature variations cause large variations of the emission current. Unfortunately this diode test is less suitable for a comparison of the emissivity of different tubes, because standardization of heater inputs in different tubes, even of the same type, provides no real uniformity of cathode temperature, especially along the cathode length. Two tubes may show close agreement between 1) their distributions of temperature along the cathode length, at heater voltage of 2.5 volts and 2) emission current. However, at normal  $E_f = 6.3$  volts operating

conditions, entirely different temperature distributions may exist due to different radiation properties and thermal conductivities. Thus, they can have different emission currents at operating temperatures.

Measurement of mutual conductance [3], [11] as a function of heater power produces quite useful data for the evaluation of emissive abilities of different tubes. At high-cathode temperatures, the emission ability of cathodes is so great that the current drain is space-charge limited. Consequently, the mutual conductance is only slightly dependent upon the heater power. At lower temperatures a saturated condition sets in, and the mutual conductance drops quickly. For production evaluation of cathode emission, this  $G_m$  method is too cumbersome and time-consuming. A dynamic  $G_m$  measuring method using a by-passed cathode resistance with a heater voltage reduced to approximately 4 volts shows that the better the emission ability of the tube under these conditions, the higher the measured  $G_m$ .

In contrast to the mutual conductance  $G_m$  which is proportional to the space-charge limited area of the cathode, the well-known shot noise [10], [12–14] of the tube depends very strongly on the area of the saturated parts of the cathode, because of the removal of the space-charge reduction of noise. Shot noise therefore represents a most sensitive measure [4] of cathode quality. The practical performance of this noise test, its evaluation for judging cathode quality, its comparison with other already mentioned cathode tests, and several applications will be described and discussed after a theoretical introduction.

## II. THEORY

The mean-square shot noise current is

$$\overline{i_p^2} = 2eI_p\Gamma^2\Delta f = 2eI_{eq}\Delta f \quad (1)$$

with  $e$  the electron charge,  $I_p$  the plate current of the tube under test,  $\Delta f$  the bandwidth of the circuit, and  $I_{eq}$  the equivalent plate current of a saturated diode delivering the same noise  $\overline{i_p^2}$  as the test tube. Introducing the well-known expression [14] for the space-charge reduction factor  $\Gamma$  of a triode into (1), we obtain the desired equivalent noise current

$$I_{eq} = \begin{cases} I_p & \text{saturated region} \\ 1.29 \frac{E_f G_m}{\sigma} & \text{space-charge-limited region} \\ I_p & \text{exponential region} \end{cases} \quad (2)$$

of the triode under test, where  $G_m$  is the mutual conductance of the triode,

\* Original manuscript received by the IRE, November 19, 1957; revised manuscript received, April 18, 1958.

† Communication of Telefunken GmbH., Ulm, Germany.

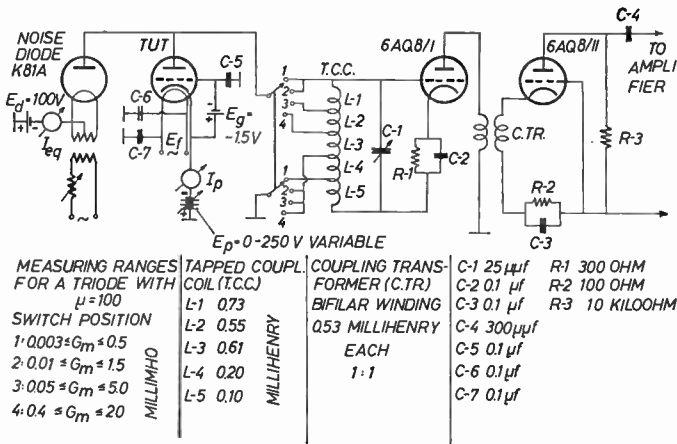


Fig. 1—Input circuit of the measuring amplifier.

$$\sigma = \frac{1}{1 + \frac{1}{\mu} \left( 1 + \frac{4d_{gp}}{3d_{cg}} \right)} \quad (3)$$

is a function of the electrostatic amplification factor  $\mu$ , and the distances  $d_{gp}$  and  $d_{cg}$  between grid plate and grid cathode respectively, and

$$E_T = \frac{kT_K}{e} \quad (4)$$

is the so-called temperature voltage of the cathode temperature  $T_K$  with  $k$  the Boltzmann constant.

### III. TEST EQUIPMENT

The principal circuit for the measurement of shot noise is shown in Fig. 1. The tube under test (TUT) is connected to the input of the preamplifier stage by means of a tapped coupling coil. For noise calibration a noise diode K81A is connected parallel to the input. Its plate voltage  $E_a=100$  volts is kept constant to ensure temperature-limited operation. The dc current  $I_{eq}$  of the diode is regulated by adjusting its heater voltage.

To enable a quick change in measuring different tube types, the tube under test is mounted on an exchangeable socket. The tube has its own voltage supply. The grid voltage is kept constant at  $E_g = -1.5$  volts to provide a rather uniform current density along the cathode. The plate voltage  $E_p$  is variable in order to regulate the dc plate current  $I_p$ .

The preamplifier consists of a twin triode 6AQ8 (see Table I) operating in a modified cascode connection [2]. A suitable position of the switch (Fig. 1) is chosen, depending on the test tube's transconductance, to give an optimal noise matching of the first section of the 6AQ8 triode to the test tube. The input admittance of the preamplifier is made large compared to the output conductance of the test tube, so that the input voltage of the preamplifier is directly proportional to the shot-noise current  $i_p$  for all plate currents  $I_p$ . The second section of the 6AQ8 tube is coupled in a normal

TABLE I  
OPERATING CHARACTERISTICS

	6AQ8 (ECC 85) Twin Triode	6BX6 (EF 80) Pentode
Heater voltage $E_f$	6.3 v	6.3 v
Plate voltage $E_p$	250 v	170 v
Screen grid voltage $E_{g2}$	—	170 v
Control grid voltage $E_{g1}$	-2.3 v	—
Cathode-Bias resistor $r_c$	—	160 ohm
Plate current $I_p$	10 ma	10 ma
Screen grid current $I_{g2}$	—	2.5 ma
Transconductance $G_m$	5.9 mmho	7.4 mmho
Amplification factor $\mu$	57	50

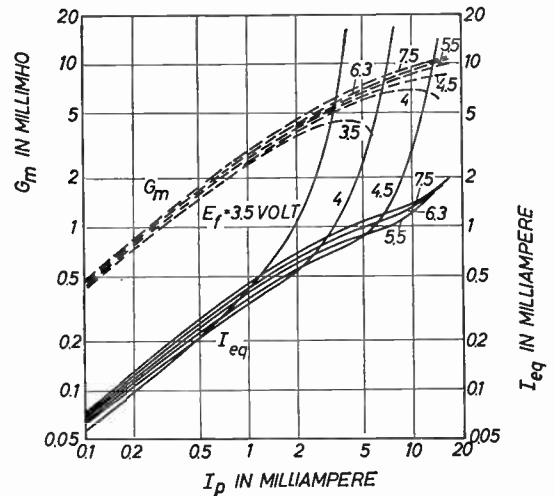


Fig. 2—Transconductance and noise characteristics of a 6BX6 pentode at  $E_g = -1.5$  volts. Heater voltage  $E_f =$  parameter.

grounded grid connection to the first system by means of a transformer with bifilar winding at one to one ratio.

The voltages of the preamplifier (not shown in Fig. 1) are supplied by the following multistage amplifier. It has a center frequency of 470 kc and a bandwidth of 20 kc. Its last stage is connected to a full-wave diode rectifier operating on a load resistor of 10k ohms where a high-resistance voltmeter serves as an output indicator. Under the described conditions of matching, the voltmeter deflection is directly proportional to the shot-noise source  $i_p$  and, according to (1), to the square root of the equivalent diode current  $I_{eq}$ , which is the desired quantity. For noise calibration, the output voltmeter is simply read as a function of the dc current  $I_{eq}$  of the noise diode with zero-plate voltage on the tube under test.

### IV. TEST RESULTS

In Fig. 2 the measured values of mutual conductance,  $G_m$ , and of the diode current  $I_{eq}$ , are plotted as a function of the plate current  $I_p$ . Eq. (1) relates  $I_{eq}$  to the shot-noise current. The results apply to a tube type 6BX6 in triode connection at  $E_g = -1.5$  volts. The normal operation conditions of this tube type are given in Table I. Heater voltage  $E_f$  is parameter.  $G_m$  curves have the usual shape [11], which is affected only slightly by the heater voltage, as long as all elements of the cathode operate space-charge limited. The curves

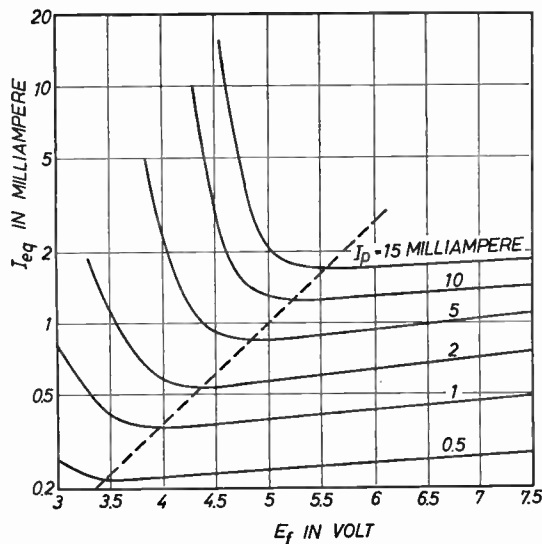


Fig. 3—Noise characteristics of a 6BX6 pentode at  $E_0 = -1.5$  volts. Plate current  $I_p$  = parameter.

shown are similar for plate currents less than 2 ma but depart progressively at higher and higher currents as the heater voltage is raised. The reduction in  $G_m$  is produced by the fact that progressively more elements of the cathode become saturated as the plate current is increased or as the heater voltage is reduced so that these elements do not contribute to the mutual conductance.

The curves for  $I_{eq}$  run approximately parallel to the  $G_m$  curves at low values of plate current. With fixed values of plate current, the curves for noise-current as well as the  $G_m$  curves for high-heater voltage are only slightly above those for low-heater voltage. With increasing plate current the  $I_{eq}$  curves begin to rise very rapidly at first for the low-heater voltages. This influence of the increased effect of saturation of the cathode which shows itself in the noise current at  $E_f = 3.5$  volts and  $I_p = 0.5$  ma very markedly as a cross-over point of several noise curves, becomes noticeable in the  $G_m$  curve only above  $I_p = 2$  ma as a barely perceptible decrease.

This behavior may be understood, if we consider that the mutual conductance is determined by all the elements of space-charge-limited emission, while the noise is determined principally by the elements with saturated emission, predominantly due to a weighting factor  $1/\Gamma^2 \gg 1$ . It must be noticed that the curves for  $I_{eq}$ , according to Fig. 2 at high values of plate current at times exceed the saturated shot-noise current prescribed by the limit  $I_{eq} = I_p$ . van der Ziel [14] kindly suggested to the authors that part of this excess noise and anomalies shown in some of the figures are due to flicker noise and that in order to find the true shot-noise effect, one has to go to frequencies of 5–15 mc.

The noise characteristics of Fig. 2 with the parameter  $E_f$  may also be described by other representations. In Fig. 3 the diode current  $I_{eq}$  is plotted in logarithmic scale as function of heater voltage  $E_f$ . The plate current

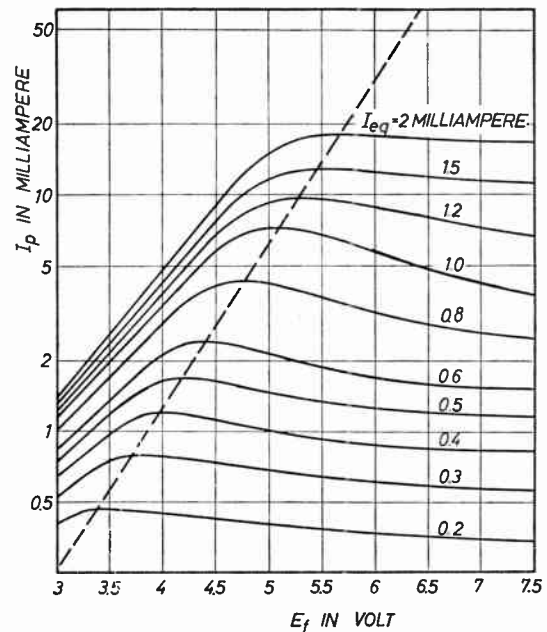


Fig. 4—Noise characteristics of a 6BX6 pentode at  $E_0 = -1.5$  volts. Equivalent diode current  $I_{eq}$  = parameter.

$I_p$  is the parameter. We see that  $I_{eq}$  is a slowly rising function of  $E_f$  at high-cathode temperatures. Saturation of  $I_p$  occurs at low values  $E_f$  accompanied by a strong increase of noise. The resulting noise minimum of the different  $I_p$  curves are joined by a dotted straight line. Every point corresponds to the cross-over points already shown in Fig. 2.

In Fig. 4 the plate current  $I_p$  is plotted on a logarithmic scale as function of  $E_f$  with  $I_{eq}$  as the parameter.  $I_p$  increases exponentially with rising  $E_f$  at low-heater voltages. Then, corresponding to the cross-overs in Fig. 2, remarkable maxima occur which are joined again by a dotted straight line. Its extrapolation to the normal heater voltage  $E_f = 6.3$  volts indicates a cross-over current of  $I_p = 50$  ma. The effect of current saturation at the fixed  $E_f$  values of 3.5 and 4 volts visible as maxima of  $G_m$  in Fig. 2 can already be detected as maxima of  $I_p$  in Fig. 4 at about 1/7 of the corresponding plate current. This relation implies the high sensitivity of the noise test.

## V. COMPARISON OF CATHODES

The results given in Section IV above relate to a well-activated cathode of a 6BX6 tube. These shall be compared now with a very poorly activated cathode of the same type. Fig. 5 shows the measured results in the same representation as Fig. 2 which was for the well-activated cathode. The differences between both of the families of characteristics are very remarkable. Comparing first the mutual conductance, the  $G_m$  maxima in Fig. 5 for the bad tube are lower by more than one decade than those in Fig. 2. Besides this difference in cathode saturation, the  $G_m$  curves of the bad tube show also a considerably higher dependence on  $E_f$  than the good one. That means, the effective space-charge-

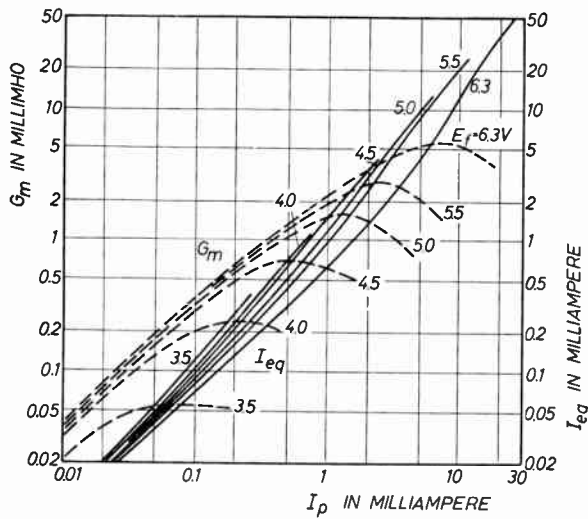


Fig. 5— $G_m$  and noise of a poorly-activated 6BX6 pentode.  $E_g = -1.5$  volts  $E_f =$  parameter.

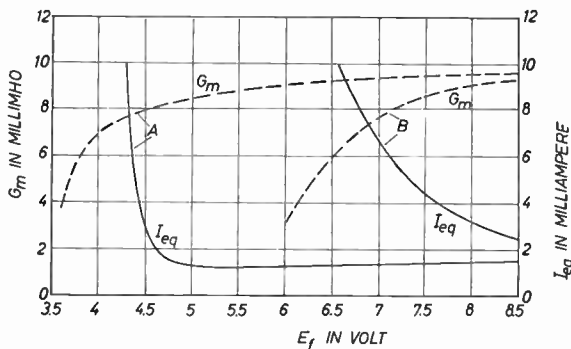


Fig. 6—Comparison of tubes 6BX6.  $A =$  well-activated,  $B =$  poorly-activated cathode.  $E_g = -1.5$  volts,  $I_p = 10$  ma.

limited area of the cathode is strongly temperature dependent. The cathode has noticeable patches, it is quite nonuniform. These conclusions are confirmed by the noise characteristics. The poor cathode does not show a cross-over point at all. Parts of the cathode are saturated even at very-low-plate currents, and normal heater voltage. The good cathode shows a rapid increase of  $I_{eq}$  with  $I_p$  when turning from space-charge limitation to saturation, while the poor cathode shows nearly straight lines of about 45 degrees slope for  $I_{eq}$  as function of  $I_p$ . The cathode is very nonuniform so that saturated patches exist independent of the operating conditions.

Curves  $A$  and  $B$  of Fig. 6 show the characteristics  $G_m$  and  $I_{eq}$  as functions of  $E_f$  in linear scales for the same well-activated cathode ( $A$ ) of Fig. 2 and the poorly activated cathode ( $B$ ) of Fig. 5. During the measurements the plate current  $I_p = 10$  ma and the grid voltage  $E_g = -1.5$  volts were kept constant for the two 6BX6. A strong correlation between  $G_m$  and  $I_{eq}$  curves is obvious. Decreasing  $G_m$  values correspond to rapidly increasing noise  $I_{eq}$ . The uniform cathode  $A$  shows a comparative sharp knee of  $I_{eq}$ , while the nonuniform cathode  $B$  has a smooth noise curve. Lowering the heater voltage, all parts of the cathode  $A$  become saturated quite

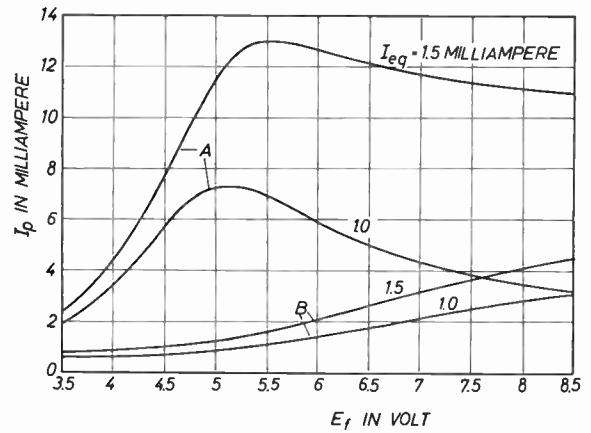


Fig. 7—Comparison of tubes 6BX6.  $A =$  well-activated,  $B =$  poorly-activated cathode.  $E_g = -1.5$  volts,  $I_{eq} =$  parameter.

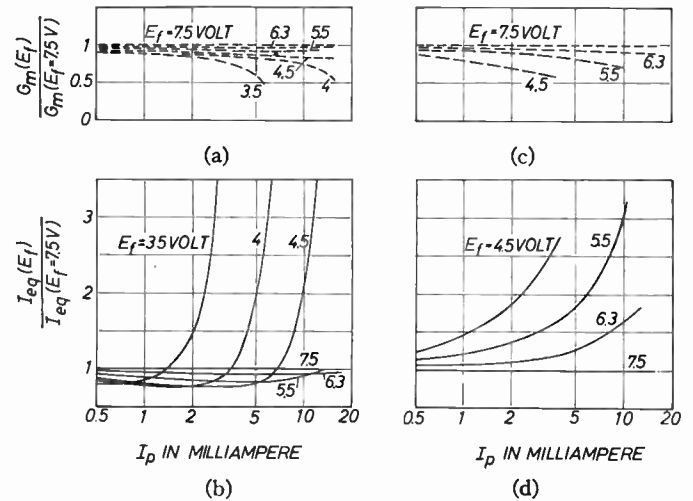


Fig. 8—Comparison of tubes 6BX6. (a), (b) well-activated, (c), (d) poorly-activated cathode.  $E_g = 1.5$  volts,  $E_f =$  parameter.

uniformly below  $E_f = 4.5$  volts. The poor cathode  $B$  has saturated patches all over the range of  $E_f$ .

Supplementing Fig. 4, the noise characteristics of the two cathodes  $A$  and  $B$  are represented now in Fig. 7 in a linear scale for the parameters  $I_{eq} = 1.0$  and  $1.5$  ma. The difference between the two cathodes is especially notable at heater voltages below 5 volts.

To get an even more suitable representation for the comparison of cathodes, the results of Fig. 2 were replotted in Fig. 8 in a different form. Figs. 8(a) and 8(b) refer to a tube with a good cathode, Figs. 8(c) and 8(d), to a tube with a poor cathode with nonuniform emission. The upper part of the figure shows the ratio of  $G_m$  at the given heater voltage to the  $G_m$  at 7.5 volts for a grid voltage  $E_g = -1.5$  volts plotted as a function of the plate current  $I_p$ . The lower part of the figure gives the noise values of  $I_{eq}$ , again referred to the reading at  $E_f = 7.5$  volts, as a function of plate current  $I_p$ . Heater voltage is the parameter.

In the tube with a good cathode (Figs. 8(a) and 8(b)), the noise shows a surprisingly steep rise with increasing current, while the mutual conductance shows a much less pronounced drop which becomes noticeable only at

considerably higher plate current. The fairly uniform cathode shows a transfer from the space-charge-limited region to the saturated region at relatively high-plate current. In the tube with a poor cathode (Figs. 8(c) and 8(d) this effect becomes noticeable at the lowest plate currents. This is produced by small areas of saturated emission from the cathode which increase continually with increasing plate current and which, at low values of plate current, reach values shown only at high currents by the good cathode.

VI. SIMPLIFIED NOISE TEST

For cathode evaluation in a manufacturing process the measurement of all the noise characteristics  $I_{eq}$  according to Fig. 2 or Fig. 8 as function of the plate current  $I_p$  is by far too time-consuming. Even the measuring of only one curve  $I_{eq}$  corresponding to Fig. 6 as function of heater voltages  $E_f$  is too lengthy for production control, although it may deliver valuable laboratory information. For this purpose a simplified noise test has been found useful which will be described below.

The tube under test is always triode connected. The grid-bias voltage  $E_g = -1.5$  volts, is chosen to give zero-grid current, the heater voltage is kept constant at a suitable value of about  $E_f = 5.0$  volts, as indicated to be desirable by Fig. 7. For testing, the plate voltage  $E_p$  of the tube is increased rather quickly and steadily starting from zero up to such a value that the amplifier of the test equipment of Fig. 1 shows a previously selected fixed noise value, i.e.,  $I_{eq} = 1.5$  ma. Then the corresponding plate current  $I_{pn}$  of the test tube is read as a measure of noise and cathode quality.

From Fig. 7 we see that the higher the test value  $I_{pn}$ , the better the cathode. For the 6BX6 the readings  $I_{pn} \geq 10$  ma correspond to very good cathodes, and  $I_{pn} \approx 1$  ma to very poor cathodes.

Besides its simple performance, the noise test  $I_{pn}$  has the advantage of running the tubes not too far from their normal grid and heater voltages, so that the above mentioned difficulties of the diode test  $I_d$  are avoided. Plate current is drawn only for a few seconds. Its peak value does not much exceed 1 ma for poor cathodes and 10 ma for good ones. Alteration of the cathode quality by the test method itself is therefore extremely small.

To study the correlation between the results of the three tests  $I_{pn}$ ,  $G_m$ ,  $I_d$ , thirty 6BX6 pentodes were tested according to the conditions of Table II. The results are shown in Fig. 9. In the upper diagram the measured values of  $G_m$  for each of the tubes are marked at the corresponding values of the diode current  $I_d$  as abscissa. In the lower diagram the data on  $I_{pn}$  are presented. The measured points are well-approximated by the so-called least square-trend lines. This proves a strong correlation among all three tests.

VII. CATHODE ACTIVATION AND NOISE

Some applications of noise measurements to the study of cathode activation are possible. Fig. 10 shows

TABLE II  
DATA ON READINGS FOR VARIOUS CATHODE TESTS ON 6BX6

	$I_{pn}$ —Noise test	$G_m$ —Test	$I_d$ —Diode Test
Fixed values	$E_f = 5$ v $E_{g1} = -1.5$ v $I_{eq} = 1.5$ ma	$E_f = 4$ v $E_p = E_{g2} = 170$ v $r_e = 160$ ohm	$E_f = 2.5$ v $E_p = E_{g1} = E_{g2} = 5$ v
Reading	Plate Current $I_{pn}$ in ma	Mutual conductance in momh	Diode current $I_d$ in ma
Note	Regulate $E_p = E_{g2}$ so that $I_{eq} = 1.5$ ma	Dynamic method	Constant heater power

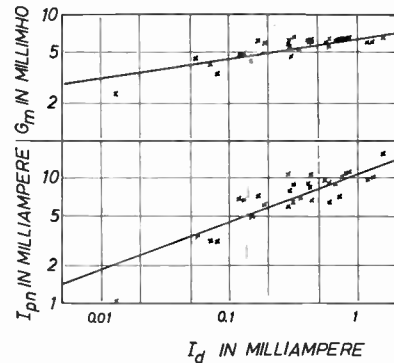


Fig. 9—Correlation of cathode tests.  $I_{pn}$ ,  $G_m$ ,  $I_d$  (see Table II).

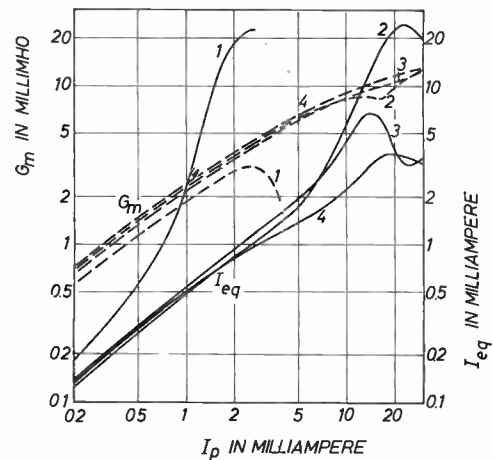


Fig. 10— $G_m$  and noise of 6BX6 in different states of cathode activation.  
Curves 1: pumped but nonactivated  
Curves 2: after activation  
Curves 3: after 120 hours operation (Table I)  
Curves 4: after 190 hours operation (Table I)  
 $E_g = -1.5$  volts;  $E_f = 6.3$  volts.

the measured mutual conductance  $G_m$  and noise characteristics  $I_{eq}$  of a 6BX6 in different states of activation as function of the plate current for a constant heater voltage  $E_f = 6.3$  volts. Coordinates are the same as in Fig. 2. Curves 1 correspond to the pumped but unactivated state of the cathode, curves 2 to its state at the end of the normal activation processing, curves 3 and 4 to the tube after 120 and 190 hours operation according to conditions shown in Table I. We see from the shape of the characteristics that a progressive increase of saturation current has occurred from curve 1 to 4. The

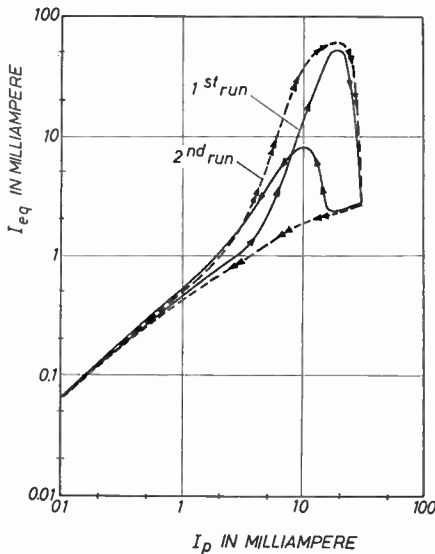


Fig. 11—Hysteresis of noise curves.  $E_c = -1.5$  volts;  $E_f = 6.3$  volts.

activation process is accompanied by a noticeable translation of the  $G_m$  lines to higher  $G_m$  values. The active and therefore space-charge-limited area of the cathode increases with activation. The noise curves show a corresponding transfer of saturated patches into space-charge limitation. Between  $I_p = 10$  and 16 ma the  $G_m$  curve 2 reveals a typical current saturation which, however, can be overcome by further rising plate current. A similar but smaller cathode saturation is hardly perceptible at  $G_m$  curve 3. The small  $G_m$  effects are accompanied with large maxima of the noise curves. Such a maximum is even detectable clearly after 190 hours of life from noise curve 4, while such an effect cannot be estimated from the corresponding  $G_m$  curve.

The described anomaly of noise shows a hysteresis loop with time as pictured in Fig. 11 for a 6BX6 at  $E_f = 6.3$  volts. With growing plate current the noise increases from a low value up to  $I_{eq} = 50$  ma, and then drops rather quickly to  $I_{eq} = 2$  ma. With falling  $I_p$  the noise again reaches its starting value after passing a lowered maximum. The activation state of the cathode has improved after a second run as indicated by the dashed curve. These noise measurements reveal changes in cathode quality that can barely be detected by other and more conventional means.

The method becomes still more sensitive when the heater voltage  $E_f$  is lowered as shown in Fig. 12. Fig. 12(a) depicts  $E_f = 6.3$  volts. Curve 1 corresponds to the activated cathode, curves 2 and 3 to the tube after operating for 120 and 190 hours respectively. Fig. 12(b) at  $E_f = 5.0$  volts shows details which cannot be perceived in the left one.

Finally, in Fig. 13 an interesting application of the simplified noise test to find optimal activation is shown. There the measured emission curves  $I_{pn}$  averaged for groups of 5 tubes 6BX6 are plotted in a double logarithmic scale as a function of activation burning time. The tubes were run with heater voltage only as indi-

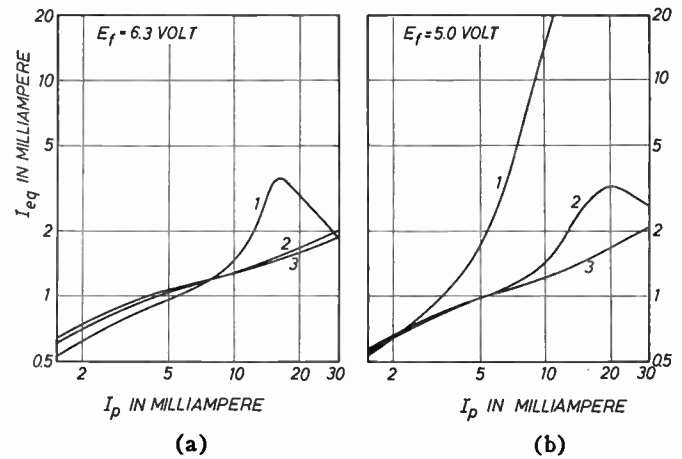


Fig. 12—Activation of a 6BX6 pentode measured at (a)  $E_f = 6.3$  volts. (b)  $E_f = 5.0$  volts with  $E_c = -1.5$  volts. Curves 1: activated; Curves 2: after 120 hours operation (Table I); Curves 3: after 190 hours operation (Table I).

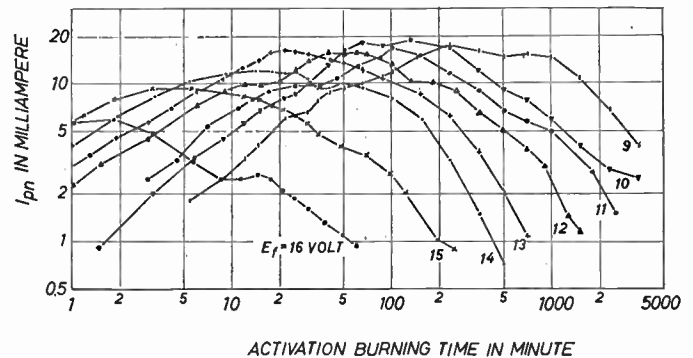


Fig. 13— $I_{pn}$  noise test for a 6BX6 pentode during activation burning time,  $E_f =$  parameter. See Table II for noise-test conditions.

cated by the parameter  $E_f$ . All the curves have essentially the same shape but differ in height and position of their maxima. Each maximum may be characterized by the corresponding coordinates of time and voltage  $E_f$ . The values that give a certain maximum of emissive ability may be called "optimal time" and "optimal heater" voltage respectively. To obtain a high emissivity at fixed cathode temperature, the time of activation should approach but not exceed the corresponding optimal time of activation. Similar results may be observed for tubes operating with plate current during the process of activation. In such cases the optimal time of activation will be somewhat shortened. With this information, tube processing and activation schedules have been improved in several cases of tube production, for instance, the method was very successful for passive cathode nickel where considerably shorter activation times and better life results were obtained.

ACKNOWLEDGMENT

The authors wish to thank R. Cantz for providing the noise amplifier and M. Bareiss, T. H. Briggs, and W. B. Nottingham, for valuable discussions and help in revising of the manuscript.

## BIBLIOGRAPHY

- [1] Briggs, T. H. "A Study of Cathode Emission and Measurements" Superior Tube Company, Norristown, Pa. January 16, 1956. (Private Communication.)
- [2] Cantz, R. "HF-Amplification with Triodes," *Telefunken-Röhre*, Vol. 30 (February, 1953), pp. 52-69.
- [3] Dahlke, W. "Long Life Radio Tubes," *Telefunken-Zeitung*, Vol. 27 (July, 1954), pp. 76-87; *Le Vide*, Vol. 10 (January, 1955), pp. 318-335. "Life Time of Oxide-Cathodes," *Telefunken-Zeitung*, Vol. 30 (March, 1957), pp. 55-61.
- [4] Dahlke, W. "Shot Noise of Triodes," *Nachrichtentechn. Fachberichte*, No. 2 (1955), pp. 56-59.
- Rothe, H. "Theorie rauschender Vierpole und deren Anwendung," *Telefunken-Röhre*, Vol. 33 (October, 1956), pp. 64-66;
- [5] Dow, W. G. *Engineering Electronics*, New York: John Wiley and Sons Co. Inc., 1952, 2nd ed., p. 139.
- [6] Nakai, J., Inuishi, Y., and Tsung-Che, Y. "On the Relations between Electron Emission, Conduction and Noise of Oxide-Coated Cathodes," *Journal of the Physical Society of Japan*, Vol. 10 (April, 1955), pp. 437-443.
- [7] North, D. O., "Fluctuations in Space-Charge-Limited Currents at Moderate High Frequencies," *RCA Review*, Vol. 4 (April, 1940), p. 463.
- [8] Nottingham, W. B. "Thermionic Emission," *Handbuch der Physik*, Vol. 21 (1956), pp. 97-157.
- [9] Metson, G. H., Wagener, S., Holmes, M. F., and Child, M. R. "The Life of Oxide Cathodes in Modern Receiving Valves," *Proceedings of the IEE*, Pt. III, Vol. 99 (March, 1952), pp. 69-81.
- [10] Rothe, H., und Kleen, W. *Elektronenröhren als Anfangsstufen-Verstärker—2. Auflage*, Leipzig: Akademie Verlagsges, 1953, pp. 291-299.
- [11] Rothe, H., und Kleen, W. *Grundlagen und Kennlinien der Elektronen-Röhren—2. Auflage*, Leipzig: Akademie Verlagsges, 1943, pp. 197-199.
- [12] Schottky, W. "About Spontaneous Current Fluctuations in Various Conductors," *Annalen der Physik*, Vol. 57 (July, 1918), pp. 541-567.
- Schottky, W., and Spenke, E. "About Space Charge Reduction of Shot Noise," *Wissenschaftliche Veröffentlichungen aus dem Siemens-Konzern*, Vol. 16 (1937), pp. 1-41.
- [13] Thompson, B. J., North, D. O., and Harris, W. A. "Fluctuations in Space-Charge-Limited Currents at Moderate High Frequencies," Part I-V, *Electron Tubes*, Vol. I (March, 1949). Published by *RCA Review*, pp. 58-190. Reprinted from *RCA Review* (January, 1940, et seq.)
- [14] van der Ziel, A. *Noise*, New York: Prentice-Hall, Inc., 1954, pp. 99-103.

## CORRECTION

The definition of VAR as published in "IRE Standards on Radio Aids to Navigation: Definitions of Terms, 1954" (Standard 54 IRE 12. S1), which appeared on pp. 189-209 of the February, 1955 issue of PROCEEDINGS, is in error. It appears in PROCEEDINGS as:

VAR (VHF Aural-Visual Range). A special type of vhf ating at vhf and providing *Radial Lines of Position* in any *Direction* as determined by *Bearing* selection within the receiving equipment. This facility emits a nondirectional "reference" modulation and a rotating pattern which develops a "variable" modulation of the same frequency as the reference modulation. *Lines of*

*Position* are determined by comparison of phase of the variable with that of the reference.

The correct definition is:

VAR (VHF Aural-Visual Range). A special type of VHF range providing a pair of *Radial Lines of Position* which are reciprocal in *Bearing* and are displayed to the pilot on a zero-center, left-right indicator. This facility also provides a pair of reciprocal *Radial Lines of Position* located 90° from the above visually-indicated lines and these are presented to the pilot as aural A-N radio range signals. The A-N aural signals provide a means for differentiating between the two visually-indicated lines (and vice versa).

# IRE Standards on Information Theory: Definitions of Terms, 1958\*

58 IRE 11. S1

## COMMITTEE PERSONNEL

### Subcommittee on East Coast Information Theory

P. L. BARGELLINI, *Chairman* 1958

P. ELIAS, *Chairman* 1955–1958

R. M. Fano, 1957–1958

### Subcommittee on West Coast Information Theory

N. M. BLACHMAN, *Chairman* 1956–1958

J. H. Tillotson, 1957–1958

### Committee on Information Theory and Modulation Systems

P. ELIAS, *Chairman* 1958–

J. G. KREER, JR., *Chairman* 1955–1958

W. G. TULLER, *Chairman* 1952–1955†

E. R. KRETZMER, *Vice-Chairman* 1958–

P. ELIAS, *Vice-Chairman* 1957–1958

M. J. E. GOLAY, *Vice-Chairman* 1955–1956

J. G. KREER, JR., *Vice-Chairman* 1952–1953

P. L. Bargellini 1952–1958

W. R. Bennett 1952–1958

N. M. Blachman 1956–1958

R. S. Caruthers 1957–1958

T. P. Cheatham, Jr., 1954–1955

W. B. Davenport, Jr., 1954–1955

L. A. DeRosa 1952–1958

P. Elias 1954–1957

M. J. E. Golay 1957–1958

S. Goldman 1956–1958

D. D. Grieg 1952–1954

J. V. Harrington 1952–1954

H. Kohler 1952–1958

J. G. Kreer, Jr. 1958–

E. R. Kretzmer 1952–1958

V. D. Landon 1952–1956

N. Marchand 1952–1958

L. A. Meacham 1952–1958

B. M. Oliver 1952–1953

W. Palmer 1952–1954

J. F. Peters 1956–1958

D. Pollack 1952–1958

K. H. Powers 1957–1958

J. R. Ragazzini 1952–1953

† Deceased.

## Standards Committee 1958–1959

R. F. SHEA, *Chairman*

J. G. KREER, JR., *Vice-Chairman*

C. H. PAGE, *Vice-Chairman*

L. G. CUMMING, *Vice-Chairman*

J. Avins

W. F. Bailey

M. W. Baldwin, Jr.

J. T. Bangert

W. R. Bennett

J. G. Brainerd

D. R. Brown

T. J. Carroll

P. S. Carter

A. G. Clavier

G. A. Deschamps

D. S. Dewire

S. Doba, Jr.

P. Elias

G. A. Espersen

D. Frezzolini

E. A. Gerber

A. B. Glenn

V. M. Graham

R. A. Hackbusch

H. C. Hardy

R. T. Haviland

A. G. Jensen

A. E. Kerwien

G. S. Ley

Wayne Mason

D. E. Maxwell

H. R. Mimno

E. Mittelmann

L. H. Montgomery, Jr.

G. A. Morton

R. C. Moyer

J. H. Mulligan, Jr.

W. Palmer

R. L. Prtichard

P. A. Redhead

R. Serrell

W. A. Shipman

H. R. Terhune

E. Weber

R. B. Wilcox

W. T. Wintringham

## Definitions Coordinator

C. H. PAGE

\* Approved by the IRE Standards Committee, June 23, 1958. Reprints of this standard, 58 IRE 11. S1, may be purchased while available from the Institute of Radio Engineers, 1 East 79th Street, New York, N. Y. at \$0.50 per copy. A 20 per cent discount will be allowed for 100 or more copies mailed to one address.

## INTRODUCTION

Information Theory, in the narrowest sense, is used to describe a body of work, largely about communication problems but not entirely about *electrical* communication, in which the information measures defined below (see *Information Content*, *Transinformation*) are central. This work is also known, particularly in Europe, as "the mathematical theory of communication." In a broader sense it is taken to include all statistical aspects of communication problems, including the theory of noise, statistical decision theory as applied to detection problems, and so forth. This broader field is sometimes called "statistical communication theory." In a still broader sense its use includes theories of measurement and observation which use other measures of information, or none at all, and indeed work on any problem in which information, in one of its colloquial senses, is important. The first and narrowest sense is the one to which the following definitions apply.

The original information measures defined in information theory were the averaged quantities *Average Information Content* (entropy) and *Average Transinformation* (transmitted information) (e.g., Shannon<sup>1</sup>). The unaveraged quantities *Information Content* and *Transinformation* (information transfer) were introduced later (e.g., Woodward<sup>2</sup>). The use of the unaveraged quantities has since spread. It has caused some controversy, since two basic theorems which justify the definitions of the averaged quantities do not apply in the unaveraged case. However, recent work in coding theory has given added significance to the unaveraged quantities (e.g., Shannon<sup>3</sup>).

The definitions of *Information Content*, *Transinformation*, *Equivocation*, *Redundancy*, *Message* and other terms whose definitions depend on these apply to the case of a communication system in which transmitted and received symbols are selected from a finite set. Only some of the defined concepts can be extended to other cases, and revision of the definition may be required before doing so. In particular, in the finite case either *Information Content* or *Transinformation* may be taken as basic, and the other as derived. However, *Information Content* does not extend conveniently to other cases, such as selection from a continuous set of possible values, while *Transinformation* can be so extended.

## DEFINITIONS

**Average Information Content (per symbol) (information rate from a source, per symbol).** The average of the *Information Content Per Symbol* emitted from a source.

*Note:* The terms *Entropy* and *Negentropy* are sometimes used to designate *Average Information Content*.

<sup>1</sup> C. E. Shannon and W. Weaver, "The Mathematical Theory of Communication," University of Illinois Press, Urbana, Ill.; 1949.

<sup>2</sup> P. M. Woodward, "Probability and Information Theory, with Applications to Radar," McGraw-Hill Book Co., Inc., New York, N. Y.; 1953.

<sup>3</sup> C. E. Shannon, "Certain results in coding theory for noise channels," *Information and Control*, vol. 1, pp. 6-25; 1957.

**Average Transinformation (of output symbols and input symbols).** *Transinformation* averaged over the ensemble of pairs of transmitted and received symbols.

**Binary Code.** Any *Code* employing two distinguishable types of *Code Elements*.

**Bit (information theory).** A unit of *Information Content* equal to the *Information Content* of a *Message* the *a priori* probability of which is one-half.

*Note:* If, in the definition of *Information Content*, the logarithm is taken to the base two, the result will be expressed in *bits*.

**Channel.** A combination of transmission media and equipment capable of receiving *Signals* at one point and delivering related *Signals* at another point.

**Channel Capacity.** The maximum possible *Information Rate* through a *Channel* subject to the constraints of that *Channel*.

*Note:* *Channel Capacity* may be either per second or per symbol.

**Channel Utilization Index.** The ratio of the *Information Rate (per second)* through a *Channel* to the *Channel Capacity (per second)*.

**Code.** A set of transformation rules to be applied to *Messages* or *Signals*.

*Note:* *Code* is sometimes used in a colloquial sense to denote the set of *Code Characters* used by a *Code*.

**Code Character.** The representation of a discrete value or symbol in accordance with a *Code*.

**Code Element.** One of a finite set of parts of which the characters in a given *Code* may be composed.

**Conditional Information Content (of a first symbol given a second symbol).** The negative of the logarithm of the conditional probability of the first symbol, given the second symbol.

*Note 1:* The choice of logarithmic base determines the unit of *Information Content*. See *Bit* and *Hartley*.

*Note 2:* The *Conditional Information Content* of an input symbol given an output symbol, averaged over all input-output pairs, is the *Equivocation*.

*Note 3:* The *Conditional Information Content* of output symbols relative to input symbols, averaged over all input-output pairs, has been called spread, prevarication, irrelevance, etc.

**Content, Average Information.** See *Average Information Content*.

**Content, Conditional Information.** See *Conditional Information Content*.

**Entropy.** See *Average Information Content*.

**Equivocation.** The *Conditional Information Content* of an input symbol given an output symbol, averaged over all input-output pairs.

**Hartley.** A unit of *Information Content* equal to the *Information Content* of a message, the *a priori* probability of which is one-tenth.

*Note:* If, in the definition of *Information Content*, the logarithm is taken to the base ten, the result will be expressed in *Hartleys*.

**Information Content (of a message or a symbol from a source).** The negative of the logarithm of the probability that this particular *Message* or symbol will be emitted from the source.

*Note 1:* The choice of logarithmic base determines the unit of *Information Content*. See *Bit* and *Hartley*.

*Note:* The probability of a given *Message* or symbol being emitted may depend on one or more preceding *Messages* or symbols.

*Note 3:* The quantity has been called *Self-Information*.

**Information Rate (from a source, per symbol).** See *Average Information Content*.

**Information Rate (from a source, per second).** The product of the *Average Information Content per Symbol* and the average number of symbols per second.

**Information Rate (through a channel, per symbol).** See *Average Transinformation*.

**Information Rate (through a channel, per second).** The product of the *Average Transinformation per Symbol* and the average number of symbols per second.

**Message.** (a) An ordered selection from an agreed set of symbols, intended to communicate information. (b) The original modulating wave in a communication system.

*Note:* Definition (a) is the sense in which the term is used in communication theory; definition (b) is the sense in which the term is often used in engineering practice.

**Message Source.** That part of a communication system where *Messages* are assumed to originate.

**Mutual Information.** See *Transinformation*.

**N-ary Code.** A *Code* employing *N* distinguishable types of *Code Elements*.

**Negentropy.** See *Average Information Content*.

**Redundancy (of a source).** The amount by which the logarithm of the number of symbols available at the source exceeds the *Average Information Content per Symbol* of the source.

*Note:* The term *Redundancy* has been used loosely in other senses. For example, a source whose output is normally transmitted over a given channel has been called redundant, if the *channel utilization index* is less than unity.

**Relative Redundancy (of a source).** The ratio of the *Redundancy* of the source to the logarithm of the number of symbols available at the source.

**Self Information.** See *Information Content*.

**Signal.** The physical embodiment of a *Message*.

**Ternary Code.** A *Code* employing three distinguishable types of *Code Elements*.

**Transferred Information.** See *Transinformation*.

**Transinformation (of an output symbol about an input symbol).** The difference between the *Information Content* of the input symbol and the *Conditional Information Content* of the input symbol given the output symbol.

*Note 1:* If  $x_i$  is an input symbol and  $y_j$  is an output symbol, the *Transinformation* is equal to

$$\begin{aligned} & [-\log p(x_i)] - [-\log p(x_i | y_j)] \\ &= \log \frac{p(x_i | y_j)}{p(x_i)} = \log \frac{p(x_i, y_j)}{p(x_i) p(y_j)} \end{aligned}$$

where  $p(x_i | y_j)$  is the conditional probability that  $x_i$  was transmitted when  $y_j$  is received, and  $p(x_i, y_j)$  is the joint probability of  $x_i$  and  $y_j$ .

*Note 2:* This quantity has been called *Transferred Information*, *Transmitted Information* and *Mutual Information*.

**Transmitted Information.** See *Transinformation*.



# Correspondence

## Optimum Finite Code Groups\*

A problem which has attracted considerable interest recently is that of determining so called "perfect words" or "optimum finite code groups." These are sequences of numbers,  $X_i$ , which satisfy the condition

$$\sum_{i=0}^{N-1-k} X_i X_{i+k} = \rho_k = \begin{cases} 0, \pm 1 & k=1, 2, \dots, N-1 \\ N & k=0 \end{cases}$$

$$X_i = \pm 1.$$

The only known solutions to date are for sequences of length  $N=1, 2, 3, 4, 5, 7, 11, 13$ . It is also known that solutions of odd length ( $N$  odd) satisfy the symmetry condition

$$X_i = X_{N-i}(-1)^{i+(N-1)/2} \quad (N \text{ odd}). \quad (1)$$

Recently, we have found another necessary condition which must be possessed by sequences of odd length. In particular, if

$$X_i = \psi_i X_{i-1}; \text{ then } \psi_{2i} = \psi_i; \quad (N \text{ odd}). \quad (2)$$

Consistency between (1) and (2) imposes very severe restrictions on the existence of solutions. It then can readily be shown that no solutions of odd length exist between  $N=13$  and  $N=101$ . Moreover, there are strong indications that there are very few, if any, solutions of odd lengths larger than  $N=13$ . We hope to submit a paper covering this material shortly.

J. E. STORER  
R. TURYN  
Sylvania Electric Products, Inc.  
Waltham, Mass.

\* Received by the IRE, April 3, 1958.

## WWV Standard Frequency Transmissions\*

Since October 9, 1957, the National Bureau of Standards radio stations WWV and WWVH have been maintained as constant as possible with respect to atomic frequency standards maintained and operated by the Boulder Laboratories, National Bureau of Standards. On October 9, 1957, the USA Frequency Standard was 1.4 parts in  $10^9$  high with respect to the frequency derived from the UT 2 second (provisional value) as determined by the U. S. Naval Observatory. The atomic frequency standards remain constant and are known to be constant to 1 part in  $10^9$  or better. The broadcast frequency can be further corrected with respect to the USA Frequency Standard as indicated in the table presented here. This correction is *not* with respect to the current value of frequency based on UT 2. A minus sign indicates that the broadcast frequency was low.

\* Received by the IRE, July 14, 1958.

## WWV FREQUENCY†

June, 1958 1500 UT	Parts in $10^9$
1	-3.4
2	-3.3
3	-3.3
4	-3.3‡
5	-3.2
6	-3.2
7	-3.1
8	-3.0‡
9	-3.0
10	-2.9
11	-2.9
12	-2.9‡
13	-2.9
14	-3.0
15	-3.1
16	-3.2
17	-3.3
18	-3.2
19	-3.2
20	-3.1
21	-3.2
22	-3.3‡
23	-3.3
24	-3.3
25	-3.3
26	-3.4
27	-3.4
28	-3.4
29	-3.4
30	-3.3

† WWVH frequency is synchronized with that of WWV.  
‡ Decrease in frequency of  $0.5 \times 10^{-9}$  at 1900 UT at WWV.

The WWV and WWVH time signals are synchronized; however, they may gradually depart from UT 2 (mean solar time corrected for polar variation and annual fluctuation in the rotation of the earth). Corrections are determined and published by the U. S. Naval Observatory.

WWV and WWVH time signals are maintained in close agreement with UT 2 by making step adjustments in time of precisely plus or minus twenty milliseconds on Wednesdays at 1900 UT when necessary; one step adjustment was made at WWV and WWVH on June 11, 1958.

W. D. GEORGE  
Radio Standards Lab.  
Nat'l. Bur. of Standards  
Boulder, Colo.

## Storage Capacity in Meteor-Burst Communication Systems\*

Campbell<sup>1</sup> has derived a differential equation, the solution of which allowed the specification of the storage capacity of a meteor-burst communication system in terms of the desired probability of filling the store. In a

\* Received by the IRE, March 27, 1958.  
<sup>1</sup> L. L. Campbell, "Storage capacity in burst-type communication systems," Proc. IRE, vol. 45, pp. 1661-1666; December, 1957.

completely independent investigation the same differential equation was derived using a different method. This method also allowed the inclusion of other factors that occur in the communication problem. It should be noticed that with  $K=0$ , (10) is the same as (34) given by Dr. Campbell.

## TRANSMITTER STORE-SIZE DETERMINATION

In this approach the first  $K$  bits transmitted are used for synchronizing. Let

$P(x)$  = probability that the information in store prior to a burst be  $x$  bits or less

$Q(x)$  = probability that the information in store after a burst be  $x$  bits or less

$a$  = arrival rate

$t$  = mean time between bursts

$s$  = decreasing rate (transmitted rate - arrival rate) =  $(n-a)$

$L$  = mean time of burst duration

$K$  = number of bits required for synchronization.

$$P(x) = \int_{z=0}^{x-\infty} e^{-z/at} \frac{1}{at} Q(x-z) dz \quad (1)$$

$$Q(x) = \int_{r=K}^{r=\infty} e^{-r/sL} \frac{1}{sL} P(x+r-K) dr + \int_{r=0} e^{-r/sL} \frac{1}{sL} P(x) dr. \quad (2)$$

From (2)

$$Q(x) = \int_{r=K}^{\infty} e^{-r/sL} \frac{1}{sL} P(x+r-K) dr + [1 - e^{-K/sL}] P(x). \quad (3)$$

In (1) let

$$y = x - z$$

$$P(x) = \int_{y=0}^{\infty} e^{-[(x-y)/at]} \frac{1}{at} Q(y) dy. \quad (4)$$

In (3) let

$$y = x + r - K$$

$$Q(x) = \int_{y=x}^{\infty} e^{-[(y-x+K)/sL]} \frac{1}{sL} R(y) dy + [1 - e^{-K/sL}] P(x). \quad (5)$$

Differentiating (4) and (5) with respect to  $x$

$$\frac{dP(x)}{dx} = \frac{1}{at} Q(x) - \frac{1}{at} P(x)$$

$$\frac{dQ(x)}{dx} = -\frac{1}{sL} P(x) + \frac{1}{sL} Q(x) \quad (6)$$

$$+ [1 - e^{-K/sL}] \frac{dP(x)}{dx}. \quad (7)$$

From (6)

$$Q(x) = at \frac{dP(x)}{dx} + P(x).$$

Substitute into (7)

$$at \frac{d^2P(x)}{dx^2} + \frac{dP(x)}{dx} = -\frac{1}{sL} P(x) + \frac{1}{sL} at \frac{dP(x)}{dx} + \frac{1}{sL} P(x) + [1 - e^{-K/sL}] \frac{dP(x)}{dx} \quad (8)$$

Collecting terms

$$at \frac{d^2P(x)}{dx^2} + \left[ e^{-K/sL} - \frac{at}{sL} \right] \frac{dP(x)}{dx} = 0 \quad (9)$$

or

$$\frac{d^2P(x)}{dx^2} + \left[ \frac{e^{-K/sL}(sL) - at}{(sL)(at)} \right] \frac{dP(x)}{dx} = 0 \quad (10)$$

Solving for  $P(x)$

$$P(x) = 1 - \exp - \left[ \frac{e^{-K/sL}(sL) - at}{(sL)(at)} \right] x \quad (11)$$

Thus

$$Pr(n > x) = \exp - \left[ \frac{e^{-K/sL}(sL) - at}{(sL)(at)} \right] x \quad (12)$$

Also let

$$m = \frac{sL}{at} \quad (13)$$

Then (12) becomes

$$Pr(n > x) = \exp - \left[ \frac{e^{-K/mat}(mat) - at}{(mat)at} \right] x \quad (14)$$

or

$$Pr(n > x) = \exp - \left[ \frac{e^{-K/mat}m - 1}{m} \right] \frac{x}{at} \quad (15)$$

With  $h$  = transmitted rate from (13)

$$m = \frac{sL}{at} = \frac{(h - a)}{a} \frac{L}{t} \quad (16)$$

In (16)  $L/t$  is the ratio of the mean time for the duration of a burst to the mean time for the period between bursts. Also,  $h/a$  is the ratio of the outgoing bit rate to the incoming bit rate, or stated in another way, the speed change effected by the transmitter. Let

$$D = \frac{L}{t},$$

$$R = \frac{h}{a},$$

then with the proper substitutions

$$m = (R - 1)D \quad (17)$$

RECEIVER STORE-SIZE DETERMINATION

Let

$L(x)$  = probability that the number of bits in store is  $x$  or less just before receipt of a transmission burst

$M(x)$  = probability that the number of bits in store is  $x$  or less just after the receipt of a transmission burst

$f$  = final service-bit rate

$m, k, t, s, L, a$  are the same as before.

$$L(x) = \int_0^\infty \frac{1}{ft} e^{-r/t} M(x+r) dr, \quad (18)$$

$$M(x) = \int_0^\infty \left\{ [1 - P(u)] e^{-u/sL} \frac{du}{sL} + \frac{\partial P(u)}{\partial u} du e^{-u/sL} \right\} L(x-u) \quad (19)$$

Substituting

$$P(u) = 1 - \exp - \left[ \frac{e^{-K/sL}(sL) - at}{(sL)(at)} \right] u,$$

(19) becomes

$$M(x) = \int_0^x L(x-u) \frac{e^{-K/sL}}{at} \exp - \left[ \frac{ue^{-K/sL}}{at} \right] du \quad (20)$$

Eqs. (18) and (20) are identical in form to (1) and (2) and because the boundary conditions are the same, the result is of the same form or

$$M(x) = 1 - \exp - \left[ \frac{e^{-K/sL}(fx) - at}{e^{-K/sL}(fx)(at)} \right] x \quad (21)$$

Therefore,

$$M(n > x) = \exp - \left[ \frac{e^{-K/sL}(fx) - at}{e^{-K/sL}(fx)(at)} \right] x \quad (22)$$

is the probability that store-size  $x$  in the receiver will not be exceeded.

Or, if it is desired, a ratio of the maximum average speed of the output device to the maximum average speed of the input device  $f/a = E$  may be used and (22) becomes

$$M(n > x) = \exp - \left[ \frac{e^{-K/sLE} - 1}{e^{-K/sLE}} \right] \frac{x}{at} \quad (23)$$

WALTER A. HELBIG  
Radio Corp. of America  
Camden, N. J.

Radio Engineering Use of the Cayley-Klein Model of Three-Dimensional Hyperbolic Space\*

The purpose of this note is to indicate how the Cayley-Klein model of three-dimensional hyperbolic space can be used in radio engineering.

The Smith chart is a useful tool for dealing with reflection coefficient transformations through bilateral two-port networks. The chart is aptly suitable for performing lossless transformations, because the rim of the Smith chart (the unit circle) is "invariant," being transformed into itself. For lossy transformations, however, the chart is not as suitable, because the unit circle does not remain invariant, being transformed into a circle inside the Smith chart. From a geometrical point of view, a lossless transformation can be performed by using real angles and real distances, whereas a lossy transformation actually requires "complex angles" (or "complex distances"). Since

it has been shown (Schilling<sup>1,2</sup>) that a geometric representation of a complex angle (distance) requires three dimensions, we may therefore state that the Smith chart is not the natural tool for treating lossy transformations. To find such a tool we have to look for a surface that is imbedded in three dimensions and transformed into itself (invariant) under the transformation—a "three-dimensional Smith chart."

Reflection coefficient transformations through bilateral two-port networks are performed analytically by the linear fractional transformation

$$\Gamma' = \frac{A\Gamma + B}{C\Gamma + D}, \quad AD - BC = 1. \quad (1)$$

For lossless two-port networks  $B=C^*$ ,  $D=A^*$ , the asterisk indicating a conjugate complex quantity. Eq. (1) can be written in the canonic form

$$\frac{\Gamma' - \Gamma_{f1}}{\Gamma' - \Gamma_{f2}} = q \frac{\Gamma - \Gamma_{f1}}{\Gamma - \Gamma_{f2}}, \quad q = e^{2\mu} = e^{2(\mu + j\nu)}, \quad (2)$$

where  $\Gamma_{f1}$  and  $\Gamma_{f2}$  are the fixed points obtained by putting  $\Gamma' = \Gamma$  in (1) and  $q$  is the multiplier.

Eqs. (1) and (2) can be graphically performed by the use of an elementary inversion method called the isometric circle method.<sup>3,4</sup> For lossless two-port networks the isometric circle method consists in two inversions. The isometric circles are orthogonal to the unit circle of the Smith chart. If the Smith chart is converted into the Cayley-Klein model of two-dimensional hyperbolic space,<sup>5-7</sup> these circles are transformed into straight lines, and the two inversions are converted into two non-Euclidean reflections.<sup>8</sup>

For lossy two-port networks the isometric circle method basically consists in four inversions in the  $\Gamma$  plane. A stereographic mapping of the  $\Gamma$  plane on the surface of the Riemann unit sphere, which is assumed to be the absolute surface of a Cayley-Klein model of three-dimensional hyperbolic space,<sup>9,10</sup> converts the four inversions in the  $\Gamma$  plane into two non-Euclidean reflections in two straight lines in space, for example,  $L_{12}$  and  $L_{13}$ , both non-Euclidean perpendiculars to an "inner

<sup>1</sup> F. Schilling, "Über die geometrische Bedeutung der Formeln der sphärischen Trigonometrie im Falle komplexer Argumente," *Math. Ann.*, vol. 39, pp. 598-600; 1891.

<sup>2</sup> —, "Beträge zur geometrischen Theorie der Schwarz'schen S-Funktion," *Math. Ann.*, vol. 44, pp. 161-260; 1894.

<sup>3</sup> E. F. Bolinder, "Impedance and polarization-ratio transformations by a graphical method using the isometric circles," *IRE TRANS. ON MICROWAVE THEORY AND TECHNIQUES*, vol. MTT-4, pp. 176-180; July, 1956.

<sup>4</sup> E. F. Bolinder, "Noisy and noise-free two-port networks treated by the isometric circle method," *Proc. IRE*, vol. 45, pp. 1412-1413; October, 1957.

<sup>5</sup> J. Van Slooten, "Meetkundige Beschouwingen in Verband met de Theorie der Electriche Vierpolen," W. D. Meinema, Delft, The Netherlands; 1946.

<sup>6</sup> G. A. Deschamps, "Geometrical representation of the polarization of a plane electromagnetic wave," *Proc. IRE*, vol. 39, pp. 540-544; May, 1951.

<sup>7</sup> E. F. Bolinder, "A survey of the use of non-Euclidean geometry in electrical engineering," *J. Franklin Inst.*, vol. 265, pp. 169-186; March, 1958.

<sup>8</sup> E. F. Bolinder, "Graphical methods for transforming impedances through lossless networks by the Cayley-Klein diagram," *Acta Pol., Elec. Eng. Series*, vol. 7, no. 202; 1956.

<sup>9</sup> F. Klein, "Vorlesungen über Nicht-Euklidische Geometrie," für den Druck neu bearbeitet von W. Rosemann, Springer Verlag, Berlin, Germany; 1928.

<sup>10</sup> F. Schilling, "Die Bewegungstheorie im Nicht-Euklidischen hyperbolischen Raum," vols. I, II, Leibniz-Verlag, Munich, Germany; 1948.

\* Received by the IRE, March 31, 1958.

axis<sup>11</sup>  $L_1$  through two points  $P_{f1}$  and  $P_{f2}$  on the surface of the unit sphere.<sup>11</sup> The points  $P_{f1}$  and  $P_{f2}$  are images of the fixed points  $\Gamma_{f1}$  and  $\Gamma_{f2}$  in the  $\Gamma$  plane. The lossy two-port network can thus be represented by the geometric configuration shown in Fig. 1. In this figure the non-Euclidean distance between  $L_{12}$  and  $L_{13}$  on  $L_1$  is  $\mu'$ , and the non-Euclidean angle between planes through  $L_{12}$  and  $L_{13}$ , and  $L_1$ , is  $\mu''$ . The quantity  $\mu' + j\mu''$  forms a "complex distance" in Schilling's sense.<sup>1,2</sup>

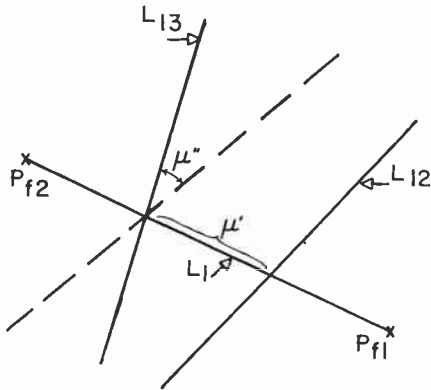


Fig. 1—Geometric configuration representing a bilateral lossy two-port network.

Van Slooten<sup>5</sup> has remarked that just as the Cayley-Klein model of two-dimensional hyperbolic space is suitable for impedance transformations through bilateral lossless two-port networks, so ought the Cayley-Klein model of three-dimensional hyperbolic space to be applicable for impedance transformations through lossy two-port networks. Although Van Slooten seems to be of the opinion that the Cayley-Klein model of three-dimensional hyperbolic space is too complicated to be of any use in electrical engineering, the model has nevertheless found many practical applications.

The geometric configuration shown in Fig. 1 can be used in studying problems dealing with bilateral two-port networks. It has been shown how the Klein generalization of the well-known Pascal theorem to three dimensions can be used to analyze such a network from three arbitrary impedances or reflection coefficient measurements.<sup>11-13</sup> The cascading of bilateral two-port networks can be studied by means of the Schilling generalization of the Hamilton theorem, a well-known theorem in spherical trigonometry. The inner axes and their perpendiculars that represent the constituent networks, together with those that represent the resultant network, form a geometric configuration consisting in six lines, all consecutively non-Euclidean perpendiculars to each other ("the Schilling

<sup>11</sup> E. F. Bolinder, "Impedance Transformations in the Three-Dimensional Hyperbolic Space," Res. Lab. of Electronics, M.I.T., Cambridge, Mass., Quart. Prog. Rep., pp. 125-128; April 15, 1956.  
<sup>12</sup> E. F. Bolinder, "Impedance transformations by extension of the isometric circle method to the three-dimensional hyperbolic space," *J. Math. Phys.*, vol. 36, pp. 49-61; April, 1957.  
<sup>13</sup> E. F. Bolinder, "General method of analyzing bilateral, two-port networks from three arbitrary impedance measurements," *Ericsson Technics*, vol. 14, pp. 3-35; 1958.

figure").<sup>11-13</sup> The Cayley-Klein model of three-dimensional hyperbolic space has also been used in studying the efficiency of two-port networks.<sup>14</sup>

The Cayley-Klein model of three-dimensional hyperbolic space has been treated by Deschamps in a basic paper<sup>15</sup> and has recently begun to be applied by de Buhr.<sup>16</sup>

Lastly, let me briefly point out the relation between the Cayley-Klein model and the Poincaré model of the three-dimensional hyperbolic space.

By the "Darboux transformation," each pair of points inverse in relation to the unit sphere is transformed into the pole of its symmetry plane. This transformation converts the Cayley-Klein model of three-dimensional hyperbolic space into the conformal Poincaré model of three-dimensional hyperbolic space, in which a straight line is represented by an arc of a circle that orthogonally cuts the absolute surface (here the surface of the unit sphere).<sup>7</sup>

From an engineering point of view the Poincaré model of three-dimensional hyperbolic space is rather impractical whereas the Cayley-Klein model of three-dimensional hyperbolic space can be used constructively in studying many important network problems, only a few of which have been outlined in this note.

E. F. BOLINDER  
 Antenna Lab., Electronics Res. Directorate  
 Air Force Cambridge Res. Center  
 Bedford, Mass.

Formerly with:  
 Research Lab. of Electronics  
 M.I.T.  
 Cambridge, Mass.

<sup>14</sup> E. F. Bolinder, "Graphical method for determining the efficiency of two-port networks," *Proc. IRE*, vol. 45, p. 361; March, 1957.

<sup>15</sup> G. A. Deschamps, "Geometric viewpoints in the representation of waveguides and waveguide junctions," *Proc. Symposium on Modern Network Synthesis*, Polytechnic Inst. of Brooklyn, N. Y., pp. 277-295; April, 1952.

<sup>16</sup> J. de Buhr, "Die geometrische Darstellungsweise hintereinandergeschalteter, allgemeiner, verlustbehalteter Vierpole," *AEÜ*, vol. 11, pp. 173-176; April, 1957.

### Properties of Root Loci\*

The roots of the polynomial  $P(s) + KZ(s)$  determine part of the transient behavior of certain types of linear feedback systems. As the constant  $K$  varies  $(0, \infty)$ , the roots trace out loci starting at the roots of  $P(s)$  and ending at the roots of  $Z(s)$ . The roots of  $P(s)$  are called poles, whereas the roots of  $Z(s)$  are called zeros.

The tangent vector of the loci is

$$u = - \frac{Z(s)}{P'(s) + KZ'(s)}$$

\* Received by the IRE, March 31, 1958. This paper presents the results of one phase of research carried out at the Jet Propulsion Lab., Calif. Inst. Techn., under Contract No. DA-04-495-Ord 18, sponsored by the Dept. of the Army Ordnance Corps.

For the constant  $K$  equal to zero the tangent vector indicates the rate of departure from the poles and the angle of departure. Both these quantities are conveniently calculated from the pole-zero pattern of complex  $s$  plane. The initial tangent vector at the pole  $s_{pj}$  is given by the expression

$$u(s_{pj})_{K=0} = - \frac{\sum_{i=1}^z (s_{pj} - s_{zi})}{\prod_{i=1, i \neq j}^p (s_{pj} - s_{pi})}$$

where

$$P(s) = \prod_{i=1}^p (s - s_{pi})$$

$$Z(s) = \prod_{i=1}^z (s - s_{zi})$$

The magnitude of the vector is the residue of the pole and is calculated by finding the ratio of the zero-to-pole vectors to the pole-to-pole vectors. The angle is given by the well-known formula

$$\phi = 180^\circ + \sum_{i=1}^z \phi_{zi} - \sum_{i=1, i \neq j}^p \phi_{pi}$$

where  $\phi$  is the angle of the zero-to-pole vectors and the pole-to-pole vectors.

Substitution of  $1/\lambda$  for the constant  $K$  yields the behavior of the tangent as  $K \rightarrow \infty$ . Similar expressions are obtained except that the roles of the zeros and poles are interchanged. As an example of pole-zero patterns, Fig. 1 has the initial tangent vectors as indicated.

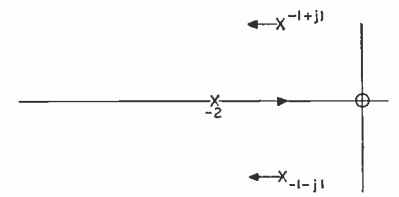


Fig. 1—Tangent vectors of a root locus.

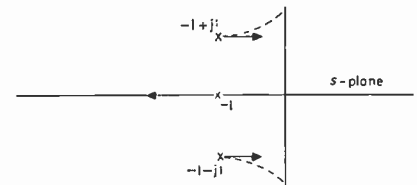


Fig. 2—Pole-zero pattern indicating curvature of the root locus.

The derivative of the tangent vector indicates the amount and direction of turning of the loci. The initial derivative is given by the expression

$$\left. \frac{du}{dK} \right|_{K=0} = 2 \frac{Z(s)Z'(s)}{[P'(s)]^2} - \frac{Z^2(s)P''(s)}{[P'(s)]^3}$$

Use of this formula is restricted to the special case of no zeros in the finite  $s$  plane. In this case  $Z(s) = 1$  and

$$\left. \frac{du}{dK} \right|_{K=0} = u^3(s)P''(s)$$

The pole-zero pattern of Fig. 2 has tangent

vectors as indicated. Use of the curvature relation indicates that the upper pole curves to the left.

The tangent vector and the curvature of the tangent vector are of interest in that they indicate the direction and curvature of a root locus. The magnitude of the tangent vector indicates the rate of motion of the roots for incremental changes in gain or other circuit parameters.

C. S. LORENS  
Jet Production Lab.  
California Institute of Technology  
Pasadena, Calif.

### A Proposed Technique for the Improvement of Range Determination with Noise Radar\*

In the above paper,<sup>1</sup> Bourret pointed out that a very sharp output could be obtained from a noise radar by using for the transmitted signal a bell-shaped power spectrum

$$\Phi(\omega) = \frac{P\beta/\pi}{\beta^2 + (\omega - \omega_0)^2} \quad (1)$$

where  $P$  is the total power and  $\beta$  is the distance on either side of  $\omega_0$  to the half-power point, and correlating this signal with the double derivative.

It is shown that the autocorrelation function  $R(\tau)$  of (1) is

$$R(\tau) = P \cos \omega_0 \tau e^{-\beta|\tau|}. \quad (2)$$

This particular  $R(\tau)$  has a cusp at  $\tau=0$ , so that its first derivative has a jump discontinuity and the second derivative has the character of an impulse function going to infinity.

The mathematics of the paper appears to be correct, but the physics of the problem leads intuitively to question the basis of the assumption as to whether an approximation to the ideal result can be reached even as a rough approximation.

The literal form of the energy spectrum (1) is impractical since the spectrum extends to infinity. If it were possible to produce and use a spectrum extending to infinity, there undoubtedly would be found a large number of functions which would provide all kinds of desirable results. The only value would lie in the possibility of being able to produce a practical approximation. But that involves a totally different mathematical problem which the paper has not touched. One should really work with a power spectrum of finite bandwidth. Then

$$R(\tau) = \int_0^{\omega} \Phi(\omega) \cos \omega \tau d\omega. \quad (3)$$

In this case, differentiation under the integral sign is permissible and one finds that

$$R'(\tau) = - \int_0^{\omega} \omega \Phi(\omega) \sin \omega \tau d\omega \quad (4)$$

so that  $R'(0)=0$ . In other words, no cusp is observed and  $R(\tau)$  has a maximum with slope 0.

This is true no matter how large a bandwidth is selected so that the cusp can never be achieved. This case is, mathematically speaking, an example of non-uniform convergence. One can proceed further and find

$$R''(\tau) = - \int_0^{\omega} \omega^2 \Phi(\omega) \cos \omega \tau d\omega \quad (5)$$

from which it follows that

$$R''(0) = - \int_0^{\omega} \omega^2 \Phi(\omega) d\omega. \quad (6)$$

Coupled with the fact that a double differentiation will introduce a great deal of noise into the system, the utility of the method is indeed doubtful.

From (6) it is evident that  $R''(0)$  is infinite for infinite bandwidth. This again shows that this method only applies to non-practical problems.

The mathematical problem of finding an optimum for finite bandwidth has not as yet been formulated rigorously.

HARRY HOCHSTADT  
The W. L. Maxson Corp.  
New York, N. Y.  
Polytechnic Institute of Brooklyn  
Brooklyn 1, N. Y.

### Estimates of Entropy of a Message Source\*

Shannon<sup>1</sup> has shown that, for an ergodic, finite-state message source

$$F_N \leq G_N, \quad (1)$$

where  $F_N$  is the conditional entropy of the next symbol when the preceding  $(N-1)$  symbols are known, and  $G_N$  is the entropy per symbol of blocks of  $N$  symbols. The purpose here is to derive a sequence of related inequalities.

Thus, let  $F_N^R$  be the conditional entropy (per symbol) of sequences of length  $R$  when the preceding sequence of length  $(N-R)$  is known.

Symbolically,

$$F_N^R = \frac{-1}{R} \sum_{i,j} P(B(N-R, i), B(R, j)) \log P(B(R, j)/B(N-R, i)), \quad (2)$$

where

$B(K, i)$  = the  $i$ th sequence of length  $K$   
 $P(X)$  = probability of sequence  $X$ ,  
 $P(X, Y)$  = probability of sequence  $X$  followed by sequence  $Y$ ,  
 $P(X/Y) = P(X, Y)/P(Y)$  = conditional probability that sequence  $X$  follows sequence  $Y$ , given  $Y$ .

Note that, in terms of Shannon's notation,

$$F_N^1 \equiv F_N, \\ F_N^N \equiv G_N. \quad (3)$$

We shall prove that

$$F_N^{R+1} \geq F_N^R, \quad (R = 1, 2, \dots, N-1). \quad (4)$$

From (2) and (4), one readily obtains

$$F_N^R = \frac{N}{R} G_N - \frac{(N-R)}{R} G_{N-R} \\ = \frac{1}{R} (N G_N - (N-R) G_{N-R}). \quad (5)$$

But Shannon<sup>1</sup> has shown that

$$N G_N = \sum_{K=1}^N F_K.$$

Hence (5) becomes

$$F_N^R = \frac{1}{R} \left( \sum_{K=1}^N F_K - \sum_{K=1}^{N-R} F_K \right) \\ = \frac{1}{R} \sum_{K=N-R+1}^N F_K. \quad (6)$$

Replacing  $R$  by  $(R+1)$  in (6) and subtracting yields

$$F_N^{R+1} - F_N^R \\ = \frac{1}{R(R+1)} \left( R \sum_{N-R}^N F_K - (R+1) \sum_{N-R+1}^N F_K \right) \\ = \frac{1}{R(R+1)} \left( R F_{N-R} - \sum_{N-R+1}^N F_K \right), \\ = \frac{1}{R(R+1)} \left( \sum_{K=N-R+1}^N (F_{N-R} - F_K) \right). \quad (7)$$

But, as Shannon has pointed out,<sup>2</sup>  $F_N$  is a monotonic decreasing function of  $N$ . Hence (7) is nonnegative, and (4) is proved.

CARMEN N. CAMPOPIANO  
Microwave Research Institute  
Polytechnic Institute of Brooklyn  
Brooklyn 1, N. Y.

*Ibid.*, p. 84.

### Minimum Weight Solenoid Systems\*

As pointed out by Worcester *et al.*,<sup>1</sup> solenoids constructed from aluminium result in a combined coil plus power supply weight which, for correct design, is less than that of the corresponding system with a copper coil, up to a certain coil size, even though the aluminium coil requires more power. However, it can be shown as follows that the advantage is never very great and exists only for coils which have rather small values of  $R$ , the ratio of the external to internal diameter. These occur in minimum weight designs only for low-field requirements or large internal diameters.

Worcester, *et al.* use a linear relation be-

\* Received by the IRE, May 5, 1958.

<sup>1</sup> W. E. Worcester, A. L. Weitzmann, and R. J. Townley, "Lightweight aluminium foil solenoids for traveling-wave tubes," IRE TRANS. ON ELECTRON DEVICES, vol. ED-3, pp. 70-74; January, 1956.

\* Received by the IRE, February 4, 1958.  
<sup>1</sup> R. Bourret, Proc. IRE, vol. 45, p. 1744; December, 1957.

\* Received by the IRE, April 21, 1958.  
<sup>1</sup> C. E. Shannon, "The Mathematical Theory of Communication," University of Illinois Press, Urbana, Ill.; 1949.

tween the power supply weight and the power, but a more general relation of the form

$$W_p = \alpha \cdot P^\beta$$

can be handled without difficulty and is needed in practical cases.

Power required by the coil is given by<sup>2</sup>

$$P = \Omega \left( \frac{R + 1}{R - 1} \right)$$

where  $\Omega$  is proportional to the field squared, the length of the coil, and the resistivity of the material, and so the total weight is

$$W_T = \alpha \Omega^\beta \left( \frac{R + 1}{R - 1} \right) + d(R^2 - 1)$$

where  $d$  is proportional to the density of the coil, its length, and its internal radius squared.

By differentiation, the condition that the system shall have minimum weight is

$$\frac{\alpha \beta \Omega^\beta}{d} = R(R - 1)^2 \cdot \left( \frac{R + 1}{R - 1} \right)^{1-\beta}$$

and eliminating  $\alpha \Omega^\beta$  from the weight equation gives the simpler form for minimum weight,

$$W_T = d(R^2 - 1) \left( \frac{R}{\beta} + 1 \right).$$

Full treatment of these equations cannot be given here, but consider the limiting forms of the last two equations when the radius ratio is taken as  $1 + r$  with  $r$  small.

$$\frac{\alpha \beta \Omega^\beta}{d} \simeq 2^{1-\beta} \cdot r^{1+\beta}$$

$$W_T \simeq 2rd \left( 1 + \frac{1}{\beta} \right).$$

$r$  can be eliminated immediately giving

$$W_T = \text{constant} \times (\Omega d)^{\beta/(1+\beta)}$$

Thus, the weight ratio for minimum weight systems of different materials can be expressed in terms of a function of the resistivity and density ratios only.

$$\frac{W_1}{W_2} = \left( \frac{\Omega_1}{\Omega_2} \cdot \frac{d_1}{d_2} \right)^{\beta/(1+\beta)}$$

If suffix 1 refers to copper and 2 to aluminium this ratio is 1.35 for  $\beta = 1$ .

Similarly, by using the limiting forms for large  $R$ , it follows that the weight ratio depends only on the resistivity ratio

$$\frac{W_1}{W_2} = \left( \frac{\Omega_1}{\Omega_2} \right)^\beta$$

which is 0.56 for  $\beta = 1$ .

Thus, copper coil systems are 35 per cent heavier for near-unity radius ratios but 44 per cent lighter for large radius ratios. In between, the ratio can be shown to decrease steadily with increasing radius ratio.<sup>3</sup>

If the main weight of the power supply is due to a transformer, which is often the case,

then it can be shown that  $\beta = \frac{1}{2}$  is the correct index for the weight-power law and the corresponding weight ratios are 1.30 and 0.65 in the two limits, which is a narrower range than before. With such relatively insignificant differences in weight it would seem that copper coils are to be preferred in view of the smaller size of both coil and power supply.

G. M. CLARKE  
Ferranti Valve Lab.  
Edinburgh 5, Scotland

### Various Definitions of the Delta Entities\*

I should like to make some comments in connection with the discussion on "the Dirac delta function  $\delta$ ."<sup>1,2</sup> Before deciding what "the  $\delta$ " really means it is better to speak quite generally about "the delta entity" or "the delta entities." There are many similar entities like "the delta"; e.g., the symbolical  $\sigma$  functions of Paul Lévy<sup>3</sup> or other entities from the quantum physics.

The delta entity can be studied from different points of view which do not eliminate one another:

- either it is a *point pseudofunction* (the point standpoint),
- or a *distribution* in the sense of Laurent Schwartz<sup>4</sup> (the functional standpoint),
- or a *class of almost everywhere equal real functions* in the sense of Heinz König<sup>5</sup> (the abstract algebraical standpoint),
- or a *pure symbol* (the symbolical standpoint).

Sketching the theory of the delta pseudofunction we must first answer two questions:

*Under what conditions does the symbol  $+\infty$  become a real (infinite) number?*

*Why is not the delta entity a (single-valued real) point function of a real independent variable?*

To find the exact response one must not only analyze the logical definition of the concept  $+\infty$  and of the point function, but must also take into account the manner in which we really use them in the mathematical analysis.

The application of  $+\infty$  is based on two principles:

First, in a given mathematical or physical problem  $P$ , the number  $+\infty$  is always a

unique result of a limiting process well-defined in  $P$ .

Second, for the calculation with  $+\infty$ , there exist well-defined arithmetical rules *not dependent* on the limiting process in the first principle; e.g.,  $a + (+\infty) = +\infty$ , where  $a =$  any real finite number.

For the concept, "the point function," there are three marks:

1) The first essential mark of the concept is the pure fact of a correspondence of a finite or infinite real number  $f(t)$  to a point  $t$  from the well-defined point set  $E$ . This mark tells us nothing about the realization of this correspondence.

2) The second essential mark is that the correspondence of  $f(t)$  to  $t$  must be *invariant* with respect to the specifications of the way in which we realize it.

3) The additional mark indicates what the relation  $f(t_0) = +\infty$  should mean. We explain it generally. Let  $t_0$  be a (finite or infinite) real point; it need not belong to  $E$ . One states that

the function  $f(t)$  has in  $t_0$  the value  $f(t_0)$  or  $f(t_0+)$  or  $f(t_0-)$  equal to  $+\infty$  or the supremum of  $f(t)$  in  $t_0$  is  $\bar{f}(t_0)$  or  $f(t_0+)$  or  $f(t_0-)$  equal to  $+\infty$  } (+)

if in every two, right, or left-sided neighborhood of  $t_0$ , there exists in  $E$  a sequence of one or another different points

$$\tau_1, \tau_2, \tau_3, \dots \rightarrow t_0$$

in which

$$f(\tau_1) < f(\tau_2) < f(\tau_3) < \dots \rightarrow \xi,$$

and if the number  $\xi$  is equal to  $+\infty$  and defines at least one of the six values (+).

In other words mark 3 indicates that the limiting process by which the number  $f(t_0) = +\infty$  is defined, *directly depends* on the fact of the correspondence of the values  $f(t)$  to the points  $t$  from  $E$ .

If we deny some of the marks 1-3 above, then  $f(t)$  will be defined as a (single-valued real) *point pseudofunction* (of a real independent variable). The name "pseudofunction" was coined by Doetsch.<sup>6</sup> Sometimes one speaks also about "an improper function". We define it by these conditions:

- 4) Mark 1 above holds good.
- 5) Mark 2 changes in the negative [non- $\beta$ ]; the correspondence of  $f(t)$  to  $t$  *depends on* the way in which it is realized.
- 6) The additional mark 3 can (but not necessarily must) be valid.

Thus, if a correspondence is realized by two essentially different ways, then we have two different point pseudofunctions. The fact of a correspondence is the same, but the way of its realization essentially determines the properties of the pseudofunction under consideration.

Let us start with the unit step function

$$U(t, k) = \begin{cases} 1 & \dots t > 0 \\ k & \dots t = 0 \\ 0 & \dots t < 0 \end{cases}$$

\* Received by the IRE, February 24, 1958; revised manuscript received, March 21, 1958.

<sup>1</sup> R. A. Johnson, "A note concerning the Dirac delta function," Proc. IRE, vol. 44, pp. 1058-1059; August, 1956.

<sup>2</sup> P. A. Clavier, R. A. Johnson, and R. B. Lackey, "The Dirac delta function," Proc. IRE, vol. 44, pp. 1876-1877; December, 1956.

<sup>3</sup> P. Lévy, "Une nouvelle classe de fonctions symboliques: les  $\sigma$ -fonctions," Bull. Sci. Math., vol. 80, pp. 83-96; May-June, 1956.

<sup>4</sup> L. Schwartz, "Théorie des distributions," Actual. scient. industr., part I, p. 1091, 1950; part II, p. 1122, 1951.

<sup>5</sup> H. König, "Neue Begründung der Theorie der 'Distribution' von L. Schwartz," Mathem. Nachricht., vol. 9, pp. 129-148; 1953.

<sup>6</sup> G. Doetsch, "Handbuch der Laplace-Transformation," Bd. II, 1. Abt., Birkhäuser, Basel-Stuttgart, Germany; 1955.

R. C. Glass and P. Gottfeldt, "Aluminium foil solenoids for traveling-wave tubes," IRE TRANS. ON ELECTRON DEVICES, vol. ED-4, p. 186; April, 1957.

<sup>3</sup> G. M. Clarke, "Weight aspects of coils for magnetic fields," to be published in *Electronic and Radio Engineer*.

where  $k$  is a real constant from the interval  $-\infty < k < +\infty$ . Every value of the parameter  $k$  defines a certain function  $U(t, k)$ . Two different values  $k_1, k_2$  define two different step functions.

It is necessary to distinguish between a certain step function and the class (set) of all these functions. Therefore we have in general two kinds of properties. Let  $K$  be a class of the elements  $e$ . We designate the property  $A$  as *individual*, when it refers to the certain element  $e \in K$  only;  $A$  is a *class property*, when it refers to all elements  $e$  which are considered as a whole set  $K$ . If the property  $A$  depends on a certain value of  $k$ , this is called the *individual property* of the mathematical entity under consideration. When  $A$  is not dependent on  $k$ , then  $A$  is a class property of these entities.

At any point  $t$  from  $-\infty < t < +\infty$ , one can compute the derivative of  $U(t, k)$  according to the classical definition. Taking  $+\infty$  as a number we can imply a correspondence of elements from the set of two elements  $\{0, +\infty\}$  to elements of the set of all real finite numbers. Therefore it is permitted (as the result of this correspondence) to define the following entity

$$\delta(t, k) = \begin{cases} \frac{dU(t, k)}{dt} & \text{(the both-sided derivative)} \\ & \text{if } 0 < k < 1, \\ \frac{d^+U(t, k)}{dt} & \text{(the right-sided derivative)} \\ & \text{if } k \leq 0, \\ \frac{d^-U(t, k)}{dt} & \text{(the left-sided derivative)} \\ & \text{if } k \geq 1. \end{cases}$$

This correspondence itself is a class property belonging to all entities  $\delta(t, k)$ . Every  $\delta(t, k)$  really has mark 1, but it is not a point function because of the validity of mark 5 and the nonvalidity of mark 3.  $\delta(t, k)$  is a point pseudofunction and cannot be treated by the methods appropriate to the point functions.

For the physical applications, it seems to be useful to restrict the values of the parameter  $k$  and to introduce the following definition:

The point pseudofunction  $\delta(t, k)$  is called the *unit impulse pseudofunction*, if  $0 \leq k \leq 1$ ; the point pseudofunction with the value  $k=1/2$  is called the *symmetrical Delta pseudofunction* or the *Dirac (improper) function*.

Delta pseudofunctions may be obtained in a more routine fashion using the limits of certain rectangles. If we introduce the number  $\rho$  by

$$\rho = 1 - k$$

then, geometrically,  $\rho$  is the portion of the area of rectangles under consideration situated on the right half plane. This number coincides with that of Johnson.<sup>1</sup>

The theorems governing the theory of the delta pseudofunctions may be stated by the use of the Riemann-Stieltjes or generally of the Lebesgue-Stieltjes integration.

Concerning the Laplace transform we have the following statement: for the pseudofunction  $\delta(t, k)(0 \leq k \leq 1)$ , the one-

sided Laplace transform has a meaning only when  $k=0$ ; if  $0 < k \leq 1$ , this transform has no meaning. But the two-sided Laplace transform always has a meaning for  $0 \leq k \leq 1$ .

Taking the delta entity as a distribution it is clear that the theory of distributions deals only with the class properties of the delta pseudofunctions, so that we omit here their individual ones. This has two important effects for the engineering applications of the delta entities:

First, in studying the impulse phenomena and the phenomena of the automatic control technique, engineers are primarily interested in their individual properties. They incline to consider the point pseudofunctions  $\delta(t, k)$  rather than the delta distribution.

Second, if we want to use the delta distribution, it would be necessary to define the notions of the impulse and automatic control technique in a new way with respect to the class properties of the phenomena under consideration, not with respect to their individual properties as is usual nowadays. Such research would be very useful for any engineering theory.

OTOMAR PANKRAZ  
Křížek-Karlín, N.E.  
Prague, Czechoslovakia

### Some Comments on Minimum Triggering Signals\*

Another theorem on minimum energy triggering signals, which is at least of academic interest, may be stated as follows.

Given a lossless network driven from a constant voltage source  $e_1(t)$  and terminated in a resistor (see Fig. 1), the optimum triggering signal  $e_1(t)$ , which will make the voltage across the terminating resistor a value of  $e_0$  at time  $t_0$ , is a doublet if  $g_{12}(+0) \neq 0$  and  $g_{12}(t)$  are bounded. Also, the minimum energy consumed is zero.  $g_{12}(t)$  is the impulse response of the network.

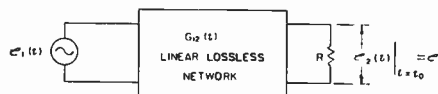


Fig. 1.

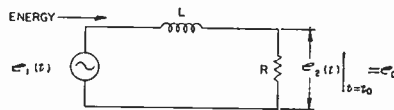


Fig. 2.

Consider a driving function  $e_1(t)$  as a positive impulse at  $t=0$  followed by a negative impulse at  $t=\Delta t$ , and let  $\Delta t \rightarrow 0$ . The energy consumed by the terminating resistor, assuming the output voltage reached the value  $e_0$  (this is easily done since it is

assumed that  $g_{12}(+0) \neq 0$ ) is as follows:

$$E = \frac{1}{R} \lim_{\Delta t \rightarrow 0} \left\{ \int_0^{\Delta t} \frac{e_0^2 g_{12}^2(t)}{g_{12}^2(+0)} dt + \int_{\Delta t}^{\infty} \left[ \frac{e_0 g_{12}(t)}{g_{12}(+0)} - \frac{e_0 g_{12}(t-\Delta t)}{g_{12}(-0)} \right] dt \right\}$$

$$E = \frac{1}{R} \lim_{\Delta t \rightarrow 0} \left\{ \int_0^{\Delta t} \frac{e_0^2 g_{12}^2(t)}{g_{12}^2(+0)} dt + \int_{\Delta t}^{\infty} \frac{e_0^2 g_{12}^2(t)}{g_{12}^2(+0)} dt + \int_{\Delta t}^{\infty} \frac{e_0^2 g_{12}^2(t-\Delta t)}{g_{12}^2(+0)} dt - 2 \int_{\Delta t}^{\infty} \frac{e_0^2 g_{12}(t) g_{12}(t-\Delta t)}{g_{12}^2(+0)} dt \right\}$$

Now, if  $g_{12}(t)$  is bounded, and  $\Delta t \rightarrow 0$ :

$$\int_0^{\Delta t} \frac{e_0^2 g_{12}^2(t)}{g_{12}^2(+0)} dt \rightarrow 0$$

$$\int_{\Delta t}^{\infty} \frac{e_0^2 g_{12}^2(t-\Delta t)}{g_{12}^2(+0)} dt \rightarrow \int_{\Delta t}^{\infty} \frac{e_0^2 g_{12}(t) g_{12}(t-\Delta t)}{g_{12}^2(+0)} dt$$

$$\rightarrow \int_{\Delta t}^{\infty} \frac{e_0^2 g_{12}^2(t)}{g_{12}^2(+0)} dt$$

Hence in the limit,

$$E = 0 \text{ and } e_1(t) \text{ is a doublet.}$$

The theorem is easily extended to cover certain classes of lossy networks; that is, if the impulse response across each resistor in the network is not zero at  $t=+0$  and is bounded, then the optimum signal is a doublet and the energy consumed is zero.

Although the above theorem and Beattie's work<sup>1</sup> are fundamental and interesting, they are of little practical importance, since the optimum signal usually requires that the signal source is capable of *absorbing energy*. That is, the generator tries to get back the energy it has put into the network. This is usually not feasible. For example, a radar receiver cannot send unused energy back to the transmitter. It would certainly be of more practical interest if the signal optimization were carried out not only subject to the constraint that the output voltage (or current) reaches a triggering level, but also the constraint that the signal source is capable of delivering but not absorbing energy. For example, find the optimum signal for the circuit of Fig. 2 subject to the above conditions. (Note that the doublet is the optimum signal under ideal conditions.) The optimum signal obviously must deliver at least

$$E_{min} = \frac{1}{2} L \frac{e_0^2}{R^2}$$

Now assume that the input signal is an impulse. Then,

$$E = \int_0^{\infty} \frac{e_0^2}{R} e^{-(2R/L)t} dt = \frac{1}{2} L \frac{e_0^2}{R} = E_{min}$$

Hence, the optimum signal for this simple case under the additional constraint, that

<sup>1</sup> L. A. Beattie, "Minimum energy triggering signals," Proc. IRE, vol. 46, pp. 751-757; April, 1958.

\* Received by the IRE, April 28, 1958.

the signal source can only deliver energy, is an impulse.

Perhaps the most interesting situation is where one has control over both the transmitter and receiver, as is often the case. This brings to mind the question, "What is the optimum receiver-transmitter combination?"

J. L. DAUTREMONT, JR.  
TelAutograph Corp.  
Los Angeles 45, Calif.

### A Low-Noise Nonlinear Reactance Traveling-Wave Amplifier\*

Nonlinear reactance amplification at high frequencies is currently receiving widespread interest for two major reasons:

1) Low-loss ferromagnetic materials and variable capacitance elements (semiconductor diodes) now available are suitable for nonlinear reactance operation at UHF and microwave frequencies.

2) The variable reactance amplifier does not depend on resistive elements for operation. Hence, it should be capable of yielding very low noise figures without refrigeration.

The general energy relations for nonlinear reactance amplification have been developed by Manley and Rowe.<sup>1</sup> Tien and Suhl have recently presented an analysis of traveling-wave amplification by means of nonlinear reactances<sup>2</sup> and have given a detailed discussion of the ferromagnetic type amplifier.

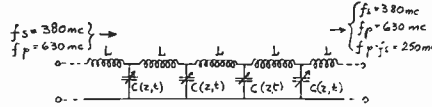
The purpose of this letter is to present some of the results obtained with a first experimental model of a traveling-wave variable reactance amplifier using nonlinear capacitances and designed for operation at UHF. The amplifier was designed and built late in 1957 and tested early in 1958. It operates under the following conditions:

- Signal frequency: 380 mc
- Pump (energizing) frequency: 630 mc
- (Idler frequency: 250 mc)
- Forward-signal gain: 10 to 12 db (signal and pump traveling in the same direction)
- Conversion gain (380 to 250 mc): 8 to 10 db
- Reverse-signal gain: -3 to -6 db (signal and pump traveling in opposite directions)
- Pump power: 1 to 2 mw
- Bandwidth: 10 to 20 mc
- Noise figure: 3.5 db.

The choice of signal and pump frequencies was governed by the availability of associated equipment (filters, etc.).

The reader is referred to Tien and Suhl<sup>2</sup> for the theory of operation of the nonlinear reactance traveling-wave amplifier. The amplifying structure used resembles that

shown in Tien and Suhl's Fig. 2 which is reproduced here.



Four diffused-junction nonlinear capacitance silicon diodes having low resistive loss were used. These are described by Uhlir<sup>3</sup> and Bakanowski, *et al.*<sup>4</sup> The circuit was designed to propagate with nearly equal velocities the signal, pump, and idler ( $f_p - f_s$ ) frequencies. With the sum frequency ( $f_p + f_s = 1010$  mc) reactively terminated, the operation of the amplifier corresponds to the "inverting modulator" case of Manley and Rowe's paper.<sup>1</sup> A more detailed presentation of the results obtained with the above amplifier and others currently under investigation is in preparation.

The writer wishes to express his thanks to A. Uhlir, Jr., for furnishing the variable capacitance diodes and to W. W. Mumford for his guidance and help.

R. S. ENGELBRECHT  
Bell Telephone Labs., Inc.  
Whippany, N. J.

<sup>3</sup> A. Uhlir, Jr., "The potential of semiconductor diodes in high-frequency communications," *Proc. IRE*, vol. 46, pp. 1099-1115; June, 1958.

<sup>4</sup> A. E. Bakanowski, N. G. Cranna, and A. Uhlir, Jr., "Diffused silicon and germanium nonlinear capacitors," presented at IRE-AIEE Semiconductor Device Res. Conf., Boulder, Colo., July, 1957.

### The Electron Optical Action of an Annular Aperture Lens\*

Until now, the only formula available to describe the deflection of an electron in an annular aperture lens has been the one derived empirically by Glewwe.<sup>1</sup> The purpose here is to present the derivation of an alternate and simpler formula which nevertheless serves to verify the work of Glewwe.

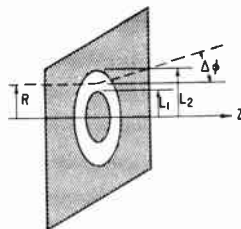


Fig. 1—Annular lens geometry.

In the annular lens shown in Fig. 1, the inner and outer radii of the aperture are  $L_1$  and  $L_2$ , respectively, and the lens is at potential  $V$  with respect to the cathode from

which electrons originate. The dashed line shows the trajectory of an electron entering the lens parallel to the axis and at a distance  $R$  from it. If  $E_z$  is the axial electric field existing on the left side of the plane in the absence of the slit, and if there is no field to the right of the plane, then Glewwe's formula for the deflection  $\Delta\phi$  of the trajectory is

$$\tan(\Delta\phi) = \frac{-E_z L_2}{2V} [1 - (1 - L_1/L_2)^{1.5}] \ln \frac{R}{\sqrt{L_1 L_2}} \quad (1)$$

This is a thin lens formula and is based on the empirical observation that there is no deflection of those electrons at  $R = \sqrt{L_1 L_2}$ .

We can derive a simpler formula in the standard way starting with this same observation. It is apparent from this fact that electric field lines which, in the uniform part of the field, lie outside  $\sqrt{L_1 L_2}$  must fringe outward and terminate on the outer part of the lens, while those inside  $\sqrt{L_2 L_1}$  must terminate on the inner part of the lens. Since no flux crosses the surface  $R = \sqrt{L_1 L_2}$ , we can construct an annular pill box with one curved surface at  $R$ , and the other at  $R = \sqrt{L_1 L_2}$ . The ends are placed sufficiently far from the lens for the box to encompass the entire range of field distortion due to the aperture (Fig. 2).

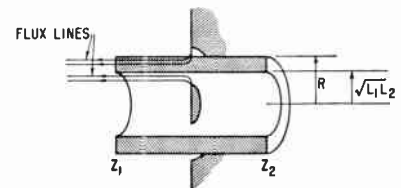


Fig. 2—Illustrating the application of Gauss' law for an annular lens.

The flux entering the curved surface at  $R$  must equal that leaving the annular end of the box, (neglecting any space charge) so that

$$-2\pi R \int_{z_1}^{z_2} E_R dz = - \int_{\sqrt{L_1 L_2}}^R 2\pi R E_z dR \quad (2)$$

The total radial impulse given an electron at  $R$  is

$$m\Delta v_R = e \int_{t_1}^{t_2} E_R dt = e \int_{z_1}^{z_2} \frac{E_R}{v_z} dz \quad (3)$$

Assuming that  $v_z$  and  $R$  are unchanged as the electron passes through the lens (thin lens approximation) we find from (2) that

$$\Delta v_R = \frac{e/m}{v_z} \frac{E_z}{R} \int_{\sqrt{L_1 L_2}}^R R dR \quad (4)$$

Integrating, and making use of  $v_z^2 = -2e/mV$

$$\frac{\Delta v_R}{v_z} = \tan(\Delta\phi) = - \frac{E_z}{2V} \frac{R^2 - L_1 L_2}{2R} \quad (5)$$

Eq. (5) has properties similar to that of Glewwe's formula. In the limit as  $L_1$  and  $L_2$  become large and  $L_1/L_2 \rightarrow 1$ , both reduce to the well-known Davisson formula for a slit.<sup>2</sup> Furthermore, both formulas predict

<sup>2</sup> K. R. Spangenberg, "Vacuum Tubes," McGraw-Hill Book Co., Inc., New York, N. Y., p. 354; 1948.

\* Received by the IRE, May 6, 1958.

<sup>1</sup> J. M. Manley and H. E. Rowe, "Some general properties of nonlinear elements—Part I," *Proc. IRE*, vol. 44, pp. 904-913; July, 1956.

<sup>2</sup> P. K. Tien and H. Suhl, "A traveling wave ferromagnetic amplifier," *Proc. IRE*, vol. 46, pp. 700-706; April, 1958.

\* Received by the IRE, April 21, 1958.

<sup>1</sup> C. W. Glewwe, "Some properties of an annular electron lens," M. S. thesis, University of Minnesota, Minneapolis, Minn.; 1955.

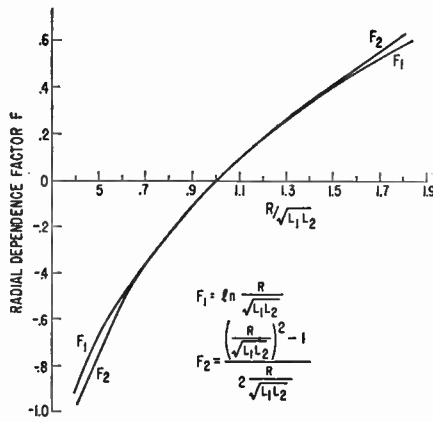


Fig. 3—Relative deflection as a function of radius predicted by the two lens formulas.

equal and opposite deflections for electrons at radii  $R_1$  and  $R_2$  so that

$$R_1 R_2 = L_1 L_2$$

The factors in both formulas showing the dependence of  $\tan(\Delta\phi)$  on  $R$  are compared in Fig. 3 which illustrates the equivalence of the two expressions in the usual range of interest. For many practical cases the factor  $[1 - (1 - L_1/L_2)^{1/2}]$  in (1) is reasonably close to 1.

L. A. HARRIS  
General Electric Co.  
P. O. Box 1088  
Schenectady, N. Y.

### Pulse Modulation Transmitted through a Linearly Modulated Transit-Time Device\*

A recent publication<sup>1</sup> discusses the use of transit-time modulation, by linear sawtooth waveforms, to accomplish frequency translation. The analysis presented has been carried out by Fourier integration over the modulation cycle, and, therefore, is restricted to problems which are quasistationary with respect to the modulation waveform. Some interesting properties of the system are lost by such an approach. The following paragraphs present a comprehensive discussion of the phenomena, without attempting analytical investigation of the problems encountered. They appear straightforward but tedious, and their evaluation would exceed the limits of the present space.

#### EXTENSION OF PREVIOUS ANALYSIS

The notation of Cumming<sup>1</sup> is used to facilitate comparison. Referring to his Figs. 4 and 5, we draw the analogous diagram for *symmetrical* sawtooth modulation.

For convenience we assume commensurate periods so that

$$T_m = kT_i \quad (1)$$

where  $k$  is a positive integer, but this restriction will be dropped in the most general case. Fig. 1 shows that neither overlapping nor holes appear in the train of samples constituting the output, at least for moderate amounts of modulation which will be assumed. In this respect our Fig. 1 differs from Figs. 4 and 5 of Cumming.<sup>1</sup>

The sampling points on the input-line of Fig. 1 represent the zero crossings of a continuous signal of frequency  $f_i = 1/T_i$ , entering the transit-time modulated device. The phase modulation converts the signal into two pulse trains of frequencies  $f_{o1} = 1/T_{o1}$  and  $f_{o2} = 1/T_{o2}$ , respectively, interlaced at a repetition rate  $f_m = 1/T_m$ . The pulses of one train fill the gaps between the pulses of the other, and vice versa. As indicated in Fig. 1, the pulses of the trains contain equal numbers of carrier cycles and, therefore, at the output are unequal in width and amplitude, in the fashion of an equal total energy per pulse relation.

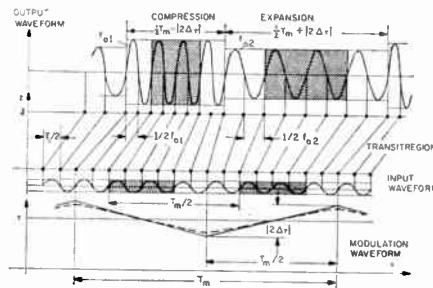


Fig. 1—Transmission of a sinusoid of frequency  $f_i$  through the transit-time device.

If condition (1) is not met, the carrier phase will vary from pulse to pulse of each train with respect to the envelope. In pulse modulation this is unimportant, since we shall integrate over the *carrier cycle* in the demodulation process. (In other words, we are only interested in the envelope of the pulses.) The basic difference in the approach of Cumming<sup>1</sup> is that Fourier integration is extended over several periods of the *modulation-waveform*,<sup>2</sup> and thus his coherence condition (1) results, which becomes irrelevant for pulse modulation.

The foregoing considerations show that pulse modulation constitutes a very natural utilization of the method, since signals may be restricted to the straight, continuous portions of the modulation cycle. Thus, even for asymmetrical linear sawtooth modulation as discussed by Cumming,<sup>1</sup> the influence of the everpresent, finite flyback interval may be completely eliminated by a pulse scheme. On the other hand, if we choose symmetrical triangular modulation, we are able to make use of both slopes for frequency shift in opposite directions for adjacent pulses. The shaded areas in Fig. 1 illustrate the situation for pulse-modulated input, and represent the signal-on periods.

The required synchronism between pulse train and modulation waveform is readily

accomplished, making use of the periodicity of the pulse-train envelope. The relation between frequency shift in the system and the transit-time modulation parameter  $\dot{\tau}$  is obtained from elementary considerations as

$$f_{o1,2} = \frac{f_i}{1 \mp \dot{\tau}} \doteq f_i(1 \pm \dot{\tau}), \quad \dot{\tau} \ll 1, \quad (2)$$

where  $\dot{\tau} = -4|\Delta\tau|f_m$  for symmetrical triangular modulation. Eq. (2) is the analogous expression to (2) in Cumming's paper. The difference is that we may assign  $\dot{\tau}$  any practical value, since we are not restricted by the coherence-condition (1) of Cumming. Introducing the  $\dot{\tau}$  just defined in his (1), we have

$$\bar{n} = -\dot{\tau}f_o/2f_m \quad (3)$$

Overlapping of significant regions of the pulse spectra is prevented if we assign  $\bar{n}$  a value between three and five. Fig. 2 illustrates the situation on hand of the unshifted and both shifted spectra, for two typical values of  $\bar{n}$ .

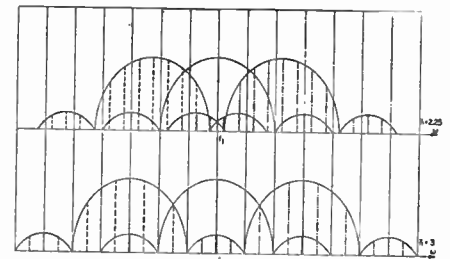


Fig. 2—Pulse spectra for  $\bar{n} = 2.25$  and 3.

The spectral distributions are sketched for square-wave envelope with repetition rate  $2f_m$ , and fixed carrier frequency  $f_i$  of the input pulses. Note that the line spacing is halved in the shifted spectra, according to the superposition of two pulse trains of repetition rate  $f_m$ . Analysis would show a phase relationship between components, due to the periodicity of the original waveform. In Fig. 2 we merely intend to present a crude estimate of crosstalk. It seems apparent that values  $\bar{n} = (2n+1)/4$ ,  $n = 0, 1, 2, \dots$ , prevent coincidence of significant components of the original, and either one of the shifted spectra. Even under practical conditions, these values should assure minimum crosstalk between channels.

The residual overlapping of the pulse spectra represents the only source of first-order crosstalk in the device, as long as we assume linear transmission. Other effects are of a CW nature and readily eliminated in the demodulation process.

The method described seems to be most applicable at microwave frequencies with pulse-repetition rates in the megacycle range. Experimental investigations — by others<sup>3</sup> demonstrates feasibility of  $n=1$  with conventional traveling-wave tubes. It seems realistic to expect  $\bar{n}=2$  with present tubes, and slight changes in tube design should lead to satisfactory performance

\* Received by the IRE, May 2, 1958.  
<sup>1</sup> R. C. Cumming, "The serrodyne frequency translator," PROC. IRE, vol. 45 pp. 175-186; February, 1957.

<sup>2</sup> The conventional spectrum viewpoint of frequency modulation cannot provide the required time resolution, and one must investigate the time-functions proper.

<sup>3</sup> D. R. Bellis and R. A. Huggins, "Phase Modulation of Traveling Wave Tubes," Eng. Notes, Huggins Lab., Menlo Park, Calif.; March, 1957

around 3 to 4 for  $\bar{n}$ . This would chiefly involve lengthening of the transit time. Narrow-band filters, to separate the resulting pulse channels, are readily constructed.

From (3) we realize that for these practical assumptions  $\bar{i} \ll 1$ , such that with  $f_i \bar{i} = \Delta f_i$  we may rewrite (2)

$$f_{01,2} \doteq f_i \pm \Delta f_i. \quad (4)$$

This implies negligible frequency asymmetry of the shifted pair, and analogously amplitude and width of the pulses will experience negligible change.

All our considerations so far have been based on symmetrical triangular transit-time modulation, but ultimately we shall employ the linear portions of a sine wave, as indicated by the dotted curve in Fig. 1. This sine wave may be directly obtained from one demodulated pulsetrain, at  $f_{01}$  for example, and the system is self-synchronizing, as soon as a signal is present. Since the sine wave introduces a certain deviation from linearity of the modulation waveform, distortion will arise, which is expected to be tolerable. Also, since the significant change in waveform occurs during the pulses only, the effective  $\bar{n}$  for the sine wave is larger than  $\bar{n}$  for a linear sawtooth of equal peak amplitude, due to the larger  $\bar{i}$ .

Thus we realize that for pulse modulation schemes the ideal transit-time modulation, waveform would be trapezoidal, the slopes being restricted to the duration of the pulses. With respect to spectral separation, this will assure best use of the total phase shift available in the transit-time device. Pulse modulation, combined with sinusoidal transit-time modulation, should render a very good approximation of this ideal case. As indicated in Fig. 3, only the

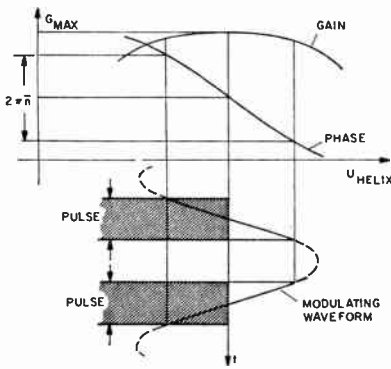


Fig. 3—Transit-time modulation characteristic for a traveling-wave tube.

portions of the modulation voltage, which correspond to the pulse-on intervals, make contributions to the output. Distortion during the rounded portions of the waveform is irrelevant, since it occurs for no-signal periods. Since  $\bar{i} = -2\pi\Delta\tau f_m$ , the effective  $\bar{n}$  is increased by a factor  $\pi/2$  over that of the symmetrical linear sawtooth of equal peak amplitude, according to (3).

SPECIFIC APPLICATIONS

Shifting of the Pulse-Carrier Frequency

If RF pulses of essentially arbitrary shape, repetition rate  $2f_m$ , proper phasing of their envelope with respect to the transit-

time modulation as indicated in Fig. 1, and carrier frequency  $f_i$  are fed into the system, adjacent output pulses have carrier frequencies  $f_i + \Delta f_i$  and  $f_i - \Delta f_i$ , respectively. Pulses spaced  $T_m$  thus experience frequency shift either up or downward, with no undesired components otherwise. The length and height of the pulses are affected according to the percentage of the frequency shift.<sup>4</sup> For  $f_i \gg \Delta f_i$  these effects are negligible.

Applications in Frequency-Script Counters or Computers

In a system which employs the carrier frequencies  $f_i$  and, for example,  $f_{01}$  of the pulses to represent binary states, the device may serve as a shift register. The clock pulses synchronize the transit-time modulation, and no appreciable pulse distortion occurs during the shifting. The repetition rate of the pulses is  $f_m$ , their length  $T_m/4$ , and a time shift  $T_m/2$  may be used to accomplish addition or subtraction.<sup>5</sup>

Pulse-Duplexing Scheme

Assume two channels to be represented on a pulse train of carrier frequency  $f_i$  by time division, odd pulses denoting channel 1 and even pulses denoting channel 2. A transit-time device may then be employed as a convenient decoder. Sinusoidal or symmetrical triangular transit-time modulation is employed, and the modulation voltage again is readily derived from the signal. The pulses then alternately fall on rising or decreasing portions of the modulation period, and the resulting frequency shift converts time division into frequency division. The two channels then are quite easily separated by filters. The inverse procedure may be used for time-division coding.

MULTIPLE REFLEX-PULSE AMPLIFIER

According to Fig. 4, the incoming information is pulse modulated and has a carrier frequency  $f_i$ . The pulses are fed into the transit-time modulator which also provides gain for the signal, and employs symmetrical triangular or sinusoidal modulation. Again the transit-time modulation voltage may be derived from the pulse train. Odd and even pulses of the train are shifted upward or downward in frequency, respectively, through junction B enter filter 1 with associated delay  $MT_m$ , and through junction A re-enter the transit-time modulator. The delay  $MT_m$  is chosen such that each pulse enters the transit-time device under identical modulation conditions, as on its first passage. The procedure is repeated, and after a certain number of recirculations, each of which is associated with delay and signal gain, two adjacent pulses of the train are at carrier frequencies symmetrically located about  $f_i$ , and eventually will reach a symmetrical pair  $f_i \pm n\Delta f_i$ , denoting the limits of the useful band.<sup>6</sup> The signals then enter filter 2,

<sup>4</sup> Large upward frequency results in shortening of RF pulses, which seems also attractive on an energy basis.  
<sup>5</sup> M. I. Disman. "Registers and Counters Based on Frequency Memory." Stanford University, Stanford, Calif., Rep. No. TR-19, August 16, 1954.  
<sup>6</sup> For this, the deviation from actual symmetry according to (2) will accumulate, but for only a few recirculations and  $\bar{i} \ll 1$  still presents no problem.

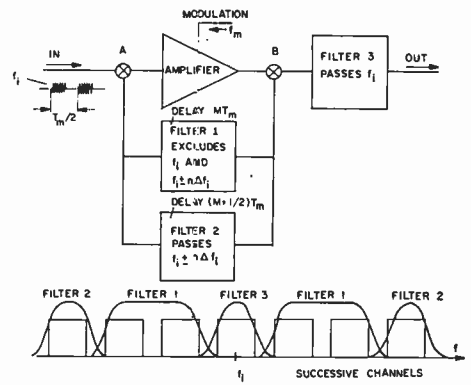


Fig. 4—Block diagram and filter characteristic for the pulse-reflex amplifier.

and the associated delay  $(M + \frac{1}{2})T_m$  brings the pulses to slopes of opposite frequency shifting. After an equal amount of total recirculations the pulses will be shifted back to  $f_i$ , again experiencing delay and gain at each recirculation, and leave the loop through junction B and filter 3. Pulse deformation due to the amplitude and compression effects is compensated, since individual pulses go through the mechanism both ways.

The system described exhibits certain memory properties, since pulses are circulating in the device for a time given by the total number of recirculations.<sup>7</sup>

To avoid coupling from the highly amplified pulses, which are about to leave the system, to the channels of the low-level incoming pulses, it might be advantageous not to run through the inverse-shifting procedure as just described. Instead, pulses at carrier frequencies  $f_i \pm n\Delta f_i$  may be shifted back to  $f_i$  with a conventional mixer. With increasing amplification, the amplified spectra move away from the low-level channels, and crosstalk is held to a minimum.

Acknowledgment is due to Dr. W. A. Edson for contributing valuable comments.

V. MET  
 General Electric Co.  
 Palo Alto, Calif.

<sup>7</sup> Construction of a frequency-division delay line, utilizing the compressed delay, seems promising.

Phase Dependence of a Ferromagnetic Microwave Amplifier\*

An amplifier using polycrystalline yttrium garnet<sup>1</sup> of 75-oersted linewidth has been tested. It is based on the degenerate, two-frequency electromagnetic mode of operation, a special case of that proposed by Suhl.<sup>2</sup> The purpose of this letter is to present

\* Received by the IRE, April 8, 1958.  
<sup>1</sup> The garnet was obtained from Harvard University through the courtesy of Prof. C. L. Hogan and Dr. J. E. Pippin.  
<sup>2</sup> H. Suhl. "Proposal for a ferromagnetic amplifier in the microwave range." *Phys. Rev.*, vol. 106, pp. 384-385; April 15, 1957.

experimental evidence of the phase-dependent operation of this type of ferromagnetic microwave amplifier.

Since the pulsed pump power and the CW signal input are not necessarily phase coherent, the output level differs from pulse to pulse. An experiment was designed to display on a single oscilloscope trace, the amplifier output pulse and a pulse showing the corresponding phase difference between pump and signal inputs. Fig. 1(a) shows approximately twelve superimposed traces. The amplifier output pulse is on the left and is seen to range between net gain (upward deflection) and attenuation. Fig. 1(b), 1(c), and 1(d) are single trace photographs show-

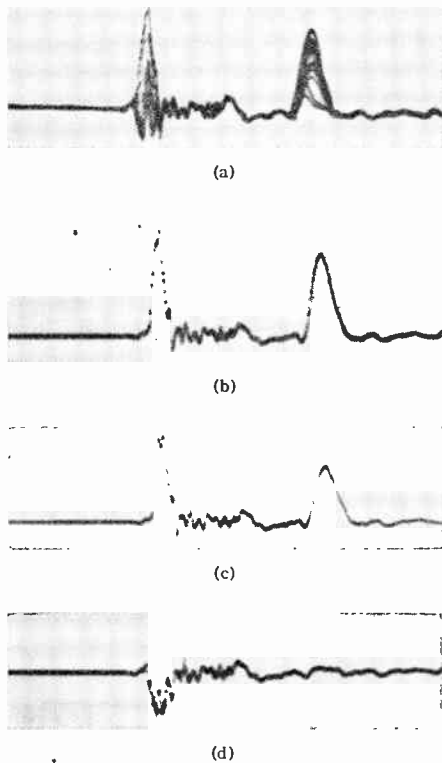


Fig. 1.

ing the maximum gain, intermediate gain, and maximum attenuation conditions, respectively, corresponding to maximum, intermediate, and zero amplitudes of the phase-comparison pulses. The phase pulse shows the shape of the magnetron pulse. It is seen that relative phase coherence is maintained over the 0.5- $\mu$ sec duration of a pulse, as would be expected. Some extraneous high-frequency transients from the pulser are also seen on all the traces.

The experimental apparatus is arranged as follows. An X-band magnetron and the sweep of an oscilloscope are triggered by a common single-pulse trigger. A portion of the pump power is added, in a magic tee, to the output of a crystal frequency doubler, which is driven phase coherently by the 4650-mc signal generator. The sum pulse, indicating their relative phases, is detected by a calibrated crystal and displayed on the oscilloscope after passing through a 1.7- $\mu$ sec delay line. The delay is introduced so

that the amplifier output pulse and its corresponding phase pulse can be displayed on the same trace. A variable phase shifter is placed between the crystal doubler and magic tee, and is adjusted so that the phase and amplifier output pulses are simultaneously a maximum.

This experiment was then repeated for a large number of pulses. It was seen that for only one setting of the phase shifter was there a one-to-one correspondence between maximum amplification and maximum phase-pulse amplitude (0 degree phase difference) and between maximum attenuation and zero phase pulse amplitude (180 degrees phase difference). It was also seen that two values of incoming pump-power phase gave zero net amplifier gain. This behavior is consistent with the phase dependence of the lumped circuit analog of the simple parametric amplifier.<sup>3</sup>

The amplifier itself consists of a strip line cavity normal to an X-band waveguide. In this respect it is similar to the one reported by Weiss.<sup>4</sup> The strip line cavity is one wavelength long; its resonant frequency is 4650 mc. The strip is 0.320 inch in width and is shorted at both ends. A garnet disk of 0.30-inch diameter and of 0.050-inch thickness is cemented to each side of the strip at its center. Coupling into and out of the cavity at signal frequency is obtained by means of probes located one-quarter wavelength from each end. X-band waveguide of one-half standard height is used to increase the filling factor of the garnet in the cavity and also to increase the effective pump field.  $H_{0e}$  is set for ferromagnetic resonance at pump frequency and is in the plane of the strip. The field direction is at 45 degrees to the long dimension of the strip and to the waveguide. The threshold pump power for oscillation in this amplifier has been observed to be 8-kw peak. For 0.1-mw signal input, a peak gain of 47 db has been observed with a bandwidth of approximately 1 mc.

W. L. WHIRRY  
F. B. WANG  
Hughes Aircraft Co.  
Culver City, Calif.

<sup>3</sup> T. J. Bridges "A parametric electron beam amplifier," Proc. IRE, vol. 46, pp. 494-495; February, 1958.

<sup>4</sup> M. T. Weiss "A solid-state microwave amplifier and oscillator using ferrites," Phys. Rev., vol. 107, p. 317; July 1, 1957.

propagation. The case of constant beam velocity and tapered circuit phase velocity may show the way to eliminating undesired backward-wave oscillations in forward-wave amplifiers. For one direction of taper, it appears that the start-oscillation CN is reduced for backward-wave oscillations, thus making possible BW oscillators of reduced size and weight.

The case of variable beam velocity is interesting because of the possibility of designing a backward-wave oscillator in the gun or acceleration region of the tube, thus yielding a minimum size and weight.

Because of the immediate application of the constant beam velocity-tapered circuit velocity case to BW oscillation suppression, an analysis of this situation has been made. Two approaches have been considered. For both methods the assumption of a linearly tapered velocity parameter  $b$  was made. One method involves graphical integration of  $x$  and  $y$  vs  $b$  curves plotted from the determinantal equation for the incremental propagation constants derived for the tapered circuit structure case. The other approach, which leads to less laborious numerical computation but is limited to small values of CN, involves finding a power series solution for the RF circuit voltage, RF beam current, and RF beam velocity differential equations, in the manner of Quate.<sup>1</sup> For the case of zero initial current and velocity modulation on the beam, the solution for the RF circuit voltage for forward-wave interaction for  $QC = d = 0$  takes the form

$$\frac{V(z)}{V(0)} = \exp -j\beta_e \left(1 + \frac{b(0)C}{2}\right) z \cdot \left[ e^{-j\pi CN(b(0) + 2\pi CN T)} - j \frac{(2\pi CN)^3}{3!} + j \frac{(2\pi CN)^5}{5!} \left(\frac{b(0)^2}{2} + j5T\right) - \frac{(2\pi CN)^6}{6!} (1 - j3b(0)T) + \dots \right] \quad (1)$$

where  $b(0)$  is the velocity parameter at  $z=0$  and  $T$  is the taper constant given by

$$T = \frac{\tau}{\beta_e C^2} \quad (2)$$

where  $\beta_e = \omega/u_0$  and  $\tau$  is defined by the set of circuit equations

$$\begin{aligned} X &= X(0)(1 + \tau z) \\ B &= B(0)(1 + \tau z) \end{aligned} \quad (3)$$

for the reactance and susceptance per unit length of the equivalent transmission line for the circuit.

For the case of backward-wave interaction it is only necessary to replace  $b(0)$  by  $-b(0)$  and  $j$  by  $-j$  in (1). For the case of zero  $T$ , (1) reduces to the solution obtained by Quate.

D. V. GEPPERT  
Microwave Tube Lab.  
Sylvania Electric Products, Inc.  
Mountain View, Calif.

<sup>1</sup> C. F. Quate, "Power Series Solution of Traveling Wave Tube Equations," Bell Telephone Labs., Rep. No. MM-53-1500-36; October 20, 1953.

\* Received by the IRE, May 14, 1958.

# Contributors

Morrel P. Bachynski (S'54-M'56) was born on July 19, 1930 in Bienfait, Saskatchewan, Canada. He received the B.E. degree in engineering physics in 1952 and the M.S. degree in 1953, both from the University of Saskatchewan, and the Ph.D. degree from McGill University, Montreal, Canada, in 1955.



M. P. BACHYNSKI

Until October, 1955, as a member of the staff of the Eaton Electronics Research Laboratory at McGill he was engaged in investigations concerning aberrations in microwave lens systems. Since that time he has been with the RCA Victor Research Laboratories, Montreal, concerned primarily with short-wave propagation problems.

He now holds the position of head of the Wave Propagation Division.



Walter E. Dahlke was born in Berlin, Germany, on August 24, 1910. He graduated Dr. phil. in 1936



W. E. DAHLKE

after having studied physics and mathematics at the University of Berlin. During the following four years, he was a research assistant at the Physical Institute of the University of Jena, Germany. Here he took the degree of Dr. phil. habil. (lecturer) in 1939, working on infrared spectroscopy. In 1940

through 1945 he was a member, and since 1944 the head, of the microwave tube laboratory at the German Aviation Research Establishment in Berlin-Adlershof.

Mr. Dahlke joined Telefunken Laboratory, Ulm, in 1949. As head of a research group he has been working specifically on problems of electron tubes for triode characteristics, tube noise, and oxide cathodes.

At present he is giving lectures on electron tubes at the Institute of Technology in Stuttgart.

He is a member of the German Physical Society.



Franz Dlouhy was born on July 10, 1914 in Hainburg, Austria. He joined Telefunken Laboratories, Ulm, Germany, in

1947, where he participated in development work and investigations concerning vacuum tubes. In 1952 he finished his technical training, which had been interrupted by World War II, and received the Diplom Ingenieur from Technische Hochschule, Karlsruhe, Southern Germany.



F. DLOUHY

He is now specifically working on studies on oxide coated cathodes.



Erwin E. Dreese was born in Millbrook, Mich., on September 10, 1895. He received the B.S. degree in electrical engineering from the University of Michigan, Ann Arbor, in 1920, the M.S. degree in 1922, and the degree of Electrical Engineer in 1929.



E. E. DREESE

In 1917 and 1918 he served with the U. S. Army Signal Corps and from 1925 to 1930 was chief engineer of the Lincoln Electric Company, Cleveland, Ohio. Since 1930 he has been professor and chairman of the Electrical Engineering Department at the Ohio State University, Columbus. Since 1937 he has also been editor of technical textbooks for the International Textbook Company and chairman of the board of trustees of the James F. Lincoln Arc Welding Foundation.

He is a member of the American Institute of Electrical Engineers, the American Society for Engineering Education, Sigma Xi, Tau Beta Pi, Theta Chi, and honorary member of Theta Tau and Eta Kappa Nu.



James P. Gordon was born in New York, N. Y., on March 20, 1928. He received the B.S. degree in physics from M.I.T., Cambridge, Mass., in 1949, and the M.A. and Ph.D. degrees in 1951 and 1955 from Columbia University, New York, N. Y. His doctoral dissertation at Columbia University resulted in the first ammonia maser.



J. P. GORDON

Since joining Bell Telephone Labora-

tories, Inc., Murray Hill, N. J., in 1955, he has continued his work on masers and is now directing a group which is investigating a number of problems relating to this field.

Dr. Gordon is a member of the American Physical Society and Sigma Xi.



George N. Hatsopoulos was born in Athens, Greece, on January 7, 1927. He attended Athens Polytechnic, School of Mechanical and Electrical Engineering. He received the B.S. and M.S. degrees in 1950, the M.E. degree in 1954, and the Sc.D. degree in 1952 all in mechanical engineering from Massachusetts Institute of Technology, Cambridge, Mass.



G. N. HATSOPoulos

He was a research assistant at M.I.T. from 1950-1951, chief engineer at the Matrad Corporation, New York, N. Y. from 1952-1953, teaching assistant at M.I.T. from 1953-1954, consultant at the Matrad Corporation and instructor in mechanical engineering at M.I.T. from 1954-1956, assistant professor in mechanical engineering at M.I.T., and a consultant with Foster Miller Associates, Watertown, Mass., Thermo Electron Engineering Corporation, Belmont, Mass., and Joseph Kaye and Company, Brookline, Mass., during 1956 to 1957.

He directed the research of M.I.T. projects concerned with isothermal surface investigation, the basic development of the thermoelectron engine, and the effects of forced vibrations of heat transfer in free convection. He is co-holder with J. Kaye of three U. S. patents.

Since January, 1958 he has been president of the Thermo Electron Engineering Corporation, Cambridge, Mass.

Dr. Hatsopoulos was a member of the Honors Group in Mechanical Engineering from 1948 to 1950 and is a member of Sigma Xi.



Joseph Kaye was born in Malden, Mass., on November 16, 1912. In 1934, he obtained the S.B. degree in physical chemistry from Massachusetts Institute of Technology, Cambridge, Mass., and was awarded the first Stratton Prize. In 1936, he received a fellowship from M.I.T.; in 1937 he was conferred the Ph.D. degree in physical chemistry, and from 1937-1939 he was a Little Post-Doctorate Fellow. From 1939-1955, he served as a research engineer, an instructor, and an associate professor in

the Mechanical Engineering Department of M.I.T. Since 1952, he has been director of the Research Laboratory of Heat Transfer in Electronics, and in 1955, he became a professor in the Mechanical Engineering Department.



J. KAYE

Dr. Kaye, a registered professional engineer in the State of Massachusetts, is a member of the American Chemical Society, American Physical Society, American Society of Mechanical Engineers, American Society for Engineering Education, Institute of Aeronautical Sciences, Sigma Xi, and Pi Tau Sigma, and a Fellow of the American Academy of Arts and Sciences.

John D. Kraus (A'32-M'43-SM'43-F'54), for a photograph and biography, please see page 369 of the January, 1958 issue of PROCEEDINGS.

H. E. J. Neugebauer was born on May 8, 1905 in Berlin, Germany. He studied mathematics and physics at the University of Berlin from 1924 to 1929.



H. NEUGEBAUER

In 1935, he received the Doctor's degree from the Technische Hochschule of Dresden with a dissertation on multicolor printing. Until 1951 he worked on various research and development projects, most of which were connected with optics or colorimetry.

Dr. Neugebauer came to Montreal Can., in 1951 and applied his experience in the field of visible light to the study of microwave optics and electromagnetic wave theory. He worked for Eaton Electronics Research Institute of McGill University, Adalia Ltd., and, recently, for RCA Victor in Montreal, as head of the Wave Propagation Section of the Research Laboratories. He is presently a consultant to RCA Victor, among others.

He is a member of the Optical Society of America, and the Technical Association of the Graphic Arts. He has published a number of papers on optics, colorimetry, and electromagnetic wave theory. At the past International Assembly of URSI in Boulder, Colo., he was elected a member of Commission VI.

George L. Turin (M'56) was born in New York, N. Y. on January 27, 1930. He received the S.B. and S.M. degrees from the Massachusetts Institute of Technology, Cambridge, Mass. in 1952



G. L. TURIN

after completing the cooperative course in electrical engineering in conjunction with Philco Corporation. In the summer of 1952 he was an M.I.T. Overseas Fellow at Marconi's Wireless Telegraph Co. in England. From 1952-1956 he worked at M.I.T.'s Lincoln Laboratory, Lexington, Mass., in the field of statistical communication theory, first as a staff member, and later as a research assistant while completing his doctoral studies. During this latter period he was also a consultant to the firm of Edgerton, Germeshausen, and Grier. He received the Sc.D. degree in electrical engineering from M.I.T. in 1956.

Since July, 1956 Dr. Turin has been engaged in communication and radar research studies at Hughes Aircraft Company, Culver City, Calif. He also has taught part-time at the University of Southern California, Los Angeles.

Dr. Turin is a member of Eta Kappa Nu, Tau Beta Pi, and Sigma Xi.

Harold A. Wheeler (A'27-M'28-F'35) was born in St. Paul, Minn., on May 10, 1903. He received the B.S. degree in physics from George Washington University, Washington, D. C., in 1925 and did post-graduate studies in physics at The Johns Hopkins University, Baltimore, Md., until 1928.



H. A. WHEELER

He was employed by the Hazeltine Corp. from 1924 to 1945, advancing to vice-president and chief consulting engineer. Since 1946, he has engaged in independent work as a consulting radio physicist, and since 1947, his principal occupation has been as President of Wheeler Laboratories, Inc. In this capacity, he is directing the Great Neck and Smithtown laboratories, specializing in microwaves and antennas.

His specialization in antennas dates back to "all-wave" antennas for broadcast receivers around 1935, then radar beacon and IFF antennas during World War II, for

which he received the Navy Certificate of Commendation. He has published basic studies of "small" antennas and "large" arrays and has directed recent developments in radar antennas for guiding missiles.

Mr. Wheeler has served IRE in such positions as Director (1934, 1940-1945), chairman of the Standards Committee, and chairman of the Long Island Section. He received the Morris N. Liebman Memorial Prize in 1940 for work on some problems of television. He is a Fellow of the AIEE and Radio Club of America, Associate Member of IEE, and member of Sigma Xi and Tau Beta Pi.

Lowell D. White (M'57) was born in New York, N. Y., on April 18, 1925. He received the A.B. degree in 1949, the M.A. degree in 1951, and the Ph.D. degree in 1956, all in physics from Princeton University, Princeton, N. J. From 1951 to 1953, he was an AEC Predoctoral Fellow and from 1953 to 1955, an instructor.



L. D. WHITE

Since joining the Bell Telephone Laboratories, Inc., Murray Hill, N. J., in 1955, he has worked on noise in traveling-wave tubes, electron beams, and the ammonia maser.

Dr. White is a member of the American Physical Society and Sigma Xi.

Ming S. Wong (S'39-A'42-SM'53) was born in China in 1914. He received the B.S. degree in communication from the University of California, Berkeley, Calif. in 1938 and the M.S. degree in the same field from Iowa State College, Ames, Iowa in 1939.



M. S. WONG

From 1941 to 1958 he was with the Wright Air Development Center, Dayton, Ohio, working on antenna and microwave measurements and later, on propagation. He is now on the staff of the Propagation Laboratory, Air Force Cambridge Research Center, Bedford, Mass.

Mr. Wong is a member of Pi Mu Epsilon, American Physical Society, and Commission II of URSI.



## Scanning the TRANSACTIONS

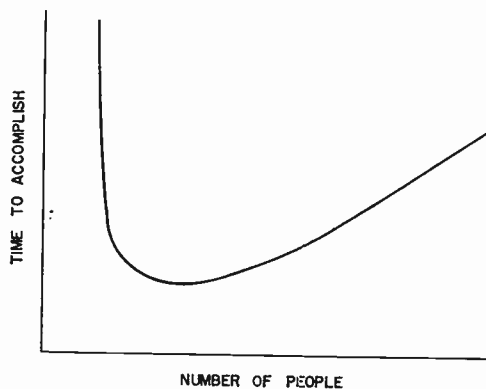
Communications engineering is undergoing a change that is probably as radical as that in any field in radio-electronics. The significance of the changes is attested to by the simultaneous appearance of guest editorials in two different TRANSACTIONS. The change, surprisingly enough, is due largely to developments in another field—digital computers. Although coded transmissions have a long history, the recent advent of high-speed data processing systems is now making it technically feasible to interconnect and coordinate countless complex activities at widely separated locations, using digital transmissions and data handling techniques. So vast are the potentialities that it is predicted that in a relatively few years there will be more communication traffic between digital machines than between humans.

This new field of digital communication is bringing with it totally new problems in communication system design. The major concern of the communications engineer will now be how to transmit digital information as accurately and efficiently as possible. Information theory tells us that low probabilities of error can be achieved either by making the channel capacity much larger than the rate of transmission of information or by increasing the size of the "packages" of information that are encoded for transmission as single units. Unfortunately, the latter alternative increases the complexity of the decoding equipment to a point where it is not presently practicable. Thus we presently can obtain an acceptable probability of error only at the expense of channel capacity. The challenge of the future lies in developing improved techniques and machines which will provide more sophisticated, and at the same time, economically feasible decoding operations. The solution of this key problem will lead to a great saving of channel capacity. Along with improved decoding apparatus will come major improvements in error-detecting and error-deletion coding techniques with a corresponding improvement in accuracy. It is likely that out of this work will come a much closer alliance, if not an actual merger of the fields of information processing and information transmission. (R. M. Fano, "The challenge of digital communication," IRE TRANS. ON INFORMATION THEORY, June, 1958. J. Z. Millar, "Search for accuracy in communications," IRE TRANS. ON COMMUNICATIONS SYSTEMS, June, 1958.)

The specter of engineering shortages, whether real or imaginary, has provoked a great deal of discussion on the training and utilization of technical manpower. One fact which has emerged from all the talk is that, however great the need for engineers may be, the need for engineering supervisors is greater. It is not enough that a supervisor be a competent engineer. He must become proficient in the special procedures and practices necessary to direct the operations of an engineering group, become conversant with and make good use of the lines of communication within his company, and most important of all, develop to the fullest his innate talents for leadership. The need for good supervisors is reflected in the fact that engineering management has come to the fore as a major field of study. Among IRE's 28 Professional Groups, Engineering Management ranks larger than all but three. This widespread interest among engineers reflects, too, the fact that most supervisors come up from the engineering ranks.

To the welter of wails about the manpower shortage, the rebuttal is frequently heard: we need to improve quality more than quantity; or, 50 per cent of what an engineer does could be done by a technician; or, empty-ump per cent of our manpower is wasted in drawing up bids for contracts the company never gets; or, somewhat facetiously, why should we match Russia's output, engineer for engineer—we're not

going to dance with them. One serious facet of the engineering utilization problem that is all too common is represented qualitatively by the curve below, which says in effect that too many cooks can spoil the broth. If we follow the curve from left to right we see that without a certain minimum number of engineers a project cannot be accomplished at all, that as engineers are added, we rapidly arrive at an optimum



number, but that adding still more people will actually make the job longer. The gradual slope of the right end of the curve vs the steep slope of the left suggests that overstaffing is a far more difficult condition to detect than understaffing, and hence apt to be much more common.

Overstaffing usually manifests itself in breaking the job down into too many small pieces. This leads to duplication of effort, poor coordination, and handcuffing the progress of the whole to the speed of the slowest few. Worst of all, the condition is self-perpetuating. As the above curve suggests, an overstaffed organization is likely to miss its project deadlines, and, as a result, add even more personnel to try to make up for it the next time, making matters even worse. Just how serious a situation this is was pointed up by an authority who recently found that if overstaffing is by roughly a factor of three with respect to the optimum number (which appears to be a fairly usual situation) then the time taken to accomplish the job is approximately twice what it would have been with the optimum number. This means that costs are high by a factor of six!

It appears we should take another look at the old grade school problem: "If two men can dig a well in eight hours, how long would it take four men." The answer may be *more* than eight hours because there isn't room in the well for four men. (H. M. Elliott, "The transition from engineer to supervisor," IRE TRANS. ON ENGINEERING MANAGEMENT, June, 1958. R. B. Kershner, "The size of research and engineering teams," *loc. cit.*)

The effects of electric shocks from TV receivers had some light shed on it, at least indirectly, by a recent series of tests on dogs. The dog was selected for the experiments because its response to electric shock is similar to that of man. Dogs were subjected to discharges from capacitors ranging in size from 250 to 3000  $\mu\text{f}$ , charged to voltages of 1 to 40 kilovolts. None of the discharges produced cardiac arrest, ventricular fibrillation, or any other detectable untoward effect. While it is impossible to predict accurately the human response to similar shocks, it seems probable that the same conclusion applies to adult men. (W. B. Konwenhoven and W. R. Milnor, "The effects of high-voltage, low-capacitance electrical discharges in the dog," IRE TRANS. ON MEDICAL ELECTRONICS, July, 1958.)

In these days of frequency spectrum congestion, there is considerable interest in any new method of compressing the time or frequency band needed to transmit information. A new system, called Ticoss, has been developed which provides a unique approach to multichannel operation. Ticoss stands for Time-Compressed Single-Sideband System. In a typical application ten two-way stations can operate over a single SSB channel by time-sharing multiplex. The multiplexing is accomplished by dividing each half-second into ten time slots. Stations are assigned a given time slot to transmit or receive and then are shut off during the rest of each half-second period to give other stations on other channels their turn. The heart of the system is the time-compression feature. Information to be transmitted is first stored during each preceding half-second and then read out and transmitted at high speed during the assigned time slot. At the receiving end, the compressed message is stored and then read out at its original slower speed, resulting in a continuous message at the receiver output. This novel system is particularly well suited to mobile operations. (M. I. Jacob and J. Mattern, "Time-compressed single-sideband system (Ticoss)," IRE TRANS. ON COMMUNICATIONS SYSTEMS, June, 1958.)

Medical applications of electronic instrumentation and control techniques offer a fertile field of development as broad as medicine itself. An interesting cross section of recent progress in the application of these techniques to studies of the brain, heart, muscles, and blood is presented in the July issue of the IRE TRANSACTIONS ON MEDICAL ELECTRONICS. The issue shows electronics in the following varied roles: detection of minute electrical responses of the brain to specific stimuli in the presence of high background noise by means of sampling, storage and averaging techniques; measurement of

oxygen saturation of blood within the body; artificial respiration; measurement of the electrical activity of muscles; heart beat simulator for demonstrating electrocardiographic equipment; and a heart rate counter that gives a direct reading in beats per minute.

Nonlinear systems, in a sense, are several dimensions removed from linear systems and they become more difficult to design and to understand. The nature of the input signals and the mode of operation affect system performance in a manner that is not easily predicted with direct mathematical analyses. However, nonlinearities are always present in control systems whether intentional or not, and efforts to provide a better understanding of nonlinear system operation have been made since the origin of automatic control.

In future control systems the effects of nonlinearities will become more important, and the solution of the associated problems will be of increasing interest. To assess some of the progress that has been attained in this field and to define some of the obstacles that prevent more rapid advances, the PGAC sponsored a Symposium on Nonlinear Control in San Francisco at the Mark Hopkins Hotel on August 19, 1957. The Symposium was divided into two parts: the morning session devoted to "Practical Applications in Nonlinear Control," consisting of three invited papers, and the afternoon session, a panel discussion on the "Obstacles to Progress in Nonlinear Control."

The symposium aroused considerable interest in the papers and the panel discussions and, fortunately, all of the recorded panel discussions and the papers for the morning sessions were procured. They are now available in a special TRANSACTIONS of the Professional Group on Automatic Control issued in June.

## Books

### Mass Spectroscopy by H. E. Duckworth

Published (1958) by Cambridge University Press, 32 E. 57 St., N. Y. 22, N. Y. 175 pages+17 bibliography pages+7 appendix pages+6 index pages+xii pages, 41 figures, 8½×5½, \$6.50.

Professor Duckworth's monograph covers the mass spectroscopy field from the viewpoint of a physicist, but in an apparent effort to keep it brief he has neglected some areas and has repeated what has been said in other books on the subject. As the author's preface says, the monograph is concerned with the operation and application of mass spectroscopy and mere mention is made of chemical reaction rates and mechanisms while electronic or high vacuum techniques are not included at all. The book has an excellent chapter on the role of mass spectroscopy in nuclear physics research.

Physicists in today's environment should have such a handy, up-to-date reference to mass spectroscopy, but the electronics engineers or chemists might do better to find books more closely akin to their needs.

The most outstanding merit of the book lies in its up-to-date bibliography and its treatment of atomic masses and nuclear physics. The most serious deficiency lies in the fact that it has not said much that has

not been said in other books on the subject. In fact Barnard's book (1953) has covered the same topics and included information useful to a much wider spectrum of technical people.

On the whole the book is very interesting and worthwhile and would make good reading for all scientific people. The book is certainly the most recent one published and if one required a general reference book on mass spectroscopy this book would adequately fill that need.

HAROLD C. MATTRAW  
General Electric Co.  
Knolls Atomic Power Lab.  
Schenectady, N. Y.

### Introduction to Electromagnetic Engineering by R. F. Harrington

Published (1958) by McGraw-Hill Book Co., Inc., 330 W. 42 St., N. Y. 36, N. Y. 291 pages+12 appendix pages+1 bibliography page+6 index pages+xii pages, 11 illus. 9¼×6¼, \$8.00.

Professor Harrington has written a very attractive book. It contains a thorough and well-organized introduction to electric and magnetic field problems, with the emphasis on the static case. He has directed it towards engineering students at the junior, senior,

and first-year graduate levels. Calculus and some circuit theory are presupposed.

Unlike most books on electromagnetic theory, this one makes use of the experimental results of circuit theory as a starting point for the field theory. In this way, continuity with the student's previous work is emphasized. Thus Kirchhoff's voltage law is generalized to include the induced voltage due to changing magnetic flux, while the current law is generalized by adding a term in the rate of change of charge accumulated at a junction. These two relations lead to Maxwell's equations quite conveniently. In the earlier part of the book, it seems that this approach to some extent sacrifices physical insight in favor of mathematical convenience. However, in the later applications of Maxwell's equations to static problems, the missing relations show up, and so do the physical meanings.

Vector analysis is adroitly introduced in the second chapter, and is used fully throughout the rest of the book. In the third chapter, electric field intensity is introduced as a quantity whose line integral equals voltage. In a similar emphasis on the circuit viewpoint, magnetic flux density is defined as a vector field having a surface integral related

to the induction of voltage in a loop. In the fourth chapter,  $D$  is introduced as vector field having divergence equal to charge, while  $H$  is essentially defined by the Maxwell-Ampere equation. The possibility that  $B$  and  $H$ ,  $E$  and  $D$  might be related in some way is explored by reference to ideal inductors and capacitors. In Chapter Five, electrostatics is treated as a special case of Maxwell's equations. The fields resulting from point charges, line charges, and dipoles are considered, as is reciprocity, and Gauss's law. In Chapter Six the field of steady electric currents is considered. Starting with the magnetic vector potential, the Biot-Savart law is derived. The fields of various one and two-dimensional current distributions are considered, including loops, quadrupoles, and solenoids. In Chapter Seven, the specification of a vector function in terms of flow and vortex sources is used to introduce the ideas of electric and magnetic polarization. Use is made of the concept of magnetic charge and magnetic current in stressing the duality between electric and magnetic field problems. In Chapter Eight consideration is given to boundary problems. Among the examples given are concentric spheres with two conducting media, a current-carrying wire in a magnetic sheath, images for a pair of conducting spheres, and a disk of constant potential in a plane of zero potential. Again, emphasis is placed on the duality of electric and magnetic problems. In Chapter Nine circuit elements are considered, including resistive, capacitive, and inductive systems. The coefficients of potential, capacitance, electrostatic induction, resistance, and conductance are clearly treated, together with methods of finding the values of circuit elements. Methods for finding upper and lower limits of approximation are included. Finally, in Chapter Ten, the electromagnetic field is dealt with. Starting with Maxwell's equations for a nonconducting medium, the wave equation is derived. The properties of plane wave solutions and of standing waves are then found. The idea of generalized current is used to generalize Maxwell's equations to conducting media. Poynting's theorem is followed by discussion of the electromagnetic potentials, and radiation. A short section on waveguides and resonant cavities closes the book.

A dominant feature of the text is the quality of the writing. Ideas are clearly stated, and care is evident in the continuity from paragraph to paragraph, chapter to chapter. Problems and review questions are included. All in all, it is a good book, and should be teachable as well.

L. A. MANNING  
Stanford University  
Stanford, Calif.

#### Transients in Electrical Circuits by G. V. Lago and D. L. Waidelich

Published (1958) by The Ronald Press Co., 15 E. 26 St., N. Y. 10, N. Y. 382 pages+7 appendix pages+3 index pages+vii pages. Illus. 9½×6¼. \$7.50.

This book is intended as a textbook for the electrical engineering student in his junior or senior year. The only mathematical background required is a standard course in differential and integral calculus. A first course in electrical circuit theory covering

Thevenin's and Norton's theorem is assumed. The growing emphasis on pulse type of circuitry and the solution of the associated transient problems by means of the Laplace transform is reflected in this book. In the first chapter trivial problems involving constant current or constant voltage sources feeding single circuit elements are presented to develop the concept of duality between currents in one form of circuit and voltages in its complement. This duality concept is continued more or less throughout the entire book. In the second chapter, complex circuits having one storage element are solved for their transient behavior by classical means using the separation of variables. In the third and fourth chapter, a simple treatment of second-order differential equations and hyperbolic function is presented with some applications to circuits having two storage elements. With the first third of the book as a background, the Laplace transform method is presented in Chapter 5 without proofs. The lack of mathematical rigor to prove the validity of the Laplace transform method in a book of this type is entirely proper. The average undergraduate student needs this method as a tool early in his training and can study the mathematical proofs in a later mathematics course. A short illustrative Laplace transform table is given in this chapter with a more complete table in the appendix. Simple problems are solved in Chapter 5 by the Laplace transform method and the results compared with the differential equation solutions of Chapters 3 and 4. Factoring of higher degree polynomials is discussed in Chapter 6 and treatment of more complicated inductive circuits having mutual inductance between coils is explained in Chapter 7 using the factoring methods of Chapter 6. Chapter 8 deals with transients in circuits having ac rather than dc sources while Chapter 9 considers sources having other than sinusoidal waveforms. Chapters 10 and 11 deal with steady-state responses to sinusoidal and nonsinusoidal waves, respectively. Chapters 12 and 13 deal with mechanical systems and servomechanisms. The remaining three chapters, comprising 10 per cent of the book, deal with the Fourier series, the Fourier integral, and some applications of each.

This appears to be an excellent undergraduate textbook. It is well written, with many interesting and practical problems as examples and exercises. Its organization is such that the graduate engineer not versed in the Laplace transform method could easily use this book as a self-study guide although the lack of problem solutions might be a handicap. It is certainly a good book for an organized course on transients and even students in their junior year should find it easy reading.

G. B. HERZOG  
RCA Labs.  
Princeton, N. J.

#### Modern Computing Methods

Published (1958) by Philosophical Library, Inc., 15 E. 40 St., N. Y. 16, N. Y. 103 pages+11 bibliography pages+14 appendix pages+vi pages. Illus. 9½×6. \$8.75.

This small but rather high-priced book has been developed from a series of lectures

delivered by staff members of the Mathematics Division of the British National Physical Laboratory to representatives of industrial firms. The course of lectures was organized by the Electrical Engineering Department of the Imperial College of Science and Technology.

A condensed guide is presented for numerical methods which are useful in problem-solving, both methods intended for the hand computer using a desk machine, and methods applicable to the solution of problems by high-speed digital computing equipment.

The first four chapters are concerned with the solution of algebraic problems, while Chapters 5 through 9 discuss methods derived from analysis. Relaxation methods are described in Chapter 10, Chapter 11 discusses the problems arising in the construction of mathematical tables, and the final chapter illustrates the need for using a variety of techniques in the course of solving a given problem.

Three appendixes offer an extensive bibliography, an example of the use of a high-speed digital machine in the solution of a set of nonlinear simultaneous differential equations, and an account of the principles and manner of working of a mechanical differential analyzer.

In view of the large and growing importance of machine computation, the present little volume is most welcome as an introduction and guide to the field. The anonymous authors are to be congratulated on the scope of the ideas they have set down so succinctly.

L. N. RIDENOUR  
Missile Systems Div.  
Lockheed Aircraft Corp.  
Sunnyvale, Calif.

#### Einführung in die Mikrowellen-Elektronik Teil II: Lauffeldröhren by Werner Kleen and Klaus Pöschl

Published (1958) by S. Hirzel Verlag, Stuttgart, N., Birkenwaldstrasse 185, Germany. 171 pages+16 appendix pages+5 index pages+ix pages. Illus. 9½×6¼. DM 28.

This textbook on traveling-wave tubes is the second volume of a series on "Introduction to Microwave Technique." Since the first volume ("Fundamentals") is not available in this country, some of the derivations referred to in the present text must be taken on faith.

However, this is no serious defect because the literature is extensively quoted and equations related to amplification, bandwidth, maximum power output, and other pertinent tube characteristics are generally derived in this text, either in the form given by the originators or modified by the authors who are active contributors to the art.

Both authors are professors at the Munich Institute of Technology and consultants for the Siemens & Halske A. G., one of the largest West German firms in the electrical and machine industry.

The book is very thorough and, in spite of its relatively short length, conveys a good understanding of all important features.

The major part is devoted to the normal forward wave tubes and treats linear theory, noise, nonlinearities, and practical designs. Separate chapters are devoted to backward wave amplifiers and oscillators,

# Abstracts of IRE TRANSACTIONS

The following issues of TRANSACTIONS have recently been published, and are now available from the Institute of Radio Engineers, Inc., 1 East 79th Street, New York 21, N. Y. at the following prices. The contents of each issue and, where available, abstracts of technical papers are given below.

Sponsoring Group	Publication	Group Members	IRE Members	Non-Members*
Automatic Controls	PGAC-5	\$0.85	\$1.25	\$2.55
Broadcast Transmission Systems	PGBTS-10	0.70	1.05	2.10
Communications Systems Engineering	Vol. CS-6, No. 1	0.85	1.30	2.55
Management	Vol. EM-5, No. 2	0.70	1.05	2.10
Information Theory	Vol. IT-4, No. 2	1.10	1.65	3.30
Medical Electronics	PGME-11	0.90	1.35	2.70

\* Public libraries and colleges may purchase copies at IRE Member rates.

## Automatic Control

PGAC-5, JUNE, 1958

Special Symposium Issue, The Editor (p. 41)

The Issue in Brief (p. 42)

Part I: Practical Applications in Nonlinear Control

The Design and Performance of a Model, Second-Order, Nonlinear Servomechanism—R. E. Kuba and L. F. Kazda (p. 43)

This paper discusses the design and performance characteristics of a model, second-order, nonlinear servomechanism. The design procedure stems from principles laid down in the authors' previous paper, in which the nonlinear differential equation characterizing this servo was synthesized. The physical aspects of the various building blocks needed for nonlinear servo construction are considered. Schemes for generating nonlinear functions are described, along with methods for accomplishing the multiplication and differentiation of the control system's variables. Schematic diagrams of the nonlinear servo are presented, in addition to instructions for adjusting the parameters to obtain the proper response behavior. The results of a comparison of equivalent nonlinear and linear servo operation are given in the form of photographs illustrating the control system's error response for various magnitudes of step inputs of position. The nonlinear system's error response is shown to be superior to the linear system's error response in that the nonlinear response exhibits no overshoot and reduces the system error to zero in approximately the time required for the linear system's error response to pass through zero for the first time. The response time of the nonlinear, model servo corresponds closely to the predicted response time.

The Practical Realization of Final-Value Systems with Limiting Constraints—R. C. Booton, Jr. and A. Rosenbloom (p. 49)

In certain applications, the desired function of a control system is to control some variable accurately only at one instant of time. Examples of this can be found in homing missile guidance systems or aircraft landing systems. In the latter case, it is desired to have the vertical component of velocity be small at the instant of touchdown. Complicating features of such systems are the constraints imposed by

physical limitations, such as the limited vertical acceleration capability of airplanes, and the noise or inaccuracy of measurements of the controlled variable. The optimum configuration for such systems has been derived, and this form can be used as the basis for the design of actual systems. The theoretical derivation of the optimum system idealized the actual situation, and a number of problems must be considered when the physical system is designed. Such problems as the closed-loop realization, the number of measurements of the system response, and the manner in which these measurements are utilized are discussed in this paper.

Combined Hysteresis and Nonlinear Gains in Complex Control Systems—R. V. Halstenberg (p. 51)

The types and sources of hysteresis commonly found in mechanical systems, and some of the effects thereof, are discussed.

The describing function technique as specifically applied to studying hysteresis-caused limit cycles is outlined.

The use of an analog computer for studying hysteresis in servosystems is reviewed.

Techniques are presented for determining active and passive compensation to eliminate or reduce hysteresis limit cycles.

Finally, a method is given for analyzing hysteresis plus a single-valued nonlinearity when they occur together or apart in a single or multiloop control system. By this method it is possible to synthesize a nonlinear gain characteristic which eliminates or reduces a hysteresis limit cycle. The validity of the method is demonstrated by comparison with analog computer results.

Part II: Obstacles to Progress in Nonlinear Control

Introduction—Harold Chestnut (p. 59)

Availability of Necessary Theory for the Analysis and Design of Nonlinear Systems—O. J. M. Smith (p. 60)

Nonlinearities in Machine Tools and Missiles—John L. Bower (p. 62)

Nonlinearity in Process Systems—Ernest G. Holzmann (p. 63)

The Role of Computers in Analysis and Design of Control Systems—George P. West (p. 65)

Problems of Nonlinearity in Adaptive or Self-Optimizing Systems—Charles F. Taylor (p. 66)

Open Panel Discussion (p. 67)

Closing Remarks (p. 70)

Committee for the 1957 PGAC Symposium on Nonlinear Control (p. 73)

Book Review (p. 74)

PGAC News (p. 75)

## Broadcast Transmission Systems

PGBTS-10, JUNE, 1958

Announcements (p. 1)

Cochannel Television Interference and its Reduction—E. W. Chapin, L. C. Middlekamp, and W. K. Roberts (p. 3)

The undesired effects of cochannel television interference vary both with the intensity and the frequency of the interfering signal. It is found that there are three types of frequency-variation of objectionability, namely: 1) A progressive decrease of objectionability as the frequency of the undesired signal is shifted away from the carrier frequency of the desired signal, which we have called the Beat Size Effect; 2) superimposed on the Beat Size Effect there is a cyclic variation in objectionability which repeats at intervals corresponding to the horizontal scanning frequency; and 3) superimposed on each of these variations there is a "fine-grain" cyclic variation which repeats at intervals corresponding to the vertical scanning frequency. We have called the cyclic variation 2) and 3) Beat Pattern Effects. Advantage may be taken of the Beat Size Effect and the Beat Pattern Effects to reduce cochannel television interference by appropriate specification of the operating frequencies and frequency tolerances of the desired and undesired stations. It is shown that it is also possible to reduce the objectionable effects of cochannel television interference by the use of certain postdetection devices in the television receiver. Narrow-band video filters, high-pass video filters, and diode clamp video correction circuits have given promising results.

IRE Professional Group on Broadcast Transmission Systems Membership Directory (as of February 28, 1958) (p. 25)

## Communications Systems

VOL. CS-6, NO. 1, JUNE, 1958

Search for Accuracy in Communications (Guest Editorial)—J. Z. Millar (p. 1)

Time-Compressed Single-Sideband System (Ticoss)—M. I. Jacob and J. Mattern (p. 2)

This paper describes a time-compressed single-sideband system (Ticoss), which, by use of time-sharing techniques, avoids many of the problems of a frequency-multiplexed system of the same capacity. Included in the discussion is a description of compressor-expander units for both voice and digital data systems.

Evaluation of IF and Baseband Diversity Combining Receivers—R. T. Adams and B. M. Mindes (p. 8)

Techniques of diversity reception have advanced rapidly with the advent of over-the-horizon communication. Because of the rapidly fluctuating signals encountered in tropospheric scatter propagation, strong-signal selection (switching diversity) has been largely supplanted by more sophisticated signal-combining techniques. Present tropospheric scatter sys-

from a Gaussian random process, a useful general relationship may be found between certain input and output statistics of the set. This relationship equates partial derivatives of the (high-order) output correlation coefficient taken with respect to the input correlation coefficients, to the output correlation coefficient of a new set of nonlinear devices bearing a simple derivative relation to the original set. Application is made to the interesting special cases of conventional crosscorrelation and autocorrelation functions, and Bussgang's theorem is easily proved. As examples, the output autocorrelation functions are simply obtained for a hard limiter, linear detector, clipper and smooth limiter.

**The Effect of Instantaneous Nonlinear Devices on Cross-Correlation**—Roy Leipnik (p. 73)

If  $X_1(t)$ ,  $X_2(t)$  are two noises (stochastic processes),  $f$  and  $g$  are functions describing the action of two instantaneous nonlinear devices, we say that the  $(m, n)$  cross-correlation property holds in case the cross-correlation of  $f(X_1(t_1))$  with  $g(X_2(t_2))$  is proportional to the cross-correlation of  $X_1(t_1)$  with  $X_2(t_2)$ , whenever  $f$  and  $g$  are polynomials of degrees not exceeding  $m$  and  $n$ , respectively. We take  $m = \infty$  or  $n = \infty$  to mean that  $f$  or  $g$  is any continuous function.

The Barrett-Lampard expansion of the second-order joint density of  $X_1(t_1)$  and  $X_2(t_2)$  is used to derive an expression for the cross-correlation of  $f(X_1(t_1))$  and  $g(X_2(t_2))$ . This expression yields necessary and sufficient conditions for the validity of the cross-correlation property in three cases:  $X_1(t)$  and  $X_2(t)$  stationary,  $m, n$  unrestricted;  $X_1(t)$  stationary,  $m, n$  unrestricted;  $X_1(t)$  stationary,  $n = 1$ .

Examples are constructed with the help of special orthonormal polynomials illustrating the necessity and sufficiency of the conditions.

**Some Properties of Nonbinary Error-Correcting Codes**—C. Y. Lee (p. 77)

An error-correcting code may be thought of as a subset  $S_0$  of points belonging to a set  $S$  in which a metric is defined such that the distance between every pair of distinct points of  $S_0$  is larger than some given number. In Hamming's original formulation,  $S$  was taken to be the set of all  $2^n$   $n$ -bit binary numbers and the distance between a pair of binary numbers  $s$  and  $t$  was taken to be the number of bits of  $s$  which do not agree with the corresponding bits of  $t$ . In this note we shall take  $S$  to be the set of all  $n$ -tuples in which each coordinate of an  $n$ -tuple can assume one of  $k$  integral values:  $0, 1, \dots, k-1$ , with  $k \geq 2$ . Properties of these nonbinary codes will be discussed.

**The Effect of Noise Upon a Method of Frequency Measurement**—T. B. Pickard (p. 83)

The effect of noise upon a method of information transmission and recovery is analyzed. The information is coded as the frequency shift of a carrier. The carrier is assumed to be transmitted over two channels which have  $90^\circ$  phase difference. The recovery of the information is accomplished in a new way by measuring the

frequency shift by means of a "coherent cycle counter."

A general expression is obtained for the expected frequency measurement of the coherent cycle counter in terms of the signal and noise autocorrelation functions. The percentage bias of the counter is shown to be a function only of the signal-to-noise ratios in the two channels. In the noise-free case, the expected frequency measurement is given by the centroid of the signal power spectrum. When no signal is present the average indicated frequency is zero, thereby effectively cancelling the average effect of the sources of noise in the system. For applications in which the transmitted frequency fluctuates about the carrier or reference frequency, the method is shown to be superior to both an axis crossing counter and an ideal phase differentiator when it is required to operate through zero frequency difference.

Correspondence (p. 88)

PGIT News (p. 89)

Roster of PGIT Members (p. 91)

## Medical Electronics

PGME-11, JULY, 1958

**A Sensitive System for the Measurement of Brain Responses in the Intact Human**—John F. Davis (p. 29)

An all-electronic method is described whereby minute electrical responses in brain recordings can be measured reliably even in the presence of large noise-to-signal ratios. The signal in this instance is a discrete response to a controlled stimulus. The "noise" is not white noise in this case, but the normal rhythmic activity of the electroencephalogram (EEG) which is randomly related to the signal. The responses are usually invisible in the EEG recording but they can be detected by means of averaging and storing techniques. The system makes use of gated integrators and floating-grid vacuum-tube voltmeters.

Oximetry—W. Paul (p. 34)

Oximetry is the estimation of per cent oxygen saturation of blood by photometric means. Incident light may be reflected from a vascular bed or cuvette and the reflected light measured, or the transmitted light may be measured to yield the required data. Theoretically, transillumination lends itself to absolute measurement with a two-color system, whereas reflection oximetry requires three colors.

The instrumentation described employs two colors along with an alternating light source to allow ac amplification. An analog computer provides a continuous ratio of the corresponding two currents recorded by an ink-writing milliammeter. The over-all response to a step change has a period of less than 0.5 second and is considered rapid enough for clinical dye curve studies. There is reason to believe that the deficient long-term stability of the photocells limits function as an absolute oximeter.

**Further Progress in Electronic Control of Artificial Respiration**—L. H. Montgomery and S. E. Stephenson, Jr. (p. 38)

It is the intention of this paper to cover work on the use of electronic amplifiers in conjunction with other instrumentation as supportive devices in cases of partial or complete muscle failure. It is a continuation of work previously published in these TRANSACTIONS and indicates the trend of further applications of electronic engineering in this field.

**The Effects of High-Voltage, Low-Capacitance Electrical Discharges in the Dog**—W. B. Kouwenhoven and W. R. Milnor (p. 41)

Reported are the results on animals of 520 discharges from capacitors ranging in size from 250 to 3000 micromicrofarads, charged to voltages of 1 to 40 kilovolts. These discharges were sent through the animals at various instants in the heart cycle, and in most cases the current path was from foreleg to hind leg (analogous to the path from hand to foot). The time constant (RC) of the discharges also was varied by inserting resistances in the discharge circuit.

None of these discharges produced ventricular fibrillation, cardiac arrest, or any other untoward effect which could be detected by the methods used. While it is impossible to accurately predict the human response to similar electric shocks, it seems probable that the same conclusion applies to adult man.

**A New Six-Channel Electromyograph for Studies on Muscle**—J. V. Basmajian (p. 45)

To study potentials from several different muscles or parts of the same muscle concurrently so that relative activity could be compared directly, a special apparatus has been developed and tested over the past several years and is reported now for the first time.

This apparatus consists essentially of six identical but entirely separate amplifiers, each fitted with a small cathode-ray tube for monitoring. Together with the control unit, they are mounted on the top of a compact metal cabinet. Situated on the floor of the cabinet is the power supply unit next to a light-proof compartment containing six recording cathode-ray tubes. The traces on these tubes are recorded by a 35-mm linagraph camera affixed to the side of the cabinet. This new instrument has been used extensively and with good results in the author's laboratory for a variety of studies on muscle function.

**An Electronic Heartbeat Simulator and a Cardiac Tachometer**—O. Z. Roy (p. 48)

The procedure for obtaining an artificial heartbeat with the use of multivibrator techniques is described. The chief feature of this design is the use of well-known circuitry to produce: 1) three pulses of variable amplitude and relatively long periods, and 2) variable time delays between the pulses of up to 0.5 second.

Also described is the circuit for a cardiac tachometer with two linear scales, the ranges of which are 0 to 75 and 0 to 180 beats per minute, a response time from zero to full scale (10 seconds), and an accuracy of better than 2 per cent.



# Abstracts and References

Compiled by the Radio Research Organization of the Department of Scientific and Industrial Research, London, England, and Published by Arrangement with that Department and the *Electronic and Radio Engineer*, incorporating *Wireless Engineer*, London, England

NOTE: The Institute of Radio Engineers does not have available copies of the publications mentioned in these pages, nor does it have reprints of the articles abstracted. Correspondence regarding these articles and requests for their procurement should be addressed to the individual publications, not to the IRE.

Acoustics and Audio Frequencies.....	1668
Antennas and Transmission Lines.....	1668
Automatic Computers.....	1669
Circuits and Circuit Elements.....	1669
General Physics.....	1671
Geophysical and Extraterrestrial Phenomena.....	1672
Location and Aids to Navigation.....	1674
Materials and Subsidiary Techniques..	1674
Measurements and Test Gear.....	1677
Other Applications of Radio and Electronics.....	1678
Propagation of Waves.....	1678
Reception.....	1679
Stations and Communication Systems..	1679
Subsidiary Apparatus.....	1680
Television and Phototelegraphy.....	1680
Transmission.....	1681
Tubes and Thermionics.....	1681
Miscellaneous.....	1682

The number in heavy type at the upper left of each Abstract is its Universal Decimal Classification number and is not to be confused with the Decimal Classification used by the United States National Bureau of Standards. The number in heavy type at the top right is the serial number of the Abstract. DC numbers marked with a dagger (†) must be regarded as provisional.

## ACOUSTICS AND AUDIO FREQUENCIES

- 534.1.087:621.395.616 **2275**  
 Absolute Calibration of a Capacitance-Type Vibration Pickup—(*Tech. News Bull. Natl. Bur. Stand.*, vol. 42, pp. 1-3; January, 1958.) See also 332 of 1958 (Koidan).
- 534.143:537.528 **2276**  
 The Electroacoustic Efficiency of a Spark Discharge in Water—N. A. Rol and D. P. Frolov. (*Doklady Akad. Nauk S.S.S.R.*, vol. 118, pp. 683-686; February 1, 1958.)
- 534.232:537.228.1 **2277**  
 Transients in Piezovibrators—P. V. Ponomarev. (*Akust. Zh.*, vol. 3, pp. 243-253; July, 1957.) An investigation of the operation of a radiating quartz plate excited by pulses of arbitrary shape.
- 534.232:537.228.1 **2278**  
 Shift of Resonant Frequencies of a Plane Piezoelectric Radiator with Resistive Load—A. A. Ananeva. (*Akust. Zh.*, vol. 3, pp. 282-285; July, 1957.) Investigation of BaTiO<sub>3</sub> ceramics and other piezoelectric materials showed the considerable influence of a resistive load on measurements of resonance frequencies. Results are presented graphically.
- 534.232-8 **2279**  
 New Technique for Measuring Transducer Blocked Impedance—G. A. Sabin. (*J. Acoust. Soc. Amer.*, vol. 30, pp. 146-150; February, 1958.) A pulse method for measurements on underwater transducers is described and results for a magnetostrictive transducer resonant at 60 kc are given.
- 534.232-8:621.318.134 **2280**  
 Testing Experimental Ferrite Ultrasonic

The Index to the Abstracts and References published in the PROC. IRE from February, 1957 through January, 1958 is published by the PROC. IRE, May, 1958, Part II. It is also published by *Electronic and Radio Engineer*, incorporating *Wireless Engineer*, and included in the March, 1958 issue of that journal. Included with the Index is a selected list of journals scanned for abstracting with publishers' addresses.

Receivers—I. P. Golyamina, A. D. Sokolov, and V. I. Chulkova. (*Akust. Zh.*, vol. 3, pp. 288-290; July, 1957.) The acoustic properties of some Ni-Zn ferrites used in ultrasonic receivers are reported and the frequency response of Ni ferrite and Ni-Zn ferrites are shown graphically.

534.232-8:621.395.623.52 **2281**  
 Theory of Ultrasonic Concentrators—L. G. Merkulov. (*Akust. Zh.*, vol. 3, pp. 230-238; July, 1957.) The properties of conical, exponential, and catenary horns are investigated and their characteristics are calculated. Experiments show that the highest magnification is obtained with the catenary type of horn.

534.241 **2282**  
 Frequency Dependence of Echoes from Bodies of Different Shapes—R. Hickling. (*J. Acoust. Soc. Amer.* vol. 30, pp. 137-139; February, 1958.) It is shown by calculation that the frequency dependence of an echo is different for a prolate spheroid, an infinite cylinder, and a sphere.

534.6:519.272 **2283**  
 Correlation Method of Measurement of Acoustic Relations—S. G. Gershman and E. F. Orlov. (*Akust. Zh.*, vol. 3, pp. 285-288; July, 1957.) Results of experiments carried out in a building of the Acoustical Institute of the U.S.S.R. are shown graphically and a method for the calculation of transmission losses is described. See also 2501 of 1955 (Goff).

534.76:534.78 **2284**  
 Stereophonic Listening and Speech Intelligibility against Voice Babble—I. Pollack and J. M. Pickett. (*J. Acoust. Soc. Amer.*, vol. 30, pp. 131-133; February, 1958.) Experiments with earphones confirm that directional information may improve intelligibility.

534.78 **2285**  
 Masking of Speech by Noise at High Sound Levels—I. Pollack and J. M. Pickett. (*J. Acoust. Soc. Amer.*, vol. 30, pp. 127-130; February, 1958.) Over a wide range of conditions a high level of background noise was found to cause deterioration of speech intelligibility for a constant speech/noise ratio.

534.861 **2286**  
 Experimental Study of Statistical Properties of Musical and Speech Signals in Broadcasting—B. A. Fersman. (*Akust. Zh.*, vol. 3, pp. 274-281; July, 1957.) An experimental installation for the investigation of the distribution function of instantaneous values of four types of signal is examined. Speech signals have been found to follow a Cauchy type of distribution.

621.395.625.3:621.317.42 **2287**  
 The Determination of the Magnetization of Magnetic Recording Tape—Schmidbauer. (See 2505.)

## ANTENNAS AND TRANSMISSION LINES

621.315.212 **2288**  
 Attenuation in Continuously Loaded Coaxial Cables—G. Raisbeck. (*Bell Sys. Tech. J.*, vol. 37, pp. 361-374; March, 1958.) A theoretical study of the attenuation in cables loaded with magnetic material is presented. Three parameters are involved, and when the line has optimum dimensions, two parameters determine the attenuation. Graphical and analytical relations are given in forms which can be applied to practical problems.

621.372.2 **2289**  
 Experimental Check of Formulas for Capacitance of Shielded Balanced-Pair Transmission Line—B. G. King, J. McKenna, and G. Raisbeck. (*PROC. IRE*, vol. 46, pp. 922-923; May, 1958.) See 1646 of 1957 (Gent).

621.372.43 **2290**  
 General Synthesis of Quarter-Wave Impedance Transformers—H. J. Riblet. *IRE TRANS. ON MICROWAVE THEORY AND TECHNIQUES*, vol. MTT-5, pp. 36-43; January, 1957. Abstract, *PROC. IRE*, vol. 45, p. 576; April, 1957.)

621.372.8:537.226 **2291**  
 Losses in Dielectric Image Lines—D. D. King and S. P. Schlesinger. (*IRE TRANS. ON MICROWAVE THEORY AND TECHNIQUES*, vol. MTT-5, pp. 31-35; January, 1957. Abstract, *PROC. IRE*, vol. 45, p. 576; April, 1957.)

621.372.8:621.372.413 **2292**  
 Resonance Properties of Ring Circuits—F. J. Tischer. *IRE TRANS. ON MICROWAVE THEORY AND TECHNIQUES*, vol. MTT-5, pp. 51-56; January, 1957. Abstract, *PROC. IRE*, vol. 45, p. 576; April, 1957.)

621.372.821:621.372.832.6 **2293**  
 Strip-Line Hybrid Junction—H. G. Pascalar. *IRE TRANS. ON MICROWAVE THEORY AND TECHNIQUES*, vol. MTT-5, pp. 23-30; January, 1957. Abstract, *PROC. IRE*, vol. 45, p. 576; April, 1957.)

621.372.825 **2294**  
 Calculation of Parameters of Ridge Waveguides—Tsung-Shan Chen. (*IRE TRANS. ON MICROWAVE THEORY AND TECHNIQUES*, vol. MTT-5, pp. 12-17; January, 1958. Abstract, *PROC. IRE*, vol. 45, p. 575; April, 1957.)

621.372.85+621.315.212:621.318.134 2295  
**Ferrite Components in Microwave Systems**—B. L. Humphreys. (*Electronic Eng.*, vol. 30, pp. 341-345; May, 1958. A review of circuit techniques.

621.396.67:621.397.62:621.317.3 2296  
**Measuring TV Aerial Performance**—F. R. W. Strafford. (*Wireless World*, vol. 64, pp. 67-69; February, 1958, pp. 120-123; March, 1958, and pp. 294-298; June, 1958.) A minimum height of 25 feet and distance/height ratio of 15 are recommended for the test transmitting and receiving antennas; conditions for accurate measurements and the selection of a suitable test site are discussed. The choice of standard antennas and of radiating and detecting equipment is considered, and methods of presenting gain and directional response characteristics are given. Techniques of antenna impedance measurement and effects of feeder mismatching are discussed.

621.396.67.095 2297  
**Use of a Fictitious Magnetic Current for the Solution of the Problem of Radiation of an Aerial over a Surface with the Heterogeneous Boundary Conditions of Leontovich**—O. N. Tereshin. (*Radiotekhnika*, vol. 12, pp. 24-31; April, 1957.) The conditions are defined in terms of a coefficient  $\alpha$ , the ratio of the tangential components of the electric and magnetic fields.

621.396.677.43 2298  
**The Behaviour of Two Concentric Rhombic Aerials**—W. Kronjäger and K. Vogt. (*Nachricht. Z.*, vol. 10, pp. 494-496; October, 1957.) Measurements of coupling factor, matching, and gain of two rhombics, one of which is placed inside the other, show that the influence of the loaded outer antenna on the inner is negligible. The installation discussed is used for reception in a 4:1 range of frequencies, each antenna covering a range of 2:1.

621.396.677.5 2299  
**Super Loop Antenna**—S. Adachi, J. R. McDougal, and Y. Mushiaki. (*Sci. Rep. Res. Inst. Tohoku Univ.*, Ser. B, vol. 9, pp. 1-8; June, 1957.) Measurements of input impedance and directional properties at 120-370 mc are presented for a multi-element antenna consisting of circular loops, positioned concentrically around a supporting pipe of relatively large diameter and connected in parallel at their feed points.

621.396.677.5 2300  
**Theoretical Formulation for Circular Loop Antennas by Integral Equation Method**—S. Adachi and Y. Mushiaki. (*Sci. Rep. Res. Inst. Tohoku Univ.*, Ser. B, vol. 9, pp. 9-18; June, 1957.) An integral equation for the current distributions in a loaded circular loop antenna is solved by the successive approximation method, thus leading to expressions for the transmitting and receiving characteristics of a loaded or short-circuited loop antenna at HF.

621.396.677.71 2301  
**Radiation and Surface Currents from a Slot on an Infinite Conducting Cylinder**—F. H. Northover. (*Canad. J. Phys.*, vol. 36, pp. 206-217; February, 1958.) The saddle-point method of calculating the far field, as used by Papas (2715 of 1949) and others, is not valid for points close to the antenna. The basis for a method which overcomes this defect is described. The ranges of validity of this method and of the Papas procedure are discussed.

621.396.677.73 2302  
**A New Broad-Band Microwave Antenna System**—R. W. Friis and A. S. May. (*Commun. and Electronics*, no. 35, pp. 97-100; March, 1958.) The antenna is an electro-

magnetic horn capped by a sector of a paraboloidal reflector. It is intended for simultaneous operation in the bands 3700-4200 mc, 5925-6425 mc, and 10,700-11,700 mc. Details of gain and directivity are given.

621.396.677.85:629.19 2303  
**Loaded-Lens Antenna tracks Missiles**—L. S. Miller. (*Electronics*, vol. 31, pp. 44-46; March 28, 1958.) An artificial dielectric lens consisting of concentric foam-plastic hemispheres each covered with metal disks is used to provide a circularly polarized feed for a 60-foot paraboloid at 216-245 mc. A waveguide feed allows independent control of  $E$  and  $H$ -plane patterns, and separate horizontal and vertical polarization outputs provide maximum polarization versatility.

#### AUTOMATIC COMPUTERS

681.142 2304  
**Simulation of Nonlinear Field Problems**—I. C. Hutcheon. (*Brit. Commun. Electronics*, vol. 5, pp. 96-99; February, 1958.) Some three-dimensional problems can be solved by using a resistance network in conjunction with a single ac amplifier, a function generator, a scanning switch, and a number of simple analog storage units.

681.142:512.831 2305  
**Matrix Analysis of Logical Networks**—E. J. Schubert. (*Commun. and Electronics*, no. 35, pp. 10-13; March, 1958.) "A novel method of matrix algebra is derived for the analysis of networks representing logical systems too complex for conventional approaches using Boolean algebra. It is shown that truth tables of system blocks may be treated as matrices and that logical operations on such matrices can be performed efficiently."

681.142:517.512.2 2306  
**An Analogue Computer for Fourier Transforms**—D. G. Tucker. (*J. Brit. IRE*, vol. 18, pp. 233-235; April, 1958.)

681.142:621.311.25:621.039 2307  
**Analogue Computers in the Nuclear Power Programme**—J. C. Nutter. (*Instrum. Practice*, vol. 12, pp. 46-51; January, 1958.)

681.142:[621.314.63+621.395.1:537.525.92 2308  
**New Applications of Impedance Networks as Analogue Computers for Electronic Space-Charge and for Semiconductor Diffusion Problems**—G. Čremošnik, A. Frei, and M. J. O. Strutt. (*Proc. IRE*, vol. 46, pp. 868-877; May, 1958.) The general second-order partial differential equation is transformed to the equivalent equation of finite differences and hence relations for analog impedance networks are derived. Resistance chains are applied to the case of one-dimensional high-vacuum diodes yielding results within about 1 per cent of the exact solutions. RC networks are applied to semiconductor diffusion with space and surface recombination, giving some new results for  $p$ - $n$  diodes. A plane resistance network applied to a triode with space charge gives the anode current/gird voltage curve within a few per cent of the published value. See also 1493 of 1958 (Čremošnik and Strutt) and back references.

681.142:621.314.7 2309  
**A Basic Transistor Circuit for the Construction of Digital Computing Systems**—P. L. Clout. (*Proc. IEE*, pt. B, vol. 105, pp. 213-220; May, 1958.) A circuit, comprising one transistor, one capacitor, and three resistors, forms the basis of a complete digital computing system for use where high operation speed is not essential. The construction of well-known computer circuits from the basic circuit is described and a complete logical computing sys-

tem, using 184 circuits, is developed to demonstrate their application.

#### CIRCUITS AND CIRCUIT ELEMENTS

621.3.049.75 2310  
**Printed Wiring**—H. Nagatsu and H. Sakai. (*Rep. Elec. Commun. Lab., Japan*, vol. 5, pp. 18-29; December, 1957.) An assessment and detailed description of processes in the production of photo-etched circuits. The properties of the copper foil used are examined and particular attention is paid to the photographic and enamelling techniques and to dip-soldering.

621.314.22 2311  
**Small Transformers with Low Magnetic Leakage**—A. Lang. (*Elektrotech. Z., Ed. A.*, vol. 79, pp. 10-14; January 1, 1958.) The external field characteristics of various types of laminated and C-core transformers are examined to determine the form of construction with lowest leakage.

621.314.22:621.372.512.2 2312  
**Wide-Band Transformer Characteristics**—A. C. Hudson. (*Electronic and Radio Engr.*, vol. 35, pp. 228-234; June, 1958.) "A parameter  $f_r$  is defined for wide-band transformers, which represents the series resonance of the leakage inductance and the primary and secondary stray capacitances. It is shown that this parameter may be determined from the low-frequency requirements on the transformer, and then used as a guide to the attainable high-frequency response."

621.318.042.1:538.24 2313  
**Terminal Properties of Magnetic Cores**—T. C. Chen and A. Papoulis. (*Proc. IRE*, vol. 46, pp. 839-849; May, 1958.) The terminal properties of the cores can be obtained from their dynamic step response; it is shown that for thick (2 mils or more), thin ( $\frac{1}{2}$  mil), and intermediate-sized cores there is a unique relation between the flux in the core and the applied coulomb-turns. The analysis is verified by experiment.

621.318.44 2314  
**New Techniques for Winding Subminiature Coils**—W. F. Kallensee. (*Electronic Ind.*, vol. 17, pp. 70-71; January, 1958.) Details of a method for winding self-supporting coils of adhesive-coated wire.

621.318.57:621.314.63 2315  
**Solid-State Thyatron switches Kilowatts**—R. P. Frenzel and F. W. Gutzwiller. (*Electronics*, vol. 31, pp. 52-55; March 28, 1958.) The operation of a controlled silicon rectifier and its application in various switching circuits and converters are described.

621.318.57:621.396.96 2316  
**Broad-Band Balanced Duplexers**—C. W. Jones. (*IRE TRANS. ON MICROWAVE THEORY AND TECHNIQUES*, vol. MTT-5, pp. 4-12; January, 1957. Abstract, *Proc. IRE*, vol. 45, p. 575; April, 1957.)

621.319.4 2317  
**Research of Condensers and its Results**—S. Hayashi, K. Kinugawa, K. Kudo, M. Chiba, and S. Sakurai. (*Rep. Elec. Commun. Lab., Japan*, vol. 5, pp. 30-34; December, 1957.) Voltage, temperature, and frequency characteristics are given for a number of types of capacitor, particularly the BaTiO<sub>3</sub> and silvered mica types.

621.319.4.001.4 2318  
**Accelerated Life Testing of Capacitors**—G. J. Levenbach. (*IRE TRANS. ON RELIABILITY AND QUALITY CONTROL*, no. PGRQC-10, pp.

9-20; June, 1958. Abstract, *PROC. IRE*, vol. 45, p. 1166; August, 1957.)

621.319.43 2319

**Precision Variable Capacitors For High-Grade Electronic Equipment**—A. A. Turnbull. (*Brit. Commun. Electronics*, vol. 4, pp. 756-759; December, 1957.) Two types of small variable capacitors are described which were designed to meet stability and accuracy specifications comparable with larger types. One gives a linear frequency variation over 15° of shaft rotation; the other gives a sinusoidal variation of frequency about a mean value as the rotor shaft is turned continuously.

621.372.413 2320

**Excitation of Higher-Order Modes in Spherical Cavities**—R. N. Ghose. (*IRE TRANS. ON MICROWAVE THEORY AND TECHNIQUES*, vol. MTT-5, pp. 18-22; January, 1957. Abstract, *PROC. IRE*, vol. 45, pp. 575-576; April, 1957.)

621.372.44:621.372.6 2321

**Some General Properties of Nonlinear Elements: Part 2—Small-Signal Theory**—H. E. Rowe. (*PROC. IRE*, vol. 46, pp. 850-860; May, 1958.) The analysis of nonlinear capacitor modulators, demodulators, and negative-conductance amplifiers, with only two signal frequencies present, gives results that agree with the general energy relations of Part 1 [2988 of 1956 (Manley and Rowe)]. In addition, the gain, bandwidth, terminal admittances, and sensitivity to changes in terminal admittances or in local-oscillator drive, are given together with their dependence upon the amount of nonlinearity. Generally the bandwidth of these devices approaches zero as the nonlinearity approaches zero.

621.372.44:621.372.632 2322

**General Properties of Frequency-Converting Networks**—S. Duinker. (*Philips Res. Rep.*, vol. 13, pp. 37-78; February, 1958, and pp. 101-148; April, 1958.) A generalized analysis of frequency-converting systems consisting of networks containing nonlinear inductors, capacitors, and resistors, and including also nonlinear  $L$ ,  $C$ , and  $R$  coupling elements. The mesh and nodal equations for a general nonlinear network are given, and it is assumed that a certain high-voltage and current distribution (the so-called fundamental state) results from the presence of (carrier) current and voltage sources. First-order perturbational equations are then derived corresponding to the disturbance of the fundamental state by small (signal) voltage or current sources. Linear differential equations with time-dependent coefficients are obtained, which yield, for a periodic fundamental state, equations in matrix form. Methods of simplifying the matrices are shown, and the method is used to examine stability, conversion gain, and loss. As an example, a polyphase magnetic modulator is analyzed.

621.372.5 2323

**Parallel Four-Terminal Networks**—F. E. Rogers. (*Electronic and Radio Engr.*, vol. 35, pp. 207-211; June, 1958.) A simple relation exists between the output/input voltage ratio for any number of four-terminal networks in parallel and their parameters of output admittance and short-circuit transfer admittance. The relation enables the voltage ratio to be stated without solving the networks.

621.372.512.3:621.374.4 2324

**A Wide-Band Multiplier Unit**—G. T. Sason. (*R.S.G.B. Bull.*, vol. 33, pp. 360-362; February, 1958.) Capacitive coupling leads to easily adjustable wide-band couplers. A practical design of a wide-band frequency-multiplier

unit incorporating these and covering all bands from 3.5 to 28 mc is given.

621.372.54:621.372.412 2325

**Ceramic I. F. Filters match Transistors**—D. Elders and E. Gikow. (*Electronics*, vol. 31, pp. 59-61; April 25, 1958.) BaTiO<sub>3</sub> resonant filters can replace IF transformers with improvement in size, cost, ruggedness, and insertion loss. Their input and output impedances are compatible with those of transistors.

621.372.543 2326

**Transient Phenomena in Band Filters**—A. Sabbatini. (*Note Recensioni Notiz.*, vol. 6, pp. 625-638; September/October, 1957.) Analysis of a filter consisting of two coupled circuits.

621.373.4 2327

**Simultaneous Asynchronous Oscillations in Class-C Oscillators**—M. I. Disman and W. A. Edson. (*PROC. IRE*, vol. 46, pp. 895-903; May, 1958.) It is shown, theoretically and practically, that self-starting asynchronous oscillations are possible in a class-C pentode oscillator. Transient and steady-state solutions are obtained for such an oscillator with one and two degrees of freedom.

621.373.42.029.64:621.3.018.41(083.74) 2328

**S.H.F. Frequency Standard uses Double Conversion**—Thompson, Vetter, and Waters. (See 2488.)

621.373.421.11 2329

**Simultaneous Oscillations at Two Frequencies in a Self-Oscillatory System with Automatic Bias**—G. M. Utkin. (*Radiotekhnika, Mosk.*, vol. 12, pp. 64-66; April, 1957.) An investigation of the self-biasing by grid current in an oscillator confirms that oscillations at two different frequencies may occur. See also 1362 of 1958.

621.373.421.14:621.3.018.41(083.74) 2330

**An Atomic Reference Oscillator**—Capelli. (See 2489.)

621.373.421.14.029.6 2331

**Frequency Stabilization of a Microwave Oscillator with an External Cavity**—I. Goldstein. (*IRE TRANS. ON MICROWAVE THEORY AND TECHNIQUES*, vol. MTT-5, pp. 57-62; January, 1957. Abstract, *PROC. IRE*, vol. 45, p. 576; April, 1957.)

621.373.431.1.018.756 2332

**Multivibrator Circuit for Millimicrosecond Pulses**—W. Gruhle. (*Elektronik*, vol. 6, pp. 261-263; September, 1957) Pulse rise times of about 20  $\mu$ sec and a repetition frequency of several mc can be achieved with the tube circuit described. Pulse width can be adjusted continuously without affecting the rise time.

621.373.44 2333

**Precision Pulse Generator**—H. L. Miller. (*IRE TRANS. ON NUCLEAR SCIENCE*, vol. NS-3, pp. 18-21; June, 1956. Abstract, *PROC. IRE*, vol. 44, p. 1084; August, 1956.)

621.374.32:621.314.7 2334

**Dekatrons and Electromechanical Registers Operated by Transistors**—G. B. B. Chaplin and R. Williamson. (*Proc. IEE*, pt B, vol. 105, pp. 231-236; May, 1958. Discussion, pp. 266-272.) Transistor circuits are described for driving cold-cathode decade tubes and electromechanical counters. In both cases the transistor circuit combines the waveform-shaping properties of the thermionic valve with the economy of power achieved with the cold-cathode valve. High reliability of performance is also attained.

621.374.4:621.318.4:621.397.6 2335

**Magnetic-Core Dividers for ITV Sync**

**Generators**—A. Rose. (*Electronics*, vol. 31, pp. 76-77; April 11, 1958.) An accurate and stable digital divider can be made with a pair of magnetic cores having rectangular hysteresis loops. Division by factors up to 17 has been obtained in a single stage in the frequency range 10-50 kc.

621.375.1 2336

**On the Problem of Synthesis of Amplifier Circuits**—S. V. Samsonenko. (*Radiotekhnika, Mosk.*, vol. 12, pp. 45-57; April, 1957.) A new mathematical method is described for the analysis of transients in amplifiers and a means of synthesis is suggested for multistage systems considering different types of distortion.

621.375.13+621-52 2337

**Design of Conditionally Stable Feedback Systems**—J. Ôizumi and M. Kimura. (*Sci. Rep. Res. Inst. Tohoku Univ., Ser. B*, vol. 9, pp. 19-38; June, 1957.) Conditionally stable systems are shown to have a greater feedback than that obtainable from unconditionally stable feedback circuits. The design of such systems is analyzed mathematically and a practical method for automatically preventing oscillation occurring in them is suggested. Experimental results obtained with a suitable circuit are presented.

621.375.3 2338

**Some Aspects of Half-Wave Magnetic Amplifiers**—G. M. Ettinger. (*Proc. IEE*, pt B, vol. 105, pp. 237-248; May, 1958. Discussion, pp. 266-272.) The performance of half-wave magnetic amplifiers is analyzed and a theory presented which allows for a finite control-circuit resistance, or rectifier reverse conductance, and imperfect core properties. Experimental results obtained with amplifiers using different cores show good agreement with theory. Various methods of bias are reviewed and a conductance-controlled amplifier is described.

621.375.3 2339

**A Fast-Response Full-Wave Magnetic Amplifier**—G. E. Lynn. (*Commun. and Electronics*, no. 35, pp. 37-41; March, 1958.)

621.375.3 2340

**The Effective Feedback Factor of Self-Balancing Magnetic Amplifiers**—W. A. Geyger. (*Commun. and Electronics*, no. 35, pp. 66-69; March, 1958.)

621.375.4.011.21 2341

**Three Output Imittance Theorems**—H. Stockman. (*Electronic Ind.*, vol. 17, pp. 61-63, 156; January, 1958.) A discussion of various theorems having practical application in the analysis of transistor circuits.

621.375.4.018.783 2342

**Nonlinear Distortion in Transistor Amplifiers**—G. Meyer-Brötz and K. Felle. (*Elektron Rundschau*, vol. 11, pp. 297-301; October, 1957.) Following an analysis of the causes of distortion in common-emitter circuits, the distortion factor is derived from the static characteristics. The dependence of distortion on temperature, collector bias, input signal level, and load resistance is determined, and calculated values are compared with results of measurements.

621.375.4.024 2343

**Some Transistor Input Stages for High-Gain D.C. Amplifiers**—G. B. B. Chaplin and A. R. Owens. (*Proc. IEE*, pt B, vol. 105, pp. 249-257; May, 1958. Discussion, pp. 266-272.) Several types of input stage are investigated and methods of reducing drift are suggested. It is shown that drift of operating point in transistor dc amplifiers depends on the type of

circuit; the lowest drift being obtained using the transistor as a chopper.

- 621.375.4.024 2344  
**A Transistor High-Gain Chopper-Type D.C. Amplifier**—G. B. B. Chaplin and A. R. Owens. (*Proc. IEE*, pt B, vol. 105, pp. 258-266; May, 1958. Discussion, pp. 266-272.) A modulated system is employed consisting of a transistor input chopper; a high-gain transistor ac amplifier and an output chopper. The system has an open loop gain of 500  $v/\mu a$  with a band extending from direct current to 25 cps. Peak output is  $\pm 10$  volts and current drift referred to input is  $4 \times 10^{-9} a$  in the range 20°C-50°C. The voltage drift at the input is less than 100  $\mu a$ .
- 621.375.4.029.3 2345  
**Designing Transistor A.F. Power Amplifiers**—M. B. Herscher. (*Electronics*, vol. 31, pp. 96-99; April 11, 1958.) The amplifier described delivers 45 w to a 4- $\Omega$  load. It contains a driver stage, a phase splitter using a transistor pair, and a push-pull output-stage.
- 621.375.9:538.569.4.029.6 2346  
**Operation of a Solid-State Quantum-Mechanical Amplifier**—M. W. P. Strandberg, C. F. Davis, B. W. Faughnan, R. L. Kyhl, and G. J. Woiga. (*Phys. Rev.*, vol. 109, pp. 1988-1989; March 15, 1958.) "The operation of an S-band solid state quantum-mechanical amplifier operated at 4.2°K with a computed noise temperature of less than 4.5°K is compared with similar devices and is used as proof of the condition of discrete phonon saturation which has been previously postulated." See also 1691 of 1958 (McWhorter and Meyer).
- 621.375.9:538.569.4.029.6 2347  
**The Solid-State Maser—a Supercooled Amplifier**—J. W. Meyer. (*Electronics*, vol. 31, pp. 66-71; April 25, 1958.) A review of maser techniques with descriptions of two-level molecular-beam and three-level solid-state devices. Amplifier and oscillator characteristics, noise measurements, and future developments are discussed.
- 621.375.9:538.569.4.029.6 2348  
**A U.H.F. Solid-State Maser**—R. H. Kingston. (*Proc. IRE*, vol. 46, p. 916; May, 1958.) Maser action at a frequency of 300 mc has been obtained by using a cavity mode at the pumping frequency and a lumped resonant circuit at the amplifying frequency.
- 621.375.9:538.569.4.029.6 2349  
**Design Considerations for Circulator Maser Systems**—F. R. Arams and G. Krayer. (*Proc. IRE*, vol. 46, pp. 912-913; May, 1958.) A general expression for effective maser system noise temperature is calculated and a working approximation is derived. The noise and stability requirements for a low-noise circulator maser system are given in terms of maser gain and of dissipative losses and SWR in various parts of the system.
- 621.375.9:538.569.4.029.6:621.396.822 2350  
**System-Noise Measurement of a Solid-State Maser**—A. L. McWhorter and F. R. Arams. (*Proc. IRE*, vol. 46, pp. 913-914; May, 1958.) A complete amplifier system with an effective input noise temperature of  $20 \pm 5^\circ K$  is described. The sources of noise are analyzed and it is shown that the noise temperature of the maser proper is close to the theoretical value.
- 621.375.9:538.569.4.029.64 2351  
**Electron Spin and Phonon Equilibrium in Masers**—Bloembergen. (See 2385.)
- 621.375.9:621.372.2 2352  
**A Travelling-Wave Parametric Amplifier**—

A. L. Cullen. (*Nature, London*, vol. 181, p. 332; February 1, 1958.) A lossless transmission line with periodically varying distributed inductance and a constant distributed capacitance will support a growing current wave. For maximum amplification the oscillator used for providing the periodic variation of inductance must be synchronized with the incoming signal. The noise figure of such an amplifier should be very favorable. An experimental investigation is in progress, and related schemes are being studied in which precise frequency and phase relations are not demanded.

621.375.9.029.6:537.311.33 2353  
**Proposed Negative-Mass Microwave Amplifier**—H. Krömer. (*Phys. Rev.*, vol. 109, p. 1856; March 1, 1958.) It is pointed out that negative masses occur in semiconductors at energies close to the band edge if the energy contours are re-entrant there. It is suggested that such a semiconductor might be used as the active element in a microwave amplifier, although preliminary experiments with germanium did not show the effect. See also 2901 of 1954 (Shockley and Mason).

#### GENERAL PHYSICS

533.6.011 2354  
**On Chandrasekhar's Theory of Turbulence**—P. C. Jain. (*Proc. Nat. Inst. Sci. India*, pt A, vol. 23, pp. 504-513; November 26, 1957.) The theory (*Proc. Roy. Soc. A*, vol. 229, pp. 1-19; April 5, 1955.) has been generalized to the case of axisymmetric turbulence, and eight differential equations in eight defining scalars of double and triple correlation tensors deduced. Two of these equations replace that of de Kármán and Howarth (*Proc. Roy. Soc. A*, vol. 164, pp. 192-215; January 21, 1938) in the theory of isotropic turbulence.

533.6.011 2355  
**On Decay of Energy Spectrum of Isotropic Turbulence**—N. R. Sen. (*Proc. Nat. Inst. Sci. India*, pt A, vol. 23, pp. 530-533; November 26, 1957.)

535.215:537.224 2356  
**Electric Field Distribution in Polarized Photoconductors**—H. Kallmann and J. R. Freeman. (*Phys. Rev.*, vol. 109, pp. 1506-1508; March 1, 1958.) The distribution is determined from changes which occur in the persistent polarization [see 2633 of 1955 (Kallmann and Rosenberg)] under various polarizing conditions.

537.12:537.311.1 2357  
**The Fundamental State of an Electron Gas**—H. Koppe. (*Z. Physik*, vol. 148, pp. 135-155; April 3, 1957.) Detailed discussion with reference to Mayer's treatment of electron correlation energy (*Phys. Rev.*, vol. 100, pp. 1579-1586; December 15, 1955).

537.226 2358  
**Force Densities in Dielectrics**—É. Durand. (*C.R. Acad. Sci., Paris*, vol. 245, pp. 1003-1006; September 16, 1957.)

537.311.1 2359  
**A New Approach to the Theory of Electrical Conductivity of Solids**—B. Meltzer. (*Physica*, vol. 23, pp. 118-124; February, 1957.) Since the electrical conductance of a body is a measure of the fluctuations of charge in a state of thermodynamic equilibrium an analysis of these fluctuations gives the value of the conductivity. The value derived agrees with that of Drude but is found to be half that for the Lorentz-Sommerfeld model.

537.311.1 2360  
**The Boltzmann Equation in the Theory of Electrical Conduction in Metals**—D. A. Greenwood. (*Proc. Phys. Soc. London*, vol. 71, pp.

585-596; April 1, 1958.) The Boltzmann equation for electrical conduction in metals is derived assuming  $\hbar/\tau \ll kT$ , where  $\tau$  is the collision time. An expression independent of this assumption is considered but not evaluated.

537.311.1 2361  
**Theory of Electrical Conductivity of Anisotropic Inhomogeneous Media**—A. Nedoluha. (*Z. Physik*, vol. 148, pp. 248-252; April 13, 1957.)

537.311.31:538.63 2362  
**Quantum Theory of the Electrical Conductivity of Metals in a Magnetic Field**—I. M. Lifshits. (*Zh. Eksp. Teor. Fiz.*, vol. 32, pp. 1509-1518; June, 1957.) The kinetic equation for the density matrix is derived and the asymptotic values of the kinetic coefficients in a strong magnetic field are analyzed.

537.56 2363  
**On the Theory of Spectral-Line Broadening in Plasma**—V. I. Kogan. (*Doklady Akad. Nauk S.S.S.R.*, vol. 118, pp. 907-910; February 11, 1958.)

537.56 2364  
**Structure of Shock Waves in a Plasma**—V. D. Shafranov. (*Zh. Eksp. Teor. Fiz.*, vol. 32, pp. 1453-1459; June, 1957.) Investigation of a shock wave in a plasma taking account of the difference in electron and ion temperatures. Three cases are examined: a) nonstationary shock wave, b) stationary shock wave, and c) stationary shock-wave in a strong magnetic field.

537.56 2365  
**Electrodynamical Acceleration of Plasma Bunches**—L. A. Artsimovich, S. Yu. Luk'yanov, I. M. Podgornyĭ, and S. A. Chuvatin. (*Zh. Eksp. Teor. Fiz.*, vol. 33, pp. 3-8; July, 1957.) A method is described of generating a gas-discharge plasma by the electric explosion of a 0.02 mm-diameter copper wire in a discharge chamber evacuated to  $1-2 \times 10^{-8}$  mm Hg. A 75- $\mu f$  capacitor is used with initial voltage 30 kv.

537.56 2366  
**Quantum Kinetic Equation for Plasma taking Account of Correlation**—Yu. L. Klimontovich and S. V. Temko. (*Zh. Eksp. Teor. Fiz.*, vol. 33, pp. 132-134; July, 1957.) A quantum kinetic equation for a system of particles with coulomb interaction is derived taking into account the correlation of the mutual position of the charged particles.

537.56 2367  
**On the Effective Field in a Plasma**—B. B. Kadomtsev. (*Zh. Eksp. Teor. Fiz.*, vol. 33, pp. 151-157; July, 1957.) Equations for the partial distribution functions are used to compute the effective field acting on charged particles in a plasma. The effective field differs from the mean field by a small quantity of the order of  $1/N$  where  $N$  is the number of particles within a sphere of radius equal to the Debye radius.

537.56:538.56 2368  
**The Dispersion Equation for Plasma Waves**—N. G. Van Kampen. (*Physica*, vol. 23, pp. 641-650; July, 1957.) The validity of different formulas is discussed. When collisions are infrequent no dispersion equation exists except in special cases. See also 2029 of 1956.

537.56:538.569 2369  
**On the Dynamics of a Bounded Plasma in an External Field**—L. M. Kovrizhnykh. (*Zh. Eksp. Teor. Fiz.*, vol. 33, pp. 72-76; July, 1957.) An investigation of the dynamics of a quasi-neutral plasma formation located in the field of a plane electromagnetic wave. The method of

successive approximations is used. Within the limits of the assumptions of the analysis a plasma bunch tends to spread out.

537.56:538.6:52 2370

**An Energy Principle for Hydromagnetic Stability Problems**—I. B. Bernstein, E. A. Frieman, M. D. Kruskal, and R. M. Kulsrud. (*Proc. Roy. Soc. A*, vol. 244, pp. 17–40; February 25, 1958.) The problem of the stability of static, highly conducting, fully ionized plasmas is investigated by means of an energy principle developed from one introduced by Lundquist (122 of 1952). The method is applied to the general axisymmetric system and to plasmas which are completely separated from the magnetic field by an interface.

537.56:538.63:538.56 2371

**Radiation of Plasma in a Magnetic Field**—B. A. Trubnikov. (*Doklady Akad. Nauk S.S.S.R.*, vol. 118, pp. 913–916; February 11, 1958.) Mathematical analysis of electromagnetic radiation in plasma taking account of electron spin in a uniform magnetic field.

537.56:538.63:538.566 2372

**Coherent Scattering and Radiation of Electromagnetic Waves by Plasma in an Inhomogeneous Magnetic Field**—G. A. Askar'yan. (*Zh. Eksp. Teor. Fiz.*, vol. 32, pp. 1576–1577; June, 1957.) The propagation of quasi-plane waves in a waveguide filled with plasma in a longitudinal magnetic field and the radiation in an electron plasma of a bunch which travels through a spatially periodic axially symmetric magnetic field are discussed. The plasma tends to focus the bunches and a longitudinal focusing effect results from the attraction between the induced currents flowing in the same direction.

538.114 2373

**Models Demonstrating the Phenomena of Ferromagnetic Hysteresis**—H. Wilde. (*Nachricht. Z.*, vol. 10, pp. 497–502; October, 1957.) Extension and refinement of the Preisach model. See also 842 of 1957 (Feldtkeller and Wilde).

538.222:539.2 2374

**Contribution to the Phenomenological Theory of Paramagnetic Relaxation in Parallel Fields**—N. K. Belousova and I. G. Shaposhnikov. (*Zh. Eksp. Teor. Fiz.*, vol. 33, pp. 238–242; July, 1957.) The role of spin-lattice interaction is examined and the applicability of the results of this analysis to paramagnetic absorption at high frequencies and temperatures of the order of 20°K is considered.

538.3 2375

**The Classical Electromagnetic Equations expressed as Complex Four-Dimensional Quantities**—E. F. Bolinder. (*J. Franklin Inst.*, vol. 263, pp. 213–223; March, 1957.) It is possible to compress the classical electromagnetic equations into three complex four-dimensional quantities representing, respectively, electromagnetic fields, currents and charges, and vector and scalar potentials. This notation is useful in problems relating to waveguides, cavities, and antennas for microwaves.

538.3:52 2376

**Theory of Magnetohydrodynamic Waves using the Energy Pulse Tensor of Abraham**—E. Richter. (*Z. Physik*, vol. 148, pp. 253–261; April 3, 1957.) See also 2423 of 1957.

538.3:52 2377

**Dynamo Effect in Magnetohydrodynamic Theory**—S. Colombo. (*Rev. gén. Élect.*, vol. 66, pp. 325–332; June, 1957.)

538.52:538.566 2378

**Surface Currents Induced by Short-Wave-**

**length Radiation**—J. A. Cullen. (*Phys. Rev.*, vol. 109, pp. 1863–1867; March 15, 1958.) "The integral equation given by Fock [1412 of 1947] for the surface currents induced in a perfectly conducting convex object by short-wavelength plane electromagnetic waves is solved directly by the method of Fourier transforms. The result agrees with Fock's indirect approach. Some general properties of the equation are also discussed."

538.561:537.56:53.087:621.383.27 2379

**The Cherenkov Effect Produced by Single Particles in Gases**—A. Ascoli-Balzanelli and R. Ascoli. (*Nuovo Cim.*, vol. 6, pp. 1392–1408; December 1, 1957.) (In English.) The application of photomultipliers for detecting Cherenkov radiation is discussed and successful experimental work is reported.

538.566:535.42 2380

**A New Formulation of Scalar Diffraction Theory for Restricted Aperture**—J. M. Cowley and A. F. Moodie. (*Proc. Phys. Soc. London*, vol. 71, pp. 533–545; April 1, 1958.)

538.566:537.53 2381

**Radiation of Charged Particles in Flight Past Ideally Conducting Bodies**—Yu. N. Dnestrovskii and D. P. Kostomarov. (*Doklady Akad. Nauk S.S.S.R.*, vol. 116, pp. 377–380; September 21, 1957.) The problem is discussed in the nonrelativistic approximation and the induced charge and currents are calculated initially without considering retardation. The radiation due to the current system determined is then estimated. The dipole approximation is used to derive expressions for the rate at which energy is radiated. The radiation resistance for a waveguide system is calculated and its dependence on the particle velocity and on the radius/wavelength ratio is shown graphically.

538.566.029.65:537.228.5 2382

**Stark Effect at 2.0 and 1.2 Millimetres Wavelength: Nitric Oxide**—C. A. Burrus and J. D. Graybeal. (*Phys. Rev.*, vol. 109, pp. 1553–1556; March 1, 1958.) "Stark-effect measurements have been made for the first time in the 1–2-mm wave region. Results of Stark-effect measurements on the  $J = \frac{1}{2} \rightarrow 3/2$  and  $J = 3/2 \rightarrow 5/2$  transitions of the  $^{2}N_{1/2}$  ground state of  $N^{14}O^{16}$ , falling at 2.0 and 1.2 mm, respectively, are reported, and are shown to fit closely existing theory; the electric dipole moment of NO in the ground state is found to be  $0.158 \pm 0.006$  Debye unit."

538.569.4.029.6 2383

**Electric Susceptibility of Ethyl Chloride in the Centimeter Region**—G. P. Srivastava. (*Z. Physik*, vol. 148, pp. 242–247; April 3, 1957.) (In English.) Results of measurements at 8780 mc over a pressure range 10–75 cm Hg and a temperature range 263°–353° K are discussed. See also 3841 of 1957 (Krishnaji and Srivastava).

538.569.4.029.64:621.375.9 2384

**Electron Spin and Phonon Equilibrium in Masers**—N. Bleembergen. (*Phys. Rev.*, vol. 109, pp. 2209–2210; March 15, 1958.) It is pointed out that the successful operation of  $KCo(Cr)(CN)_6$  in three-level steady-state masers is incompatible, regardless of the operating frequencies of the maser, with the assumption that the relaxation rates are determined by the interaction between the lattice vibrations and the helium bath [see *ibid.*, vol. 109, pp. 302–311; January 15, 1958.] (Giordmaine *et al.*).

539.1.01:538.569.4 2385

**Identity of Spin Temperature and Thermodynamic Temperature**—A. Abragam and

W. Proctor. (*C.R. Acad. Sci., Paris*, vol. 245, pp. 1048–1050; September 23, 1957.)

539.2:537.311.1 2386

**Generalized Mobility Theory**—M. Lax. (*Phys. Rev.*, vol. 109, pp. 1921–1926; March 15, 1958.) A formal theory of mobility is presented that does not depend on the existence of a transport equation. In particular the Hamiltonian describing the electron plus the scattering system is not decomposed into an unperturbed part plus a perturbation. Only the applied field is treated as small. The result is shown to reduce to the usual transport result when the scattering perturbation is weak, without assuming the existence of a relaxation time. The relation between a many-electron treatment and the one-electron treatment is demonstrated for the case of Fermi as well as Boltzmann statistics.

539.2:537.311.31:061.3 2387

**The Band Theory of Metals**—(*Nature, London*, vol. 181, pp. 525–527; February 22, 1958.) Brief report of a conference held by the Physical Society at Imperial College, London, December 20–21, 1957. Some 20 papers are noted.

#### GEOPHYSICAL AND EXTRATERRESTRIAL PHENOMENA

523.164:523.35 2388

**A "Lunar" Radio Interferometer**—G. A. Gurzadyan. (*Doklady Akad. Nauk S.S.S.R.*, vol. 118, pp. 1094–1097; February 21, 1958.) In a two-antenna interferometer used in radio astronomy one of the antennas can be replaced by the surface of the sea. In the instrument described the ionosphere of the moon is used in place of the second antenna. With meter wavelengths the minimum angle of refraction of the lunar ionosphere is found to be of the order of  $0.1^{\circ}$ – $0.2^{\circ}$ .

523.164.31:523.35 2389

**Radio Interference Phenomena due to the Ionosphere of the Moon**—G. A. Gurzadyan. (*Doklady Akad. Nauk S.S.S.R.*, vol. 118, pp. 884–887; February 11, 1958.) An attempt to explain the increase of solar radio emission observed before and after a solar eclipse, by interference effects due to refraction of radio waves in the lunar ionosphere.

523.164.32 2390

**A Remarkable Solar Radio Event**—(*Nature, London*, vol. 181, pp. 542–543; February 22, 1958.) Increased solar radio noise at a frequency of 200 mc was recorded at Nera Observatory, Netherlands, from 0848 V.T. on November 4, 1957. The maximum value was approximately 900 times the noise level of the quiet sun. Fluctuations with a period of 0.2–0.3 second occurred and are attributed to solar phenomena.

523.164.32:621.396.677.833 2391

**A Radio Image of the Sun on 3.2-cm Wavelength**—V. V. Vitkevich, A. D. Kuz'min, A. E. Salomonovich, and V. A. Udal'tsov. (*Doklady Akad. Nauk S.S.S.R.*, vol. 118, pp. 1091–1093; February 21, 1958.) In June, 1957 at a station of the Physical Institute in the Crimea a new stationary radio telescope with a parabolic reflector of 31 inches diameter, was put into commission. Isophotes of the sun obtained at 3.2 and 10.0 cmλ are shown.

523.165 2392

**Energy Spectrum of Cosmic Radiation**—H. Alfvén and E. Åström. (*Nature, London*, vol. 181, pp. 330–331; February 1, 1958.) A theory is given for the observed spectrum  $f = \text{const. } p^{-n}$  where  $n = 2.5$  for a wide range of values of momentum  $p$ .

circuit; the lowest drift being obtained using the transistor as a chopper.

621.375.4.024 2344  
A Transistor High-Gain Chopper-Type D.C. Amplifier—G. B. B. Chaplin and A. R. Owens. (*Proc. IEE*, pt B, vol. 105, pp. 258–266; May, 1958. Discussion, pp. 266–272.) A modulated system is employed consisting of a transistor input chopper; a high-gain transistor ac amplifier and an output chopper. The system has an open loop gain of  $500 \text{ v}/\mu\text{a}$  with a band extending from direct current to 25 cps. Peak output is  $\pm 10$  volts and current drift referred to input is  $4 \times 10^{-9}$  a in the range  $20^\circ\text{C}$ – $50^\circ\text{C}$ . The voltage drift at the input is less than  $100 \mu\text{a}$ .

621.375.4.029.3 2345  
Designing Transistor A.F. Power Amplifiers—M. B. Herscher. (*Electronics*, vol. 31, pp. 96–99; April 11, 1958.) The amplifier described delivers 45 w to a  $4\text{-}\Omega$  load. It contains a driver stage, a phase splitter using a transistor pair, and a push-pull output-stage.

621.375.9:538.569.4.029.6 2346  
Operation of a Solid-State Quantum-Mechanical Amplifier—M. W. P. Strandberg, C. F. Davis, B. W. Faughnan, R. L. Kyhl, and G. J. Wolga. (*Phys. Rev.*, vol. 109, pp. 1988–1989; March 15, 1958.) "The operation of an S-band solid state quantum-mechanical amplifier operated at  $4.2^\circ\text{K}$  with a computed noise temperature of less than  $4.5^\circ\text{K}$  is compared with similar devices and is used as proof of the condition of discrete phonon saturation which has been previously postulated." See also 1691 of 1958 (McWhorter and Meyer).

621.375.9:538.569.4.029.6 2347  
The Solid-State Maser—a Supercooled Amplifier—J. W. Meyer. (*Electronics*, vol. 31, pp. 66–71; April 25, 1958.) A review of maser techniques with descriptions of two-level molecular-beam and three-level solid-state devices. Amplifier and oscillator characteristics, noise measurements, and future developments are discussed.

621.375.9:538.569.4.029.6 2348  
A U.H.F. Solid-State Maser—R. H. Kingston. (*Proc. IRE*, vol. 46, p. 916; May, 1958.) Maser action at a frequency of 300 mc has been obtained by using a cavity mode at the pumping frequency and a lumped resonant circuit at the amplifying frequency.

621.375.9:538.569.4.029.6 2349  
Design Considerations for Circulator Maser Systems—F. R. Arams and G. Krayer. (*Proc. IRE*, vol. 46, pp. 912–913; May, 1958.) A general expression for effective maser system noise temperature is calculated and a working approximation is derived. The noise and stability requirements for a low-noise circulator maser system are given in terms of maser gain and of dissipative losses and SWR in various parts of the system.

621.375.9:538.569.4.029.6:621.396.822 2350  
System-Noise Measurement of a Solid-State Maser—A. L. McWhorter and F. R. Arams. (*Proc. IRE*, vol. 46, pp. 913–914; May, 1958.) A complete amplifier system with an effective input noise temperature of  $20 \pm 5^\circ\text{K}$  is described. The sources of noise are analyzed and it is shown that the noise temperature of the maser proper is close to the theoretical value.

621.375.9:538.569.4.029.64 2351  
Electron Spin and Phonon Equilibrium in Masers—Bloembergen. (See 2385.)

621.375.9:621.372.2 2352  
A Travelling-Wave Parametric Amplifier—

A. L. Cullen. (*Nature, London*, vol. 181, p. 332; February 1, 1958.) A lossless transmission line with periodically varying distributed inductance and a constant distributed capacitance will support a growing current wave. For maximum amplification the oscillator used for providing the periodic variation of inductance must be synchronized with the incoming signal. The noise figure of such an amplifier should be very favorable. An experimental investigation is in progress, and related schemes are being studied in which precise frequency and phase relations are not demanded.

621.375.9.029.6:537.311.33 2353  
Proposed Negative-Mass Microwave Amplifier—H. Krömer. (*Phys. Rev.*, vol. 109, p. 1856; March 1, 1958.) It is pointed out that negative masses occur in semiconductors at energies close to the band edge if the energy contours are re-entrant there. It is suggested that such a semiconductor might be used as the active element in a microwave amplifier, although preliminary experiments with germanium did not show the effect. See also 2901 of 1954 (Shockley and Mason).

#### GENERAL PHYSICS

533.6.011 2354  
On Chandrasekhar's Theory of Turbulence—P. C. Jain. (*Proc. Nat. Inst. Sci. India*, pt A, vol. 23, pp. 504–513; November 26, 1957.) The theory (*Proc. Roy. Soc. A*, vol. 229, pp. 1–19; April 5, 1955.) has been generalized to the case of axisymmetric turbulence, and eight differential equations in eight defining scalars of double and triple correlation tensors deduced. Two of these equations replace that of de Kármán and Howarth (*Proc. Roy. Soc. A*, vol. 164, pp. 192–215; January 21, 1938) in the theory of isotropic turbulence.

533.6.011 2355  
On Decay of Energy Spectrum of Isotropic Turbulence—N. R. Sen. (*Proc. Nat. Inst. Sci. India*, pt A, vol. 23, pp. 530–533; November 26, 1957.)

535.215:537.224 2356  
Electric Field Distribution in Polarized Photoconductors—H. Kallmann and J. R. Freeman. (*Phys. Rev.*, vol. 109, pp. 1506–1508; March 1, 1958.) The distribution is determined from changes which occur in the persistent polarization [see 2633 of 1955 (Kallmann and Rosenberg)] under various polarizing conditions.

537.12:537.311.1 2357  
The Fundamental State of an Electron Gas—H. Koppe. (*Z. Physik*, vol. 148, pp. 135–155; April 3, 1957.) Detailed discussion with reference to Mayer's treatment of electron correlation energy (*Phys. Rev.*, vol. 100, pp. 1579–1586; December 15, 1955).

537.226 2358  
Force Densities in Dielectrics—É. Durand. (*C.R. Acad. Sci., Paris*, vol. 245, pp. 1003–1006; September 16, 1957.)

537.311.1 2359  
A New Approach to the Theory of Electrical Conductivity of Solids—B. Meltzer. (*Physica*, vol. 23, pp. 118–124; February, 1957.) Since the electrical conductance of a body is a measure of the fluctuations of charge in a state of thermodynamic equilibrium an analysis of these fluctuations gives the value of the conductivity. The value derived agrees with that of Drude but is found to be half that for the Lorentz-Sommerfeld model.

537.311.1 2360  
The Boltzmann Equation in the Theory of Electrical Conduction in Metals—D. A. Greenwood. (*Proc. Phys. Soc. London*, vol. 71, pp.

585–596; April 1, 1958.) The Boltzmann equation for electrical conduction in metals is derived assuming  $\hbar/\tau \ll kT$ , where  $\tau$  is the collision time. An expression independent of this assumption is considered but not evaluated.

537.311.1 2361  
Theory of Electrical Conductivity of Anisotropic Inhomogeneous Media—A. Nedoluha. (*Z. Physik*, vol. 148, pp. 248–252; April 13, 1957.)

537.311.31:538.63 2362  
Quantum Theory of the Electrical Conductivity of Metals in a Magnetic Field—I. M. Lifshits. (*Zh. Eksp. Teor. Fiz.*, vol. 32, pp. 1509–1518; June, 1957.) The kinetic equation for the density matrix is derived and the asymptotic values of the kinetic coefficients in a strong magnetic field are analyzed.

537.56 2363  
On the Theory of Spectral-Line Broadening in Plasma—V. I. Kogan. (*Doklady Akad. Nauk S.S.S.R.*, vol. 118, pp. 907–910; February 11, 1958.)

537.56 2364  
Structure of Shock Waves in a Plasma—V. D. Shafranov. (*Zh. Eksp. Teor. Fiz.*, vol. 32, pp. 1453–1459; June, 1957.) Investigation of a shock wave in a plasma taking account of the difference in electron and ion temperatures. Three cases are examined: a) nonstationary shock wave, b) stationary shock wave, and c) stationary shock-wave in a strong magnetic field.

537.56 2365  
Electrodynamical Acceleration of Plasma Bunches—L. A. Artsimovich, S. Yu. Luk'yanov, I. M. Podgornyĭ, and S. A. Chuvatin. (*Zh. Eksp. Teor. Fiz.*, vol. 33, pp. 3–8; July, 1957.) A method is described of generating a gas-discharge plasma by the electric explosion of a 0.02 mm-diameter copper wire in a discharge chamber evacuated to  $1-2 \times 10^{-8}$  mm Hg. A  $75\text{-}\mu\text{f}$  capacitor is used with initial voltage 30 kv.

537.56 2366  
Quantum Kinetic Equation for Plasma taking Account of Correlation—Yu. L. Klimontovich and S. V. Temko. (*Zh. Eksp. Teor. Fiz.*, vol. 33, pp. 132–134; July, 1957.) A quantum kinetic equation for a system of particles with coulomb interaction is derived taking into account the correlation of the mutual position of the charged particles.

537.56 2367  
On the Effective Field in a Plasma—B. B. Kadomtsev. (*Zh. Eksp. Teor. Fiz.*, vol. 33, pp. 151–157; July, 1957.) Equations for the partial distribution functions are used to compute the effective field acting on charged particles in a plasma. The effective field differs from the mean field by a small quantity of the order of  $1/N$  where  $N$  is the number of particles within a sphere of radius equal to the Debye radius.

537.56:538.56 2368  
The Dispersion Equation for Plasma Waves—N. G. Van Kampen. (*Physica*, vol. 23, pp. 641–650; July, 1957.) The validity of different formulas is discussed. When collisions are infrequent no dispersion equation exists except in special cases. See also 2029 of 1956.

537.56:538.569 2369  
On the Dynamics of a Bounded Plasma in an External Field—L. M. Kovrizhnykh. (*Zh. Eksp. Teor. Fiz.*, vol. 33, pp. 72–76; July, 1957.) An investigation of the dynamics of a quasi-neutral plasma formation located in the field of a plane electromagnetic wave. The method of

successive approximations is used. Within the limits of the assumptions of the analysis a plasma bunch tends to spread out.

537.56:538.6:52 2370

**An Energy Principle for Hydromagnetic Stability Problems**—I. B. Bernstein, E. A. Frieman, M. D. Kruskal, and R. M. Kulsrud. (*Proc. Roy. Soc. A*, vol. 244, pp. 17–40; February 25, 1958.) The problem of the stability of static, highly conducting, fully ionized plasmas is investigated by means of an energy principle developed from one introduced by Lundquist (122 of 1952). The method is applied to the general axisymmetric system and to plasmas which are completely separated from the magnetic field by an interface.

537.56:538.63:538.56 2371

**Radiation of Plasma in a Magnetic Field**—B. A. Trubnikov. (*Doklady Akad. Nauk S.S.S.R.*, vol. 118, pp. 913–916; February 11, 1958.) Mathematical analysis of electromagnetic radiation in plasma taking account of electron spin in a uniform magnetic field.

537.56:538.63:538.566 2372

**Coherent Scattering and Radiation of Electromagnetic Waves by Plasma in an Inhomogeneous Magnetic Field**—G. A. Askar'yan. (*Zh. Eksp. Teor. Fiz.*, vol. 32, pp. 1576–1577; June, 1957.) The propagation of quasi-plane waves in a waveguide filled with plasma in a longitudinal magnetic field and the radiation in an electron plasma of a bunch which travels through a spatially periodic axially symmetric magnetic field are discussed. The plasma tends to focus the bunches and a longitudinal focusing effect results from the attraction between the induced currents flowing in the same direction.

538.114 2373

**Models Demonstrating the Phenomena of Ferromagnetic Hysteresis**—H. Wilde. (*Nachricht. Z.*, vol. 10, pp. 497–502; October, 1957.) Extension and refinement of the Preisach model. See also 842 of 1957 (Feldtkeller and Wilde).

538.222:539.2 2374

**Contribution to the Phenomenological Theory of Paramagnetic Relaxation in Parallel Fields**—N. K. Belousova and I. G. Shaposhnikov. (*Zh. Eksp. Teor. Fiz.*, vol. 33, pp. 238–242; July, 1957.) The role of spin-lattice interaction is examined and the applicability of the results of this analysis to paramagnetic absorption at high frequencies and temperatures of the order of 20°K is considered.

538.3 2375

**The Classical Electromagnetic Equations expressed as Complex Four-Dimensional Quantities**—E. F. Bolinder. (*J. Franklin Inst.*, vol. 263, pp. 213–223; March, 1957.) It is possible to compress the classical electromagnetic equations into three complex four-dimensional quantities representing, respectively, electromagnetic fields, currents and charges, and vector and scalar potentials. This notation is useful in problems relating to waveguides, cavities, and antennas for microwaves.

538.3:52 2376

**Theory of Magnetohydrodynamic Waves using the Energy Pulse Tensor of Abraham**—E. Richter. (*Z. Physik*, vol. 148, pp. 253–261; April 3, 1957.) See also 2423 of 1957.

538.3:52 2377

**Dynamo Effect in Magnetohydrodynamic Theory**—S. Colombo. (*Rev. gén. Élect.*, vol. 66, pp. 325–332; June, 1957.)

538.52:538.566 2378

**Surface Currents Induced by Short-Wave-**

**length Radiation**—J. A. Cullen. (*Phys. Rev.*, vol. 109, pp. 1863–1867; March 15, 1958.) "The integral equation given by Fock [1412 of 1947] for the surface currents induced in a perfectly conducting convex object by short-wavelength plane electromagnetic waves is solved directly by the method of Fourier transforms. The result agrees with Fock's indirect approach. Some general properties of the equation are also discussed."

538.561:537.56:53.087:621.383.27 2379

**The Cherenkov Effect Produced by Single Particles in Gases**—A. Ascoli-Balzanelli and R. Ascoli. (*Nuovo Cim.*, vol. 6, pp. 1392–1408; December 1, 1957.) (In English.) The application of photomultipliers for detecting Cherenkov radiation is discussed and successful experimental work is reported.

538.566:535.42 2380

**A New Formulation of Scalar Diffraction Theory for Restricted Aperture**—J. M. Cowley and A. F. Moodie. (*Proc. Phys. Soc. London*, vol. 71, pp. 533–545; April 1, 1958.)

538.566:537.53 2381

**Radiation of Charged Particles in Flight Past Ideally Conducting Bodies**—Yu. N. Dnestrovskii and D. P. Kostomarov. (*Doklady Akad. Nauk S.S.S.R.*, vol. 116, pp. 377–380; September 21, 1957.) The problem is discussed in the nonrelativistic approximation and the induced charge and currents are calculated initially without considering retardation. The radiation due to the current system determined is then estimated. The dipole approximation is used to derive expressions for the rate at which energy is radiated. The radiation resistance for a waveguide system is calculated and its dependence on the particle velocity and on the radius/wavelength ratio is shown graphically.

538.566.029.65:537.228.5 2382

**Stark Effect at 2.0 and 1.2 Millimetres Wavelength: Nitric Oxide**—C. A. Burrus and J. D. Graybeal. (*Phys. Rev.*, vol. 109, pp. 1553–1556; March 1, 1958.) "Stark-effect measurements have been made for the first time in the 1–2-mm wave region. Results of Stark-effect measurements on the  $J = \frac{3}{2} \rightarrow 3/2$  and  $J = 3/2 \rightarrow 5/2$  transitions of the  $^2\Pi_{1/2}$  ground state of  $N^{14}O^{16}$ , falling at 2.0 and 1.2 mm, respectively, are reported, and are shown to fit closely existing theory; the electric dipole moment of NO in the ground state is found to be  $0.158 \pm 0.006$  Debye unit."

538.569.4.029.6 2383

**Electric Susceptibility of Ethyl Chloride in the Centimetre Region**—G. P. Srivastava. (*Z. Physik*, vol. 148, pp. 242–247; April 3, 1957.) (In English.) Results of measurements at 8780 mc over a pressure range 10–75 cm Hg and a temperature range 263°–353° K are discussed. See also 3841 of 1957 (Krishnaji and Srivastava).

538.569.4.029.64:621.375.9 2384

**Electron Spin and Phonon Equilibrium in Masers**—N. Bleembergen. (*Phys. Rev.*, vol. 109, pp. 2209–2210; March 15, 1958.) It is pointed out that the successful operation of  $KCo(Cr)(CN)_6$  in three-level steady-state masers is incompatible, regardless of the operating frequencies of the maser, with the assumption that the relaxation rates are determined by the interaction between the lattice vibrations and the helium bath [see *ibid.*, vol. 109, pp. 302–311; January 15, 1958.] (Giordmaine *et al.*).

539.1.01:538.569.4 2385

**Identity of Spin Temperature and Thermodynamic Temperature**—A. Abragam and

W. Proctor. (*C.R. Acad. Sci., Paris*, vol. 245, pp. 1048–1050; September 23, 1957.)

539.2:537.311.1 2386

**Generalized Mobility Theory**—M. Lax. (*Phys. Rev.*, vol. 109, pp. 1921–1926; March 15, 1958.) A formal theory of mobility is presented that does not depend on the existence of a transport equation. In particular the Hamiltonian describing the electron plus the scattering system is not decomposed into an unperturbed part plus a perturbation. Only the applied field is treated as small. The result is shown to reduce to the usual transport result when the scattering perturbation is weak, without assuming the existence of a relaxation time. The relation between a many-electron treatment and the one-electron treatment is demonstrated for the case of Fermi as well as Boltzmann statistics.

539.2:537.311.31:061.3 2387

**The Band Theory of Metals**—(*Nature, London*, vol. 181, pp. 525–527; February 22, 1958.) Brief report of a conference held by the Physical Society at Imperial College, London, December 20–21, 1957. Some 20 papers are noted.

#### GEOPHYSICAL AND EXTRATERRESTRIAL PHENOMENA

523.164:523.35 2388

**"Lunar" Radio Interferometer**—G. A. Gurzadyan. (*Doklady Akad. Nauk S.S.S.R.*, vol. 118, pp. 1094–1097; February 21, 1958.) In a two-antenna interferometer used in radio astronomy one of the antennas can be replaced by the surface of the sea. In the instrument described the ionosphere of the moon is used in place of the second antenna. With meter wavelengths the minimum angle of refraction of the lunar ionosphere is found to be of the order of  $0.1''$ – $0.2''$ .

523.164.31:523.35 2389

**Radio Interference Phenomena due to the Ionosphere of the Moon**—G. A. Gurzadyan. (*Doklady Akad. Nauk S.S.S.R.*, vol. 118, pp. 884–887; February 11, 1958.) An attempt to explain the increase of solar radio emission observed before and after a solar eclipse, by interference effects due to refraction of radio waves in the lunar ionosphere.

523.164.32 2390

**A Remarkable Solar Radio Event**—(*Nature, London*, vol. 181, pp. 542–543; February 22, 1958.) Increased solar radio noise at a frequency of 200 mc was recorded at Nera Observatory, Netherlands, from 0848 V.T. on November 4, 1957. The maximum value was approximately 900 times the noise level of the quiet sun. Fluctuations with a period of 0.2–0.3 second occurred and are attributed to solar phenomena.

523.164.32:621.396.677.833 2391

**A Radio Image of the Sun on 3.2-cm Wavelength**—V. V. Vitkevich, A. D. Kuz'min, A. E. Salomonovich, and V. A. Udal'tsov. (*Doklady Akad. Nauk S.S.S.R.*, vol. 118, pp. 1091–1093; February 21, 1958.) In June, 1957 at a station of the Physical Institute in the Crimea a new stationary radio telescope with a parabolic reflector of 31 inches diameter, was put into commission. Isophotes of the sun obtained at 3.2 and 10.0 cmλ are shown.

523.165 2392

**Energy Spectrum of Cosmic Radiation**—H. Alfvén and E. Åström. (*Nature, London*, vol. 181, pp. 330–331; February 1, 1958.) A theory is given for the observed spectrum  $f = \text{const. } p^{-n}$  where  $n = 2.5$  for a wide range of values of momentum  $p$ .

- 523.5:621.396.11 2393  
**Diurnal Variation in the Number of Shower Meteors Detected by the Forward Scattering of Radio Waves: Part 3—Ellipsoidal Theory**—C. O. Hines. (*Canad. J. Phys.*, vol. 36, pp. 117-126; January, 1958.) The ellipsoidal geometry inherent in the forward-scatter process is developed fully. The more rigorous results obtained are compared at various stages in the analysis with those given by the simplifying "cylindrical approximation" developed in Part 1 (738 of 1956). The "potentially observable" trails are first located and their distribution determined. The fraction of these providing a signal exceeding some given level is found and the total number of these observable trails as a function of trail orientation is determined by integrating over the spatial distribution. Part 2: 1046 of 1956 (Forsyth *et al.*).
- 523.5:621.396.11 2394  
**Resonance Effects in the Theory of Meteor Observability**—D. R. Moorcroft and C. O. Hines. (*Canad. J. Phys.*, vol. 36, pp. 134-136; January, 1958.) The observability theory for forward scattering is revised to cover the resonance that occurs when there is a component of the incident electric vector transverse to the axis of the meteor trail. Normalized contours are given.
- 523.75:523.165 2395  
**Solar Activity and Cosmic Radiation**—R. R. Brown. (*J. Geomag. Geoelect.*, vol. 9, no. 2, pp. 79-85; 1957.) Experimental observations of cosmic radiation during intense solar activity are presented and examined with particular attention to the period around the solar flare of February 23, 1956. The results obtained are discussed in relation to models of solar activity involving corpuscular streams.
- 523.75:550.385.4 2396  
**On the Asymmetry of the Heliographic Distribution of the Storm-Producing Probability of Flares**—Y. Hakura. (*J. Radio Res. Labs. Japan*, vol. 5, pp. 57-64; January, 1958.) The probability is greatest for flares near the center of the disk and for those in the NE and SW quadrants. The greater probability for flares in the western hemisphere is not statistically significant.
- 523.755:523.72 2397  
**The Distribution over the Emitting Area of X Radiation from the Solar Corona and the Residual Intensity during Total Solar Eclipses**—G. Elwert. (*J. Atmos. Terr. Phys.*, vol. 12, nos. 2/3, pp. 187-199; 1958.) (In German.) The E layer is assumed to be ionized by X rays of approximate wavelength 50-100 Å. The intensity of coronal radiation in this waveband is calculated and the results lead to a considerable degree of limb-brightening and to emission of radiation at radii greater than that of the visible disk. The intensity of the residual radiation during total eclipses can be calculated and is estimated to have been about 20 per cent in 1952 and 1954, and about 10 per cent in 1955.
- 550.385:523.75 2398  
**Magnetic Activity following a Solar Flare**—M. A. Ellison. (*J. Atmos. Terr. Phys.*, vol. 12, nos. 2/3, pp. 214-215; 1958.) The conclusions reached by Watson (3853 of 1957) that solar flares and increases of magnetic activity are not correlated is not correct. When the magnitude of the flare and its position on the disk are taken into account, there is a positive correlation as was shown by Newton (see, *e.g.*, 3398 of 1944).
- 550.389.2 2399  
**International Geophysical Year**—H. Odishaw. (*Science*, vol. 127, pp. 115-128; January 17, 1958.) A report on the U. S. program with a brief account of some of the activities during the first five months.
- 550.389.2:629.19 2400  
**Estimating the Life of a Satellite**—J. M. C. Scott. (*Nature, London*, vol. 180, pp. 1467-1468; December 28, 1957.)
- 550.389.2:629.19 2401  
**Lifetime of an Artificial Earth Satellite**—D. C. M. Leslie. (*Nature, London*, vol. 180, pp. 403-404; February 8, 1958.) The approximate formulas given by Fejer (2087 of 1958) and Scott (2400 above) are compared with those given by a more exact method and found to be accurate provided the eccentricity is not large.
- 550.389.2:629.19 2402  
**British Radio Observation of the Satellite**—(*Brit. Commun. Electronics*, vol. 4, pp. 770-772; December, 1957.) Brief reports of the observations made on the first Russian satellite at the B.B.C. Station, Tatsfield, the Radio Research Station, Slough, and Ministry of Supply establishments are given. These include measurements of the signal characteristics, field strength, Doppler frequency shift, and bearing and elevation of the satellite.
- 551.510.535 2403  
**The Effect of Diffusion on the Vertical Distribution of Ionization in a Quiet F Region**—V. C. A. Ferraro and I. Özdoğan. (*J. Atmos. Terr. Phys.*, vol. 12, nos. 2/3, pp. 140-149; 1958.) Electrons are assumed to disappear by attachment to neutral molecules and by diffusion. The coefficient of attachment is assumed to be constant while the diffusion constant is calculated according to classical theory. Using rocket measurements of air density and temperature, the vertical distribution of electrons can be calculated. The results are at variance with those actually observed, possibly because the diffusion constant is much less than that assumed.
- 551.510.535 2404  
**Ambipolar Diffusion in the F<sub>2</sub> Layer**—A. Dalgarno. (*J. Atmos. Terr. Phys.*, vol. 12, nos. 2/3, pp. 219-220; 1958.) Diffusion in the F<sub>2</sub> layer probably depends on the diffusion of O<sup>+</sup> in O; the coefficient is estimated to be about one quarter of the value normally assumed to be applicable in the F<sub>2</sub> layer.
- 551.510.535 2405  
**Horizontal Wind Systems in the Ionospheric E Region Deduced from the Dynamo Theory of the Geomagnetic Sq Variation**—(*J. Geomag. Geoelect.*, vol. 9, no. 2; 1957.)  
 Part 3—H. Maeda. (pp. 86-93.) Wind systems are deduced from Sq data for the solstice seasons in both northern and southern hemispheres and the diurnal and semi-diurnal components are examined. A comparison of the theoretical system with observed winds is made.  
 Part 4—S. Kato. (pp. 107-115.) Wind velocities are calculated taking account of Coriolis forces and assuming the electron density at night to be 1/12th that at noon.  
 Parts 1 and 2: 1080 of 1957.
- 551.510.535 2406  
**Non-Chapmanlike Variations in the Ionospheric E and F<sub>1</sub> Layers. Effect of the Sq Current System: Part 2**—T. Shimazaki. (*J. Radio Res. Labs. Japan*, vol. 5, pp. 35-56; January, 1958.) Variations in f<sub>0</sub>E and f<sub>0</sub>F<sub>1</sub> are examined in various months in addition to those of March which have already been discussed (see 3472 of 1957). It is shown that, in non-equinoctial months, f<sub>0</sub>E is larger in the winter hemisphere than in the summer hemisphere for the same solar zenith distance. This unsymmetrical distribution is interpreted as being due to the Sq current system effect in the E layer, the Sq current system developing more strongly in summer than in winter. Somewhat similar results are observed for the F<sub>1</sub> layer but detailed examination shows that they can be explained by the temperature difference between the summer and winter hemispheres.
- 551.510.535:523.164 2407  
**Radio-Star Scintillations at an Equatorial Station**—J. R. Koster. (*J. Atmos. Terr. Phys.*, vol. 12, nos. 2/3, pp. 100-109; 1958.) Scintillation of radio stars has been measured at 45 mc in Ghana for four years. It is unusually intense, occurs only at night, and is correlated with spread echoes from the F layer and with equatorial scatter of radio signals near sunspot maximum.
- 551.510.535:523.164 2408  
**The Diurnal and Seasonal Variations of Spread-F Ionospheric Echoes and the Scintillations of a Radio Star**—B. H. Briggs. (*J. Atmos. Terr. Phys.*, vol. 12, nos. 2/3, pp. 89-99; 1958.) The degree of spreading is greater at Inverness (57°N) than at Slough (52°N) but the diurnal and seasonal variations are similar and can be correlated with the scintillations of the radio star in Cassiopeia provided an allowance is made for the zenith angle of the star. See also 1737 of 1958.
- 551.510.535:523.746 2409  
**A Method of Determining the Correlation between f<sub>0</sub>F<sub>2</sub> and Sunspot Number**—H. Shibata. (*J. Radio Res. Labs. Japan*, vol. 5, pp. 65-73; January, 1958.) The monthly median critical frequency *f* and the smoothed sunspot number *R* can be represented for a month *m* and time of day *t* by  $f(m, t) = a(m, t)R + b(m, t)$ . The continuous periodic functions *a* and *b* are examined using data obtained at six places in Japan.
- 551.510.535:523.75:621.396.11 2410  
**Solar Activity and the Ionosphere**—C. M. Minnis. (*Nature, London*, vol. 181, pp. 543-544; February 22, 1958.) Observations at Slough showed that the intensity of the ultraviolet and X radiation responsible for the existence of the E layer of the ionosphere, was higher in September, October, and November, 1957 than ever before recorded, and that on individual days in November the critical frequency of the F<sub>2</sub> layer at noon was above 16 mc. See also 1153 of 1958 (Bennington).
- 551.510.535:550.385 2411  
**Disturbances in the Ionospheric F<sub>2</sub> Region associated with Geomagnetic Storms: Part 3—Auroral Latitudes**—T. Sato. (*J. Geomag. Geoelect.*, vol. 9, no. 2, pp. 94-106; 1957.) Results of a statistical treatment show that the deviation of f<sub>0</sub>F<sub>2</sub> on a disturbed day is similar to the negative disturbance in middle latitudes (see Part 2: 127 of 1958); the deviation of h<sub>p</sub>F<sub>2</sub> is different. Main features of the F<sub>2</sub> disturbances can be accounted for by vertical electron drift.
- 551.510.535:621.396.11 2412  
**Electron Density Fluctuations and Scattering of Radio Waves in the Ionosphere**—Ya. L. Al'pert. (*Zh. Eksp. Teor. Fiz.*, vol. 33, pp. 213-225; July, 1957.) Discussion of theoretical and experimental determinations of electron density fluctuations and of energy scattered at VHF indicates that in vertical-incidence soundings at frequencies below the critical frequency the scattered field is chiefly due to waves first scattered in the forward direction and then reflected from higher levels in the ionosphere.
- 551.510.535:621.396.11 2413  
**Control of the Ionosphere by Means of Radio Waves**—V. A. Bailey. (*J. Atmos. Terr. Phys.*, vol. 12, nos. 2/3, pp. 216-217; 1958.) A note on the possibility of using radio waves near the gyrofrequency of electrons in the

ionosphere to control the electron temperature and hence the rates of diffusion, attachment, and recombination.

551.510.535:621.296.11.029.62:629.136.3 2414  
An Artificial Ionosphere—(Brit. Commun. Electronics, vol. 5, p. 117; February, 1958.) The release from rockets of potassium into the high atmosphere produces an ionized cloud, lasting for about an hour, suitable for returning micro-wave signals.

551.594.2 2415  
Waveform Studies of Electric Field Changes during Cloud-to-Cloud Lightning Discharges—B. A. P. Tantry, R. S. Srivastava, and S. R. Khastgir. (Proc. Natl. Inst. Sci. India, pt. A, vol. 23, pp. 499-503; November 26, 1957.) Assuming that cloud-to-cloud discharges may be identified from the sign of the field change and the time separation of the individual strokes, such discharges exhibit all the features known to be associated with ground discharges. They include: a) precursors, b) multiple strokes, c) return strokes, d) slow field changes and "hook" components, and e) junction field changes between strokes.

551.594.5 2416  
Auroral Display Observed from Unusually Low Geomagnetic Latitudes—B. McInnes. (Met. Mag. London, vol. 86, pp. 114-117; April, 1957.) Observations of the aurora display of September 8, 1956 are reported with brief details of some related effects.

551.594.5 2417  
Horizontal Movements of Aurora—J. S. Kim and B. W. Currie. (Canad. J. Phys., vol. 36, pp. 160-170; February, 1958.) The drift of auroral forms has been measured at three stations in Canada south of the auroral zone. No evidence is found of a motion due to the earth's rotation relative to a fixed point in space. The distribution and magnitude of the drift speeds parallel and normal to the geomagnetic meridians are similar to those found for ionospheric drifts. The drift speeds increase with geomagnetic activity particularly in an E-W direction.

551.594.5:621.396.96 2418  
A Continuously Recording Automatic Auroral Radar—A. G. McNamara. (Canad. J. Phys., vol. 36, pp. 1-8; January, 1958.) A low-power 50-mc system with fixed antennas is used to give a continuous photographic record. The echo intensity is also integrated electronically to give a chart record which is immediately available.

551.594.6 2419  
Abnormal Polarization of the Atmospheric Pulses Reflected Successively from the Ionosphere—S. R. Khastgir. (Nature, London, vol. 181, pp. 404-405; February 8, 1958.) Elliptical patterns of gradually decreasing eccentricity and tilt angle have been observed in cathode-ray direction finders used to record atmospheric due to lightning discharges at a distance of about 500 km.

551.594.6:621.396.11.029.45 2420  
Electromagnetic Radiation from Lightning Strokes—E. L. Hill. (J. Franklin Inst., vol. 263, pp. 107-119; February, 1957.) A theory is given of the spectral distribution and the amount of VLF radiation emitted from a vertical lightning stroke from cloud to ground. The radiated energy has a maximum intensity at about 11 kc and a total width at half-maximum of 12 kc. The total energy radiated in one leader and return stroke is estimated to be about 220,000 joules.

551.594.6:621.396.822 2421  
Atmospheric Radio Noise at Frequencies between 10 kc/s and 30 kc/s—J. Harwood.

(Proc. IEE, pt. B, vol. 105, pp. 293-300; May, 1958.) The results are described in terms of a voltage envelope at the output of a narrow-band receiver (300 cps between 3 db points). The rms voltage deduced by integrating the measured amplitude distributions varies between four and eight times the average voltage. The noise is always much more impulsive than fluctuation noise. The structure of the voltage envelope is considered in two ways: a) the amplitude distribution of pulse peaks and b) the amplitude distribution of voltage. See also 445 of 1957 (Horner and Harwood).

#### LOCATION AND AIDS TO NAVIGATION

621.396.933.1 2422  
Marconi Doppler Navigator—Wireless World, vol. 64, pp. 260-261; June, 1958.) Further technical details are given and performance during a demonstration flight is described. See also 3146 of 1957.

621.396.96:551.594.5 2423  
A Radarously Recording Automatic Auroral Radar—McNamara. (See 2418.)

621.396.969.33 2424  
A Doppler Collision Course Indicator for Use at Sea—H. R. Whitfield and C. M. Cade. (J. Inst. Nav., vol. 11, pp. 81-87; January, 1958.) A system is proposed for the instantaneous measurement of the radial component of relative velocity. This, together with the range and bearing data from a PPI, gives the aspect of the target. Possible errors in deducing true aspect and speed are discussed and the mode of operation and principal design parameters of a suitable Doppler radar are given.

#### MATERIALS AND SUBSIDIARY TECHNIQUES

535.215:537.311.33 2425  
Temperature Dependence of Photoelectromotive Force—F. F. Kodzheshirov. (Zh. Eksp. Teor. Fiz., vol. 32, pp. 1593-1594; June, 1957.) The difficulties of reconciling experimental results with theories concerning photoelectric effects are considered. The temperature dependence of the EMF is discussed with reference to amorphous Se exposed to X rays of different intensity.

535.215:546.472.21 2426  
Photovoltages Larger than the Band Gap in Zinc Sulphide Crystals—S. G. Ellis, F. Herman, E. E. Loebner, W. J. Merz, C. W. Struck, and J. G. White. (Phys. Rev., vol. 109, p. 1860; March 1, 1958.) Ultraviolet illumination produces photovoltages greater than the band gap in ZnS crystals grown from the vapor. The crystals contained random stacking faults.

535.215:546.482.21:538.6 2427  
Surface Photoconductivity of Cadmium Sulphide Modified with Magnetic Field—S. Tanaka and T. Masumi. (J. Phys. Soc. Japan, vol. 13, pp. 22-32; January, 1958.) Report and discussion of measurements made on CdS single crystals.

535.37 2428  
Energy Storage in ZnS and ZnCdS Phosphors—H. Kallmann and E. Sucov. (Phys. Rev., vol. 109, pp. 1473-1478; March 1, 1958.) It was found that the trap concentration was of the order of  $10^{16}/\text{cm}^3$  in all the phosphors examined. The observed slow rate of decay of the stored energy is explained by predominant retrapping in traps of various depths. It is concluded that the decay of stored electrons can take place radiatively and/or nonradiatively and that the rate for both processes is of the same order of magnitude. It is also shown that the light sum under a stimulation curve does not give a true picture of the trap population.

535.37 2429  
Temperature Characteristics of Barium Strontium Lithium Silicate Phosphors—A. H. McKeag. (J. Electrochem. Soc., vol. 105, pp. 78-81; February, 1958.) "The changes in spectral emission, efficiency, and temperature stability are discussed which result from changes in the following variable parameters in phosphor preparation: the Ba:Sr ratio, Li content, base:acid ratio, activator concentrations, and firing conditions."

535.371.07.002.2:621.397.62:535.623 2430  
Photodeposition of Luminescent Screens—M. Sadowsky and P. D. Payne, Jr. (J. Electrochem. Soc., vol. 105, pp. 105-107; February, 1958.) The method of deposition of the phosphor on a CRT screen for color television is described, with details of how to overcome faults which are liable to occur.

535.376 2431  
The Luminescence Response of Phosphors to Low-Energy Ion Bombardment—C. F. Eve and H. E. Duckworth. (Canad. J. Phys., vol. 36, pp. 104-116; January, 1958.) The response of ZnS-Ag and  $\text{Zn}_2\text{SiO}_4\text{-Mn}$  was determined as a function of the ion energy and the form of the dependence derived. Experimental results for ZnS-Ag are consistent with a theory that the bombarding particles penetrate the phosphor as neutral atoms and produce luminescence by electronic excitation.

537.221/.227:546.431.824-31 2432  
Surface- and Space-Charge Effects in Ceramic Barium Titanate—W. R. Büsser and E. C. Subbarao. (Naturwissenschaften, vol. 44, p. 509; October, 1957.) Interim report on the results of X-ray tests on  $\text{BaTiO}_3$  specimens subjected to ultraviolet radiation and to various surface treatments.

537.226/.227:546.817.824 2433  
Dielectric Properties of Lead Titanate and its Solid Solutions at Low Temperature under Strong Electric Field—S. Nomura and J. Kobayashi. (J. Phys. Soc. Japan, vol. 13, pp. 114-115; January, 1958.)

537.226.3:621.315.616 2434  
On Dielectric Absorption in Plastic Insulators—A. Kelen. (Phys. and Chem. Solids, vol. 2, pp. 150-151; April, 1957.)

537.226.31 2435  
Motion of a Charge Parallel to the Axis of a Cylindrical Channel in a Dielectric—L. S. Bogdankevich and B. M. Bolotovskii. (Zh. Eksp. Teor. Fiz., vol. 32, pp. 1421-1428; June, 1957.) The field produced by a charge moving parallel to the axis of a cylindrical channel is determined. The field and energy losses of the charge are calculated for various conditions of the medium.

537.226.31 2436  
Anomalous Dispersion of Permittivity in Feldspars—V. A. Ioffe and G. I. Khvostenko. (Doklady Akad. Nauk S.S.S.R. vol. 118, pp. 709-712; February 1, 1958.)

537.228.1:549.514.51 2437  
Theory of Plane Elastic Waves in a Piezoelectric Crystalline Medium and Determination of Elastic and Piezoelectric Constants of Quartz—I. Koga, M. Aruga, and Y. Yoshinaka. (Phys. Rev., vol. 109, pp. 1467-1473; March 1, 1958.) In the case of a plane elastic wave only the component of piezoelectric polarization in the direction of wave propagation produces a restoring force against mechanical strain. Thus the elastic and piezoelectric constants can be determined from experimental data. A discrepancy between theory and experiment in the results of earlier workers [see 1452 of 1941 (Atanasoff et al.)] is explained.

- 537.228.1:549.514.51 2438  
**Anelasticity of Synthetic Crystalline Quartz at Low Temperatures**—J. C. King. (*Phys. Rev.*, vol. 109, pp. 1552–1553; March 1, 1958.) "This is a preliminary report of an examination of the anelasticity and frequency-temperature behavior of synthetic quartz resonators, vibrating in thickness shear at low temperatures. The stress-induced relaxation absorption occurring at 50°K for a frequency of vibration of 5 mc in natural quartz is found to be three orders of magnitude larger in some samples of the synthetic quartz."
- 537.311.33 2439  
**Theory of Interstitial Impurity States in Semiconductors**—P. E. Kaus. (*Phys. Rev.*, vol. 109, pp. 1944–1952; March 15, 1958.) "The ionization energy and expectation value of the radius corresponding to the states of several interstitial impurities in Ge and Si are calculated. The range of the valence electron of the impurity is divided into two regions: an inner region, which is treated microscopically, and an outer region, which is treated macroscopically. The separation radius, which is primarily a function of the host crystal, is a parameter of the calculation. At a critical separation radius a rapid change of ionization energy and wavefunction results. The calculations are carried out for several impurities in column I of the periodic table."
- 537.311.33 2440  
**On the Exciton Mechanism for Capture of Current Carriers in Homopolar Semiconductors**—V. L. Bonch-Bruевич. (*Zh. Eksp. Teor. Fiz.*, vol. 32, pp. 1470–1478; June, 1957.) The capture of charge carriers by structural defects with energy transfer to small-radius excitons is investigated. The probability of this transfer and the temperature dependence of the recombination coefficients are also examined.
- 537.311.33 2441  
**On the Mass-Action Laws in Degenerate Semiconductors**—F. W. G. Rose. (*Proc. Phys. Soc. London*, vol. 71, pp. 699–701; April 1, 1958.) An analysis which defines the effective density of the energy levels in the conduction band and valence band. See also 482 of 1958.
- 537.311.33 2442  
**Decay Law for the Concentration of Non-Equilibrium Charge Carriers in Semiconductors**—G. M. Guro. (*Zh. Eksp. Teor. Fiz.*, vol. 33, pp. 158–165; July, 1957.) The kinetics of the decay of non-equilibrium carriers in a semiconductor containing a small concentration of traps is examined. In addition to monomolecular and bimolecular modes, a constant-rate recombination is identified. This occurs at low temperature when the recombination cross-section for minority carriers is much larger than that for the majority carriers.
- 537.311.33 2443  
**On the Equivalence of the Fokker-Planck Method and the Free-Energy Method for the Calculation of Carrier Density Fluctuations in Semiconductors**—K. M. Van Vliet. (*Physica*, vol. 23, pp. 248–252; March, 1957.) The Fokker-Planck method is applied to a semiconductor with transitions between the valence band, the conduction band, and one kind of impurity level. The results are consistent with the equations of Burgess (793 of 1956) obtained by the thermodynamic free-energy method.
- 537.311.33 2444  
**Electrical and Optical Properties of some  $M_2^{VI}N_3^{VIb}$  Semiconductors**—J. Black, E. M. Conwell, L. Seigle, and C. W. Spencer. (*Phys. and Chem. Solids*, vol. 2, no. 3, pp. 240–251; 1957.) A number of compounds of group Vb and VIb elements, with chemical formula  $M_2^{VI}N_3^{VIb}$ , have been synthesized as single crystals of fairly good purity. Experimental results are interpreted according to the usual semiconductor model. Energy gaps range from 1.7ev for  $Sb_2S_3$  to 0.16ev for  $Bi_2Te_3$ , decreasing as the atomic number of the components increases.
- 537.311.33:537.29 2445  
**Influence of an External Electric Field on the Adsorption Properties of a Semiconductor**—F. F. Vol'kenstein and V. B. Sandomirskii. (*Doklady Akad. Nauk S.S.S.R.*, vol. 118, pp. 980–982; February 11, 1958.) A theoretical treatment to determine the variation of absorption due to a uniform electric field directed perpendicularly to the semiconductor surface.
- 537.311.33:546.23 2446  
**The Field-Strength Dependence of the Electrical Conductivity of Selenium Single Crystals**—H. Gobrecht and H. Hamisch. (*Z. Physik*, vol. 148, pp. 218–232; April 3, 1957.) Report on investigations of the influence of a strong alternating field on the conductivity perpendicular to the field. It is concluded that the dependence of conductivity on field strength may be explained as being due to the influence of the field on the concentration of charge carriers. See also 2447 below.
- 537.311.33:546.23:537.228.1 2447  
**The Piezoelectric Effect in Selenium**—H. Gobrecht, H. Hamisch, and A. Tausend. (*Z. Physik*, vol. 148, pp. 209–217; April 3, 1957.) Report on investigations of the influence of ultrasonic oscillations on the conductivity of single-crystal Se. The piezoelectric constant was determined by a dynamic as well as a quasi-static method.
- 537.311.33:546.24 2448  
**On the Structure of the Electron Spectrum in Lattices of the Tellurium Type**—Yu. A. Firsov. (*Zh. Eksp. Teor. Fiz.*, vol. 32, pp. 1350–1367; June, 1957.) The general properties of the energy spectrum of an excess electron are studied by group-theory methods. The possibility of contact between the zone in definite directions in the k-space is considered and the effect of the spin-orbit interaction is examined. In semiconductors of this type there can be two kinds of carriers of the same sign.
- 537.311.33:546.26–1:538.21 2449  
**The Electric and Magnetic Properties of Graphite**—R. R. Haering and P. R. Wallace. (*Phys. and Chem. Solids*, vol. 3, nos. 3/4, pp. 253–274; 1957.)
- 537.311.33:[546.28+546.289] 2450  
**The Manufacture of High-Purity Germanium and Silicon Crystals**—H. F. Mataré. (*Elektron Rundschau*, vol. 11, pp. 293–296; October, 1957.) Outline of some techniques used, particularly those designed to overcome the greater difficulties inherent in the purification of Si.
- 537.311.33:[546.28+546.289] 2451  
**Tight-Bonding Calculation of Acceptor Energies in Germanium and Silicon**—R. G. Shulman. (*Phys. and Chem. Solids*, vol. 2, pp. 115–118; April, 1957.) "The differences of hole ionization energies among the group-III elements acting as acceptors in silicon indicate the necessity of considering the specific contribution of the acceptor atom. Energies of two electron bonds are calculated using Morse curves to approximate interatomic potentials. The additional binding energy increases sharply from gallium to indium in accord with experiment. Arguments are presented to show why varying the acceptor element is less important in germanium."
- 537.311.33:546.28 2452  
**Ionization Rates for Electrons and Holes in Silicon**—A. G. Chynoweth. (*Phys. Rev.*, vol. 109, pp. 1537–1540; March 1, 1958.) The ionization rate for electrons is found to be higher than that for holes for the following ranges of field-strength  $E$ : for holes,  $(2.5-6.0) \times 10^6$  v/cm; for electrons,  $(2.0-5.0) \times 10^6$  v/cm. The results suggest that the field dependence of the ionization rate for holes and probably for electrons also, could be expressed by  $aexp(-b/E)$ .
- 537.311.33:546.28:669.046.54/.55 2453  
**Zone Purification of Silicon**—E. A. Taft and F. H. Horn. (*J. Electrochem. Soc.*, vol. 105, pp. 81–83; February, 1958.) "A procedure is described for the zone purification of high purity Si using thin-walled quartz boats. Data are given that show that improved lifetime and more uniform electrical resistivity result from the zone purification of commercially available Si."
- 537.311.33:546.289 2454  
**The Low-Temperature Electrical Conductivity of  $n$ -Type Germanium**—S. H. Koenig and G. R. Gunther-Mohr. (*Phys. and Chem. Solids*, vol. 2, no. 4, pp. 268–283; 1957.) Samples of reasonably pure  $n$ -type Ge single crystals were investigated at temperatures between 1.8 and 5.1°K. The dominant conductivity mechanism is associated either with the conduction band or with an impurity conduction mechanism according to whether the temperature is greater or less than about 4°K. The mechanism of impurity conduction fits a model proposed by Mott (see 2088 of 1957). The conductivity of the conduction band deviates from Ohm's law at fields as low as 3 per cent of the threshold field for breakdown generally ascribed to impact ionization.
- 537.311.33:546.289 2455  
**Electrical Methods for Determining the Positions of Dislocation Regions in Germanium**—C. A. Hogarth and A. C. Baynham. (*Proc. Phys. Soc. London*, vol. 71, pp. 647–653, plate; April 1, 1958.) In Ge crystals grown on a deformed seed, edge dislocations occur. This gives regions of high electrical conductivity in  $n$  and  $p$ -type samples. The positions of dislocation walls determined from point-contact rectification measurements or by plotting potential against distance at constant current, agree with the positions located by etch-pit examination of the surfaces. Evidence of the  $p$ -type character of dislocations in  $n$ -type Ge is shown.
- 537.311.33:546.289 2456  
**The Fermi Level in Germanium at High Temperatures**—J. S. Blakemore. (*Proc. Phys. Soc. London*, vol. 71, pp. 692–694; April 1, 1958.) Some results are given of calculations on the Fermi level in doped and intrinsic Ge from room temperature to 1200°K.
- 537.311.33:546.289 2457  
**Precipitation of Nickel and Copper from Supersaturated Solutions in Germanium**—P. Penning. (*Philips Res. Rep.*, vol. 13, pp. 17–36; February, 1958.) During the anneal of Ge samples supersaturated with Ni, unidentified acceptors with a low activation energy are observed in addition to the acceptor levels arising from substitutional Ni atoms. A mechanism is suggested in which these acceptors are associated with vacancies left behind in the lattice when a substitutional Ni atom jumps to an interstitial site. The interstitial Ni atoms then diffuse rapidly to nuclei of precipitation. Copper gives rise to a similar behavior. The presence of a high density of vacancies during the precipitation of one of these elements greatly facilitates the penetration of the other, permitting concentrations much larger than the saturation value. See also 3779 of 1956.

- 537.311.33:546.289 2458  
**Generation of Imperfections in Germanium Crystals by Thermal Strain**—P. Penning. (*Philips Res. Rep.*, vol. 13, pp. 79-97; February, 1958.) Thermal strain is induced in a crystal if it is heated inhomogeneously or quenched from a high temperature, the strain resulting in either plastic flow or cracking. The distribution of dislocations resulting from plastic flow shows marked characteristics which can be explained by assuming that plastic flow is proportional to the elastic strain induced by the nonuniform temperature. The sources and effects of these strains on crystals grown from a melt are discussed.
- 537.311.33:546.289:535.215:538.639 2459  
**On the Anisotropy of the Even (Transverse) Photomagnetic Effect in Germanium Single Crystals**—I. K. Kikoin and Yu. A. Bykovskii. (*Doklady Akad. Nauk. S.S.S.R.*, vol. 116, pp. 381-384; September 21, 1957.) Experiments carried out on a round disk-like specimen of *n*-type Ge in a magnetic field with illumination normal to the field showed that the potential difference between opposite points on the disk varied with the angle of rotation of the specimen about the axis parallel to the field. The anisotropy of the transverse photomagnetic effect in a sample with its (111) axis perpendicular to its surface is shown graphically. No correlation was found between transverse and usual photomagnetic effects. See also 491 of 1957.
- 537.311.33:546.289:538.569.4 2460  
**Cyclotron Resonance over a Wide Temperature Range**—D. M. S. Bagguley, J. A. Powell, and D. J. Taylor. (*Proc. Phys. Soc. London*, vol. 70, pp. 759-762; October 1, 1957.) Cyclotron resonance experiments on Ge doped with Au were carried out at temperatures in the range 4°K to 90°K. See also 1121 of 1957 (Dexter *et al.*).
- 537.311.33:546.289:538.6 2461  
**Direct-Transition Exciton and Fine Structure of the Magneto-absorption Spectrum in Germanium**—S. Zwerdling, L. M. Roth, and B. Lax. (*Phys. Rev.*, vol. 109, pp. 2207-2209; March 15, 1958.) Report of the observation of exciton absorption just below the direct gap in germanium, together with the fine structure of the related oscillatory magneto-absorption. The exciton was also studied at various magnetic field strengths.
- 537.311.33:546.289:538.63 2462  
**Magnetoresistive Phenomena in *n*-type Ge Semiconductors in Strong Magnetic Fields**—M. I. Klinger and P. I. Voronyuk. (*Zh. Eksp. Teor. Fiz.*, vol. 33, pp. 77-87; July, 1957.) The equilibrium electron concentration, the Hall constant and resistivity are examined and their dependence on the magnetic field strength is discussed. The nature of the anisotropy of these quantities is determined by the anisotropy of the electron mass and by the number and mutual arrangement of the constant-energy ellipsoids.
- 537.311.33:546.46.284 2463  
**Semiconducting Properties of Mg<sub>2</sub>Si Single Crystals**—R. G. Morris, R. D. Redin, and G. C. Danielson. (*Phys. Rev.*, vol. 109, pp. 1909-1915; March 15, 1958.) A report of resistivity and Hall-effect measurements on high-purity *n* type and *p*-type Mg<sub>2</sub>Si single crystals obtained from melts of the constituents. The *p*-type crystals were obtained by doping the melt with silver or copper. The room-temperature Hall mobilities were 406 cm<sup>2</sup>/vsec for *n*-type and 56 cm<sup>2</sup>/vsec for *p*-type material. Carrier concentrations in the saturation region were as low as 8×10<sup>14</sup> cm<sup>-3</sup> for *n*-type and 4×10<sup>17</sup> cm<sup>-3</sup> for *p*-type samples.
- 537.311.33:546.46.289 2464  
**Semiconducting Properties of Mg<sub>2</sub>Ge Single Crystals**—R. D. Redin, R. G. Morris, and G. C. Danielson. (*Phys. Rev.*, vol. 109, pp. 1916-1920; March 15, 1958.) A report of resistivity and Hall-effect measurements on single crystals of Mg<sub>2</sub>Ge obtained from melts of the constituents. Undoped crystals which were *n*-type had saturated impurity concentrations as low as 3×10<sup>16</sup> cm<sup>-3</sup>; silver-doped crystals were *p*-type and had saturated impurity carrier concentrations roughly proportional to the amount of added silver. Room-temperature Hall mobilities were 280 cm<sup>2</sup>/vsec for electrons and 110cm<sup>2</sup>/vsec for holes.
- 537.311.33:546.682.86 2465  
**Properties of *p*-type Indium Antimonide: Part 1—Electrical Properties**—C. Hilsum and R. Barrie. (*Proc. Phys. Soc. London*, vol. 71, pp. 676-685; April 1, 1958.) The variation of Hall coefficient and resistivity with applied magnetic field is used to calculate the dependence of electron and hole mobilities on carrier concentration. The decrease of electron mobility with acceptor concentration is explained in terms of polar scattering and electron-hole scattering.
- 537.311.33:546.682.86:537.312.9 2466  
**Piezoresistance Constants of *P*-Type InSb**—A. J. Tuzzolino. (*Phys. Rev.*, vol. 109, pp. 1980-1987; March 15, 1958.) The change of resistance in uniaxial tension was measured for several single-crystal specimens of *p*-type InSb over the range 77°-350°K. The piezoresistance coefficients were found to depend on impurity concentrations. The elasto-Hall constant was measured at 77°K for the purest specimens and the experimental results indicate that, in the extrinsic range, the large piezoresistance is primarily due to stress-induced changes in the tensor mobility of the holes. It is concluded that the valence band extrema occur at, or very near, *K*=0 in the Brillouin zone with energy surfaces similar to those of Si and Ge.
- 537.311.33:546.682.86:537.32 2467  
**Electron Scattering in InSb**—H. Ehrenreich. (*Phys. and Chem. Solids*, vol. 2, pp. 131-149; April, 1957.) The effects of electron scattering by acoustical and optical phonons as well as electron-hole scattering on the mobility and thermoelectric power of intrinsic InSb are considered using the conduction band theory of Kane (*ibid.*, vol. 1, pp. 249-261; January, 1957). Good agreement is found between theory and experiment for both mobility and thermoelectric power.
- 537.311.33:546.682.86:537.32 2468  
**On the Scattering of Electrons by Optical Modes in Indium Antimonide**—M. Rodot. (*C. R. Acad. Sci., Paris*, vol. 245, pp. 1051-1054; September 23, 1957.) Measurements of the magneto-thermoelectric effect and the Nernst effect in specimens of *n*-type InSb at various temperatures gave results in accordance with the theory of polar scattering. See also 3772 of 1956.
- 537.311.33:546.682.86:539.23 2469  
**Resistivity and Hall Effect of Thin Films of Indium Antimonide**—J. Launey and A. Colombani. (*C. R. Acad. Sci., Paris*, vol. 245, pp. 1009-1011; September 16, 1957.) Films were reheated and then cooled to room temperature before tests were made. Hall effect was found to increase with reheat temperature and to be strictly proportional to current intensity. Consistent results were not obtained if the reheat temperature was above 470°C. Resistivity decreased rapidly with increase in film thickness.
- 537.311.33:546.682.86:539.23 2470  
**Hall Effect and Magnetoresistance of Thin Films of Indium Antimonide**—J. Launey. (*C. R. Acad. Sci., Paris*, vol. 245, pp. 1122-1124; September 30, 1957.) See also 2469 above.
- 537.311.33: [546.873.241+546.863.241+546.193.241 2471  
**Preparation and some Physical Properties of Bi<sub>2</sub>Te<sub>3</sub>, Sb<sub>2</sub>Te<sub>3</sub> and As<sub>2</sub>Te<sub>3</sub>**—T. C. Harman, B. Paris, S. E. Miller, and H. L. Goering. (*Phys. and Chem. Solids*, vol. 2, no. 3, pp. 181-190; 1957.) The preparation of the above intermetallic compounds from purified elements by several techniques is discussed. Electrical and thermal properties are presented as functions of temperature and impurity concentration. The variation of carrier mobility with temperature is approximately T<sup>-1/2</sup> for As<sub>2</sub>Te<sub>3</sub> and Bi<sub>2</sub>Te<sub>3</sub>.
- 537.311.33:546.873.241:537.323 2472  
**The Electrical Conductivity and Thermoelectric Power of Bismuth Telluride**—H. J. Goldsmid. (*Proc. Phys. Soc., London*, vol. 71, pp. 633-646; April 1, 1958.) The electrical conductivity and thermoelectric power of Bi<sub>2</sub>Te<sub>3</sub> are measured over a range of temperatures and for *n*-type and *p*-type samples. This gives the fundamental semiconductor parameters. Samples show extrinsic conduction and partial degeneration over parts of the temperature range necessitating the use of Fermi-Dirac statistics in interpretation of the results.
- 537.311.33:621.314.63 2473  
**Electrical Breakdown in *p*-*n* Junctions**—A. G. Chynoweth. (*Bell Lab. Rec.*, vol. 36, pp. 47-51; February, 1958.) The sudden breakdown which occurs when an increasing reverse voltage is applied to a *p*-*n* junction is explained by the creation of free electrons and holes in an avalanche process.
- 538.22 2474  
**Thermodynamic Theory of "Weak" Ferromagnetism in Antiferromagnetic Substances**—I. E. Dzyaloshinskii. (*Zh. Eksp. Teor. Fiz.*, vol. 32, pp. 1547-1562; June, 1957.) This type of ferromagnetism is attributed to relativistic spin-lattice interaction and magnetic dipole interaction. The dependence of the properties of these substances on the magnetic symmetry of the crystal is examined and the effect of an external magnetic field is also considered.
- 538.22 2475  
**Solid Solutions between Ferromagnetic and Antiferromagnetic Compounds with NiAs Structure**—F. K. Lotgering and E. W. Gorter. (*Phys. and Chem. Solids*, vol. 3, nos. 3/4, pp. 238-249; 1957.) The aim of the investigation is to see whether continuous series of mixed crystals between a ferromagnetic and an anti-ferromagnetic binary compound with NiAs structure exist, and to study the magnetic properties. Several solid solutions were prepared. Saturation magnetizations were measured between 20°K and the Curie temperatures, and susceptibilities between Curie temperatures and 850°-1100°K. Results are discussed.
- 538.22:537.3 2476  
**Electrical Properties of FeTiO<sub>3</sub>-Fe<sub>2</sub>O<sub>3</sub> Solid Solution Series**—Y. Ishikawa. (*J. Phys. Soc. Japan*, vol. 13, pp. 37-42; January, 1958.) The dc electrical conductivity and Seebeck voltage of the synthesized solid solution  $x\text{FeTiO}_3 \cdot (1-x)\text{Fe}_2\text{O}_3$  of ilmenite (FeTiO<sub>3</sub>) and hematite (Fe<sub>2</sub>O<sub>3</sub>) have been measured for a composition range of  $1 \geq x \geq 0.33$ , over a range of temperature. Both ordered (ferrimagnetic) and disordered (antiferromagnetic) specimens with the same composition were investigated. See also 1199 of 1958 (Ishikawa and Akimoto).
- 538.221 2477  
**Temperature Dependence of Ferromagnetic Anisotropy**—W. J. Carr, Jr. (*Phys. Rev.*, vol.

- 621.317.3:621.396.822:621.396.41 2497  
The White-Noise Method of Measuring Crosstalk and Noise Interference in Multichannel Telephone Link System—J. F. Golding. (*Electronic Eng.*, vol. 30, pp. 349–351; May, 1958.) Description of the method with details of a commercially available test set.
- 621.317.32 2498  
Measurement of Peak Values of Periodic High Voltages in a Steady State—J. Lagasse, R. Lacoste, and G. Giralt. (*Rev. gén. Élect.*, vol. 66, pp. 307–324; June, 1957.) The design and construction of a standard variable capacitor is described and the merits of different types of rectifier are discussed. See 1851 of 1957 (Lagasse and Giralt).
- 621.317.33:538.632 2499  
A Method of Measuring Specific Resistivity and Hall Effect of Disks of Arbitrary Shape—L. J. van der Pauw. (*Philips Res. Rep.*, vol. 13, pp. 1–9; February, 1958.) The method is based on a theorem applicable to a flat specimen of arbitrary shape if the contacts are sufficiently small and located at its circumference; the disk must be free of holes.
- 621.317.341:621.374.015.7 2500  
Sensitive Measurements of Pulse-Amplifier Gain—K. A. McCollom, D. R. deBoisblanc, and J. B. Thompson. (*Nucleonics*, vol. 16, pp. 74–76, 78; January, 1958.) The design of an amplifier comparator is described. Gain stability can be checked to within 0.01 per cent, and amplitude stability of two pulse generators can be compared to within 0.02 per cent.
- 621.317.35:621.391 2501  
The Measurement of Power Spectra from the Point of View of Communications Engineering: Parts 1 and 2—R. B. Blackman and J. W. Tukey. (*Bell Sys. Tech. J.*, vol. 37, pp. 185–282; January, 1958, and pp. 485–569; March, 1958.) A comprehensive mathematical and statistical study is presented, with details of analysis and planning for measurement. The analysis is then reconsidered in greater detail and from alternative points of view. Over 50 references.
- 621.317.361:538.569.4:539.1.08 2502  
Measurement and Control of Microwave Frequencies by Lower Radio Frequencies—R. C. Mackey and W. D. Hershberger. (*IRE TRANS. ON MICROWAVE THEORY AND TECHNIQUES*, vol. MTT-5, pp. 64–68; January, 1957. Abstract, *PROC. IRE*, vol. 45, p. 576; April, 1957.)
- 621.317.411 2503  
The Determination of the Permeability of Ferromagnetic Materials from the Thermal Noise Voltage of Coils—W. Nonnenmacher and L. Schweizer. (*Z. angew. Phys.*, vol. 9, pp. 239–245; May, 1957.) The complex permeability is measured as a function of frequency without the use of an externally applied alternating field. The thermal fluctuations in the ferromagnetic core material give rise to a noise voltage across the test coil. Results obtained agree well with those from conventional bridge measurements at low field strengths.
- 621.317.42:621.395.625.3 2504  
The Determination of the Magnetization of Magnetic Recording Tape—O. Schmidbauer. (*Elektron Rundschau*, vol. 11, pp. 302–305; October, 1957.) The magnetization of tape is best defined on the basis of short-circuit flux measurements; a suitable method is described. The determination of transverse magnetization, where it is undesirable or where it is used for synchronizing purposes, and the calibration of heads used in such measurements are also discussed. A specially designed electronic fluxmeter is briefly detailed.
- 621.317.44 2505  
Adaptation of the Ilivici Permeameter to the Investigation of Hypermagnetic Materials—L. Garde. (*Rev. gén. Élect.*, vol. 66, pp. 375–379; July, 1957.) To reduce the error of the instrument which can be excessive in measurements on samples of high permeability, the second yoke is constructed of mumetal.
- 621.317.715:621.375.024 2506  
Device for Matching a Galvanometer or D.C. Indicator to its Associated Circuit—T. M. Dauphinee. (*Rev. Sci. Instrum.*, vol. 29, pp. 240–241; March, 1958.) "Impedance matching is achieved by use of a chopper and transformer circuit which permits near optimum use of the available power."
- 621.317.727:621.316.93:621.314.63 2507  
Silicon Diodes as Protective Meter Shunts—A. S. Penfold and E. L. Garwin. (*Rev. Sci. Instrum.*, vol. 29, pp. 252–253; March, 1958.) Relies on the very small current through the diode for forward voltages less than 0.5 volt.
- 621.317.733 2508  
Impedance Bridges—J. F. Golding. (*Brit. Commun. Electronics*, vol. 5, pp. 104–109; February, 1958.) "After a short discussion of impedance, various types of impedance bridge and their applications are described. A table gives brief specifications of representative bridges available in Britain."
- 621.317.755 2509  
Modern Oscilloscope Practice—(*Electronic and Radio Engr.*, vol. 35, pp. 212–225; June, 1958.) A review of instruments manufactured in the U. K., with simplified circuits of various parts, showing how particular facilities are provided. Oscilloscope cameras are discussed briefly.
- 621.317.755:621.385.832 2510  
Broadband Oscilloscope Tube—D. J. Brangaccio, A. F. Dietrich, and J. W. Sullivan. (*Bell Sys. Tech. J.*, vol. 37, pp. 447–460; March, 1958.) The design and operation of a special oscilloscope tube is described. Traveling-wave tube principles are applied to the design of a helix-type vertical deflection system to give a flat bandwidth characteristic over 600 mc. Novel features are the particular deflection system and a trace on the screen which is readable without other optical means. The construction is similar to commercial tubes except for closer tolerance in electrode alignment. Repetitive pulses a few millimicroseconds in width can be viewed directly.
- 621.317.784.029.63 2511  
U.H.F. Power Meter for Operation in the 200-Mc/s Communication Band—J. K. Murray. (*Electronic Eng.*, vol. 30, pp. 345–348; May, 1958.) Description of the design of a direct-reading power meter for the frequency range 1700–2300 mc.
- 621.317.794:621.319.4 2512  
Notes on Capacitance Bolometers—H. J. Albrecht. (*Proc. IRE, Aust.*, vol. 18, pp. 128–129; April, 1957.) Note on the principles and design of an instrument comprising temperature-sensitive capacitors, with BaTiO<sub>3</sub> or SrTiO<sub>3</sub> dielectric, in two tuned circuits.
- 621.317.794:621.319.4 2512  
Notes on Capacitance Bolometers—H. J. Albrecht. (*Proc. IRE, Aust.*, vol. 18, pp. 128–129; April, 1957.) Note on the principles and design of an instrument comprising temperature-sensitive capacitors, with BaTiO<sub>3</sub> or SrTiO<sub>3</sub> dielectric, in two tuned circuits.
- 621.317.794:621.319.4 2512  
Notes on Capacitance Bolometers—H. J. Albrecht. (*Proc. IRE, Aust.*, vol. 18, pp. 128–129; April, 1957.) Note on the principles and design of an instrument comprising temperature-sensitive capacitors, with BaTiO<sub>3</sub> or SrTiO<sub>3</sub> dielectric, in two tuned circuits.
- 621.38:62 2514  
Electronics in Heavy Industry—G. M. Ettinger. (*Elect. Rev. London.*, vol. 162, pp. 30–35; January 3, 1958.) Survey of applications in measurement, control, data handling, and processing.
- 621.384.612 2515  
About Damping and Antidamping Betatron Oscillations, taking into account Non-Adiabatic Properties of the Radiation—A. N. Matveev. (*Nuovo Cim.*, vol. 6, pp. 1296–1304; December 1, 1957.) (In English.) An analysis of betatron oscillations in high-energy electron synchrotrons shows that damping and antidamping effects would only occur if radiation were an adiabatic process.
- 621.384.612 2516  
Electron Motion in Synchrotrons in the Presence of Radiation—A. N. Matveev. (*Nuovo Cim.*, vol. 6, pp. 1305–1317; December 1, 1957.) (In English.) A stochastic theory of betatron and phase oscillations induced by radiation fluctuations is presented. See also 240 of 1957.
- 621.387.424 2517  
Influence of the Effective Length and Diameter of the Cylinder on the Plateau Characteristic of Externally Graphited Glass-Walled Geiger-Müller Counters—D. Blanc. (*Nuovo Cim.*, vol. 6, pp. 974–976; October 1, 1957.) (In French.)

## PROPAGATION OF WAVES

- 621.396.11 2518  
On the Theory of Propagation of Electromagnetic Waves Along a Curved Surface—J. R. Wait. (*Canad. J. Phys.*, vol. 36, pp. 9–17; January, 1958.) The case of vertically polarized waves propagated across a discontinuity in curvature and electrical properties is considered. An approximate expression is derived for the mutual impedance between two antennas on either side of the boundary by using the principle of stationary phase and the concept of surface impedance. The first-order effects of the boundary changes are shown to be additive corrections to the mutual impedance for a homogeneous surface.
- 621.396.11 2519  
Some Methods for Studying Wave Propagation in a Uniform Magneto-ionic Medium—V. A. Bailey. (*J. Atmos. Terr. Phys.*, vol. 12, nos. 2/3, pp. 118–125; 1958.) The Appleton-Hartree expression for complex refractive index can be simplified by using the approximations:  

$$(1+s^2)^{1/2} = (4+3s^2)/(4+s^2)$$

$$\text{or } s(4s^2+3)/(4s^2+1).$$

The resulting expressions have errors of less than 1 per cent except under limited sets of conditions.

- 621.396.11:551.510.535 2520  
The Distance Attenuation of Radio Waves Reflected at Vertical Incidence from the Ionosphere—J. D. Whitehead. (*J. Atmos. Terr. Phys.*, vol. 12, nos. 2/3, pp. 150–152; 1958.) "It is shown that the assumption that the amplitude of radio waves propagated from a point source falls off inversely as the group path  $P'$  leads to a value of apparent reflection coefficient of the ionosphere which may be seriously in error, and in particular to a large error in the measurement of the electronic collision frequency in the F region."

- 621.396.11.029.4(204) 2521  
On Communication in the Sea by V. L. F. Electromagnetic Waves—K. Furutsu. (*J. Radio Res. Labs. Japan*, vol. 5, pp. 19–33; January 1958.) A theoretical analysis of the various modes of propagation when either transmitter or receiver or both are immersed

- fading to that without fading for the same signal/noise ratio. A method of measuring this quantity is described and results obtained with three different teletype VHF circuits are presented. It is concluded that knowledge of the quantity facilitates the design of communication circuits and enables the noise and fading susceptibility of various systems to be compared.
- 621.396.41 2544  
Wide-Band Ultra-high-Frequency Over-the-Horizon Equipment—R. A. Felsenheld, H. Havstad, J. L. Jatlow, D. J. LeVine, and L. Pollack. (*Commun. and Electronics*, no. 35, pp. 86-93; March, 1958.) A description of wide-band equipment for use in toll-quality multichannel telephone or television circuits in the frequency range 680-900 mc. The receivers can be used for dual or quadruple diversity by combining the signals at the 70-mc intermediate frequency.
- 621.396.41:621.376.3:621.396.813 2545  
Distortion in Frequency-Division Multiplex F.M. Systems due to an Interfering Carrier—R. G. Medhurst, E. M. Hicks, and W. Grossett. (*Proc. IEE*, pt B, vol. 105, pp. 282-292; May, 1958.) It is found that the distortion generated in a particular channel is accurately proportional to the relative level of the interfering carrier. Thus it is possible to plot curves of distortion in the worst channel against frequency separation of wanted and unwanted carriers; a permissible level of interfering carrier may be deduced. Numerical results are shown for various carrier frequency separations that arise under the CCIR frequency plan for 6 RF channels each carrying 600 speech channels. Provided the frequency separation is less than 9 mc the theory is in good agreement with experiment. See also 4005 of 1957 (Medhurst and Hodgkinson).
- 621.396.41:621.396.65 2546  
The Miami-Havana Radio System and its Integration into the Telephone Networks—K. P. Stiles, F. G. Hollins, E. T. Fruhner, and W. D. Siddall. (*Commun. and Electronics*, no. 35, pp. 94-96; March, 1958.) A description of a system developed for radio and television facilities, its method of operation, and the results obtained.
- 621.396.41:621.396.822:621.317.3 2547  
The White-Noise Method of Measuring Crosstalk and Noise Interference in Multichannel Telephone Link Systems—Golding. (See 2497.)
- 621.396.65 2548  
Surveying for Microwave Relay Systems—L. E. Strazza and R. C. S. Joyce. (*Electronic Eng.*, vol. 30, pp. 262-267; May, 1958.) Surveys in well-mapped regions may involve only site and path inspections, but path tests are necessary if accuracy of path profiles plotted from maps is doubtful. Short-duration tests are used to confirm a calculated mean path loss and hence to confirm tower heights, antenna gains, and other system parameters. Long-term tests give statistical information on fading where the path profile is unfavorable. Typical test methods are described.
- 621.396.65 2549  
A Radio Link System with Frequency Modulation for 120 Telephony Channels in the Frequency Range 1700-2300 Mc/s (FM 120/2000)—H. Holzwarth, G. Bosse, C. Colani, and E. Seibt. (*Nachricht. Z.*, vol. 10, pp. 485-493; October, 1957.)
- 621.396.65:621.385.029.63/64 2550  
All-Travelling-Wave-Tube Systems—S. Fedida. (*Electronic Eng.*, vol. 30, pp. 283-290; May, 1958.) The intrinsic features of microwave repeaters using traveling-wave tubes throughout are discussed and their advantages are described. Possible sources of distortion are analyzed and methods of reducing their effect to acceptable values are indicated.
- 621.396.65:621.385.029.64 2551  
S.H.F. Radio Links using Travelling-Wave Output Amplifiers—G. Dawson and T. K. M. Korytko. (*Electronic Eng.*, vol. 30, pp. 276-282; May, 1958.) The problems that have arisen in the planning and installation of wide-band links in many different countries are discussed. A description is given of the techniques which have been evolved in the design of the equipment and the associated supervisory and switching gear.
- 621.396.65:621.385.3.029.63 2552  
Broad-band Microwave Systems employing U.H.F. Triodes—G. W. S. Griffith and B. Wilson. (*Electronic Eng.*, vol. 30, pp. 297-302; May, 1958.) The advantages of economy and convenience in arranging for the modulation, demodulation, and as much amplification as possible to be carried out at an intermediate frequency are discussed. In the 1700-2300-mc band, triodes are the most satisfactory means of providing amplification. Systems employing such principles are described.
- 621.396.65:621.396.41 2553  
Microwave Radio Toll Systems—E. W. Anderson. (*Electronic Eng.*, vol. 30, pp. 267-271; May, 1958.) The function of the radio link in telephone networks is outlined and some of the problems requiring solution in the design of a short-haul or toll system carrying one supergroup are discussed. A typical system is described. The basic defect of nonlinearity in a FM system is avoided by using over-all feedback with a resulting over-all simplification of the repeater station.
- 621.396.65:621.397.7 2554  
Portable U.H.F.-S.H.F. Links in the B.B.C. Television Service—T. H. Bridgewater. (*Electronic Eng.*, vol. 30, pp. 291-296; May, 1958.) The various types of system in use for television outside-broadcast purposes are described together with their auxiliary and test equipment.
- 621.396.65.029.64 2555  
Microwave Link Development in the Radio Laboratories of the Post Office Engineering Department—C. F. Floyd and R. W. White. (*Electronic Eng.*, vol. 30, pp. 253-261; May, 1958.) The contribution made to wide-band microwave system development is surveyed. Work includes the design and installation of complete point-to-point 4-kmc television and multichannel telephony systems and associated test equipment. A description is given of a single-hop FM telephony link carrying 240 channels on an over-sea path of 55 miles, and a two-hop link for television transmission. Recent work on system equipment and measuring techniques is discussed and trends of development are considered.

## SUBSIDIARY APPARATUS

- 621.314.214 2556  
Variable-Output Mains Transformer—H. E. Styles. (*Wireless World*, vol. 64, pp. 262-263; June, 1958.) A design using eight windings giving voltages 2<sup>n</sup>, 2<sup>n-1</sup>, . . . 2<sup>1</sup> volts produces any integral output voltage between 0 and 255 volts by simple switching. Auto-transformer operation above 255 volts extends the range to 511 volts.
- 621.314.58:621.314.7 2557  
Voltage Conversion with Transistor Switches—P. L. Schmidt. (*Bell Lab. Rec.*, vol. 36, pp. 60-64; February, 1958.) The conversion of a dc voltage to ac at high audio frequencies at powers of 10-100 watts is achieved using a circuit containing transistors and modern magnetic-core components.
- 621.314.63:546.28 2558  
Failure-Rate Studies on Silicon Rectifiers—N. F. Bechtold and C. L. Hanks. (*Commun. and Electronics*, no. 35, pp. 49-56; March, 1958.) A study of the failure rate of rectifiers rated at 100-400 peak inverse volts under various conditions. Average failure rates for the 400-volt type are approximately three times those for the 100-volt type under identical conditions.
- 621.316.72:621.314.7 2559  
Transistor filters Ripple—F. Oakes and E. W. Lawson. (*Electronics*, vol. 31, p. 95; April 11, 1958.) In a low-voltage dc power supply a capacitance of 3500  $\mu$ f is effectively multiplied by 60 by the addition of a junction transistor operating as an impedance transformer.
- 621.316.722.1.076.25 2560  
Magnetic Voltage Stabilizers—W. Taeger. (*Elektronik*, vol. 6, pp. 265-269; September, 1957.) The use of saturation effects in a number of basic designs is described; brief details of a tube-controlled automatic stabilizer circuit are given.

## TELEVISION AND PHOTOTELEGRAPHY

- 621.397.5:535.623:778.5 2561  
The Optics of the Lenticular Colour-Film Process—R. Kingslake. (*J. Soc. Mot. Pict. Telev. Engrs.*, vol. 67, pp. 8-13; January, 1958.) This type of film, which has a possible use in color television, is described and the capabilities and limitations are given. Designs of cameras, projectors, printers, and viewers are outlined.
- 621.397.5:778.5 2562  
Monochrome Television Film Standards—K. B. Benson and J. R. Whittaker. (*J. Soc. Mot. Pict. Telev. Engrs.*, vol. 67, pp. 1-5; January, 1958.) Each stage in the production, processing, and reproduction of the film is examined. Standards for optimum results with the combined film and television system are developed.
- 621.397.6:621.374.4:621.318.4 2563  
Magnetic-Core Dividers for ITV Sync Generators—Rose. (See 2335.)
- 621.397.611.2 2564  
Beam Temperature, Discharge Lag and Target Biasing in some Television Pick-Up Tubes—B. Meltzer and P. L. Holmes. (*Brit. J. Appl. Phys.*, vol. 9, pp. 139-143; April, 1958.) The relation between discharge lag and the acceptance of the electron beam by the target, is analyzed and related to the calculated effective beam temperature. Results are given of the direct measurement of lag and its reduction by target biasing, and anomalous beam temperatures are discussed with regard to electron-optical measurements.
- 621.397.62:535.623:535.371.07.002.2 2565  
Photodeposition of Luminescent Screens—Sadovsky and Payne. (See 2430.)
- 621.397.62:621.396.662.078 2566  
Sound Signal tunes TV Automatically—C. W. Baugh, Jr., and L. J. Sienkiewicz. (*Electronics*, vol. 31, pp. 54-58; April 25, 1958.) The amplitude of the 4.5-mc intercarrier sound signal is used to control the local-oscillator frequency. As the picture level is held constant by AGC, this provides automatic fine tuning of the receiver.
- 621.397.7 2567  
The Tasks and Structure of the Swiss Television Network—W. Gerber. (*Tech. Mitt.*

*PTT*, vol. 35, pp. 441-455; November 1, 1957.) (In German and French.) After tracing the development of the Swiss television network on the basis of the 625-line system details are given of its present extent and its function as part of the Eurovision network. Future planning with regard to system expansion, progress policy, and types of links to be used is discussed.

## TRANSMISSION

621.396.61:621.376.3 2568  
Design and Construction of a F.M. Transmitter—D. F. Bowers. (*Brit. Commun. Electronics*, vol. 5, pp. 110-114; February, 1958.) The design and performance figures of a 3-6 kw transmitter for band II are given. Parallel operation is also considered.

## TUBES AND THERMIONICS

621.314.63:621.318.57 2569  
Solid-State Thyatron switches Kilowatts—Frenzel and Gutzwiller. (See 2315.)

621.314.63:621.373.51:621.372.413 2570  
A Proposed High-Frequency Negative-Resistance Diode—W. T. Read, Jr. (*Bell Sys. Tech. J.*, vol. 37, pp. 401-446; March, 1958.) A comprehensive description and analysis is given of a proposed semiconductor diode designed to operate as an oscillator when mounted in a suitable microwave cavity. The frequency would be in the range 1-50 kmc, the  $Q$  as low as 10 (negative), and the efficiency as high as 30 per cent. Reverse bias establishes a depletion layer of fixed width in a high-resistance region, bounded by very low-resistance end regions. The electric field has a maximum at one end of the space-charge region where hole-electron pairs are generated by avalanche; the holes (or electrons) produce diode current which is delayed about half a cycle relative to the alternating voltage, thus delivering power to the ac signal. When the diode is mounted in an inductive microwave cavity tuned to the diode capacitance, an oscillation will build up. It appears possible to exceed 20 watts in continuous operation at 5 kmc.

621.314.63+537.525.92]:681.142 2571  
New Applications of Impedance Networks as Analogue Computers for Electronic Space-Charge and for Semiconductor Diffusion Problems—Čremošnik, Frei, and Strutt. (See 2308.)

621.314.632:621.372.632 2572  
An Analysis of the Diode Mixer Consisting of Non-linear Capacitance and Conductance and Ohmic Spreading Resistance—A. C. Macpherson. *IRE TRANS. ON MICROWAVE THEORY AND TECHNIQUES*, vol. MTT-5, pp. 43-51; January, 1957. Abstract, *PROC. IRE*, vol. 45, p. 576; April, 1957. See also 4036 of 1957 (Messenger and McCoy).

621.314.632:621.372.632:621.396.822 2573  
Mixer Crystal Noise—N. Houlding. (*PROC. IRE*, vol. 46, pp. 917-918; May, 1958.) The effect of mismatches on the noise temperature ratio is considered and it is suggested that the assumption of thermal equilibrium [4036 of 1957 (Messenger and McCoy)] is unsound.

621.314.7 2574  
Transient Response of Drift Transistors—R. C. Johnston. (*PROC. IRE*, vol. 46, pp. 830-838; May, 1958.) The short-circuit transient response of a drift transistor to a step input current is found by solving the one-dimensional partial differential equation for minority carriers in the base, using a Laplace transform technique. The improvement in rise time due to the built-in field is less in the common-emitter than in the common-base connection. The built-in field lengthens the storage time, but reduces  $\alpha$ .

621.314.7:621.317.3 2575  
An Investigation of the Current Gain of Transistors at Frequencies up to 105 Mc/s—Hyde and Smith. (See 2494.)

621.314.7:621.318.57 2576  
Semiconductor Switching Devices—(*Electronic and Radio Engr.*, vol. 35, pp. 235-236; June, 1958.) A note on the characteristics of three new types of transistor. Information is condensed from articles in *IRE TRANS. ON ELECTRONIC DEVICES*, vol. ED-5; January, 1958.

621.314.7:621.396.822 2577  
Transistor Noise: its Origin, Measurement and Behaviour—B. L. H. Wilson. (*J. Brit. IRE*, vol. 18, pp. 207-225; April, 1958.) "The sources of noise in semiconductors and the mathematical techniques needed in their discussion are indicated in order to survey the theory of noise in transistor amplifiers and to consider methods of measurement. The variation of transistor noise with operating point and frequency is discussed and a comparison is made of noise levels in audio amplifiers using transistors and tubes respectively."

621.314.7.001.4(083.74) 2578  
I.R.E. Standards on Solid-State Devices: Methods of Testing Point-Contact Transistors for Large-Signal Applications, 1958—(*PROC. IRE*, vol. 46, pp. 878-888; May, 1958.) Standard 58 IRE 28.S1.

621.314.7.002.2:546.28 2579  
Manufacture of Silicon Transistors—J. T. Kendall. (*Electronic and Radio Engr.*, vol. 35, pp. 202-207; June, 1958.) Current techniques for the production of six types of transistor are described, with a discussion of impurity distributions. Types manufactured in the U.K. and their main characteristics are listed.

621.314.7.004.2 2580  
Naval Material Laboratory Transistor Reliability Study—R. E. Martin. (*IRE TRANS. ON RELIABILITY AND QUALITY CONTROL*, no. PGRQC-10, pp. 49-56; June, 1957.) The effects of collector voltage, of collector power dissipation, and of ambient temperature on the reliability of low power  $p-n-p$  alloy-junction transistors are to be investigated in a special laboratory. 3000 samples are to be tested for 10,000 hours or longer.

621.314.7.004.2 2581  
Success Story—Transistor Reliability—1956—C. H. Zierdt, Jr. (*IRE TRANS. ON RELIABILITY AND QUALITY CONTROL*, no. PGRQC-10, pp. 57-68; June, 1957.) The electrical characteristics of a wide range of samples of Ge and Si junction transistors were examined under various temperature conditions and for various periods of time. Preliminary tests of the effects of nuclear radiation are also reported.

621.314.7.004.2:546.289 2582  
Factors in the Reliability of Germanium Power Transistors—A. B. Jacobsen. (*IRE TRANS. ON RELIABILITY AND QUALITY CONTROL*, no. PGRQC-10, pp. 43-48; June, 1957.) The reliability of a  $p-n-p$  alloy-junction transistor used for car receivers is discussed.

621.385.004.15 2583  
A Basic Study of the Effects of Operating and Environmental Factors on Electron-Tube Reliability—W. S. Bowie. (*IRE TRANS. ON RELIABILITY AND QUALITY CONTROL*, no. PGRQC-6, pp. 46-56; February, 1956. Abstract, *PROC. IRE*, vol. 44, p. 277; February, 1956.)

621.385.004.15 2584  
Electron-Tube Life and Reliability—Built-

In Tube Reliability—M. A. Acheson. (*IRE TRANS. ON RELIABILITY AND QUALITY CONTROL*, no. PGRQC-7, pp. 33-43; April, 1956. Abstract, *PROC. IRE*, vol. 44, p. 957; July, 1956.)

621.385.004.2 2585  
Environmental Effects on Vacuum-Tube Life—H. C. Pleak and A. V. Baldwin. (*IRE TRANS. ON RELIABILITY AND QUALITY CONTROL*, no. PGRQC-9, pp. 93-101; January, 1957. Abstract, *PROC. IRE*, vol. 45, p. 577; April, 1957.) See 2956 of 1957.

621.385.004.6 2586  
Prediction of Tube Failure Rate Variations—M. P. Feyerherm. (*IRE TRANS. ON RELIABILITY AND QUALITY CONTROL*, no. PGRQC-9, pp. 65-71; January, 1957. Abstract, *PROC. IRE*, vol. 45, p. 577; April, 1957.)

621.385.029.6 2587  
Industrial Magnetrons—W. Schmidt. (*Elektron Rundschau*, vol. 11, pp. 306-309; October, 1957.) The differences in the requirements to be met in radar and industrial applications of magnetrons are summarized. Brief details are given of some German industrial types for operation at 2400 mc.

621.385.029.6 2588  
Very-Low-Noise Travelling-Wave Amplifier—E. W. Kinaman and M. Magid. (*PROC. IRE*, vol. 46, pp. 861-867; May, 1958.) A general explanation of beam noise is given with a description of noise-reduction systems lowering noise figures from 9 to 6 db.

621.385.029.6 2589  
Backward-Wave Oscillators—A. G. Stainsby. (*Electronic Eng.*, vol. 30, pp. 329-334; May, 1958.) These oscillators can be tuned electronically with a frequency range greater than an octave. There are two distinct types of oscillator, the  $O$  type which is mainly suited to low power operation as a local oscillator or test source, and the  $M$  type which is capable of delivering high powers with good efficiency and is thus suitable for use as a transmitter.

621.385.029.6 2590  
Understanding the Backward-Wave Oscillator—D. A. Dunn. (*Electronic Ind.*, vol. 17, pp. 72-76; January, 1958.) An explanation of the physical processes which take place in backward-wave oscillators.

621.385.029.63/.64 2591  
Travelling-Wave Tubes in Communications.—R. B. Coulson. (*Electronic Eng.*, vol. 30, pp. 302-304; May, 1958.) Their application in microwave repeaters and the use of electromagnets in preference to permanent magnets for beam focusing is discussed.

621.385.029.63/.64 2592  
Travelling-Wave-Tube Amplifiers—D. H. O. Allen. (*Electronic Eng.*, vol. 30, pp. 305-309; May, 1958.) [The major advances made towards a reliable and useful tube are discussed with particular reference to noise characteristics and focusing methods. Applications to microwave links and the distortions that may arise under various operating conditions are also discussed.]

621.385.029.63/.64 2593  
S-Band Travelling-Wave Tube with Noise Figure below 4 dB—M. Caulton and G. E. St. John. (*PROC. IRE*, vol. 46, pp. 911-912; May, 1958.) Modifications to the electrode configuration and voltage profile of a conventional low noise traveling-wave tube produced a hollow beam and a low velocity drift region near the cathode. Noise figures down to 3.5 db were obtained.

621.385.029.63/.64 2594

**Reflex Klystrons**—A. H. Atherton. (*Electronic Eng.*, vol. 30, pp. 315-320; May, 1958.) A general description of the construction and operation of reflex klystrons is given, with typical examples.

621.385.029.63/.64 2595

**Multicavity Klystrons**—V. J. Norris. (*Electronic Eng.*, vol. 30, pp. 321-323; May, 1958.) "A review is given of the factors determining the gain, efficiency, and bandwidth of multicavity klystrons, together with results which have been achieved in practice."

621.385.029.63/.64:621.372.414 2596

**Coaxial-Line Velocity-Modulated Oscillator Valves**—D. E. Lambert. (*Electronic Eng.*, vol. 30, pp. 324-328; May, 1958.) The principle of operation of these tubes is discussed, and also their advantages and limitations. A list of tubes in production is given.

621.385.029.64 2597

**Traveling-Wave Tubes for 4000 Mc/s**—P. F. C. Burke. (*Electronic Eng.*, vol. 30, pp. 310-314; May, 1958.) Traveling-wave tubes may be used in microwave radio links as output amplifiers, low-noise receivers, and intermediate-level amplifiers. Examples are given of applications at frequencies near 4 km.

621.385.032.213.13 2598

**High-Emission Hot Cathodes of New Type**—T. Hashimoto, M. Uchida, and A. Yokoyama. (*Rep. Elect. Commun. Lab., Japan*, vol. 5, pp. 4-8; December, 1957.) Research has been carried out on cathodes impregnated with various barium compounds for use in microwave tubes. Work has also been done on sintered cathodes. Details of life tests are given. See also 1927 of June (Hashimoto).

621.385.032.213.13 2599

**A Sintered Nickel Matrix Cathode**—R. W. Fane. (*Brit. J. Appl. Phys.*, vol. 9, pp. 149-153; April, 1958.) Cathodes containing alkaline earth carbonates and boron have given 8000

hours life at current densities in excess of 0.5 a/cm<sup>2</sup>. Processing schedules and operating temperatures are similar to those for normal oxide-coated types. Possible mechanisms of operation are discussed.

621.385.032.269.1 2600

**A New Type of Low-Noise Electron Gun for Microwave Tubes**—M. R. Currie. (*PROC. IRE*, vol. 46, p. 911; May, 1958.) Noise figures of 3.5 db are obtained with the gun system whose basic features are described.

621.385.1+621.387 2601

**Thermionic and Cold-Cathode Valves**—W. H. Aldous. (*Proc. IEE*, pt B, vol. 105, pp. 273-281; May, 1958.) A full survey of tube development since 1933 is given, with particular emphasis on the decrease in size of all types of tubes.

621.385.3 2602

**On the Amplification Factor of a Triode Valve: Part 2**—E. B. Moullin. (*Proc. IEE*, pt. C, vol. 105, pp. 196-202; March, 1958.) A description of measurements designed to test the degree to which the amplification factor is independent of the anode current (see 2649 of 1957).

621.385.3/4:029.63/.64 2603

**Triodes and Tetrodes for U.H.F.-S.H.F. Operation**—C. A. Tremlett and A. D. Williams. (*Electronic Eng.*, vol. 30, pp. 335-340; May, 1958.) A review of the advances made over the last ten years in the development of space-charge-controlled tubes for operation above 300 mc. Tube geometry and performance data for various types are listed.

621.385.832:621.317.755 2604

**Broad-Band Oscilloscope Tube**—Brangaccio, Dietrich, and Sullivan. (See 2510.)

## MISCELLANEOUS

061:621.3(436)(091) 2605

75 Years of the Elektrotechnischer Verein

Österreichs—(*Electrotech. u. Maschinenb.*, vol. 75, pp. 177-340; May 1, 1958.) The history of the Association and its journal are outlined and the contributions of Austrian scientists and engineers in the field of electrical engineering are summarized in a number of papers which include the following:

1) **The Development of Electrical Communications in Austria**—H. Schmid. (pp. 300-320.)

2) **The Contribution of Austria in the Development of High-Frequency Engineering**—C. Caspar. (pp. 320-326.)

3) **Austria's Contribution in the Development of Electroacoustics**—F. Lachner. (pp. 330-332.)

621.3.029.6(091) 2606

**Microwaves**—E. L. Ginzton. (*Science*, vol. 127, pp. 841-851; April 18, 1958.) The historical development of microwave research is reviewed and current applications and techniques are outlined.

621.3.049 2607

**Optimum Tolerance Assignment to Yield Minimum Manufacturing Cost**—D. H. Evans. (*Bell Sys. Tech. J.*, vol. 37, pp. 461-484; March, 1958.) The basic item considered is a unit with a single nominal design response, having several components with given nominal design values such that the unit response is as required. Tolerance assignment is considered in relation to cost and salvage value of a unit, and statistical results are presented.

621.3.049:621-52 2608

**Automatic Methods in Radio Component Manufacture**—D. Stevenson and R. B. Shepherd. (*J. Brit. IRE*, vol. 18, pp. 227-231; April, 1958.) Two special systems are described: a) an electronic counter technique applied to the accurate control of a high-speed coil winding machine; b) a power press producing ferrous piece-parts protected from jamming by detecting each ejected part magnetically.

